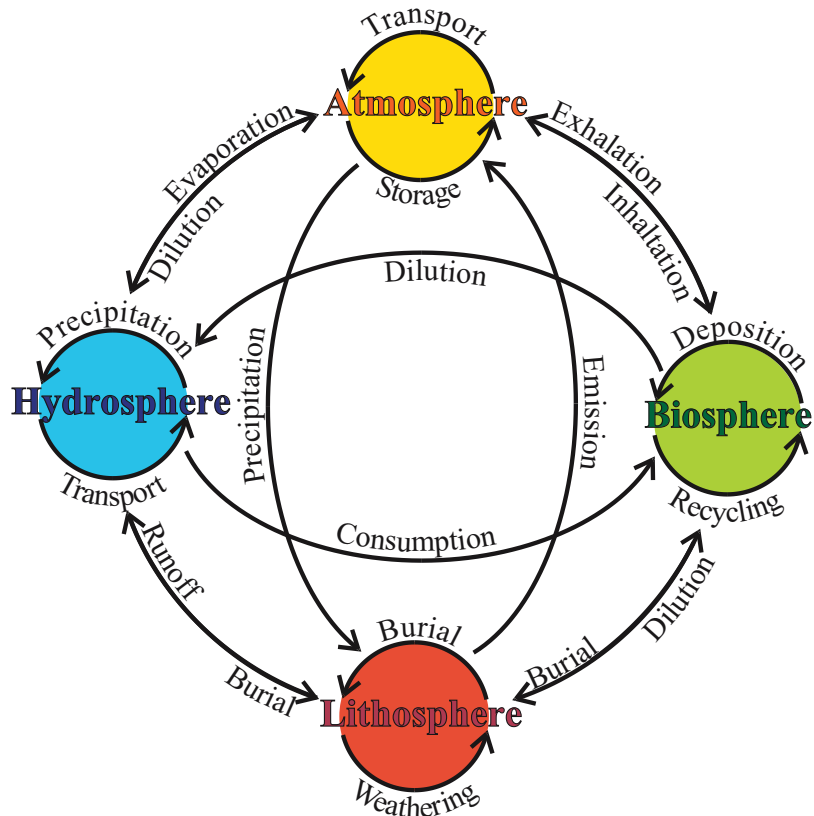


Box models of volatile cycles over the entire Phanerozoic



Dissertation
zur Erlangung des Doktorgrades
der Mathematisch-Naturwissenschaftlichen Fakultät
der Christian-Albrechts-Universität
zu Kiel

vorgelegt von
Oliver Bartdorff

Kiel 2006

Referent: Prof. Dr. Klaus Wallmann

Korreferent: PD. Dr. Thor Hansteen

Tag der mündlichen Prüfung: 03. November 2006

Zum Druck genehmigt:

Der Dekan

*“The time has come,” the Walrus said,
“To talk of many things:
Of shoes – and ships – and sealing wax
– of cabbages – and kings ...
and why the sea is boiling hot –
and whether pigs have wings.”*

Lewis Carroll (1871)
Through the Looking-Glass

Preface

This study comprises a general introduction presented in Chapter I, and three stand-alone chapters - Chapter II - IV. Each of the chapters contains a separate introduction, a box model set-up, model results, and a discussion of the results, as well as a separate reference list. For a better understanding of the models by the enthusiastic readers, a complete list of the model relevant calculations is added to the corresponding chapters. The last chapter gives a summary outline of the present study.

The titles of the chapters are briefly listed below:

Chapter I

Introduction

Chapter II

Modeling the chemical evolution of seawater (S, P, C, Sr, O)
over the entire Phanerozoic

Chapter III

A model of atmospheric methane over the entire Phanerozoic

Chapter IV

Evolution of oxygen concentrations in the deep ocean and marine nutrient inventories
over the entire Phanerozoic

Chapter V

Conclusion

The research project from which this dissertation emerged, is embedded in the Sonderforschungsbereich (SFB) 574 "Volatiles and Fluids in Subduction Zones", hosted at the University of Kiel. One general aim of the SFB 574 is to obtain a better understanding of the material transfer through subduction zones concerning input-output budgets.

The present work considers processes, such as subduction, deposition, weathering, and emission which are controlled through subduction. The models decipher the significance of subduction processes on selected volatiles, and on the global biogeochemical cycles over a long time scale (570 Ma).

Abstract

Three stand-alone geochemical box models have been developed to simulate globally coupled biogeochemical cycles. These models reflect the evolution of the participating biotic and abiotic constituents in marine and terrestrial environments, including the lower atmosphere. The single models focus on the calculation of: 1) the chemical evolution of seawater, 2) the atmospheric methane concentration, and 3) the concentration of oxygen in surface and deep ocean water over the entire Phanerozoic (570 Ma). The models are driven by geological and evolutionary forcings and are controlled by proxy data. Internal feedback is provided by model outputs serving as input to other model components. The Phanerozoic biogeochemical evolution of seawater (dissolved inorganic carbon, alkalinity, nutrients, and oxygen), its isotope sulfur and carbon composition, as well as the atmospheric partial pressures of oxygen (pO_2), carbon dioxide (pCO_2), and methane (pCH_4) are calculated by standard runs of the individual models.

The first model calculates the chemical evolution of seawater (S, P, C, Sr, O), its sulfur and carbon isotope composition, as well as the atmospheric partial pressures of oxygen and carbon dioxide. It successfully reproduces independent proxy data recorded in marine carbonates ($\delta^{13}C$) and evaporite rocks ($\delta^{34}S$) and basically confirms the Phanerozoic evolution of atmosphere and oceans as suggested by previous models and proxy data. However, new results and perspectives were obtained for the sulfur cycle. Thus, the seawater model revealed that both volcanic and sedimentary processes significantly affect the marine $\delta^{34}S$ record, while previous models often assumed that the evolution of seawater $\delta^{34}S$ values only reflects the sedimentary cycling - e.g. sedimentary pyrite burial and weathering. The new model uses sulfate concentrations in seawater, derived from fluid inclusion data, to calculate the net burial flux of evaporites (net burial = burial - weathering) over the entire Phanerozoic. This new estimate indicates a high net burial flux during warm periods and a high net weathering during cold periods, confirming that the deposition of evaporites is mainly controlled by the prevailing climatic conditions.

Seawater $^{87}Sr/^{86}Sr$ ratios recorded in marine carbonates were applied to derive rates of tectonic/volcanic activity over the entire Phanerozoic, because a strong relation was found between the variations of $^{87}Sr/^{86}Sr$ ratios in seawater and volcanic emissions and hydrothermal processes. The predicted rates show an oscillating trend over the Phanerozoic, with high activities during the Mesozoic and Cenozoic. The new record of tectonic/volcanic activity derived from marine $^{87}Sr/^{86}Sr$ data shows little correlation with the global sea-level evolution, thus confirming that sea level change is a poor proxy for estimating changes in spreading and subduction rates. Some of the maxima occurring in the new record are correlated to major flood basalts and superplume periods observed in the geological record. Considering that the ancient flood basalts and superplumes as well as oceanic crust production are not fully documented in the geological record, it is not surprising that periods of strong basaltic strontium release are not always accompanied by known magmatic events. Nevertheless, changes in tectonic/volcanic activity reconstructed from the marine $^{87}Sr/^{86}Sr$ record are arguably more valid than previously used proxies.

With the second model the first attempt has been made to calculate the atmospheric partial pressure of methane ($p\text{CH}_4$) over the entire Phanerozoic. According to the model, $p\text{CH}_4$ increased up to approx. 10 ppmV during the Carboniferous coal swamp era, a value which is six times higher than the present partial pressure and twenty-eight times higher than the pre-industrial Holocene value. This implies a maximum radiative forcing of about 3.5 W m^{-2} via methane, which is twice as much as the recent radiative forcing via atmospheric CO_2 . By its radiative forcing and due to its decomposition into CO_2 , methane has caused an increase of the average global surface temperature by up to 1°C .

The elevated $p\text{CH}_4$ values during the cold period of the Permo-Carboniferous may have moderated the temperature decline caused by the coeval draw-down of atmospheric CO_2 . Both the decrease in $p\text{CO}_2$ and the increase in $p\text{CH}_4$ are intimately linked to the spread of land plants during the Permian and Carboniferous. The high methane emissions from swamps during this period may have prevented the development of a “snowball earth” state repeatedly encountered during the Precambrian prior to the advent of land plants.

Combined runs of the methane model with the full global carbon model (the first model explained above) indicate that the heating induced by elevated $p\text{CH}_4$ favored the draw down of atmospheric $p\text{CO}_2$ via enhanced rates of silicate weathering during the Permian-Carboniferous.

The effects of episodic gas hydrate decomposition - according to the “clathrate gun hypothesis” (sudden break down of large amounts of methane clathrates from the seafloor due to changing stability conditions) - were investigated using an extended model simulating the evolution of $\delta^{13}\text{C}$ values in seawater and marine carbonates. These model runs confirm that the conspicuous negative $\delta^{13}\text{C}$ excursions documented in the geological record were indeed accompanied by a significant increase in atmospheric $p\text{CH}_4$ and $p\text{CO}_2$ values.

Phanerozoic changes in the redox state of the deep ocean were simulated - for the first time - with the third model presented in this thesis. The model includes a) surface water and b) deep water boxes which are coupled to diagenetic models simulating the biogeochemical turnover in surface sediments deposited on the continental shelf, slope and rise, and deep-sea floor. It is used to calculate the concentrations of dissolved oxygen, nitrate and phosphate in the two water boxes and in the pore waters of marine sediments.

The surface water receives nutrients from land and exchanges oxygen with the atmosphere. Moreover, nitrogen fixation adds nitrate to the surface ocean. Nutrients are removed from surface waters by marine export production. Within the deep water column oxygen is consumed and nutrients are released by the degradation of exported organic matter while nitrate is consumed via denitrification. Dissolved species are exchanged between these two water segments by vertical mixing while the underlying sediments exchange solutes with the surface and deep ocean by molecular diffusion across the sediment/water interface.

According to this model, the deep ocean was almost completely anoxic during the Early Paleozoic, since the low oxygen concentrations in the Early Paleozoic surface ocean - caused by low atmospheric $p\text{O}_2$ values and high surface temperatures - inhibited an effective ventilation of the

deep ocean. The ocean evolved into a fully oxic state during the Permian-Carboniferous cold period, when the oxygen concentration in surface water ventilating the deep ocean was very high because of high atmospheric pO_2 and low surface temperature values. Since these atmospheric and climatic conditions probably were caused by the spread of land plants, the development of a fully oxic deep ocean should be regarded as an additional - and previously not recognized - consequence of this major ecological transition.

The newly developed model shows that both the phosphate content and the productivity of the ocean have increased continuously over the Phanerozoic. This trend is neither observed in the burial of organic carbon nor in the marine $\delta^{13}C$ record showing that these parameters do not reliably reflect the ocean's changing productivity.

The oxygen model also predicts that the nutrient N : P ratio in seawater changes with the redox state of the ocean and that nitrogen fixation can not fully compensate for these changes. Thus, the nutrient N : P ratio was low in the anoxic oceans of the Early Paleozoic but reached very high values during the Permian-Carboniferous cold period. The model was calibrated using Holocene data and was tested to decipher the sensitivity of the marine biogeochemical system with respect to external perturbations. These tests showed that marine productivity, nutrient inventories and the oxygen content of the deep ocean are very sensitive to changes in ocean ventilation, whereas the nutrient input from land has a comparably small effect on the oceans. Reducing sediments are a more important source of phosphate to the oceans than rivers. Therefore, the positive feedback between ocean anoxia and eutrophication, which is rooted in the redox-dependent phosphorus turnover in sediments, dominates the evolution of the marine biogeochemical system. This model result implies that the state of the ocean is mainly regulated by climatic conditions and the O_2 content of the atmosphere.

Furthermore, the oxygen model was applied to investigate the triggering of oceanic anoxic events (OAEs). Nutrient input from the continents and ocean ventilation had to be changed simultaneously by 60 % to attain a fully anoxic Cretaceous ocean. Additional model runs showed that methane released from the seafloor via destabilization of gas hydrates may exhaust the entire oxygen replenished by ventilation if hydrate melting is completed within 10 kyr.

Kurzfassung

Unter der Berücksichtigung gekoppelter globaler biogeochemischer Kreisläufe wurden drei eigenständige geochemische Box Modelle entwickelt. Sie stellen die Entwicklung der beteiligten biotischen und abiotischen Komponenten sowohl in marinen und terrestrischen Ablagerungsräumen als auch in der Atmosphäre dar. Schwerpunkte der einzelnen Modelle sind die Berechnung: 1) der chemischen Entwicklung von Meerwasser, 2) der Methankonzentration in der Atmosphäre und 3) der Sauerstoffkonzentration im Oberflächen- und Tiefenwasser der Ozeane für des gesamte Phanerozoikum (570 Ma). Die Modelle werden von geologischen und evolutionären Größen gesteuert und durch unabhängige geologisch überlieferte Daten kontrolliert. Die Ergebnisse der jeweiligen Modelle greifen in die Prozesse der anderen Modelle als externe Steuergrößen ein. Der Standardlauf der einzelnen Modelle berechnet sowohl die phanerozoische biogeochemische Entwicklung von Meerwasser (gelöster anorganischer Kohlenstoff, Alkalinität, Nährstoffe und Sauerstoff), seine Isotopenzusammensetzung (Schwefel und Kohlenstoff) als auch die atmosphärischen Partialdrücke von Sauerstoff (pO_2), Kohlendioxid (pCO_2) und Methan (pCH_4).

Der Standardlauf des Modells zur Berechnung der chemischen Entwicklung der Ozeane (S, P, C, Sr, O), seiner Schwefel- und Kohlenstoffisotopenzusammensetzung stellt ebenfalls die atmosphärischen Partialdrücke von Sauerstoff und Kohlendioxid dar. Die Modellergebnisse korrelieren sehr gut mit unabhängigen, auf marinen Karbonaten ($\delta^{13}C$) und Evaporiten ($\delta^{34}S$) basierenden Daten, und bestätigen somit die chemische Entwicklung der Atmosphäre und der Ozeane über das gesamte Phanerozoikum, wie sie bereits in früheren Modellen und mit Hilfe anderer unabhängiger Daten beschrieben wurde. Ferner zeigten Sensitivitätstests, dass sowohl vulkanische als auch sedimentäre Prozesse die geologisch überlieferten marinen Schwefelisotopenzusammensetzungen beeinflusst haben. Dies steht im Gegensatz zu früher veröffentlichten Modellergebnissen, zu deren Ermittlungen ausschließlich sedimentäre Prozesse herangezogen wurden.

Zusätzlich werden in diesem Modell die Sulfatkonzentrationen im Meerwasser, welche von Lösungseinschlüssen in Evaporiten abgeleitet werden können, verwendet, um den Netto-Ablagerungsfluss von Evaporiten (Netto-Ablagerungsfluss = Ablagerung - Abtragung) für das gesamte Phanerozoikum berechnen zu können. Diese neue Abschätzung verdeutlicht, dass der Netto-Ablagerungsfluss hauptsächlich während warmer Phasen, und der netto Abtragungsfluss während kalter Phasen besonders hoch war, sie bestätigen damit, dass die Ablagerung von Evaporiten im wesentlichen von den vorherrschenden Klimabedingungen kontrolliert wird.

Eine der fundamentalen Voraussetzungen dieses Modells ist, dass die in marinen Karbonaten erhaltenen Strontiumverhältnisse im Meerwasser ($^{87}Sr/^{86}Sr$) die tektonischen und vulkanischen Aktivitäten des Phanerozoikums widerspiegeln. Diese Annahme wurde verwendet, um aus den überlieferten Meerwasserstrontiumverhältnissen die tektonischen und vulkanischen Aktivitäten der Vergangenheit zu berechnen. Die ermittelten Raten weisen einen oszillierenden Trend während des gesamten Phanerozoikums auf, mit deutlich höheren Werten als heute, vor allem im Mesozoikum und im Känozoikum. Die Ergebnisse dieser neuen Berechnungsmethode weisen nur wenige

Übereinstimmungen mit den globalen Meeresspiegelschwankungen auf, und bestätigen, dass die Meerwasserstände, wie sie in früheren Modellansätzen verwendet wurden, eine schlechte Grundlage zur Ermittlung der Spreizungs- und Subduktionsraten sind. Die geologischen Belege über Flutbasalte und „Superplumes“ zeigen im Vergleich zu den im Modell errechneten Raten hauptsächlich gute aber auch weniger gute Übereinstimmungen. Da die geologische Überlieferungen über frühere Flutbasalte und „Superplumes“ aber auch der Ozeankrustenneubildung naturgemäß nicht vollständig sind, ist es nicht verwunderlich, dass Phasen erhöhten Strontiumausstoßes nicht vollständig in allen Punkten mit den bekannten magmatischen Ereignissen deckungsgleich sind. Dennoch ist zu erwähnen, dass Änderungen in der tektonischen und vulkanischen Aktivität, ermittelt mit Hilfe von marinen Strontiumverhältnissen, gut vertretbar von den geologischen Daten ableitbar sind.

Das hier vorgestellte zweite Modell berechnet erstmals die Methankonzentration in der Atmosphäre für das gesamte Phanerozoikum. Die Modellberechnungen zeigen, dass der Partialdruck der Atmosphäre von Methan während der Kohlenepoche des Karbons auf 10 ppmV anstieg. Dieser Wert ist sechs mal höher als der heutige und achtundzwanzig mal höher als der des vorindustriellen Holozäns. Dieser hohe atmosphärische Wert bedeutet eine methanbedingte Wärmerückstrahlung von $3,5 \text{ W m}^{-2}$. Dieser Wert ist doppelt so hoch wie die rezente Wärmerückstrahlung von atmosphärischem Kohlendioxid. Durch die eigene Wärmerückstrahlung des Methans und die Wärmerückstrahlung des Kohlendioxids, welches als Folge des Methanabbaus entstanden ist, erhöhte Methan auf direktem und indirektem Weg die globale Durchschnittstemperatur um $1 \text{ }^\circ\text{C}$.

Die erhöhten pCH_4 Werte während der Kälteperiode des Permo-Karbons könnten zu einem weniger starken Absinken der Temperaturen geführt haben. Diese ursprüngliche Temperaturabnahme wäre bedingt durch die Abnahme des atmosphärischen Kohlendioxids. Sowohl der sinkende atmosphärische Kohlendioxidpartialdruck als auch der steigende atmosphärische Methanpartialdruck waren stark mit der Ausbreitung der Landpflanzen während des Permo-Karbons verknüpft. Die hohen Emissionsraten aus den Sümpfen während dieser Periode haben somit möglicherweise die Bildung einer „Schneeball-Erde“ verhindert, welche sich lange vor der Entwicklung der Landpflanzen im Präkambrium mehrfach ausbildete.

Ergänzende, mit dem Kohlenstoffmodell gekoppelte Testläufe, ergaben des Weiteren einen Anstieg der Silikatverwitterung bei erhöhten Temperaturen und ein dadurch verursachtes weiteres Absinken des atmosphärischen Kohlendioxidpartialdrucks.

Die Effekte von episodischen massiven Gashydratzersetzungen, in Anlehnung an die „Clathrate Gun Hypothesis“, wurden verwendet, um ergänzende Modellläufe durchzuführen. Dies geschah unter Berücksichtigung der Entwicklung der Kohlenstoffisotopenzusammensetzung im Meerwasser und in marinen Karbonaten, welche im vorhergenannten Modell berechnet wurden. Die Modellläufe bestätigen, dass die geologisch überlieferten auffälligen Kohlenstoffisotopenexkursionen tatsächlich mit dem starken Anstieg des atmosphärischen Methans und des Kohlendioxids einhergehen.

Das dritte in dieser Arbeit vorgestellte Modell berechnet - erstmalig - die Sauerstoffkonzentrationen des tiefen Ozeans für das Phanerozoikum. Dieses Modell ist zweigeteilt, in je eine Box für

Oberflächen- und eine für Tiefenwasser. Beide sind gekoppelt mit einem Sedimentdiagenesemodell für Schelfe, Kontinentallänge und Tiefseeboden. Dieses Modell berechnet demnach die Konzentration an gelöstem Kohlenstoff, Stickstoff und Phosphat nicht nur in den beiden Wasserboxen, sondern zusätzlich auch in den Porenwässern mariner Sedimente.

Zusammengefasst kann die Entwicklung einer sauerstoffdurchfluteten Tiefsee wie folgt beschrieben werden: das Oberflächenwasser erhält seine Nährstoffe von Land und den Sauerstoff durch den Austausch mit der Atmosphäre. Überdies reichert sich Nitrat im Oberflächenwasser durch den Prozess der Nitratfixierung an. Verursacht durch die marine Exportproduktion werden die Nährstoffe dem Oberflächenwasser entzogen. Durch den Abbau organischer Substanz wird im Tiefenwasser Sauerstoff verbraucht. Nährstoffe werden freigesetzt, während Nitrat durch die Denitrifikation verbraucht wird. Die gelösten Bestandteile des Oberflächen- als auch des Tiefenwassers werden durch den vertikalen Austausch in der Wassersäule umgelagert, während die jeweiligen Sedimente mittels molekularer Diffusion ihre Lösungen sowohl mit dem Tiefenwasser als auch mit dem Oberflächenwasser entlang der Sedimentoberfläche austauschen.

Basierend auf den hier präsentierten Modellergebnissen war die Tiefsee während des frühen Paläozoikums anoxisch. Der derzeit vorherrschende geringe atmosphärische Sauerstoffpartialdruck und eine hohe Oberflächentemperatur bedingten eine geringe Sauerstofflöslichkeit im Oberflächenwasser, was dort zu einer geringeren Sauerstoffkonzentration führte. Erst in der Kältephase des Permo-Karbons entwickelten sich die Ozeane zu vollständig sauerstoffhaltigen Systemen. Der Grund hierfür liegt in der verstärkten Sauerstoffversorgung des Tiefenwassers aufgrund des höheren Sauerstoffangebotes im Oberflächenwasser. Die Erhöhung der Sauerstoffkonzentration im Oberflächenwasser ist das Resultat eines erhöhten Sauerstoffaustauschs zwischen Ozeanen und Atmosphäre bei niedrigen Oberflächentemperaturen. Diese veränderten atmosphärischen und klimatischen Bedingungen wurden wahrscheinlich durch die Ausbreitung der Landpflanzen eingeleitet. Die Entwicklung einer vollständig sauerstoffdurchfluteten Tiefsee kann als zusätzliche Konsequenz ebenso auf ökologische Veränderungen zurückgeführt werden - eine Ursache, die bisher nicht erkannt wurde.

Die Modellberechnungen ergaben einen kontinuierlichen Anstieg der Phosphatkonzentration und die Produktivität des Ozeans während des gesamten Phanerozoikums. Dieser Trend lässt sich weder in der Ablagerung von organischem Kohlenstoff noch durch die marinen $\delta^{13}\text{C}$ Daten erkennen, wie es im Gegensatz zu den neuen Erkenntnissen in der Literatur häufig diskutiert wird. Sie weisen somit darauf hin, dass diese Parameter die Änderungen der Ozeanproduktion nicht zuverlässig wiedergeben werden können.

Das hier diskutierte Modell veranschaulicht ferner, dass sich das ändernde Nährstoffverhältnis von Stickstoff und Phosphor (N : P) im Meerwasser mit den ändernden Redox-Bedingungen der Ozeane verschiebt, und dass die Stickstofffixierung diese Änderungen nicht kompensieren kann. Demnach sind die Nährstoffverhältnisse von Stickstoff und Phosphor im anoxischen Ozean während des frühen Paläozoikums niedrig und während der kalten Phase im Permo-Karbon sehr hoch. Die Modelle wurden daher mittels holozäner Daten abgeglichen und zu Tests herangezogen, mit dem

Ziel, die Sensitivität mariner biogeochemischer Systeme unter Berücksichtigung von externen Einflüssen zu entschlüsseln. Diese Tests ergaben, dass die marine Produktion, der Nährstoffvorrat und die Sauerstoffkonzentration des Tiefenozeans sehr empfindlich auf Änderungen in der Ozeanbelüftung reagieren, der Nährstoffeintrag vom Land jedoch einen verhältnismäßig geringen Einfluss auf den Ozean hat. Reduzierende Bedingungen in marinen Sedimenten sind bedeutendere Phosphatquellen für die Ozeane als der Eintrag durch Flüsse. Dementsprechend dominiert die positive Rückkopplung zwischen anoxischen Bedingungen im Ozean und der Eutrophierung die Entwicklung des biogeochemischen Systems, welche durch die Redoxabhängigkeit des Phosphorverbrauches in Sedimenten bedingt wird. Demnach wird der Redox-Zustand der Ozeane hauptsächlich durch klimatische Bedingungen und die Sauerstoffkonzentration der Atmosphäre gesteuert.

Abschließend wurde das Sauerstoffmodell genutzt, um die Ursachen sauerstoffarmer ozeanischer Ereignisse (OAEs) zu beschreiben. Die Nährstoffversorgung und die Ozeanbelüftung wurden gleichermaßen verändert. Erst bei einer Veränderung (einer Verstärkung der Nährstoffzufuhr und einer Verringerung der Ventilation) um 60 % wurde der Ozean der Kreide komplett anoxisch. Ferner konnte mittels einer Kopplung der Modellberechnungen des Methan- und des Sauerstoffmodells bestätigt werden, dass ein plötzliches Schmelzen und Freisetzen von großen Mengen Gashydrat den Verbrauch des der Tiefsee durch Belüftungsprozesse zugeführten Sauerstoffs innerhalb von sehr kurzen Entgasungszeiträumen (10.000 a) verursachen kann.

Contents

Preface	i
Abstract	iii
Kurzfassung	vi
1 Introduction	1
1.1 Box models.....	5
1.2 Global biogeochemical cycles.....	6
1.2.1 Carbon cycle.....	7
1.2.2 Methane cycle.....	11
1.2.3 Phosphorus cycle.....	15
1.2.4 Sulfur cycle.....	18
1.2.5 Nitrogen cycle.....	20
1.2.6 Oxygen cycle.....	22
1.2.7 Isotope cycles.....	24
1.2.7.1 Carbon isotopes.....	25
1.2.7.2 Sulfur isotopes.....	25
1.2.7.3 Strontium isotopes.....	25
1.2.8 Summary.....	26
References.....	27
2 Modeling the chemical evolution of seawater (S, P, C, Sr, O) over the entire Phanerozoic	33
Abstract.....	35
2.1 Introduction.....	35
2.2 Set up of the model.....	36
2.2.1 Sulfur model.....	41
2.2.2 Phosphorus model.....	43
2.2.3 Carbon model.....	46
2.2.4 Strontium model.....	48
2.2.5 Oxygen model.....	50
2.3 External forcings of the model.....	50
2.4 Results and discussion.....	50
2.4.1 Sulfur model.....	51
2.4.1.1 Standard case.....	51
2.4.1.2 Sensitivity tests.....	53
2.4.2 Phosphorus model.....	57
2.4.2.1 Standard case.....	57
2.4.2.2 Sensitivity tests.....	58
2.4.3 Carbon model.....	59
2.4.3.1 Standard case.....	59
2.4.3.2 Sensitivity tests.....	61
2.4.4 Strontium model.....	64
2.4.4.1 Standard case.....	64
2.4.5 Oxygen model.....	66
2.4.5.1 Standard case.....	66
2.4.5.2 Sensitivity tests.....	67
2.5 Conclusions.....	67
References.....	69
Appendix.....	72

3	A model of atmospheric methane over the entire Phanerozoic	79
	Abstract.....	81
3.1	Introduction.....	81
3.2	Set up of the methane model.....	83
3.2.1	Source of atmospheric methane.....	83
3.2.1.1	Wetlands.....	83
3.2.1.2	Marine sources.....	86
3.2.1.3	Mud volcanoes.....	87
3.2.1.4	Volcanic emission.....	88
3.2.1.5	Gas hydrates.....	88
3.2.1.6	Insects.....	90
3.2.1.7	Methane release.....	90
3.2.2	Sinks of atmospheric Methane.....	91
3.2.2.1	Oxidation in the atmosphere.....	91
3.2.2.2	Oxidation within the soils.....	93
3.2.2.3	Loss of atmospheric methane.....	94
3.2.3	Budget of atmospheric methane.....	94
3.2.4	Isotope modeling.....	95
3.2.5	Climate effects of methane.....	96
3.3	Results and discussion.....	97
3.3.1	The Phanerozoic evolution of atmospheric methane.....	97
3.3.2	Effects of atmospheric methane on global average temperature.....	98
3.3.3	Methane oxidation in the Phanerozoic atmosphere.....	99
3.3.4	Gas hydrate dissociation.....	100
3.3.5	Feedbacks between methane and climate change.....	104
3.4	Conclusions.....	105
	References.....	107
	Appendix.....	112
4	Evolution of oxygen concentration in the deep ocean and marine nutrient inventories over the entire Phanerozoic	115
	Abstract.....	117
4.1	Introduction.....	118
4.2	Set up of the model.....	121
4.2.1	Surface water box.....	123
4.2.2	Deep water box.....	124
4.2.3	Benthic model.....	124
4.3	Results and discussion.....	125
4.3.1	Holocene oxygen and nutrients budget.....	125
4.3.2	Sensitivity tests.....	127
4.3.3	Phanerozoic evolution.....	134
4.3.4	Oceanic Anoxic Events (OAEs).....	137
4.4	Conclusions.....	139
	References.....	141
	Appendix.....	146
5	Conclusions	151
	 Outlook	 157

Chapter I

Introduction

Throughout the past decades the interests in global environmental and global change have increased, combined with the ongoing knowledge about Earth's forming processes. Since Earth was born its elements reside in permanent cycles, above and below Earth's surface. Almost all elements and compounds on Earth are involved in these cycles. Of course, the quality of the cycles varied prevalently in the past, and will vary in the future. But the character of the cycles stays more or less similar over time. In general, cycling elements are emitted from the mantle, and pass through reservoirs into the atmosphere, oceans and hydrosphere, as well as lithosphere for more or less time (Stanley, 1989) (Fig. 1.1). The appearances of reservoirs is strongly affected by the cyclicity of elements (Berner and Berner, 1996). The particular cycles are more or less interacting with each other (Fig. 1.1). Changes of the driving forces and different residence times of the elements in the reservoirs vary the behavior of the cycles and the appearances of the reservoirs. Hence, all elements are permanent in recycling processes due to exchange processes between exosphere and endosphere.

The main driving force for the physical and chemical changes on Earth is the tectonic activity, since without plate movement/plate tectonic no subduction, overthrusting, and no faulting would exist. Tectonic activity controls the roughness of the relief, the rate of subducting crust material into the mantle, and the recycling of the subducted matter by volcanoes at plate boundaries. Hence, the biogeochemical appearance of Earth is designed by the movement of its crust. Basically, Earth's elements and compounds are emitted from the mantle, through failures in the oceanic and continental crust. At oceanic spreading centers mantle plumes achieve the crust surface and compose the basaltic mid ocean ridges. On the other side of the moving plates the heavier plate is forced to subduct under the lighter crust. The subducting plate is heated up, and the released water, which ascent, lowers the melting point of the magma in the mantle. The ascending water rich magma penetrates the crust and creates at ocean-ocean-boundaries chains of andesitic volcanoes, whereas at ocean-continents-boundaries chains of andesitic-rhyolitic volcanoes arise. The collision of plates with equal weight arises in faulting of both crusts, accompanied by metamorphism of deeper layers. A special case of volcanism are intraplate volcanoes. Intraplate volcanoes are not bounded to plate boundaries, they occur on the oceanic crust as well as on the continental crust due to hot spots. Basically the basaltic material of the effusiva of intraplate volcanoes is different from the former mentioned volcanoes. Different rock types weather unequal, and different weathering processes - physical, chemical or biological weathering - result in different residuals and sediments.

As already hinted, the tectonic activity forms Earth's relief. The higher the relief intensity, the higher is the potential physico-biochemical erosion and denudation sensitivity, and the higher is the deposition rate. The eroded matter moves from heights to depressions for sedimentation, or is transported to the oceans. After transportation the eroded matter precipitates, if it is from dissolved origin, or sedimentates, if it is from particulate origin. Sediments become compacted by overlying matter, and pass through diagenesis or metamorphism to become eroded after exhumation and to re-enter transportation processes to the oceans. The runoff of continents rains down to the oceanic seafloor, where it is sedimentated or precipitated, to follow the subduction processes of the oceanic crust. The subducted matter passes through a number of transformation processes during its way

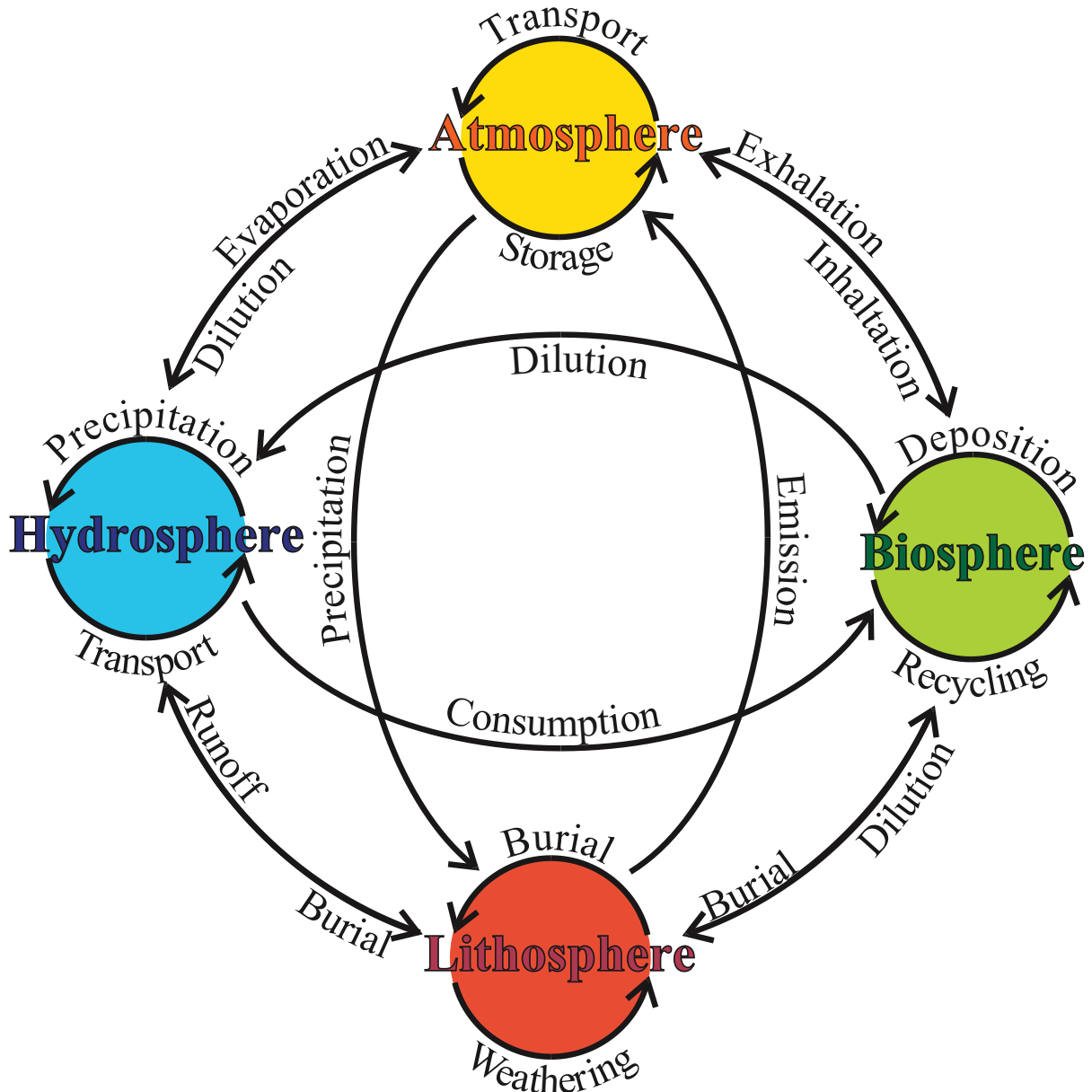


Figure 1.1: Schematic illustration of global element and compound (EC) cycles, and the cycle interactions, separated into the prevailing main environments.

The cycles are supported by gaseous, dissolved, or particulate ECs. The mantle emits ECs via eruption and forms the lithosphere. During weathering, erosion, and denudation the deposits are exhausted, and the released ECs are used up due to mineral forming, and repeatedly deposited into the lithosphere, - as soil minerals- in the upper rim of the lithosphere, or are consumed by the biosphere as nutrients. The unused weathered ECs from the lithosphere are transported via rivers or aeolian transport to fresh water lakes, or mainly to the oceans. The cycles of the biosphere and hydrosphere are strongly linked, since the supply of nutrients to the biosphere mainly occurs by aqueous solutions. The ECs in the biosphere reside in a permanent recycling process due to their consumption by consumer and destruent. Beside that the biosphere stores its ECs within long time storages, e.g. in swamps or other organic matter rich terrestrial and marine sediments. The biosphere exchanges its ECs via respiration with the atmosphere. The atmosphere acts as a short time store for ECs, since it is a good and fast transport environment. All kind of ECs which are released from the lithosphere and atmosphere, and the biosphere as well, reach the hydrosphere. After their precipitation on the seafloor they become a part of the lithosphere or reside dissolved in the water column to e.g. serve as a nutrient. Via evaporation the hydrosphere supplies the atmosphere with ECs, and due to precipitation processes the atmosphere returns ECs. The precipitated and sedimentated matter on the seafloor becomes buried, and later subducted or overthrust onto other crusts.

down into the mantle. In dependency on pressure-temperature conditions, the subducted matter is completely or partially released from its origin deposition place, or becomes remineralized, and at the end more or less melted. The melted matter ascends to the crust surface. After its emission via volcanoes the recycling is completed (Stanley, 1989).

Based on one of the fundamental assumptions of geology, that there are indefeasible laws of nature, not changing over time, so called uniformitarianism, it is possible to apply our knowledge about recent processes to interpret ancient corresponding processes. Hence, processes operating inside Earth and on Earth's surface follow principle geophysical and geochemical laws. This kind of actualism, such as transport, equilibrium constants, redox-reactions, precipitation and dissolution processes, chemical weathering, and stable isotopes have already been used to solve geochemical problems and enhanced our understanding of global natural fluxes and processes, with onward success in the past decades (Berner, 1980). Biogeochemical cycles of elements and compounds are generally portrayed in the form of box models. With ongoing knowledge about the processes computer-assisted models become more and more necessary.

1.1 Box models

A computer simulation or a computer model is a calculation program that attempts to simulate an abstract model of a particular system. Traditionally, the formal modeling of systems has been via a mathematical model, which attempts to find analytical solutions of problems, which enables the prediction of the behaviour of the system from a set of parameters and initial conditions. Box models combine overall processes in large environments in discrete boxes. These boxes attend to external inputs, e.g. from different boxes, to internal processes, and to element outputs, e.g. to different boxes (Fig. 1.2).

Biogeochemical box models describe processes of natural open systems. These equilibrium systems are controlled by the supply of elements and external limiting factors and lose their elements via output fluxes (Fig. 1.2). Several open systems are interlinked with each other. Due to the exchange of elements the prevailing systems may be buffered and stabilized. The boundaries of an open system are not distinct, the distribution of a modeled system depends on the demand of the problem, and the feasibility to solve the attended processes.

The geochemical processes presented here are calculated via two different computer programs. For model development I used ModelMaker 3.0.2 by Cherwell Scientific and Mathematica 5.2 by Wolfram Research to run numerical simulation of simple mathematical terms and differential equations, as well as mathematical formulations, which cannot be solved analytically. To solve the set of ordinary differential equations the 4th order Runge-Kutta method was used for modeling. Some of the driving forces of a model are not analytical definable, e.g. geological settings, if this information was preserved in the geological record it was used as external input. The model passed through multiple analyses within modification of adjustable parameters to produce model outputs,

which were comparable to geochemical proxy data. It was basically the aim to reproduce the well known processes of the pre-industrial Holocene or the natural processes of today.

The description and detailed explanation of the model approaches are given in the prevailing chapter (Chapter II – IV). Unmodified calculation approaches which are constructed by former authors are listed, for the sake of completeness, in the Appendix of the prevailing chapter.

A model calculation begins with an initial system, which represents the initial equilibrium state at the prevailing time with prevailing conditions. Arranged on the initial state in - and out - fluxes, environment conditions, and exchanges to other systems shift the initial equilibrium state into different phases. The following calculation steps portrayed the mathematical description of biogeochemical processes of ancient times. The end of a successful calculation is the reproduction of the biogeochemical condition of the pre-industrial Holocene, which is illustrated by representable elements or compounds.

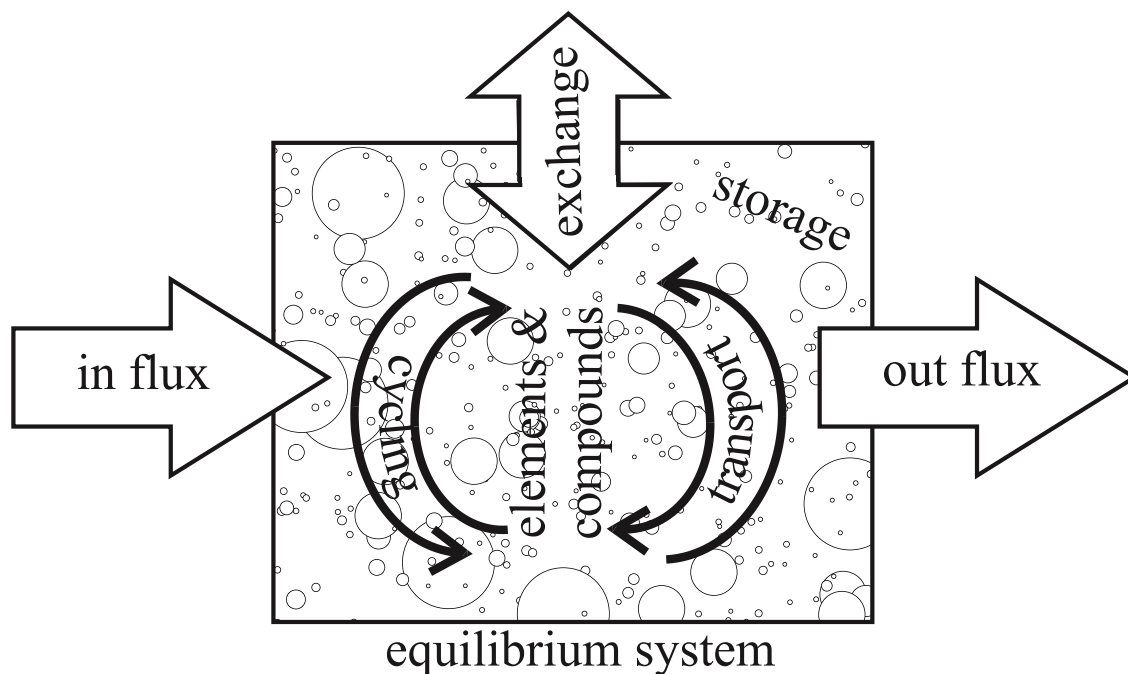


Figure 1.2: Schematic diagram of a reaction model.

Cycling elements and compounds in open systems are supplied via input fluxes, and removed via output fluxes, whereas the exchange with different equilibrium systems may buffer the present system.

1.2 Global biogeochemical cycles

All biogeochemical cycles - the movement of specie, in its many forms, between the biosphere, atmosphere, hydrosphere, and lithosphere (Fig. 1.1) - are affected by a countless number of constituent parts, which are interlinked to each other and which attend with different impact and

different residence times in the cycles. The transfer of elements and compounds between the boxes occurs via fluxes. Hence, a biogeochemical cycle is a circuit or pathway by which a chemical element or molecule moves through both biotic - *bio* - and abiotic - *geo* - compartments of Earth's system (Chester, 2000). All chemical elements occurring in organisms are part of biogeochemical cycles on short term processes. As already mentioned, this study is concerned to long term processes, but in addition to being a part of living organisms, these chemical elements also cycle through abiotic environments of ecosystems such as water (*hydrosphere*), sediments and rocks (*lithosphere*), and the air (*atmosphere*) during longer periods of time; the living factors of the planet can be referred to collectively as the biosphere (Fig. 1.1).

To keep the number of species and constituents parts for modeling on geological time scales manageable, it is essential to focus on the main parts without a falsification of the real character of the cycle. The present study focuses on the nutrients, phosphate, nitrate, sulphate, and carbon with their associated species, and further on oxygen and the greenhouse gas methane. The principle strategy for biogeochemical modeling is the reconstruction and compilation of the well known pre-industrial Holocene processes. After the pre-industrial Holocene was rebuild, the calculation for these processes were expanded to larger time frames, with respect to the changing quantity of the prevailing processes.

In the following section the principle character of the important biogeochemical cycles, such as the carbon cycle (Chapter 1.2.1) are described. In addition to the carbon cycle I described the methane cycle (Chapter 1.2.2), the phosphorus cycle (Chapter 1.2.3), the sulfur cycle (Chapter 1.2.4), the nitrogen cycle (Chapter 1.2.5), and the oxygen cycle (Chapter 1.2.6), auxiliary the biogeochemical relevant isotope cycles of carbon, strontium and sulfur were presented (Chapter 1.2.7). It was meant to decipher the functionality of several elements in the particular cycles, on a geological time scale, through the entire Phanerozoic. It should be denoted, that the present illustrated cycles (Chapter 1.2.1 - 1.2.7 & Fig. 1.3 - 1.8) are only simple overviews about long time processes, the natural short time cycles are more complex, and charged with processes which were negligible for the overall understanding.

1.2.1 Carbon cycle

All life is based on the element carbon, but carbon is also essential to the maintenance of climate and to the composition of atmosphere and oceans (Berner, 2004b). Carbon is stored on the surface (Fig. 1.3) - as organic acids and molecules in living and dead organisms, deposited in organic rich sediments and soils (*POM*); in the lithosphere as sedimentary rock e.g. deposited as limestone, dolomite, chalk and as calcium carbonate shells in marine organisms ($CaCO_3$); in the oceans as dissolved bicarbonate (HCO_3) as well as the gaseous carbon dioxide in the atmosphere (CO_2) - or it is lost at subduction zones (*M*). Furthermore, the atmospheric carbon dioxide concentration decreases during enhanced silicate weathering ($CaSiO_3$).

Carbon is released due to several processes (Fig. 1.3): weathering of organic matter (*POM*), burial of carbonate carbon (CaCO_3) and due to emission from the mantle (*M*). It is important to point out, that the global carbon cycle is splitted-up into two parts, the long term carbon cycle and the short term carbon cycle (Berner, 1999). The latter one occupies with carbon exchanges between different stores during short times, ranging between days and thousands of years. But with respect to the age of Earth and slower processes, the long term carbon cycle has got a higher outrank on geological time scales (Berner, 1982). Whereas the short term cycle “only” accounts to the exchange between plants, animals and soils, and vice versa, the long term cycle accounts to the transfer of carbon out of and into rocks. To consider processes during the entire Phanerozoic (570 Ma), solely the long term cycle was considered for this study.

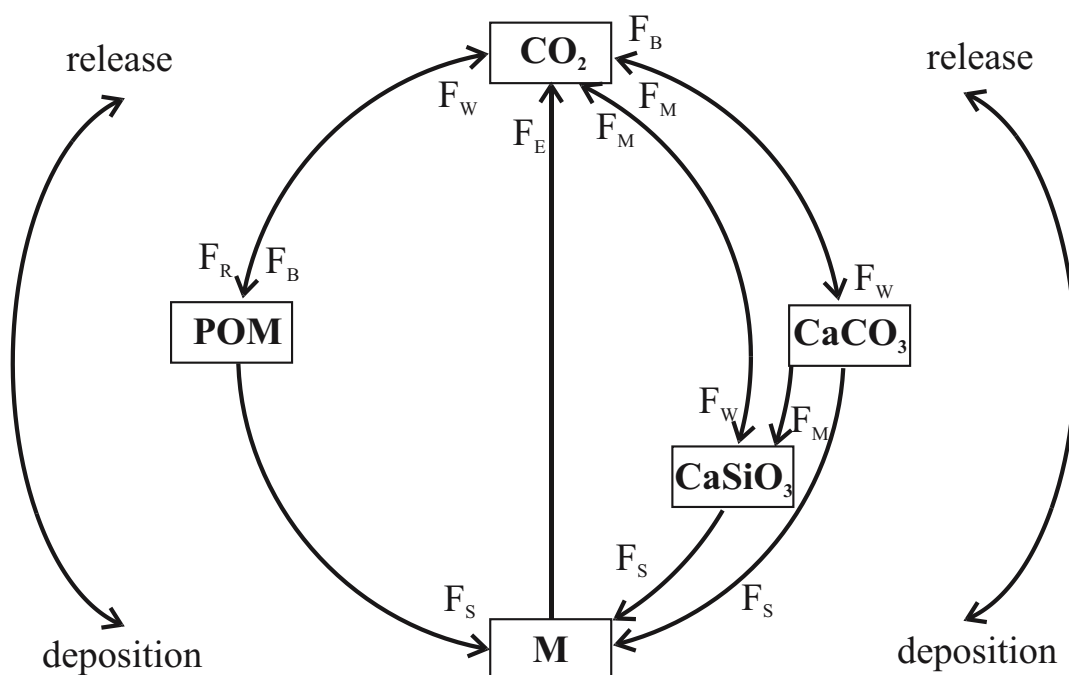


Figure 1.3: Schematic carbon cycle with carbon fluxes (arrows) and carbon storages (boxes).

CO_2 : carbon dioxide in atmosphere and oceans; CaCO_3 : inorganic carbon on the oceanic and continental crust; CaSiO_3 : silicate rocks; *M*: mantle carbon; *POM*: organic matter, on the oceanic and continental crust

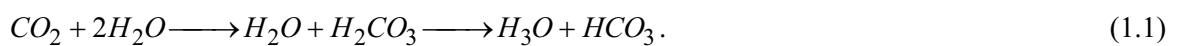
F_b : carbon burial flux; F_w : carbon weathering flux; F_m : carbon metamorphic flux; F_s : carbon subduction flux; F_r : carbon respiration flux; F_e : carbon emission flux; considered in the models.

The arrows represent the direction of carbon fluxes.

CO_2 : Over several hundreds of million years in the geologic history, the quantity of carbon dioxide found in the atmosphere and ocean has been steadily decreasing (Berner, 1990), due to enhanced silicate weathering. It was theorized that this natural long time change is in response to an increase in the sun’s output and the forced weathering over the same time period. During younger times - since the Middle Phanerozoic - the deposition (F_b) of particulate organic matter (*POM*) assists this decreasing process.

Weathering feedbacks helped to regulate Earth's temperature. An enhanced carbon dioxide sink occurs due to increasing of exposed silicate rock ($CaSiO_3$) weathering, induced due to enhanced weathering efficiency while high surface temperature. Atmospheric carbon dioxide is involved in atmospheric physics and chemistry. Atmospheric carbon dioxide let short solar wave radiation pass through the atmosphere almost completely, but reflects the backscattered long wave radiation from the Earth's surface, and heats up the atmosphere (Elrod, 1999). Due to this behavior - the so called greenhouse effect (Fourier, 1827) - atmospheric carbon dioxide affects the global climate significantly. Because an enhanced greenhouse effect, due to the greater concentration of carbon dioxide gas in the atmosphere, supplemented the production of heat energy through higher levels of long wave backscatter radiation (Elrod, 1999). As the sun shone more intense, several biological mechanisms gradually locked some of the atmospheric carbon dioxide into fossil fuels and sedimentary rocks. In summary, this regulating process has kept Earth's global average temperature more or less constant over the recent past.

Carbon dioxide enters the oceans simply by diffusion. Carbon dioxide reacts with water, and produces, via the interstage product carbonic acid (H_2CO_3), the acidic hydronium ion (H_3O) and hydrogen bicarbonate (HCO_3):



Increasing dissolution of gaseous carbon dioxide, originated from the atmosphere and biogenic respiration, decreases the seawater pH-value and intervene the chemical behavior of seawater.

POM: Ecosystems gain most of their carbon, in general as carbon dioxide, from the atmosphere (F_R). A number of autotrophic organisms have developed specialized mechanisms, allowing them the absorption of this gas into their cells. With the addition of water (H_2O) and energy ($h\nu$) from solar radiation, these organisms use photosynthesis to chemically convert the carbon dioxide to carbon-based sugar molecules ($C_6H_{12}O_6$), with the "by-product" oxygen (O_2). Some of the organic matter produced in plants is passed down to heterotrophic animals through consumption. The main part of this carbon cycle gets recycled on a very short time scale (short term cycle), but a remaining part gets deposited as particulate organic matter (*POM*) on continents and the seafloor (Degens et al., 1984) (F_B). The overall stoichiometry for the conversion of carbon dioxide (CO_2) into particulate organic matter can be summarized as:



whereas the burial of organic matter (F_R & F_B) is represented by the reaction from left to right, and the decomposition and weathering (F_W) of the organic carbon store from right to left. Due to weathering the stored carbon dioxide is released. The organic carbon stored on the seafloor enters the long time deposition in the mantle. Due to subduction (F_S) of deposited particulate organic matter (*POM*) and the following thermogenic breakdown, some of the carbon is released through failures

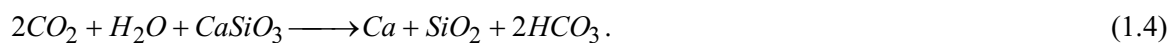
within the sedimentary cover and re-enters the seawater, the remaining part enters the mantle and gets remineralized due to melting.

$CaCO_3$: Carbon is also stored (F_B) in the lithosphere and soils in its inorganic forms. Certain forms of sea life biologically fix hydrogen bicarbonate (HCO_3) with calcium (Ca) to produce calcium carbonate ($CaCO_3$), the overall stoichiometry can be described as:



Calcium carbonate is used to produce shells and other body parts by organisms such as coral, mussel by exhalation of carbon dioxide (CO_2) and water (H_2O). When these organisms die, their shells and bodies, as well as dead or dying animals and plants, fecal matter, sand, soot and other inorganic dust sink to the ocean floor – so called marine snow - where they accumulate as carbonate-rich deposits. But most of the sinking $CaCO_3$, produced in the upper water column of the oceans, does not reach the seafloor sediments. Because of the undersaturation of $CaCO_3$ in greater depths sinking shells and comparable matter dissolve (Eq. 1.1 & 1.3). Weathering of calcium carbonate on the continents and on the ocean seafloor occurs under the same conditions (Eq. 1.1 & 1.3) (F_w). It is obvious from equation 1.3 that the overall net-effect calcium carbonate precipitation and weathering is negligible on geological time scales, with respect to the carbon dioxide concentration, but the indirect effect to different element cycles could be significant (Berner, 2004a). Ocean deposits are by far the biggest sinks of carbon on Earth. But with respect on long term cycles, the deposition of carbon within carbonates can be negligible, because due to weathering of carbonates carbon dioxide gets consumed, and due to precipitation it is released (MacKenzie and MacKenzie, 1995). On geological time scales the net carbon flux is within the carbonate carbon burial and weathering processes in balance.

$CaSiO_3$: In a real sense silicate rocks are not a carbon store, but due to its weathering great amounts of atmospheric carbon dioxide are consumed. Thus, silicate rocks are part of the carbon cycle. The weathering (F_w) process is enhanced by the formation of carbonic acid (Eq. 1.1). The overall stoichiometry for silicate weathering can be described as:



At the exosphere the silicate bounded carbon processes are one-way processes, meaning that silicates intervene the carbon cycle only during the consumption of atmospheric carbon dioxide due to weathering processes. In comparison to weathering and burial of carbonate rocks, the weathering of silicate rocks is the most important carbon sink in the exosphere (Walker et al., 1981). Furthermore this process acts as a negative feedback to atmospheric carbon dioxide. Higher atmospheric pCO_2 increases the global average temperature, higher temperature increases the silicate weathering, which lowers the atmospheric pCO_2 and the global average temperature.

M : In the common sense the mantle produces carbon dioxide (CO_2) via gaseous emission, but carbon compounds bounded are also bound to volcanic rocks in various ways, which are released due to weathering processes. This mantle derived carbon becomes recycled when carbon-rich sediments

and sedimentary rocks are subducted (F_s) and partially melted beneath tectonic boundary zones. Further this kind of decarbonisation occurs within processes during metamorphism and diagenesis (Skinner and Porter, 1992). The overall stoichiometry for decarbonisation processes can be described as:



In this way, volcanoes, especially volcanoes at plate boundaries, represent a recycling system of CO_2 (Eq. 1.5 from left to right).

Chapters II to IV are engaged with processes within the carbon cycle and their global interactions with other cycles over the entire Phanerozoic.

1.2.2 Methane cycle

In a broader sense the methane cycle (Fig. 1.4) is a component of the carbon cycle, but in a closer sense it is worth to survey natural methane separately, because of its own evolution and its significant impact on the global surface temperature as an associated driver to the greenhouse gas carbon dioxide (Crutzen, 1995).

However, methane (CH_4) is considered as one of the most important trace gases in the atmosphere because of its role as a greenhouse gas and as an aggressor in the chemistry of stratospheric ozone destruction, and water vapor and carbon dioxide producer (Crutzen, 1991; Crutzen, 1995). Methane today is the third important greenhouse gas, after carbon dioxide and water vapor, and it is the sink for the main atmospheric cleaning power, the hydroxyl radicals (OH). In that way it is weakening the global protection layer of stratospheric ozone (Bekki et al., 1994). In spite of the high global warming potential (GWP) of methane the effect on the atmosphere is negligible during low atmospheric methane level, but with increasing contents, methane intervenes. The methane cycle is restricted to anoxic environments for the production of methane (Belyaev et al., 1980), and to oxygen rich environments for its decomposition (Jacob, 2000), with exception to anaerobic methane oxidation (AMO) near the ocean floor sediments (Orphan et al., 2001; Valentine et al., 2001). However, methane is oxidized by dissolved oxygen and under presence of sulfate, thus methane can solely be released within anaerobic environments.

During pre-anthropogenic times methane was mainly produced within waterlogged soils - which e.g. occur in permafrost soils and in wetlands - in digestive tracts of herbivores - mammals and insects - and microorganisms in anoxic and sulfate depleted regimes (Wahlen, 1993) (POM_{land}). It is permanently produced by bacterial organic matter consumption on the ocean's seafloor (POM_{sea}). In general methane is produced due to the decomposition of "buried" organic matter, biologically, and thermogenic within subducted sediments, together with the by-product carbon dioxide (CO_2). A minor, more or less negligible, part of atmospheric methane is abiological produced due to the

emission from the mantle (M). Methane destruction is mainly placed in the atmosphere, only to a minor part within the soils (Jacob, 2000; Zhuang et al., 2004). However, the overall reaction of the breakdown of organic matter, in terrestrial soils, marine sediments, and digestive tracts, as well as the thermogenic processes can be simplified as (Berner and Berner, 1996):

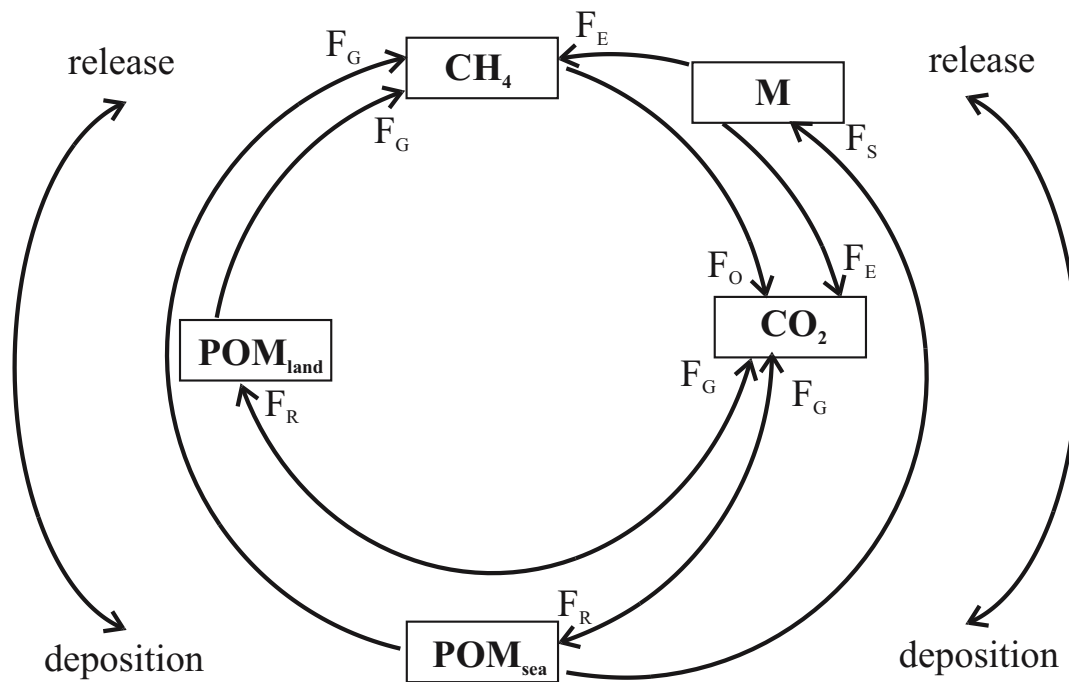


Figure 1.4: Schematic methane cycle with carbon/methane fluxes (arrows) and carbon/methane storages (boxes).

CH_4 : atmospheric methane; M : mantle methane and carbon; CO_2 : carbon dioxide in the atmosphere; POM : particulate organic matter.

F_E : carbon/methane emission flux; F_S : carbon subduction flux; F_O : methane oxidation flux; F_R : carbon respiration flux; F_G : methanogenic flux. The arrows represent the direction of fluxes.

CH_4 : The records of atmospheric methane concentration and ancient methane production are very sparse, there are only information about the last hundred of thousands years, recorded in polar ice sheets (Caillon et al., 2003). The “Vostock ice core” illustrates significant changes during the last two hundred thousand years, with remarkable heights 160 kyrs ago (Raynaud et al., 1993). The polar ice caps portrayed a significant increase in atmospheric methane concentration since the human activity in livestock breeding, agriculture, and fossil fuel burning rise (IPCC, 2001).

The main destruction of CH_4 reaching the atmosphere takes place in the modern troposphere (Seinfeld and Pandis, 1998), because more than 80 % (Sudo et al., submitted) of the cleaning power - which means primarily hydroxyl radicals (OH) (Jöckel et al., 2003) - of the atmosphere is housed in its lower 16 km (Budyko et al., 1987). A minor part of atmospheric CH_4 is consumed within the soils (1 - 10 %) (King and Schnell, 1994). Some of the reactants in the reaction chain of methane destruction are formed in the troposphere (Jacob, 2000), some others, e.g. O_3 - one of

the main agents in tropospheric chemistry (Wang et al., 1997) - move out of the stratosphere into the troposphere (Schultz et al., 1998). There are two types of triggers for the whole reaction chain of the CH_4 destruction/oxidization: One is the solar flux, which triggers the photolytic reaction, and the other ones are the radicals, which affect the chain reaction (Schmidt and Shindell, 2004). The reaction chain for the production of the oxidizing agents is very complex and is discussed in detail in Seinfeld and Pandis (1998). However the main oxidizing agents removing methane from the atmosphere are hydroxyl radicals produced in the mentioned chain reactions (Lelieveld et al., 2002). Due to the rapid recycling rate of hydroxyl radicals at moderate CH_4 levels, the oxidization processes do not significantly deplete the hydroxyl radicals (Lelieveld et al., 2002). However, at high CH_4 concentrations the cleaning power of the atmosphere decreases substantially (Schmidt and Shindell, 2003). Consequently, the atmosphere cleaning power adjusts to pollution when moderate CH_4 emissions prevail while CH_4 accumulates in the atmosphere during times of enhanced emission. In conclusion, atmospheric methane causes some changes in the atmosphere, increasing methane concentration lowers the surface protected ozone layer in the stratosphere, but produces due to decomposition toxic ozone within the troposphere. In the strict sense the decomposition of methane by hydroxyl radicals, can be described as:



The instable alkane CH_3O_2 is decomposed in the reaction chain, further, with a lot of following interstage products, such as carbon monoxide and carbon dioxide (Seinfeld and Pandis, 1998). At the end, due to methane destruction (F_o) a few other greenhouse gasses were produced, primarily carbon dioxide, ozone and water vapor, which affect the global surface temperature and atmospheric chemistry beyond methane's disappearances. The overall net stoichiometry can be described as:



whereas the gaseous toxic formaldehyde stays in the troposphere, and the gaseous toxic ozone is consumed by organisms on Earth's surface (IPCC, 2001). Hence, the effects of methane to the atmosphere can be divided into two groups, direct and indirect effects (Gassmann, 1994). The indirect part is more significant for the atmosphere and the processes on Earth's surface than the direct part. Due to the production of carbon dioxide with a longer atmospheric resistance time than methane, the depletion of hydroxyl radicals, as well as the production of agents of the acidic rain prevail the direct effect due to methane's global warming potential.

POM_{sea} : The oceanic methane cycle is a complex and intricate process, starting hundreds of meters beneath the ocean seafloor (Davie and Buffett, 2003). Organic sediments beneath the seafloor originated due to the deposition of sinking organic matter out of the upper water column, form the basis of the marine methane cycle, providing the catalyst hydrogen and carbon that are used as an energy source by a primitive life form, known as Archaea that in turn produces methane gas (Eq.

1.6). This process is called methanogenesis (F_G). Methane gas produced in a deeper sediment layer, ascent into shallower sediment regions and accumulates beneath the seafloor within the sediment pores. Much of it remains in gaseous form, but a significant amount enters into a gas hydrate state as the ambient temperature decreases and pressure increases. This hydrate state is generated when individual methane molecules form a bond with six water molecules and link together with other methane-water formations, crystallizing (Sloan, 1997). This methane gas hydrate form is extremely unstable, requiring only slight variations in temperature and pressure to trigger a gas discharge (F_G), larger sudden variations could initiate rapid gas releases, specified as clathrate gun hypothesis (Kennett et al., 2003). As fresh sediment is added to the seafloor, the prevailing pressure is gradually increased, and at a certain point the pressure and temperature increases to the critical point where the methane hydrate returns to the gaseous state (Wood et al., 2002) (F_G). An extremely small amount of this gaseous methane eventually escapes through failure in the seafloor known as cold seeps and enters the marine biosphere (Paull et al., 2002). The vast majority of this escaped methane is immediately consumed by a second species of Archaea that works in tandem with bacteria that reduces sulfate in the surrounding sediment into hydrogen sulfide (Orphan et al., 2001). This hydrogen sulfide is the primary food source of a number of life forms in the water column that cluster around these cold seeps much like the animals that receive their sustenance from their thermal counterparts. Anyway, it is under debate what triggers wide spread sudden gas release, and what does denote it to the atmosphere and biosphere (Dickens, 2001; Kennett et al., 2003; Kvenvolden, 2002; Paull et al., 2002; Schmidt and Shindell, 2003; Valentine et al., 2001). But it seems to be proofed, that such events occurred multiple times in the past. Sharp excursions of the $\delta^{13}\text{C}$ values in ancient seawater indicate a sudden release of great amounts of very light carbon (Beerling et al., 2002; Dickens, 2001; Hinrichs et al., 2003; Nisbet, 2002). Besides that the ocean floor also acts as a quiescent emitter, sediment passing methane gasses ascend through mud volcanoes or other zones of weakness and enter the water column where they gets consumed more or less completely (Mau et al., 2006; Orphan et al., 2001; Valentine et al., 2001) (F_G). However oceans emit methane, produced due to decomposing of organic matter in oxygen depleted water column and on the seafloor surface, and probably emitted methane via the release of gas out of long time storages (Kopf, 2003).

POM_{land} : The continental methane cycle is also associated to the production and decomposition of remained organic matter, as validated for the oceans (Eq. 1.6). Dead organic matter is deposited on the surface, or sinks through the water column of fresh water lakes onto the oxygen and sulfate depleted lake floor. An enhanced deposition of organic matter due to bacteria requires less oxygen environments, which mainly occur in wetlands, especially in swamps, and once in a while in deep fresh water lakes (Ehhalt, 1974). Natural wetlands are responsible for approximately 76 % of global permanent methane emissions from natural sources (IPCC, 2001) (F_G). Global emissions of insects, especially termites, account for approximately 11 % of the global methane emissions from natural sources (F_G). Methane is produced by termites as part of their normal digestive process, and the generated amount varies among different species (Crutzen, 1991). Furthermore, recent studies point out, that plants also release methane under oxygen conditions, the detailed processes are still

undeciphered, but it was detected, that the impact by living plants on the atmospheric methane cycle is significant (Keppler et al., 2006) (F_G).

M: The direct emission of methane out of volcanoes (F_E) is negligible since the first land plants has appeared in the Silurian, but it was thought that the release, permanently and explosive, has influenced the atmosphere evolution at the beginning of Earth's history (IPCC, 2001). Because of the devilish instability of methane gas hydrate, methane never passes complete through the subduction process, but the origin of natural methane, the organic matter (*POM*), gets partially subducted, on that way a few of the potential alkanes is lost in the subduction zones (F_S).

Chapter III is engaged with processes within the methane cycle, and its global interaction with other cycles, over the entire Phanerozoic.

1.2.3 Phosphorus cycle

Phosphorus can be found on Earth in water, soils and sediments, and any other environments. The phosphorus cycle (Fig. 1.5) intervenes into the carbon cycle and thus indirect on the global climate. Unlike the compounds of other matter cycles phosphorus cannot be found in the air as fine particulate compounds and not in the gaseous state. The main reservoir of more or less available phosphorus on Earth is the lithosphere. Dissolved phosphorus (PO_4) mainly cycles through water, soil and sediments, and bypasses the biosphere to a significant part. In the atmosphere phosphorus can mainly be found as very small dust particles, which mainly fertilize the continents and the oceans during dry deposition, e.g. ashes after a volcanic eruption (Duggen et al., submitted) and lesser as wet deposition, e.g. rain (Seinfeld and Pandis, 1998). Phosphorus moves slowly from deposits on land in sediments (Sed_{land}), to living organisms, and than much more slowly back into the soil and water within sediments. Phosphorus is most commonly found in rock formations (e.g. carbonate-fluoride-apatite (CFA)) and ocean sediments (Sed_{sea}) as phosphate salts or adsorbed onto iron, aluminum, and manganese oxides (Compton et al., 2000; Delaney, 1998) (*Rock*), and within the long time storage phosphorite (Berner and Berner, 1996). The phosphorus storage in the marine environment is more stable than the storage in terrestrial environments. Terrigenous phosphate dissolves comparably shortl after its precipitation, enters the biological cycle again or gets scoured out of the sediments, and move, via rivers and groundwater flow, in the oceans, where it gets consumed by organisms or precipitated on the seafloor. Over time, geologic processes can deliver ocean sediments to land, due to weathering and erosion, denudation will carry terrestrial phosphates back into the terrestrial cycle and than back into the ocean. Additionally the ocean phosphorus is recycled via subduction and emission via arc volcanism.

Phosphate salts, released from rocks (*Rock*) through weathering, usually dissolve in soil water. Plants absorb - consume - phosphates from the soil (PO_4). The plants may then be consumed by herbivores, which in turn may be consumed by carnivores. After death, the animal or plant decays, and phosphates is returned to the soil (*POM*). Because of the relative insolubility of phosphorus its

quantities in soils are generally small, hence it is often the limiting factor for plant growth (Berner and Berner, 1996). Phosphates are also limiting factors for plant-growth in marine ecosystems, because phosphates are not very water-soluble. However animals absorb phosphates by eating plants or plant-eating animals. The phosphorus cycle through plants and animals is much faster than it is through rocks (*Rock*) and sediments (*Sed*). When animals and plants die, phosphates will return to the soils or oceans, during organism decay. After that, phosphorus will end up in sediments or rock formations again, remaining there for millions of years. Eventually, phosphorus is released again

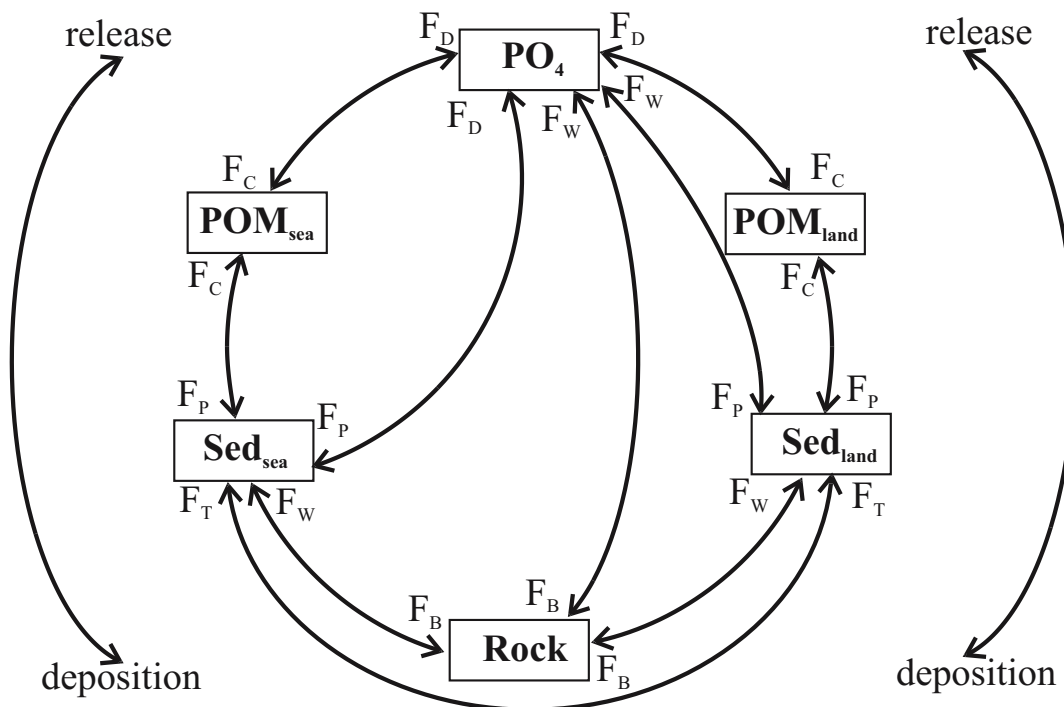


Figure 1.5: Schematic phosphorus cycle with phosphorus fluxes (arrows) and phosphorus storages (boxes).

PO₄: dissolved phosphate on continents and in the oceans; *Rock*: phosphorous bearing rocks, carbonate-fluoride-apatite (CFA), iron, aluminum and manganese oxides; *Sed*: phosphorous rich sediments on continental and oceanic crust, as dissolved phosphate in pore water, and reactive phosphate; *POM*: particulate organic matter.

F_w : phosphorus weathering flux; F_B : phosphorus burial flux; F_P : phosphorus sedimentation flux; F_C : phosphorus consumption flux; F_D : phosphorus decomposition flux; F_T : phosphorus transformation flux. The arrows represent the direction of fluxes.

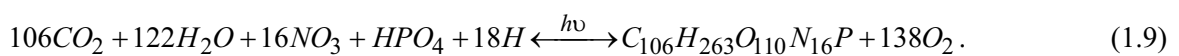
through weathering, and the cycle (Fig. 1.5) starts all over again.

PO₄: There are no records about ancient dissolved phosphorus inventories, neither for the oceans, nor for the continents. There are only nutrient model calculations via interpolation of organic matter burial (Bergman et al., 2004; Holland, 1978; Kershaw and Cundy, 2000). Recent measurements of ocean waters show an increase of dissolved phosphate in the water column from surface water to deeper regimes. The supply of dissolved phosphorus from continental rocks to the ocean mainly occurs due to riverine input (F_w), and to a smaller part by aeolian transport (Berner and Berner, 1996). The amount of dissolved phosphorus in the ocean is mainly controlled by the

effectiveness of the primary production. Thus the allocation of phosphate is strongly controlled by the development of the primary producers (F_c). Because of the fast consumption of phosphate in the upper water column in the oceans, dissolved phosphate is rare. But with increasing water depth the phosphate concentration increases, because of the decreasing consumption of dissolved species and the increasing decomposition (F_d) of sinking and of remaining particulate particles (Turekian, 1985). Thus, the amount of dissolved phosphate is controlled by the effectiveness of phosphate bounding organisms, and the rain ratio in the oceans. In general, the phosphorus cycle is strongly interlinked with the carbon cycle, since the growth of organic matter is limited by phosphorus and the supply of this nutrient is controlled by weathering of phosphorus bearing rocks. On that way phosphorus affects the carbon dioxide uptake and thus climate conditions.

Rock: Carbonate-fluoride-apatite ($\text{Ca}_5(\text{PO}_4)_3\text{F}$) (CFA) is an accumulation (F_B) of organic derived phosphorus in aquatic systems, mainly on marine sediments. In the next step, and under the absence of oxygen sulfur bacteria produce phosphorite (Berner, 1980), which are weathered (F_w) and reloaded into the phosphorus cycle after ocean-crust uplifting. CFA is the main phosphorus storage on a geological time scale (Delaney, 1998). CFA bounded to iron, aluminum, and manganese oxides on the ocean floor as well as at hydrothermal systems are also significant marine phosphorus storages. Oceanic upwelling systems supply shallow water systems with phosphate rich water, on the oxygen rich shelves phosphate bearing sediments are resulted, and found in the geological records as phosphorite.

POM: The organic bounded phosphorus (F_c) resides in a permanent recycling. Because of the fast recycling food chain, the short time bounded phosphorus resides in fast exchange between different organisms, until such time as dead particles descend out of the food chamber (F_p), e.g. to build CFA or other long time storages (Delaney, 1998) (F_r), or gets released by decomposing bacterial (F_d). Generally, organic matter is formed - in surface water and on land - by the processes of photosynthesis (Eq. 1.2). Therefore, equation 1.2 can be expand by the contribution of the main nutrients phosphate and nitrate:



Equation 1.9 illustrates the ratios between different nutrients in organisms, which is called the Redfield ratio. Redfield ratio or Redfield stoichiometry is the molecular ratio of carbon, nitrogen, phosphorus, etc. in phytoplankton. Redfield (1958) observed this relation within a large number of studies, and assume a systematic biogeochemical law. Today it seems to be proven, that these relations are prescribed rather by the offer of nutrients, than by a biogeochemical connection (Hall et al., 2005). However, organisms are a temporary storage for phosphate within the phosphorus cycle.

Chapter II and especially IV are engaged with processes within the phosphorus cycle, and its global interaction with other cycles, over the entire Phanerozoic.

1.2.4 Sulfur cycle

Sulfur is an important factor for life. But it also significantly affects the oxygen content of the atmosphere, and the character of aquatic systems. Besides that it also is an aggressor for carbonate weathering. Most of Earth's sulfur is tied up in rocks and salts or buried deep inside marine sediments. Besides that it can also be found in the atmosphere. The sulfur cycle (Fig. 1.6) contains processes in the lithosphere, biosphere, hydrosphere, and atmosphere and is an important part of the endogenous and exogenous cycles of matter. In oceans and evaporites sulfur occurs in its oxidized term as sulfate (SO_4), or as sulfur dioxide (SO_2). In magmatic and sedimentary rocks, hydrothermal solutions, and sulfur bearing gasses sulfur occurs in its reduced terms as carbonyl sulfide (OCS) and hydrogen sulfide (H_2S). Natural sources for instance occur as volcanic emission from the mantle (M), weathering of evaporite rocks (E) as well as of sedimentary pyrite (Sed) and decaying organisms (POM). Natural sinks occur due to bacterial precipitation processes, and evaporation from water. Due to weathering of sedimentary pyrite sulfur dioxide is released, under the usage of elemental sulfur and great amounts of oxygen, whereas due to sedimentary pyrite burial oxygen is released additionally.

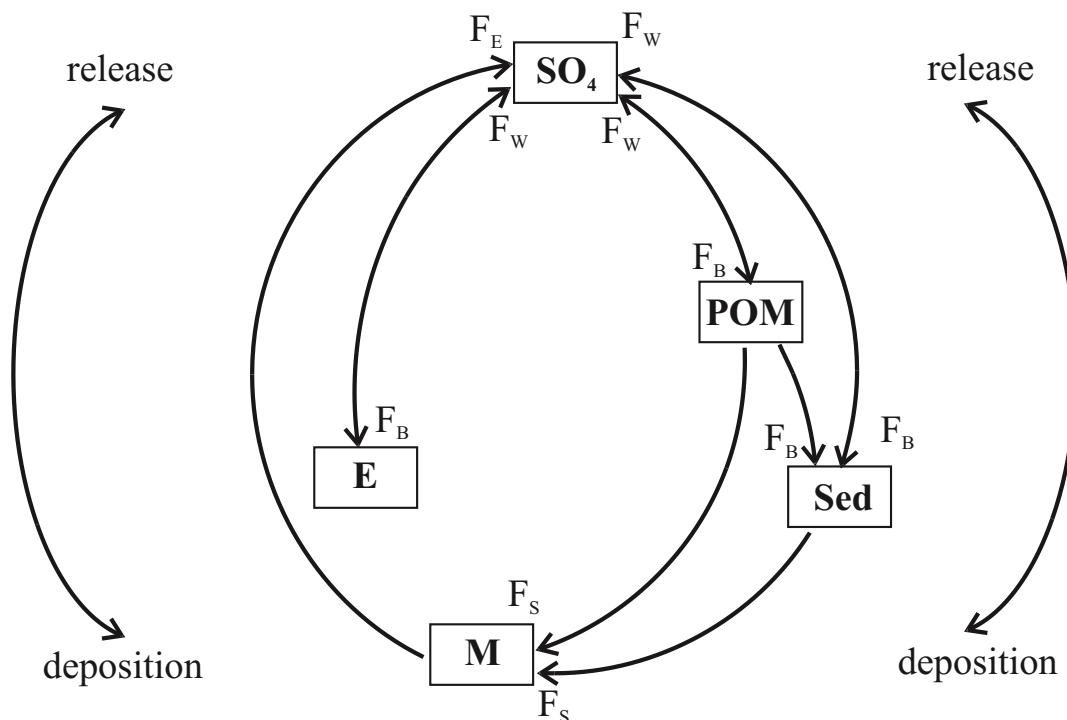


Figure 1.6: Schematic sulfur cycle with sulfur fluxes (arrows) and sulfur storages (boxes).

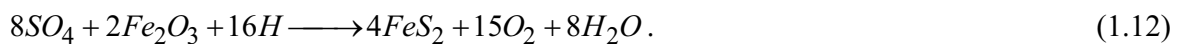
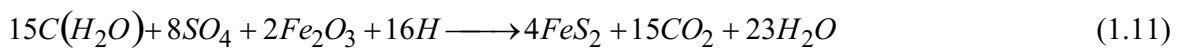
SO_4 : sulfate in the atmosphere and ocean; POM : particulate organic matter; Sed : sulfur rich sediments, especially sedimentary pyrite; M : mantle sulfur; E : sulfur rich evaporites.

F_W : sulfur weathering flux; F_B : sulfur burial flux; F_E : sulfur emission flux; F_S : sulfur subduction flux. The arrows represent the direction of fluxes.

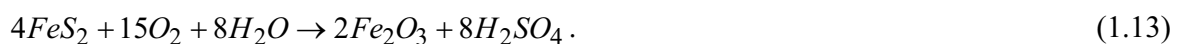
SO_4 : The records of ancient seawater sulfate concentration found in brine inclusions in evaporite rocks are well known. The composition of fluid inclusions in evaporite rocks portrayed two major long-term shifts in the chemistry of seawater during the Phanerozoic (Horita et al., 2002). The concentration of SO_4 has varied quite dramatically. The SO_4 concentrations may have been as low as a third to a fifth of the modern value during the Jurassic and Early Paleozoic. During the Permian and at the turn from the Vendian to the Cambrian the sulfate seawater concentration are as high as the modern value (Horita et al., 2002). Dramatically shifts in tectonic activity and biological evolution are possible causes for such significant changes.

Because of the continuous supply of sulfate to the oceans via runoff, the seawater is enriched in sulfate, but in environments, e.g. in the deep sea, with low water mixing rates anaerobe sulfate reducing bacteria decrease the sulfate concentration significantly.

Sed: The accumulation of sedimentary pyrite (F_b) is strongly coupled to the accumulation of organic matter (Bernier, 1980). In marine sediments on oceanic and continental crust sulfate reducing bacteria decompose organic matter (CH_2O) under anaerobic conditions and under usage of seawater sulfate (SO_4) and iron oxide (Fe_2O_3) into sedimentary pyrite (FeS_2), the overall reaction stoichiometry is:



The reaction stoichiometry portrayed an indirect oxygen release – originated by photosynthesis - due to anaerobic decomposition of organic matter, whereas during pyrite oxidation the process direct remove oxygen out of the environment:



The latter process intervenes significantly the ocean's chemistry, not only by the removal of great amounts of oxygen, it also lowers the pH-value due to the release of sulfuric acid (H_2SO_4) during weathering.

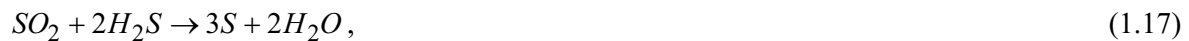
E: The evolution of evaporites deposition (F_b) is under debate (Gordon, 1975; Hay et al., sub), because of the evaporites' little resistance against erosion these deposits rapidly disappear. Already a long time ago Ochsenius (1877) proposed his theory about arid climate conditions and oceanic basins of sufficient water depth which continuously refresh their water due to a connection to a common ocean. The water of the temporarily insulated basin evaporates and is replenished by a temporarily or constant inflow of salt rich seawater. The concentrated surface layers sink to the basin floor, encountering layers differently composed, giving rise to the deposition of various compounds, mainly being sulfur within salt (e.g. $MgSO_4$), anhydrite ($CaSO_4$) and gypsum ($CaSO_4 \cdot 2H_2O$).

However, irrespective if such deep basins and the simple precipitation processes, as assumed, are comprehensible or not, evaporites are great storages of ancient sulfur and affects the ocean chemistry significant. Due to evaporation sulfur is removed out of the ocean for more or less time, whereas sulfur is returned to the ocean due to evaporite weathering (F_w).

M: The Earth's mantle emits sulfur throughout zones of weakness in the oceanic as well as continental crust (F_e). During subduction (F_s) ascending volatiles passes through the superimposed crust. Arc volcanoes release sulfur into the atmosphere (F_a) from subducted sediments, ocean crust, and mantle as sulfur dioxide (SO_2) and carbonyl sulfide (OCS) and hydrogen sulfide (H_2S) and exhaust oxygen to form sulfuric acid (Graf et al., 1997):



Elemental sulfur only occurs in company to several volcanisms, during the release of aquatic solutions due to the reaction of hydrogen sulfide and sulfur dioxide at volcanic fumaroles (Schmincke, 2004):



whereas mantle sulfur solely escapes as sulfur dioxide (SO_2) at intraplate volcanoes and spreading zones. The volcanic derived sulfur is released into atmosphere where it gets oxidized with oxygen and water to sulfuric acid (Eq. 1.14) (Halmer et al., 2002). This atmospheric sulfuric acid reaches the oceanic and continental surface by wet deposition, e.g. rain.

Chapter II is engaged with processes within the sulfur cycle, and its global interaction with other cycles, over the entire Phanerozoic.

1.2.5 Nitrogen cycle

Nitrogen is a part of vital organic compounds in microorganisms. Nitrogen in its gaseous form (N_2), makes up 78 % of the troposphere. Atmospheric nitrogen is the greatest nitrogen store, but in the gaseous form it cannot be absorbed and used as a nutrient by higher plants and animals; it must be converted first by nitrifying bacteria, so that it can enter the food chains as a part of the nitrogen cycle (Fig. 1.7). During the biological conversion of nitrogen - nitrogen fixation - cyan bacteria will first convert nitrogen (N_2) into ammonia (NH_3) and ammonium (NH_4). Abiological nitrogen is produced by photolysis due to lightning on the atmosphere. Plants can use ammonia as a source of nitrogen, but they prefer nitrate (NO_3), which is probably produced by nitrite - and nitrate, a processes, so called nitrification. In general ammonium is used during the primary production. Nitrate is bacterial reduced to ammonium, if ammonium is not available for the primary production. After the nutrients

are converted back into ammonia, anaerobic bacteria will convert them back into nitrogen gas, during a process called denitrification. Remaining matter (*POM*) from plants and animals on continents as well as in the oceans presents a short time storage of nitrogen, due to decomposition processes, such as denitrification, these storage were used as a nutrient supply. Small amounts of these nutrient deposits are preserved over longer times, e.g. deposits such as wetlands and swamps.

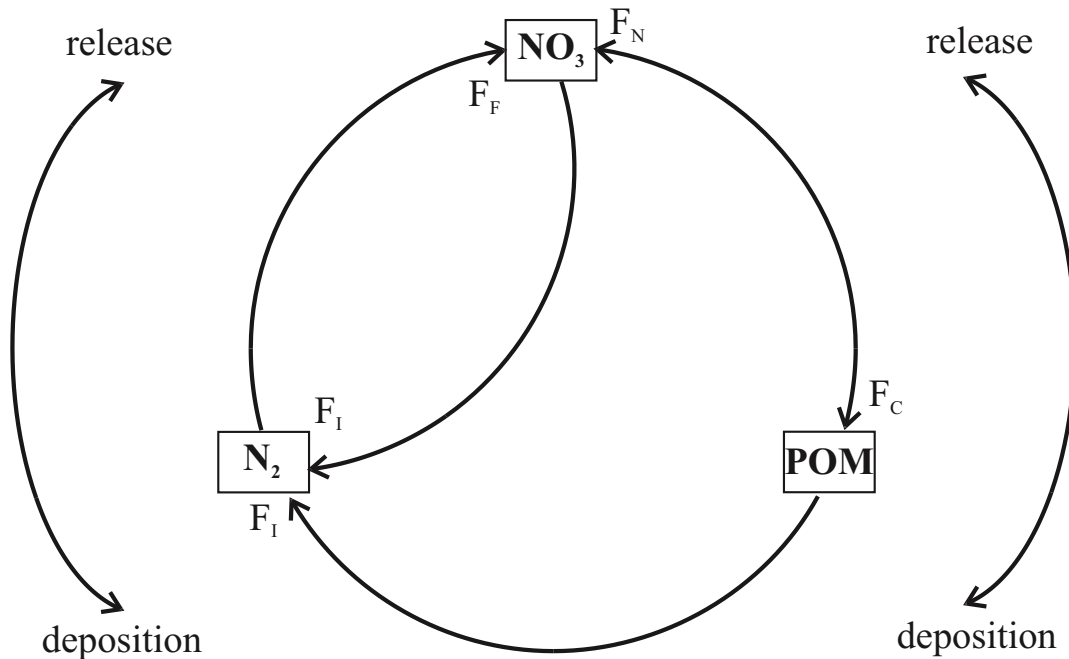


Figure 1.7: Schematic nitrogen cycle with nitrogen fluxes (arrows) and nitrogen storages (boxes).

NO_3 : nitrate in the oceans; *POM*: particulate organic matter; N_2 : atmospheric inert nitrogen.

F_I : nitrification flux; F_C : nitrate consumption flux; F_D : denitrification flux; F_F : nitrogen fixation flux. The arrows represent the direction of fluxes.

NO_3 : There are no comprehensible storages of nitrogen, which recorded information about ancient nitrogen inventory in the atmosphere or oceans. Also the recent nitrogen cycle is sparsely understood. However, after ammonium fixation, the ammonia and ammonium that is formed will be transferred further, during the nitrification process (F_F). Aerobic bacteria use oxygen to convert these compounds. Nitrosomonas bacteria will first convert nitrogen gas to nitrite (NO_2) and then nitrobacter will convert nitrite to nitrate (NO_3), a marine and terrestrial plant nutrient. The end member of nitrification takes place according to the following reactions:



N_2 : Elemental nitrogen (N_2) is a main part of the air, its atmospheric concentration stays more or less constant over long time scales (Budyko et al., 1987). A few numbers of microorganisms are able to convert the inert elemental nitrogen into plant available nitrate (NO_3), ammonia (NH_3),

and ammonium (NH_4). Generally, nitrogen fixation (F_F) is carried out according to the following reaction:



Furthermore nitrogen fixation occurs due to chemical reaction induced due to lightning in the atmosphere. This kind of nitrogen fixation produces nitric acid (HNO_3), which rains down in the oceans and on the continents. The overall stoichiometry can be described as:



POM: Plants absorb the converted ammonium and nitrate during the assimilation process (F_C), after which they are decomposed into nitrogen-containing organic molecules. Animals cannot absorb nitrates directly. They receive their nutrient supply by consuming plants or plant-consuming animals (F_C).

Nitrate is reduced by bacteria denitrification to elemental nitrogen (F_I). This inert nitrogen disappears out of the biochemical cycle. These bacteria use nitrate instead of oxygen for their respiration. The overall stoichiometry can be described as:



The nitrogen will then be released into the atmosphere again, this is the single process, which regenerate atmospheric nitrogen.

Chapter IV is engaged with processes within the nitrogen cycle, and its global interaction with other cycles, over the entire Phanerozoic.

1.2.6 Oxygen cycle

Oxygen is the most abundant element in the earth's crust, it accounts for 89 % of the mass of the ocean, and it is the second most abundant element, after nitrogen, of the mass of the Earth's atmosphere accounting for 21 % (Lenton and Watson, 2000). The oxygen cycle (Fig. 1.8) accounts for the movement of oxygen within and between its three main reservoirs: the atmosphere (O_2), the biosphere (*POM*), and the lithosphere (*Rock*) in the biogeochemical system. The oxygen cycle is strongly coupled to the cycles of carbon and water, because the oxygen transport mainly occurs within carbon dioxide, water, and organic matter. But oxygen also plays a significant part for several of elements within oxidation and reduction processes, e.g. during the alteration of the oceanic crust (Wallmann, 1999) (*M*), and it is controlled by these processes (Berner, 2004b).

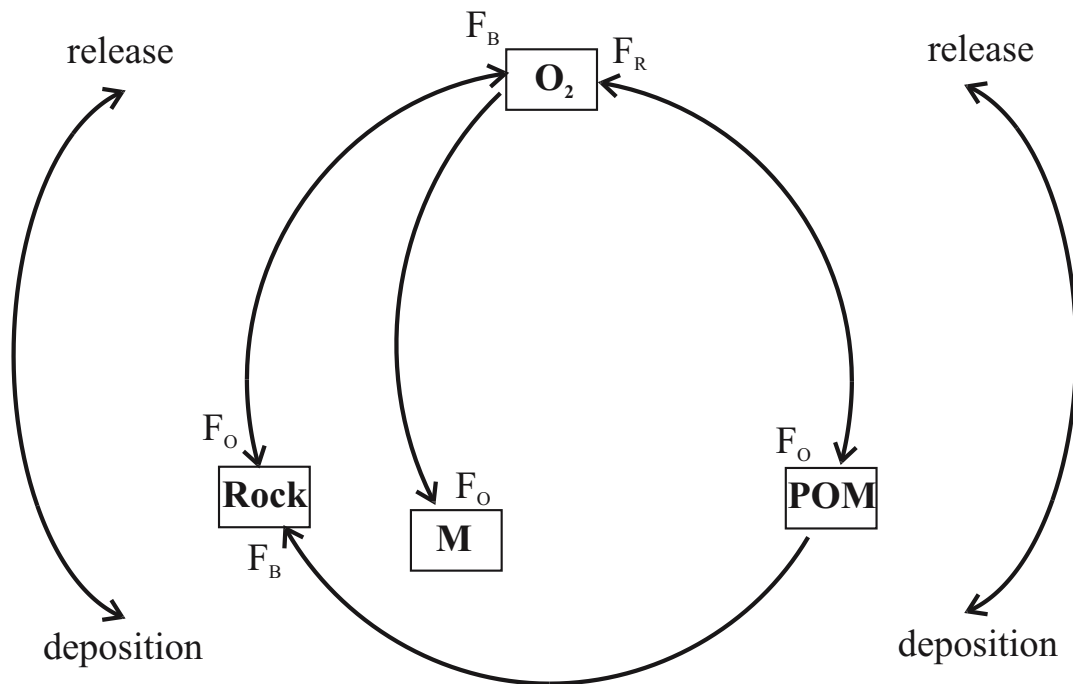


Figure 1.8: Schematic oxygen cycle with oxygen fluxes (arrows) and oxygen storages (boxes).

O_2 : atmospheric and seawater oxygen; Rock: organic carbon rocks; POM: particulate organic matter; M: mantle derived matter.

F_R : oxygen respiration flux; F_W : oxygen weathering flux; F_B : oxygen burial flux, F_O : oxidation flux. The arrows represent the direction of fluxes.

O_2 : The Phanerozoic atmospheric oxygen content faced dramatic changes during its evolution (Berner, 2001). Aquatic systems, oceans included, are in a permanent gas exchange with the atmosphere, thus their oxygen content is depending on the atmospheric oxygen content, but also on the ambient temperature, which controls the solubility of gaseous species in solutions (Broecker and Peng, 1982). At the beginning of the oxygen evolution the atmosphere was driven by oxidation and reduction processes on land as well as within the oceans, but later also by the biological processes inside the oceans. Due to the evolution and first appearance of land plants during the Silurian, the atmospheric oxygen concentration changed significantly, but stayed within a range between 17 and 35 % (Berner, 2001; Broecker and Peng, 1982). This range is prescribed by the occurrences of oxidation processes during the past 570 Ma. According to Watson et al. (1978) carbon matter requires an atmospheric oxygen content of 17 % to burn - to oxidize. The geological record shows the occurrences of charcoal for at least the past 570 Ma, thus the oxygen content must have been higher than the minimum level, which is required for carbon matter burning, whereas the upper level is given by the assumption that up to a specific atmospheric oxygen content (> 35 %) carbon matter would burn without a typical natural trigger (Wildman et al., 2004). However, since the Middle Paleozoic the atmospheric oxygen content is controlled by biogeochemical oxidation and reduction processes, and the respiration of the biosphere.

POM : The main source of oxygen within the biosphere and atmosphere is photosynthesis, which breaks down (F_R) carbon dioxide and water to create sugars and oxygen (Eq. 1.2). Due to the

decay of organic matter (F_p) atmospheric and seawater oxygen is consumed (Eq. 1.2).

Rock: Because lithosphere derived minerals are reduced in oxygen, surface weathering/oxidation of exposed rocks (F_o) also consumes oxygen (Eq. 1.13). Thus, oxygen is consumed during pyrite weathering (F_o), and released due to pyrite burial (F_b) (Berner, 1980). A further sink occurs due to weathering or alteration of iron-rich crust material, during the conversion from bivalent iron to trivalent iron (Wallmann, 1999).

M: The mantle emits elemental sulfur and mainly hydrogen sulfide (H_2S). Mantle derived sulfur is oxidized during the contact with the oxygen and hydroxyl radicals within the atmosphere, in this way decreasing the oxygen content of the atmosphere, and producing sulfate (SO_4), sulfur dioxide (SO_2), and sulfur acid (H_2SO_4):



Chapter II and IV is engaged with processes within the oxygen cycle, and its global interaction with other cycles, over the entire Phanerozoic.

1.2.7 Isotope cycles

Stable isotopes are atoms whose nuclei contain the same number (atomic number) of protons but a different number of neutrons (mass number). Hence isotopes are atoms of an element, which differ in numbers of neutrons of the atomic nucleus (Hoefs, 1997). Generally, every element on Earth has one or more isotopes. Thus an environment contains a mixture of the elements and their isotopes. Due to variations in chemical and physical forces during weathering, burial, transport, and precipitation processes the isotopes become fractionated and the isotope ratios are changed, the so called isotope effect. Thus the isotope ratios of an element in an environment allow the interpretation of the evolution of the element.

Generally, the results of the isotope analyses are given in isotope ratios (R_{sample}), presented in the relative difference ($\delta^m E$) to the standard value (R_{standard}) (Hoefs, 1997):

$$\delta^m E(\%) = \frac{R_{\text{sample}} - R_{\text{standard}}}{R_{\text{standard}}} * 1000. \quad (1.24)$$

Whereas the ratios of carbon and sulfur are used in the form:

$$R = \frac{^{13}C}{^{12}C}, \quad (1.25)$$

$$R = \frac{^{34}S}{^{32}S}. \quad (1.26)$$

However, the analyses of the strontium isotope are presented in the ratios of ^{87}Sr to ^{86}Sr .

As denoted in the former subchapters, stable isotope composition of the prevailing element cycles are also portrayed in box modeling. Stable isotope modeling has become an important part of biogeochemistry to solve fundamental problems of different geological topics. In the present study isotope ratios of carbon, sulfur, and strontium were used to decipher significances of different element and compound fluxes.

1.2.7.1 Carbon isotopes

Carbon isotopes, recorded in marine carbonates and shells, are mainly the references for the biological evolution and decipher the impact of biological productivity on seawater carbon inventory, e.g. organisms prefer the light carbon (^{12}C) variation instead of the heavier (^{13}C), thus the carbon inventory of the prevailing environment becomes heavier (Berner, 1982). Hence, environments - e.g. seawater - with heavier carbon inventory denote enhanced bioactivity.

A detailed portray of the carbon isotope cycle is given in Chapter II and III.

1.2.7.2 Sulfur isotopes

Sulfur isotopes, recorded in brine inclusions, mainly assist to differ the significance of precipitation by sulfate reducing bacteria and mantle derived sulfur on seawater sulfur inventory, e.g. the sulfur reducing bacteria remove light sulfur (^{32}S) out of seawater, whereas the volcanoes and hydrothermal systems release light sulfur isotopes to seawater (Berner, 1982). Hence, enhanced bacterial activity tends to heavier, whereas enhanced volcanic activity tends to lighter seawater sulfur inventory.

A detailed portray of the sulfur isotope cycle is given in Chapter II.

1.2.7.3 Strontium isotopes

Strontium isotopes, recorded in marine carbonates and shells, are mainly controlled by changing erosion activity on land and changing mantle degassing rates, thus strontium isotopes are used to decipher the changes in the dynamic of endogenic and exogenic processes, e.g. volcanoes tend to release more light strontium (^{86}Sr), whereas due to erosion of old rocks the river runoff to the ocean deliver more heavier strontium (^{87}Sr) (Veizer et al., 1999). Hence, light strontium ratios in seawater portrayed a significant impact by mantle degassing, whereas heavier strontium ratios in seawater indicate a significant impact due to erosion.

A detailed portray of the strontium isotope cycle is given in Chapter II.

1.2.8 Summary

All elements on Earth are permanently resided in biogeochemical cycles, they pass through biological and abiological processes and stay for more or less time in different storages. Different cycles are in contact with each other and exchange their elements and compounds continuously. Some elements shift from one cycle to another, in dependency to the compounds in which they are bounded. Changes in the character of one cycle could vary the character of different cycles. The isotope variations of the single cycles serve as information tool for the prevailing events and processes. The introduced six cycles intertwine into each other. They very well portray well the global biogeochemical conditions on a comprehensible way, and allow expanding the considered time span of their evolution.

*“Models of course, are never true
but fortunately it is only necessary
that they are useful”
(Box, G. E. P. 1979)*

References

- Beerling D. J., Lomas M. R., and Gröcke D. R. (2002) On the nature of methane gas-hydrates dissociation during the Torarcian and Aptian oceanic anoxic events. *American Journal of Science* **302**, 28 - 49.
- Bekki S., Law K. S., and Pyle J. A. (1994) Effect of ozone depletion on atmospheric CH₄ and CO concentrations. *Nature* **371**, 595 - 597.
- Belyaev S. S., Lein A. Y., and Ivanov M. V. (1980) Role of methane-producing and sulfate-reducing bacteria in the destruction of organic matter. In *Biogeochemistry of ancient and modern environments* (ed. P. A. Trudinger, M. R. Walter, and B. J. Ralph), pp. 235 - 242. Springer-Verlag.
- Bergman N. M., Lenton T. M., and Watson A. J. (2004) COPSE: a new model of biogeochemical cycling over Phanerozoic time. *American Journal of Science* **304**, 397 - 437.
- Berner E. K. and Berner R. A. (1996) *Global environment, water, air, and geochemical cycles*. Prentice - Hall, inc.
- Berner R. A. (1980) *Early diagenesis, a theoretical approach*. Princeton University Press.
- Berner R. A. (1982) Burial of organic carbon and pyrite sulfur in the modern ocean: its geochemical and environmental significance. *American Journal of Science* **282**, 451 - 473.
- Berner R. A. (1990) Atmospheric carbon dioxide levels over Phanerozoic time. *Science* **249**(1), 1382 - 1386.
- Berner R. A. (1999) A new look at the long-term carbon cycle. *GSA Today* **9**(11), 1 - 6.
- Berner R. A. (2001) Modeling atmospheric O₂ over Phanerozoic time. *Geochimica et Cosmochimica Acta* **65**(5), 685-694.
- Berner R. A. (2004a) A model for calcium, magnesium and sulfate in seawater over Phanerozoic time. *American Journal of Science*.
- Berner R. A. (2004b) *The Phanerozoic carbon cycle: CO₂ and O₂*.
- Broecker W. S. and Peng T.-H. (1982) *Tracers in the sea*. Eldigio Press.
- Budyko M. I., Ronov A. B., and Yanshin A. L. (1987) *History of the earth's atmosphere*. Springer-Verlag.
- Caillon N., Jouzel J., Severinghaus J. P., Chappellaz J., and Blunier T. (2003) A novel method to study the phase relationship between Antarctic and Greenland climate. *Geophysical Research Letters* **30**(17), 4,1 - 4,4.
- Chester R. (2000) *Marine Geochemistry*. Blackwell Science Ltd.
- Compton J., Mallinson D., Glenn C. R., Filipelli G., Föllmi K., Shields G., and Zanin Y. (2000) Variations in the global phosphorus cycle. *Marine Authogenesis: From Global to Microbial* **66**, 21 - 33.
- Crutzen P. J. (1991) Methane's sinks and sources. *Nature* **350**, 380 - 381.
- Crutzen P. J. (1995) My life with O₃, NO_x and other YZO_xs. *Nobel Lecture*, 189 - 242.

- Davie M. K. and Buffett B. A. (2003) Sources of methane for marine gas hydrate: inferences from a comparison of observations and numerical models. *Earth and Planetary Science Letters* **206**, 51 - 63.
- Degens E. T., Kempe S., and Spitzky A. (1984) Carbon dioxide: a biogeochemical portrait. In *The handbook of environmental chemistry*, Vol. 1, Part C (ed. O. Hutzinger), pp. 127 - 215. Springer-Verlag.
- Delaney M. L. (1998) Phosphorus accumulation in marine sediments and the oceanic phosphorus cycle. *Global Biogeochemical Cycles* **12**(4), 563 - 572.
- Dickens G. R. (2001) On the fate of past gas: What happens to methane released from bacterially mediated gas hydrate capacitor? *Geochemistry, Geophysics, Geosystem, an electronic journal of the Earth sciences* **2**.
- Duggen S., Croot P., Schacht U., and Hoffmann L. (submitted) High-speed ocean water fertilization with subduction zone volcanic ash and rapid phytoplankton response. *Science*.
- Ehhalt D. H. (1974) The atmospheric cycle of methane. *Tellus* **XXVI**(1 - 2), 58 - 70.
- Elrod M. J. (1999) Greenhouse Warming Potentials from the infrared spectroscopy of atmospheric gases. *Journal of Chemical Education* **76**(12), 1702 - 1705.
- Fourier J. J. B. (1827) Mémoire sur les températures du globe terrestre et des espaces planétaires. *Mémoires de l'Académie royale des sciences de l'Institut de France* **VII**, 97 - 125.
- Gassmann F. (1994) *Was ist los mit dem Treibhaus Erde?* Verlag der Fachvereine Zürich.
- Gordon W. A. (1975) Distribution by latitude of Phanerozoic evaporite deposits. *Journal of Geology* **83**(6), 671 - 684.
- Graf H. F., Feichter J., and Langmann B. (1997) Volcanic sulfur emissions: Estimates of source strength and its contribution to the global sulfate distribution. *Journal of Geophysical Research* **102**, 10727-10738.
- Hall S. R., Smith V. H., Lytle D. A., and Leibold M. A. (2005) Constraints on primary producer N:P stoichiometry along N:P supply ratio gradients. *Ecology* **86**(7), 1894 - 1904.
- Halmer M. M., Schmincke H.-U., and Graf H.-F. (2002) The annual volcanic gas input into the atmosphere, in particular into the stratosphere: a global data set for the past 100 years. *Journal of Volcanology and Geothermal Research* **115**, 511 - 528.
- Hay W. W., Migdisov A., Balukhovskiy A. N., Wold C. N., Floegel S., and Soeding E. (submitted) The decline in salinity of the ocean during the Phanerozoic: implications for climate, ocean circulation and life. *Marine Geology*.
- Hinrichs K. U., Hmelo L. R., and Sylva S. P. (2003) Molecular fossil record of elevated methane levels in late Pleistocene coastal waters. *Science* **299**, 1214 - 1217.
- Hoefs J. (1997) *Stable isotope geochemistry*. Springer-Verlag.
- Holland D. H. (1978) *The chemistry of the atmosphere and oceans*. John Wiley & sons, Inc.
- Horita J., Zimmermann H., and Holland H. D. (2002) Chemical evolution of seawater during the Phanerozoic: Implications from the record of marine evaporites. *Geochimica et Cosmochimica Acta* **66**(21), 3733 - 3756.

- IPCC. (2001) *Climate change 2001: The scientific basis*. Cambridge University Press.
- Jacob D. J. (2000) The oxidizing power of the atmosphere. In *Handbook for the weather, climate and water* (ed. T. Potter, B. Colman, J. Fishman, and M.-G. Hill).
- Jöckel P., Brenninkmeijer C. A. M., and Crutzen P. J. (2003) A discussion on the determination of atmospheric OH and its trends. *Atmospheric Chemistry and Physics Discussion* **3**, 107 - 118.
- Kennett J. P., Cannariato K. G., Hendy I. L., and Behl R. J. (2003) *Methane hydrates in quaternary climate change, the clathrate gun hypothesis*. American Geophysical Union.
- Keppeler F., Hamilton J. T. G., Brass M., and Roeckmann T. (2006) Methane emission from terrestrial plants under aerobic conditions. *Nature* **439**(12), 187 - 191.
- Kershaw S. and Cundy A. (2000) *Oceanography, an Earth science perspective*. Stanley Thornes.
- King G. M. and Schnell S. (1994) Effect of increasing atmospheric methane concentration on ammonium inhibition of soil methane consumption. *Nature* **370**, 282 - 284.
- Kopf A. J. (2003) Global methane emission through mud volcanoes and its past and present impact on the Earth's climate. *International Journal of Earth Science (Geologische Rundschau)* **92**, 806 - 816.
- Kvenvolden K. A. (2002) Methane hydrate in the global organic carbon cycle. *Terra Nova* **14**, 302 - 306.
- Lelieveld J., Peters W., Dentener F. J., and Krol M. C. (2002) Stability of tropospheric hydroxyl chemistry. *Journal of Geophysical Research* **107**(D23), 17,1 - 17,11.
- Lenton T. M. and Watson A. J. (2000) Redfield revisited, 2. What regulates the oxygen of the atmosphere? *Global Biogeochemical Cycles* **14**(1), 249 - 268.
- MacKenzie F. T. and MacKenzie J. A. (1995) *Our changing planet, An introduction to Earth system science and global environmental change*. Prentice Hall.
- Mau S., Sahling H., Rehder G., Suess E., and Soeding E. (2006) Estimates of methane output from mud extrusions at the erosive convergent margin off Costa Rica. *Marine Geology* **225**, 129 - 144.
- Nisbet E. G. (2002) Have sudden large release of methane from geological reservoirs occurred since the Last Glacial Maximum, and could such release occur again? *The Royal Society* **360**, 581 - 607.
- Ochsenius C. (1877) *Die Bildung der Steinsalzlager und ihre Mutterlaugensalze unter specieller Berücksichtigung der Flöze von Douglasshall in der Egelnschen Mulde*. C.E.M. Pfeffer.
- Orphan V. J., House C. H., Hinrichs K. U., McKeegan K. D., and DeLong E. F. (2001) Methane-consuming Archaea revealed by directly coupled isotopic and phylogenetic analysis. *Science* **293**, 484 - 487.
- Paull C. K., Brewer P. G., Ussler III W., Peltzer E. T., Rehder G., and Clague D. (2002) An experiment demonstrating that marine slumping is a mechanism to transfer methane from seafloor gas-hydrate deposits into the upper ocean and atmosphere. *Geo-Marine Letters*, 13.

- Raynaud D., Jouzel J., Barnola J. M., Chappellaz J., Delmas R. J., and Lorius C. (1993) The ice record of greenhouse gases. *Science* **259**, 926 - 934.
- Redfield A. C. (1958) The biological control of chemical factors in the environment. *American Scientist* **46**, 205 - 221.
- Schmidt G. A. and Shindell D. T. (2003) Atmospheric composition, radiative forcing, and climate change as a consequence of a massive methane release from gas hydrates. *Paleoceanography* **18**(1), 4,1 - 4,9.
- Schmidt G. A. and Shindell D. T. (2004) A note on the relationship between ice core methane concentration and insolation. *Geophysical Research Letters*.
- Schmincke H.-U. (2004) *Volcanism*. Springer-Verlag.
- Schultz M. G., Jacob D. J., Wang Y., Logan J. A., Atlas E., Blake D. R., Blake N. J., Bradshaw J. D., Browell E. V., Fenn M. A., Flocke F., Gregory G. L., Heikes B. G., Sachse G. W., Sandholm S. T., Shetter R. E., Singh H. B., and Talbot R. W. (1998) On the Origin of Tropospheric Ozone and NO_x over the Tropical South Pacific. *Journal of Geophysical Research*.
- Seinfeld J. H. and Pandis S. N. (1998) *Atmospheric chemistry and physics; from air pollution to climate change*. John Wiley & Sons, Inc.
- Skinner B. J. and Porter S. C. (1992) *The dynamic Earth, an introduction to physical geology*. John Wiley & Sons, Inc.
- Sloan E. D. (1997) *Clathrate hydrates of natural gases, second edition, revised and expanded*. Marcel Dekker, Inc.
- Stanley S. M. (1989) *Earth and life through time*. W.H. Freeman and Company.
- Sudo K., Takahashi M., and Akimoto H. (sub.) CHASER: A global chemical model of the troposphere, 2. Model results and evaluation. *Journal of Geophysical Research*.
- Turekian K. K. (1985) *Die Ozeane*. Ferdinand Enke Verlag.
- Valentine D. L., Blanton D. C., Reeborgh W. S., and Kastner M. (2001) Water column methane oxidation adjacent to an area of active hydrate dissociation, Eel River Basin. *Geochimica et Cosmochimica Acta* **65**(16), 2633 - 2640.
- Veizer J., Ala D., Azym K., Bruckschen P., Buhl D., Bruhn F., Carden G. A. F., Diener A., Ebner S., Godderies Y., Jasper T., Korte C., Pawellek F., Podleha O. G., and Strauss H. (1999) ⁸⁷Sr/⁸⁶Sr, ^δ¹³C and ^δ¹⁸O evolution of Phanerozoic seawater. *Chemical Geology* **161**, 59-88.
- Wahlen M. (1993) The global methane cycle. *Annual Reviews of Earth and Planetary Sciences* **21**, 407 - 426.
- Walker J. C. G., Hays P. B., and Kasting J. F. (1981) A negative feedback mechanism for the long-term stabilization of Earth's surface temperature. *Journal of Geophysical Research* **86**(C10), 9776 - 9782.
- Wallmann K. (1999) Die Rolle der Subduktionszonen im globalen Wasser- und Kohlenstoffkreislauf. Habilitation, Christian-Albrechts-Universität.
- Wang C., Prinn R. G., and Sokolov A. P. (1997) A global interactive chemistry and climate model. *Journal of Geophysical Research*.

- Watson A. J., Lovelock J. E., and Margulis L. (1978) Methanogenesis, fires, and the regulation of atmospheric oxygen. *Biosystems* **10**, 293-298.
- Wildman J. R. A., Hickey L. J., Dickinson M. B., Berner R. A., Robinson J. M., Dietrich M., Essenhight R. H., and Wildman C. B. (2004) Burning of forest materials under late Paleozoic high atmospheric oxygen levels. *Geological Society of America* **32**(5), 457 - 460.
- Wood W. T., Gettrust J. F., Chapman N. R., Spence G. D., and Hyndman R. D. (2002) Decreased stability of methane hydrates in marine sediments owing to phase-boundary roughness. *Nature* **420**, 656 - 660.
- Zhuang Q., Melillo J. M., Kicklighter D. W., Prinn R. G., McGuire A. D., Steudler P. A., Felzer B. S., and Hu S. (2004) Methane fluxes between terrestrial ecosystems and the atmosphere at northern high latitudes during the past century: A retrospective analysis with a process-based biogeochemistry model. *Global Biogeochemical Cycles* **18**, 23.

CHAPTER II

**Modeling the chemical evolution of seawater
(S, P, C, Sr, O) over the entire Phanerozoic**

Abstract

A numerical model has been developed considering global coupled biogeochemical cycles over the entire Phanerozoic (570 Ma). It reflects the evolution of the participating biotic and abiotic constituents in marine and terrestrial environments. The model is driven by geological and evolutionary forcings, and controlled by proxy data. The standard run of the model calculates the Phanerozoic evolution of seawater (dissolved inorganic carbon, alkalinity, phosphate), its sulfur and carbon isotope composition, as well as the partial pressures of oxygen and carbon dioxide in the atmosphere. It successfully reproduces independent proxy data recorded in marine carbonates ($\delta^{13}\text{C}$) and evaporite rocks ($\delta^{34}\text{S}$) and confirms the Phanerozoic evolution of atmospheric composition as constrained by previous models and proxy data. The model shows that both the phosphate content and the productivity of the ocean have increased continuously over the Phanerozoic. This trend is neither observed in the burial of organic carbon nor in the marine $\delta^{13}\text{C}$ record showing that these parameters do not reliably reflect the ocean's changing productivity. The model uses sulfate concentrations in seawater, derived from fluid inclusion data, to calculate the net burial flux of evaporites (burial - weathering) over the entire Phanerozoic. This new estimate indicates high net burial during warm periods and net weathering during cold periods and thus confirms that the deposition of evaporites is mainly controlled by the prevailing climatic conditions. Seawater $^{87}\text{Sr}/^{86}\text{Sr}$ ratios recorded in marine carbonates are applied to derive rates of tectonic/volcanic activity over the entire Phanerozoic. This new record shows little correlation with the global sea-level curve and confirms that sea level is a poor proxy for changes in spreading and subduction rates. Sensitivity tests showed that both volcanic and sedimentary processes determine the marine $\delta^{34}\text{S}$ record while previous models often assumed that the evolution of seawater $\delta^{34}\text{S}$ values only reflect the sedimentary cycling of sulfur.

2.1 Introduction

Box models simulating the global cycling of elements consider the transport and turnover of these elements and their stable isotopic composition to enhance our understanding of global natural fluxes and processes. Long term variations in the ocean's water chemistry are recorded as isotope composition changes of carbon, strontium, and sulfur in ancient sedimentary minerals (Hayes et al., 1999; Horita et al., 2002; Steuber and Veizer, 2003; Strauss, 1999; Veizer et al., 1999). The strontium isotope composition ($^{87}\text{Sr}/^{86}\text{Sr}$) of ancient seawater, archived in marine shells and carbonate rocks, is affected by the strontium input from rivers and hydrothermal systems (Veizer et al., 1999). The strontium isotopic trend reflects the evolution of physical properties, like the tectonic evolution - in particular volcanism - and erosion on land. The isotope composition of carbon ($\delta^{13}\text{C}_{\text{CaCO}_3}$) is affected by the partial pressure of carbon dioxide and oxygen ($p\text{CO}_2$, $p\text{O}_2$), the paleobioproductivity and accumulation of organic matter and carbonates on land as well as in the oceans (Berner, 2004b). Last but not least the sulfur isotope ($\delta^{34}\text{S}_{\text{SO}_4}$) composition of seawater is also affected by the

paleobioproductivity as well as by tectonic activity and evaporization (Berner, 2004a).

Proxy data of carbon in pedogenic terrestrial and marine carbonates indicate that the partial pressure of atmospheric CO₂ (pCO₂) has varied over the Phanerozoic (Royer et al., 2001). Geochemical box models reconstruct the fluctuation of pCO₂ due to time-dependent parameterizations of weathering and burial of organic and carbonate carbon as well as mantle degassing (Berner, 1991; Berner, 1994; Berner and Kothavala, 2001; Hansen and Wallmann, 2003; Manabe and Wetherald, 1975; Rothman, 2002; Wallmann, 2001; Wallmann, 2004). However, proxy data of carbon isotopes ($\delta^{13}\text{C}$) indicate the significance of the particular carbon fluxes (Berner, 1991; Berner, 1994; Berner and Kothavala, 2001; Peters-Kottig et al., 2003; Veizer et al., 1999; Veizer et al., 2000).

Proxy data of brine inclusions demonstrate the Phanerozoic evolution of seawater concentrations of e.g. sulphate, magnesium, and calcium (Hardie, 1996; Horita et al., 2002; Lowenstein et al., 2001; Strauss, 1999). Geochemical box models reconstruct ancient seawater sulfur concentrations due to time-dependent parameterizations of weathering and burial of marine evaporites, sedimentary pyrite, organic and carbonate carbon as well as mantle degassing (Bergman et al., 2004; Berner, 1982; Berner, 1987; Berner, 1999; Compton et al., 2000; Hansen and Wallmann, 2003; Lasaga and Ohmoto, 2002; Lenton and Watson, 2000a; Lenton and Watson, 2000b; Wallmann, 2003).

In this chapter I present a geochemical box model for the entire Phanerozoic to investigate the effects of geochemical processes on secular C-, Sr-, and S isotope composition changes and the linkage of O₂, CO₂, PO₄ and SO₄ cycles in the past. When possible I followed former models by Bergman et al. (2004), Berner and Kothavala (2001), Hansen and Wallmann (2003), Wallmann (2001), and Wallmann (2004) in order to apply or expand their compilations, or to replace them with new approaches, and to permit a comparison with previous models. By applying a new numerical model, one of my goals was to calculate the Phanerozoic $\delta^{13}\text{C}_{\text{CaCO}_3}$ - and $\delta^{34}\text{S}_{\text{SO}_4}$ concentrations in ancient oceans to compare them with proxy data recorded in marine carbonate shells (Hayes et al., 1999), as well as in marine evaporites (Strauss, 1999). Isotope ratios of marine carbonates are used to reconstruct secular time-dependent isotope fractionation processes during carbon burial. By using isotope ratios of strontium in the model, I derive an expression of the tectonic activity, in particular the volcanic degassing rate on land, at ocean margins as well as on the seafloor. Furthermore, I calculated the long-term changes of the atmospheric partial pressure of carbon dioxide and oxygen. By predicting the sulfur concentration of seawater I reconstructed the evolution of marine evaporites during the entire Phanerozoic. The model is enhanced by new parameterization of organic matter and sedimentary pyrite burial due to phosphorus net burial fluxes.

2.2 Set up of the box model

Based on previous geochemical box models (GEOCARB I - III, Berner (1991), Berner (1994), Berner and Kothavala (2001)), as well as the carbon and sulfur models of Wallmann (2001),

Wallmann (2004) and Hansen and Wallmann (2003) a new model approach has been developed to present the evolution of pO_2 and pCO_2 in the atmosphere and the isotope composition of seawater during the entire Phanerozoic.

The model consists of three boxes - atmosphere, ocean, and continents -, which again were cut, into five submodels of sulfur, phosphorus, carbon, strontium, and oxygen (Tab. 2.1). These submodels consist of 15 species generated by 38 processes (Appendix A2.1 - A2.3). Via these species the submodels as well as the boxes were interlinked and controlled by each other.

For model development I used ModelMaker 3.0.2 from Cherwell Scientific. To solve the set of ordinary differential equations I used the 4th order Runge-Kutta method, and calculated with a time step of one million years.

Below I describe the principle set up of the five submodels, the changes as well as the improvements. The complete set of the model equations and parameter are summarized in Table 2.1 - 2.3, and Appendix A2.1 - A2.3. The detailed description of the model can be found in Hansen and Wallmann (2003), Wallmann (2001) and Wallmann (2004).

Table 2.1: Model reservoirs of carbon, strontium, oxygen, phosphorus, and sulfur masses and the initial values at 570 Ma, (strontium and ^{87}Sr masses in 10^{16} mol, all other elements in 10^{18} mol).

Reservoir	Equation	Initial value
CO ₂ in atmosphere	$\frac{dCO_2}{dt} = F_{EX}$	0.378
Carbonate alkalinity in seawater	$\frac{dCA}{dt} = F_{WS} + 2 * F_{WC} - 2 * F_{BC} - F_{ALT}$	3.562
Total dissolved inorganic carbon in seawater	$\frac{dTC}{dt} = F_M + F_{MC} + F_{SC} + F_{WO} + F_{WC} - F_{BC} - F_{ALT} - F_{BO} - F_{EX}$	3.562
Carbon in the mantle	$\frac{dM}{dt} = F_{SM} + F_{SZO} - F_{EO} - F_M$	5000
CaCO ₃ on continental crust	$\frac{dCC}{dt} = F_{BCC} - F_{MC} - F_{WC}$	5250
CaCO ₃ on oceanic crust	$\frac{dCO}{dt} = F_{BCO} + F_{ALT} - F_{SM} - F_{SC}$	1200
Total dissolved inorganic ^{13}C in seawater	$\frac{d^{13}TC}{dt} = \Phi_M^{13} * F_M + \Phi_{Cin}^{13} * (F_{MC} + F_{SC} + F_{WC}) + \Phi_{POCin}^{13} * F_{WO} - \Phi_C^{13} * (F_{BC} + F_{ALT} + F_{EX}) - \Phi_{POCout}^{13} * F_{BO}$	-3
POC in sediment	$\frac{dPOC}{dt} = F_{BO} - F_{WO} - F_{SZO}$	1000
O ₂ amount in seawater and atmosphere	$\frac{dO}{dt} = F_{BO} + O_{BP} - O_{WP} - O_{SZ} - O_{IP} - F_{WO} - O_{Fe}$	30.8
Pyrite in sediments	$\frac{dP}{dt} = F_{BP} - F_{WP} - F_{SZP}$	79.2
SO ₄ in seawater	$\frac{dSO_4}{dt} = F_{WP} + F_E - netF_{BE} - F_{BP}$	30
$^{34}SO_4$ in seawater	$\frac{d^{34}SO_4}{dt} = \Phi_{WP}^{34} * F_{WP} + \Phi_{EM}^{34} * F_E - \Phi_{BE}^{34} * netF_{BE} - \Phi_{BP}^{34} * F_{BP}$	1.328
PO ₄ in seawater	$\frac{dPO_4}{dt} = F_W^{PO_4} - F_{Bland}^{PO_4} - F_{Bsea}^{PO_4} - F_{Hy}^{PO_4} - F_{BFe}^{PO_4} - F_{BCa}^{PO_4}$	0.0025
Sr in seawater	$\frac{dSr}{dt} = F_{HY}^{Sr} + F_{WS}^{Sr} + F_{WC}^{Sr} - F_B^{Sr}$	12.33
^{87}Sr in seawater	$\frac{d^{87}Sr}{dt} = \Phi_{HY}^{87} * F_{HY}^{Sr} + F_{WS}^{87Sr} + \Phi_{WC}^{87} * F_{WC}^{Sr} - \Phi_{SW}^{87} * F_B^{Sr}$	0.862

Table 2.2: Forcings of carbon, strontium, oxygen, phosphorus, and sulfur fluxes applied to the box model.

Parameter	Forced modeled processes	References	Phanerozoic range of values
Γ	Constant relating pCO ₂ and surface temperature	Berner (1987)	3.3 (Paleozoic) to 4 (Carboniferous & Cenozoic)
f_{LA}	Area of exposed carbonates (normalized on recent value)	Berner (1994)	0.5 (Cambrian) to 1.3 (Triassic)
$f_{ER}f_{coal}$	Coal distribution (normalized on recent value)	Berner (2004) and Berner and Kothavala (2001)	0 (Paleozoic) to 5 (Carboniferous)
r_M	Fraction of total POC buried in marine sediments	Berner and Kothavala (2001)	0.73 (Carboniferous) to 1 (Cambrian)
f_{BCC}	Fraction of CaCO ₃ depositing on continental crust	Hay (1998)	1 (Pre-Cenozoic) to 0.09 (present)
$\delta^{13}C_{POC}$	$\delta^{13}C$ fraction during POC burial (‰)	Hayes et al. (1999)	-30.3 (Cretaceous) to 22 (present)
$\delta^{13}C_{CaCO_3}$	$\delta^{13}C$ in CaCO ₃ subject to weathering and subduction (‰)	Hayes et al. (1999)	2.8 (Cambrian) to 3.9 (Carboniferous)
$\delta^{13}C_{POCin}$	$\delta^{13}C$ in POC subject to weathering and subduction (‰)	Hayes et al. (1999)	-3 (Cambrian) to 4.4 (Carboniferous)
cCaSW	Calcium concentration in seawater (mmol l ⁻¹)	Horita et al. (2002)	0.01 (present) to 0.03 (Silurian)
ΔT	Difference between surface temperature and water temperature at the calcite saturation depth	Wallmann (2004)	5 (Paleozoic) to 10 Permo-Carboniferous)
P_L	Pressure at the calcite saturation depth	Wallmann (2004)	50 (Paleozoic) to 200 Permo-Carboniferous)
cSO ₄ SW	SO ₄ concentration in seawater (mmol l ⁻¹)	Horita et al. (2002)	0.0081 (Silurian) to 0.029 (present)
$\delta^{34}S_{SO_4}$	$\delta^{34}S$ of marine sulfate (‰)	Strauss (1999)	10.95 (Permo-Carboniferous) to 30.32 (Cambrian)
R_{Ca}^{Sr}	Ratio of Sr and Ca in seawater	Steuber and Veizer (2003)	5 (Carboniferous) to 13 (Silurian)
$R^{87}CaCO_3$	Ratio of Sr isotopes in marine carbonates	Steuber and Veizer (2003)	0.707 (Cretaceous) to 0.709 (Cambrian)
R_{SW}^{87}	Ratio of Sr isotopes in seawater	Steuber and Veizer (2003)	0.707 (Jurassic) to 0.709 (Cambrian)
R_{Hy}^{87}	Isotope ratio in Sr released during the weathering of non-volcanic silicate rocks	Wallmann (2001)	0.716 (Pre-Paleocene) to 0.718 (Paleocene)
f_{AN}	Evolution of land plants	Berner (1994)	0.15 (Cambrian) to 1 (present)
GEOG	Effect of paleogeography on albedo and surface temperature (normalized on recent value)	Berner and Kothavala (2001)	0.07 (present) to 1.35 (Silurian)
f_{ER}	Physical erosion efficiency (normalized on recent value)	Berner and Kothavala (2001)	0.04 (Cambrian) to 1 (present)
RUN	Impact of temperature on runoff	Berner (2004)	0.025 to 0.045 (Carboniferous & Cenozoic)
f_A	Changes in total ice-free land area (normalized on recent value)	Gibbs et al. (1999)	0.59 (Ordovician) to 1 (present)
f_D	Continental discharge (normalized on recent value)	Gibbs et al. (1999)	0.9 (Carboniferous) to 1.6 (Ordovician)

Table 2.3: Parameter of carbon, strontium, oxygen, phosphorus, and sulfur fluxes (10^{18} mol Ma^{-1} , 10^{16} mol Ma^{-1} for Sr, mol/kg , for concentration) considered in the box model value used for the standard run.

Parameter / constant	Description	Range	Reference	Value
CO(rec)	Recent value CaCO_3 in and on oceanic crust (10^{18} mol Ma^{-1})	1000 - 1200	Berner (2004)	1200
eBO	Exponent describing the coupling intensity of POC burial and pO_2	0 - 1	this study	1
eWC	Exponent describing the dependence of carbonate weathering and erosion rate	0 - 1	this study	0.7
eWO	Exponent describing the dependence of POC weathering and the erosion rate	0 - 1	this study	0.7
G	Isotopic fractionation of POC in dependency on pO_2	2 - 3	Berner and Kothavala (2001)	3
k_{BC}	Kinetic constant for carbonate precipitation (Ma^{-1})	-	this study	10^9
k_{C}	Equilibrium constant for carbonate dissolution	-	Berner and Berner, (1996)	0.0044
k_{EO}	Kinetic constant for CO_2 release from subducted POC (Ma^{-1})	0.00005 - 0.000325	Berner and Kothavala (2001)	0.00005
k_{EX}	Kinetic constant for CO_2 exchange from seawater to atmosphere	-	Wallmann (2004)	10^5
k_{MC}	Kinetic constant for metamorphic CO_2 release from continental carbonates (Ma^{-1})	0.0001 - 0.0005	Berner and Kothavala (2001)	0.0004
k_{SC}	Kinetic constant for CaCO_3 subduction (Ma^{-1})	0.003083 - 0.003833	Hay et al. (1988)	0.003083
k_{SZO}	Kinetic constant for POC flux into subduction zones (Ma^{-1})	-	Wallmann (2001)	0:000432
k_{VO}	Kinetic constant for CO_2 release (10^{18} mol Ma^{-1})	-	this study	100000
k_{WO}	Kinetic constant for POC weathering (Ma^{-1})	0.002 - 0.018	Hansen and Wallmann (2003)	0.006
r_{ALT}	Fraction of HCO_3^- fixation in oceanic crust that occurs close to the spreading zones	0 - 1	Wallmann, (2001)	1
r_{BOAN}	POC fraction accumulating in anoxic environments	0.9 - 1	Berner and Canfield (1989)	0.9
$r_{\text{M(i)}}$	Initial POC fraction in marine sediments	-	Berner and Canfield (1989)	0.8
r_{S}	CaCO_3 recycling efficiency at subduction zones	0 - 1	GEOCARB	0.32
r_{VO}	Fraction of volcanic rocks weathered soon after deposition	0 - 1	Wallmann (2001)	0.5
O(i)	Initial ocean/atmosphere reservoir size of O_2 (10^{18} mol)	30.8 - 54.4	Berner and Canfield (1989)	30.8
$Z_{1/2}$	Molar O_2/S ratio during oxidation of SO_2 with O_2 to H_2SO_4	-	Hansen and Wallmann (2003)	0.5
$Z_{15/8}$	Molar O_2/S ratio during pyrite weathering	-	Hansen and Wallmann (2003)	15/8
Z_2	Molar O_2/S ratio during sulfate reduction and sulfide oxidation	-	Hansen and Wallmann (2003)	2
$\left(\frac{\text{S}}{\text{M}}\right)_{\text{M}}$	$\frac{\text{S}}{\text{C}}$ molar ratio in marine sediments	0.2 - 0.35	Hansen and Wallmann (2003)	0.23
eBP	Impact of pO_2 on pyrite formation	0 - 1	Hansen and Wallmann (2003)	0.5
eBP _{iso}	Impact of pO_2 on sulfur isotope fractionation during pyrite formation	0 - 1	Hansen and Wallmann (2003)	0.5
eWE	Exponent for coupling intensity of evaporite weathering and erosion rate	0 - 1	this study	0.1
eWP	Exponent describing the dependence of pyrite weathering and the erosion rate	0 - 1	this study	0.1

Table 2.3: Continued

Parameter / constant	Description	Range	Reference	Value
k_{BE}	Kinetic constant for evaporite precipitation (10^{18} mol Ma^{-1})	-	this study	10000
$r_{1/2}$	Contribution of SO_2 to total S emission at subduction zones	0.38 - 0.78	Halmer et al. (2002)	0.38
$\delta^{13}CO_2M$	$\delta^{13}CO_2$ value of mantle CO_2 (‰)	-	Alt and Teagle (1999)	-5
δ^{34}_{EM}	$\delta^{34}S$ -values of mantle sulfur (‰)	-0.4 - 0.6	Carpenter and Lohmann (1997)	-0.4
δ^{34}_{WP}	Average $d_{34}S$ value of weathering pyrite (‰)	-17 to -15	Petsch and Berner (1998)	-17
eBPO4	Parameter for pO_2 dependence of P-burial	0 - 1	this study	1
k_B^{PO4}	Kinetic constant for phosphorus precipitation (10^{18} mol Ma^{-1})	-	this study	30
$\left(\frac{^{87}Sr}{^{86}Sr}\right)_{Hy}$	^{87}Sr ratio in hydrothermal fluids (‰)	0.7026 - 0.703	Veizer et al. (1999)	0.7026
$\left(\frac{^{87}Sr}{^{86}Sr}\right)_{VO}$	^{87}Sr ratio volcanic deposits (‰)	0.703 - 0.705	Wallmann (2001)	0.705
k_B^{Sr}	Kinetic constant for carbonate bounded strontium precipitation (10^{18} mol Ma^{-1})	-	this study	20
R^{87}_{HY}	^{87}Sr ratio in hydrothermal fluids	0.7026 - 0.705	Jones and Jenkyns (2001)	0.7026
R^{87}_{VO}	^{87}Sr ratio in volcanic deposits	0.702 - 0.708	Wallmann (1999)	0.708
r_{Sr}	Mole fraction of Sr in weathering carbonates	0.000425 - 0.000825	Gaillardet et al. (1999)	0.000425
r_{Sr}^S	Molar ratios Sr/ CO_2 during weathering of non-volcanic silicates	0.001 - 0.002	Gaillardet et al. (1999)	0.001
r_{Sr}^{VO}	Molar ratios Sr/ CO_2 during weathering of young volcanic rocks	0.0015 - 0.0035	Gaillardet et al. (1999)	0.0015
eER	Parameter describing the dependence of weathering on erosion rate	0 - 1	this study	0.1
eWS	Exponent describing the dependence of silicate weathering and erosion rate	0.466 - 0.494	GEOCARB	0.466
W_s	Constant describing the increase of insolation	-	Berner (1994)	7.4
$\Phi^{13}M$	Mole fraction of $\delta^{13}C$ in mantle CO_2	$\Phi^{13}C_M = \frac{1000 + \delta^{13}C_{CO_2M}}{89990 + \delta^{13}C_{CO_2M}}$		
k_{WP}	Kinetic constant for weathering of sedimentary pyrite (Ma^{-1})	$k_{WP} = \frac{F_{WP}(rec) * 0.5^{eWO}}{P(q)}$		
Φ_{EM}	Mole fraction of $\delta^{34}S$ degassing from the mantle	$\Phi^{34}S_{EM} = \frac{1000 + \delta^{34}S_{EM}}{23220 + \delta^{34}S_{EM}}$		
Φ_{WP}	Mole fraction of ^{34}S of pyrite weathering	$\Phi^{34}S_{WP} = \frac{1000 + \delta^{34}S_{EM}}{23220 + \delta^{34}S_{EM}}$		
$\Phi^{87}Hy$	Mole fraction of ^{87}Sr in hydrothermal fluids	$\Phi^{87}Sr_{Hy} = \frac{\left(\frac{^{87}Sr}{^{86}Sr}\right)_{Hy}}{9.43 + \left(\frac{^{87}Sr}{^{86}Sr}\right)_{Hy}}$		
$\Phi^{87}VO$	Mole fraction of ^{87}Sr in volcanic deposits	$\Phi^{87}Sr_{VO} = \frac{\left(\frac{^{87}Sr}{^{86}Sr}\right)_{VO}}{9.43 + \left(\frac{^{87}Sr}{^{86}Sr}\right)_{VO}}$		

2.2.1 Sulfur model

Sulfur constitutes an important part of the lithosphere, biosphere, hydrosphere, as well as the atmosphere and is an essential component in exogenous and endogenous geochemical cycles. During the anaerobic decomposition of particulate organic carbon (POC) seawater sulphate (SO_4) is microbially reduced to hydrosulphide (HS^-), which in turn reacts with terrigenous iron to sedimentary pyrite (F_{BP}) (Berner, 1980). Seawater sulphate is also fixed during the formation of marine evaporites ($\text{net}F_{BE}$) in ocean basins with restricted water exchange like e.g. in arid climates (Gordon, 1975). In turn, the weathering of pyrite-bearing (F_{WP}) and evaporite rocks ($\text{net}F_{BE}$) causes the sulfur input into the ocean. Mantle derived sulfur (SO_2) is mainly emitted at intraplate volcanoes, arc volcanoes (Graf et al., 1997) and middle oceanic ridges. However, only sulfur emitted at intraplate and arc volcanoes actually reaches the atmosphere. Within the atmosphere gaseous sulfur (F_E) reacts immediately with oxygen forming sulphate. Transported by wet and dry deposition, e.g. rain, volcanic sulfur induces an additional source of sulfur to the oceans.

The sulfur model by Hansen and Wallmann (2003) has been used as the basis for the simulation of the sulfur cycle. Its complexity of six species (ocean, sedimentary evaporites, sedimentary pyrite, sulfides and hydrothermal anhydrite in oceanic crust, and mantle sulfur) has been reduced into three species (ocean, marine evaporites, sedimentary pyrite) with a simplified but time enhanced calculation. This reduction results out of the output of the model by Hansen and Wallmann (2003) which clarifies the hydrothermal turnover of sulfur at mid-ocean ridge spreading centers has no significant net effect on the sulphate concentration in the ocean in long-term cycles. My new approach for the determination of sulfur fluxes considers to sedimentary pyrite burial (F_{BP}), the net burial flux of marine evaporites ($\text{net}F_{BE}$), and sulfur emission via volcanoes (F_E). Changes are given in the text below, solely, for detailed description see Table 2.1 - 2.3 and Appendix A2.1 - A2.3.

Anaerobic decomposition of accumulated POC on the seafloor by sulphate reducing bacteria is required for sedimentary pyrite formation (Berner, 1980). This implies that sulfur fixation due to pyrite burial (F_{BP}) depends on the particulate organic matter burial flux to the oceans (F_{BOsea}), and that it is coupled to the marine sulfur content normalized to the modern sulphate inventory of the oceans ($\text{RSO}_4 = \text{SO}_4/\text{SO}_4(q)$), which is proceeding more rapidly under low oxygen conditions:

$$F_{BP} = r_{BOAN} * F_{BOsea} * \left(\frac{S}{C}\right)_M * \text{RSO}_4^{eBS} * \left(\frac{1}{RO_2}\right)^{eBP}, \quad (2.1)$$

where r_{BOAN} (0.9) represents the fraction of POC accumulation in anoxic sediments covered by oxic bottom water, and $(S/C)_M$ the molar ratio of sulfur to carbon (0.11). The exponent applied to the normalized sulfur inventory ($eBS = 0$ to 1) describes the coupling intensity of sedimentary pyrite burial to the oceanic sulfur content, and the exponent ($eBP = 0$ to 1) applied to the atmospheric oxygen concentration, normalized to the Quaternary value RO_2 ($pO_2/pO_2(q)$), describes the coupling intensity of sedimentary pyrite burial to the oxygen conditions.

Evaporites are highly soluble, therefore many evaporite deposits of the past may have been

completely dissolved by weathering processes. The geological record of marine evaporite deposition (Wold and Hay, 1993) is thus not very reliable. Hence I used the seawater sulphate concentrations reconstructed reliable from brine inclusion data (Horita et al., 2002) to constrain net sulphate burial in marine evaporites ($netF_{BE}$ = burial - weathering) over the Phanerozoic. The net sulphate burial of marine evaporites is calculated by forcing the seawater sulphate concentration predicted in the model ($cSO_{4(MOD)}$) to track the brine inclusion record ($cSO_{4(DAT)}$), Fig. 2.1):

$$netF_{BE} = k_{BE} * ((cSO_4)_{MOD} - (cSO_4)_{DAT}), \quad (2.2)$$

where k_{BE} is a kinetic burial constant (10^4 mol SO_4 Ma^{-1}). This calculation approach allows adjusting the net burial flux of marine evaporites dynamically so that the sulphate inventory in the ocean follows the proxy data.

Moreover, I assumed that the past emission of sulfur out of intraplate and subduction zone volcanoes (F_E) is proportional to the changing degassing rate (f_{VO}):

$$F_E = f_{VO} * F_E(q), \quad (2.3)$$

with $F_E(q)$ as the recent subaerial sulfur emission (0.29 to $0.85 * 10^{18}$ mol Ma^{-1} , Halmer et al. (2002)) out of volcanoes.

Thus, as mentioned above the inventory of dissolved sulphate in the oceans (SO_4) depends mainly on the burial and weathering of sedimentary pyrite (F_{BP} , F_{WP}), the emission of sulfur gases out of intraplate and arc volcanoes (F_E), and the net burial of marine evaporites ($netF_{BE}$):

$$\frac{dSO_4}{dt} = F_{WP} + F_E - netF_{BE} - F_{BP}. \quad (2.4)$$

The sulfur isotope ($\delta^{34}S$) composition of seawater during the Phanerozoic is predicted in the model, to compare model results to geological data (Strauss, 1999). The isotopic signature of sulfur is assumed for burial and release fluxes of sulfur. The fluxes of sulfur isotopes of weathered pyrite, volcanic derived sulfur, and marine evaporite fluxes are assumed not to fractionate (Hansen and Wallmann, 2003), whereas the sulfur isotope deposition during sedimentary pyrite burial has a fractionation factor, which depends on the pO_2 (Berner and Kothavala, 2001). The mole fraction (Φ) of the isotopes buried in marine evaporites and in sedimentary pyrite in the past depends on the isotope ratio of ancient seawater, whereas the isotope ratio of mantle derived sulfur and weathered sedimentary pyrite are proportional to the Quaternary isotope ratio and sulfur amount (Hansen and Wallmann, 2003) (detailed formulation are listed in Table 2.1 - 2.3 and Appendix A2.1 - A2.3):

$$\frac{d\delta^{34}SO_4}{dt} = \Phi_{WP}^{34} * F_{WP} + \Phi_{EM}^{34} * F_E - \Phi_{BE}^{34} * netF_{BE} - \Phi_{BP}^{34} * F_{BP}. \quad (2.5)$$

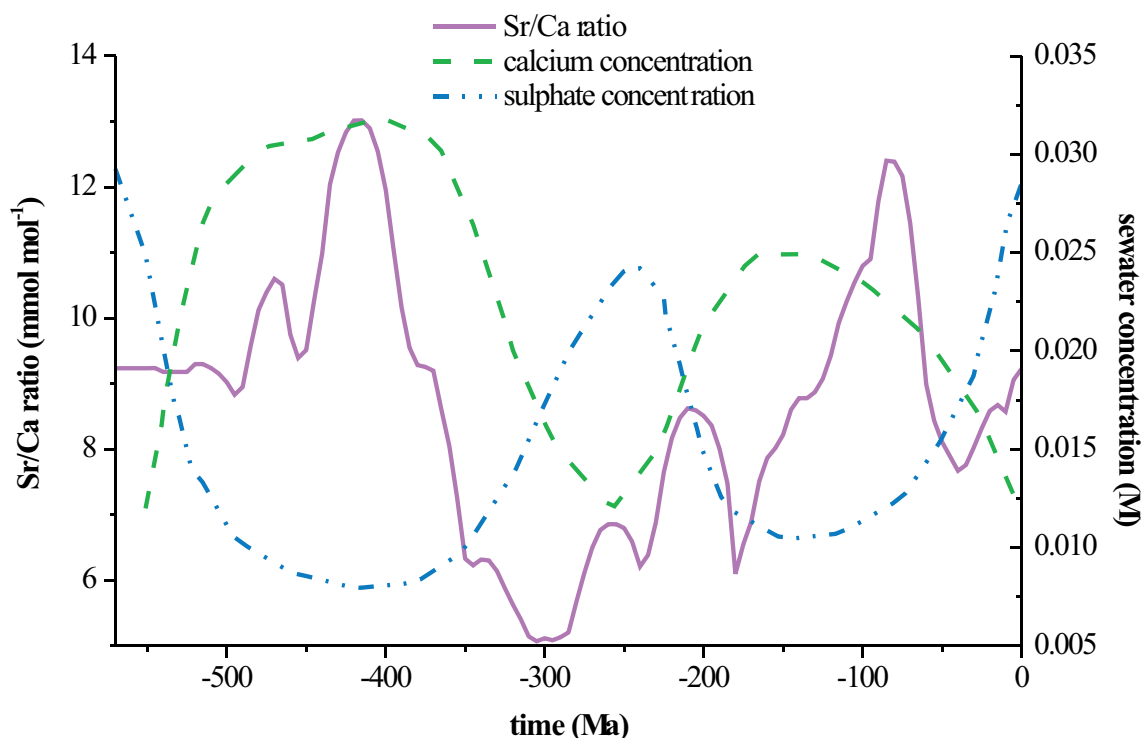


Figure 2.1: External forcings considered in the model. They are described by changes in the Sr/Ca ratio of Phanerozoic seawater derived from marine carbonate data (Steuber and Veizer, 2003) (solid line), changes in dissolved Ca concentration derived from brine inclusions in evaporites (Horita et al., 2002) (dashed line), and changes in sulphate concentrations (Horita et al., 2002) (dotted line).

2.2.2 Phosphorus model

Phosphorus (PO_4) is an essential nutrient for all organisms, which remove carbon dioxide from the atmosphere and bind it into organic matter through photosynthesis. To constrain the rate of particulate organic matter burial in marine and terrestrial sediments I have developed a simple model describing the global phosphorus cycle. The phosphorus submodel accounts for weathering fluxes of phosphorus bearing rocks, burial on land and on the seafloor, uptake at hydrothermal systems, as well as the fixation due to authigenic carbonate burial, and within oxides on the seafloor. As implied, the here described long-term phosphorus cycle interacts with the carbon cycle and, as suggested above, on this way affects the cycles of sulfur and oxygen. In the following I describe the consolidation of approaches by Bergman et al. (2004) and Wallmann (2003) to predict the ancient PO_4 seawater concentration.

Most phosphorus is found in rocks, where it is bounded into minerals (mostly apatite) (Wallmann, 2003). It is released due to the weathering of terrigenous carbonate carbon ($F_{\text{wc}}, F_{\text{wc}}(q)$, with (q)=quaternary value) and organic carbon ($F_{\text{wo}}, F_{\text{wo}}(q)$) as well as from silicates ($F_{\text{ws}}, F_{\text{ws}}(q)$, $F_{\text{wsvo}}(q)$) (Wallmann, 2001) - the main constituent of volcanic deposits and rocks in general - (e.g. Deer et al. (1992)). The weathering fluxes can be described as:

$$F_W^{PO_4} = \frac{F_{WO} + F_{WS} + F_{WC}}{F_{WO}(q) + F_{WSS}(q) + F_{WSVO}(q) + F_{WC}(q)} * F_W^{PO_4}(q). \quad (2.6)$$

A small fraction of phosphate released by weathering ($F_w^{PO_4}$) is not delivered to the ocean since it is retained on land ($F_{Bland}^{PO_4}$) mainly by plants. Its long-time storage occurs in environments with long time POC accumulation, e.g. in swamps or wetlands. Coals are formed from plant material deposited in swamps and terrestrial wetlands. Coals and coal basin sediments - which are preserved in the geological record - are, thus, a proxy for the abundance of phosphorus burial in wetlands during the past.

Ronov (1993) investigated the abundance of terrigenous sedimentary rocks, including coal basin sediments, deposited over various periods of the Phanerozoic and preserved until today (S_p). These data were later updated and re-compiled by W. W. Hay (personnel communication) and applied by Berner and Kothavala (2001) and Berner (2004b). It should, however, be considered that a large fraction of the initially deposited sediments was not preserved but converted into metamorphic rocks and lost by erosion and subduction. Previous tests on sedimentary rock cycling showed that this loss follows a simple first order decay law (Veizer and Jansen, 1979). Hence, the initial terrigenous sedimentation rate S_i was calculated as (Wallmann, 2001):

$$S_i = S_p \cdot e^{b \cdot t}, \quad (2.7)$$

using the S_p values listed in Berner and Kothavala (2001) while the decay constant (b) was set to the value $5 \cdot 10^{-3} \text{ Ma}^{-1}$ previously derived by Gregor (1985) and Wallmann (2001). The resulting sedimentation rate plotted in Fig. 2.2a (f_{ER}) was multiplied with the fraction of terrigenous sediments deposited in coal basins (Fig. 2.2b, f_{coal}) taken from Berner (2004b) to calculate the accumulation rate of coal basin sediments over the Phanerozoic. Finally, these values were normalized to the values derived for the most recent period considered in Ronov's compilations (the Pliocene) to calculate the relative change in coal basin sedimentation over the Phanerozoic (Fig. 2.2c, $f_{ER} f_{coal}$).

The coal distribution ($f_{ER} f_{coal}$) can be used to calculate the sink of phosphorus on land:

$$F_{Bland}^{PO_4} = f_{ER} f_{coal} * f_{PO_4} * F_W^{PO_4}, \quad (2.8)$$

where f_{PO_4} (0.015) is the fraction of weathered PO_4 ($F_w^{PO_4}$) buried on land.

Due to plankton growth in the oceans phosphorus is fixed, via aggregation, within the upper water column to be partly buried as particulate organic phosphorus ($F_{Bsea}^{PO_4}$) after its deposition in marines sediments. The burial flux mainly depends on the phosphate inventory of the oceans (PO_4):

$$F_{Bsea}^{PO_4} = k_{Bsea} * PO_4, \quad (2.9)$$

where k_{Bsea} (24 Ma^{-1}) is a kinetic constant for the nutrient burial within ocean floor sediments.

Another significant loss of dissolved phosphorus out of the oceans can be accounted to hydrothermal vent sites at mid-ocean ridges and ridge flanks (Wheat et al., 1996). Inside these hydrothermal plumes phosphate is removed in contact with iron oxyhydroxide particles due to precipitation processes and is bounded into the oceanic crust:

$$F_{Hy}^{PO_4} = f_{VO} * F_{Hy}^{PO_4}(q) * RPO_4 . \quad (2.10)$$

Equation 2.10 is scaled to the rate of plate movement (f_{VO}) as a dimension for hydrothermal activities, while RPO_4 describes the PO_4 amount in seawater normalized to the pre-industrial Holocene value ($PO_4/PO_4(q)$) and $F_{Hy}^{PO_4}(q)$ is the Quaternary loss of phosphorus out of seawater at hydrothermal systems ($1.2 * 10^{16}$ mol PO_4 Ma^{-1} , Compton et al. (2000)).

Additionally, phosphate is fixed in manganese and iron oxides. I calculated the iron and manganese bounded phosphorus burial ($F_{BFe}^{PO_4}$) as:

$$F_{BFe}^{PO_4} = F_{BFe}^{PO_4}(q) * anox , \quad (2.11)$$

according to Bergman et al. (2004), where $F_{BFe}^{PO_4}(q)$ describes the Quaternary loss of phosphorus during iron and manganese burial ($6 * 10^{15}$ mol PO_4 Ma^{-1} , Lenton and Watson (2000a)), and $anox$ the oxygen limiting factor (Bergman et al., 2004):

$$anox = RO_2 * (117 * PO_4) , \quad (2.12)$$

with RO_2 ($pO_2/pO_2(q)$) the normalized to recent oxygen concentration of seawater.

The burial in authigenic carbonate-fluoride-apatite (CFA) is calculated following again the approach introduced by Bergman et al. (2004):

$$F_{BCa}^{PO_4} = F_{BCa}^{PO_4}(q) * (117 * PO_4)^2 , \quad (2.13)$$

with $F_{BCa}^{PO_4}(q)$, the Quaternary consumption of phosphorus during CFA burial ($1.5 * 10^{18}$ mol PO_4 Ma^{-1} , Lenton and Watson (2000a)).

Thus, the development of the seawater PO_4 concentration over time can be described as:

$$\frac{dPO_4}{dt} = F_W^{PO_4} - F_{Bland}^{PO_4} - F_{Bsea}^{PO_4} - F_{Hy}^{PO_4} - F_{BFe}^{PO_4} - F_{BCa}^{PO_4} . \quad (2.14)$$

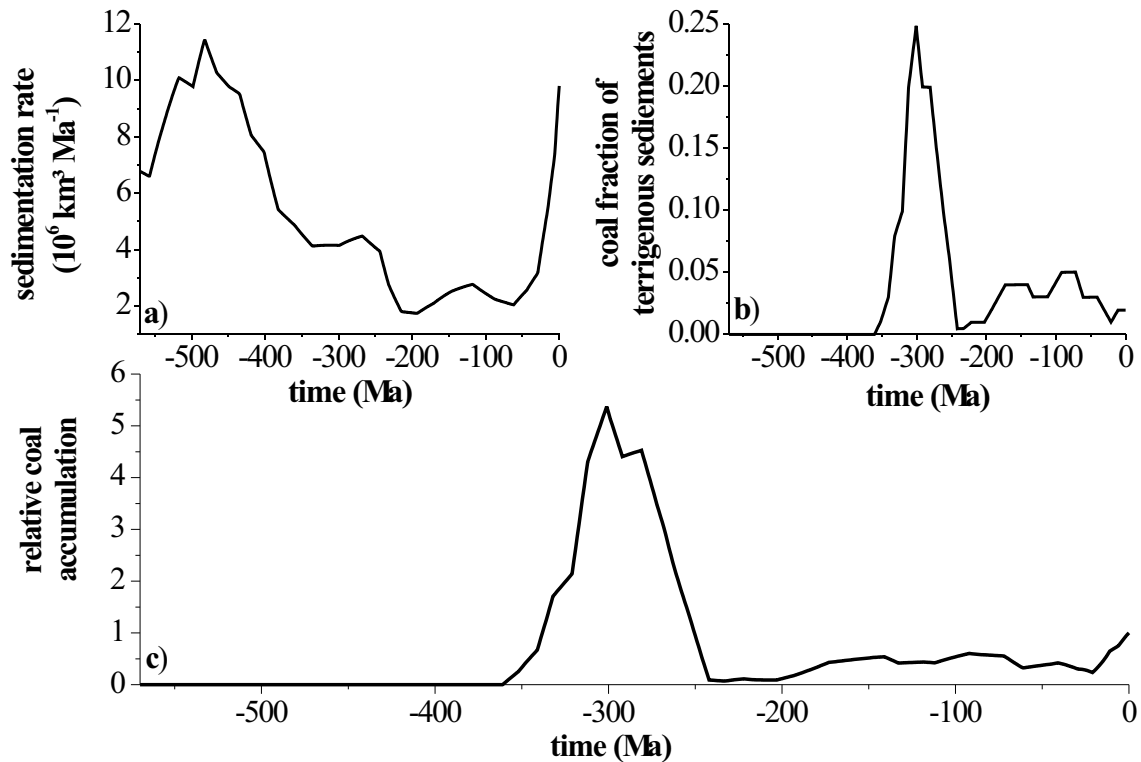


Figure 2.2 a - c: Changes in Phanerozoic a) sedimentation rates (Berner, 2004), b) coal fraction of terrigenous sediments (Berner and Kothavala, 2001), and c) relative coal accumulation derived from a) & b), normalized to the recent value (see text), considered in the model ($f_{ER} f_{coal}$).

2.2.3 Carbon model

Carbon is an essential ingredient of oceans and atmosphere, e.g. as a controlling component of life and climate. The carbon submodel accounts for organic and inorganic carbon. It predicts ancient masses in the oceans and atmosphere, in carbonate rocks, in particulate organic carbon (POC), and in the mantle. Major processes considered in the model are mantle degassing and hydrothermal fluxes, chemical weathering, and metamorphism of carbonates, carbonate and POC accumulation, and carbonate loss in subduction zones.

The carbon submodel generally follows the approaches previously presented in Wallmann (2001) and Wallmann (2004). Additionally it was advanced by adding the simulation of separated particulate organic carbon burial processes on land and at the seafloor, and the new coupling of the carbon cycle to the phosphorus cycle. Modifications and additions of the organic carbon model are outlined and given below, whereas the complete calculation approach of inorganic and organic carbon cycles are listed in Tab. 2.1 & 2.2, as well as in the Appendix (A2.1 - A2.3).

I separated the burial of particulate organic carbon into two large burial environments, seafloor and land. The POC burial at the seafloor ($F_{B_{Osea}}$) is associated to the burial of phosphorus out of the ocean ($F_{B_{sea}}^{PO4}$) and proceeds more rapidly under low oxygen conditions (Berner and Berner,

1996):

$$F_{BOsea} = F_{Bsea}^{PO_4} * 106 * \left(\frac{1}{RO_2} \right)^{eBO}, \quad (2.15)$$

with the exponent ($eBO = 0$ to 1) applied to the atmospheric oxygen concentration, normalized to the Quaternary value RO_2 ($pO_2/pO_2(q)$), describes the coupling intensity of particulate organic matter burial to the oxygen conditions.

The burial of POC on land (F_{Boland}) is proportional to the corresponding burial flux of organic phosphorus on land ($F_{Bland}^{PO_4}$):

$$F_{Boland} = F_{Bland}^{PO_4} * 450. \quad (2.16)$$

The different atomic C:P ratios of 450 and 106 (in Eqs. 2.15 & 2.16) are applied to consider the fact that terrestrial POC contains less P than marine organic matter (Redfield, 1958; Sterner and Elser, 2002).

The total burial of particulate organic carbon, on the continents as well as on the seafloor therefore can be described as:

$$F_{BO} = F_{BOsea} + F_{Boland}, \quad (2.17)$$

now.

The comprehensive carbon isotope models by Hansen and Wallmann (2003), Wallmann (2001) and Wallmann (2004) was slightly modified. In contrast to Hansen and Wallmann (2003), Wallmann (2001) and Wallmann (2004) I considered that the isotope composition of weathering carbonate rocks and POC changes through time. I applied a running mean to the recorded $\delta^{13}C$ data published by Veizer et al. (1999) and Hayes et al. (1999) and assumed that the weathering fluxes have the isotope composition ($\delta^{13}CCaCO_3$) of $CaCO_3$ and POC deposited over a period of 30 Ma prior to the considered time step (Fig. 2.3).

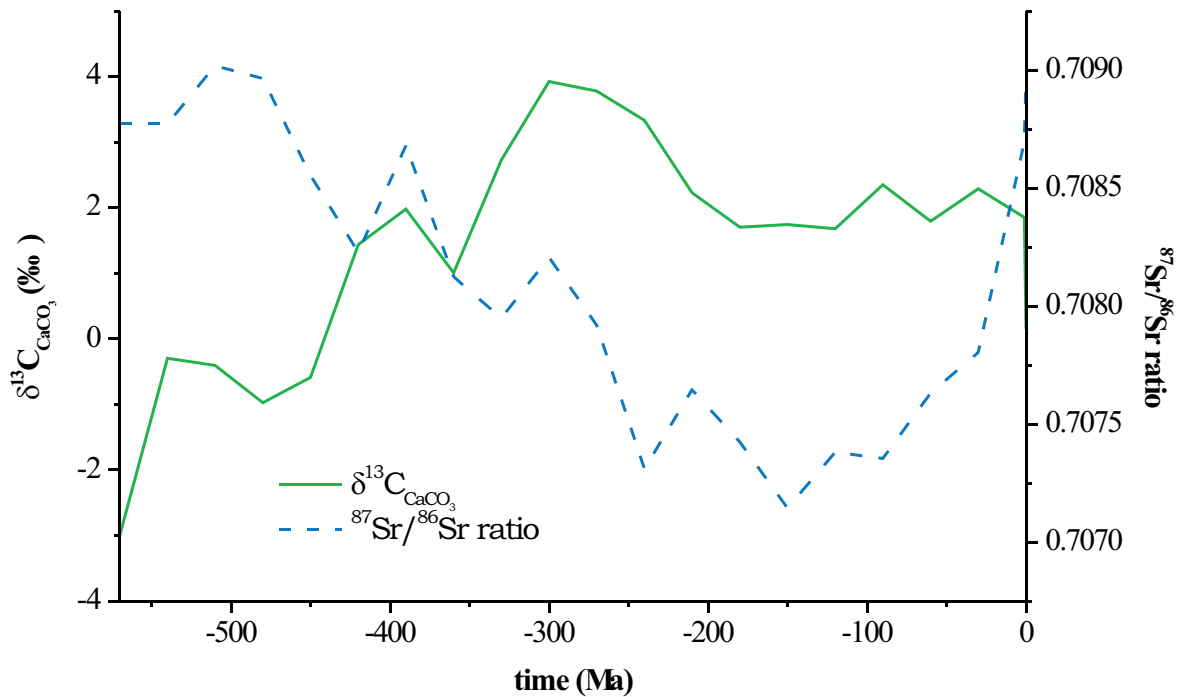


Figure 2.3: Changes in carbon and strontium isotope compositions of marine carbonates subjected to weathering ($\delta^{13}\text{C}_{\text{CaCO}_3}$, $^{87}\text{Sr}/^{86}\text{Sr}_{\text{CaCO}_3}$), in running mean data according to the data of Hayes et al. (1999) (solid line) and Veizer et al. (1999) (dashed line). Data representing a mean value, applying that the weathering fluxes have the isotopic composition of CaCO_3 and POC deposited over a period of 30 Ma prior to the considered time step, used as a external forcing in the model.

2.2.4 Strontium model

The strontium isotope composition of ancient seawater, recorded in marine carbonate shells and rocks, can be utilized as a proxy parameter for the physical - e.g. tectonic and erosion - evolution of the Earth's crust. The variations of the $^{87}\text{Sr}/^{86}\text{Sr}$ ratio reflects the interplay between mantle derived as well as continental derived strontium fluxes (Veizer et al., 1999). The strontium submodel generally follows the approaches published by Wallmann (2001) and Wallmann (2004). It accounts for masses in oceans, in silicate and carbonate rocks. Major processes considered in the model are hydrothermal release, release due to weathering of silicate and carbonate rocks, as well as the burial at the seafloor. The existing model by Wallmann (2001) and Wallmann (2004) is revised by new flux calculation for burial of strontium out of seawater, and a new approach for prediction of tectonic and volcanic rates of the Earth's crust.

Strontium is removed from the ocean by a number of different processes including carbonate burial, alteration of oceanic crust and inverse weathering. Both, modern and ancient removal rates are poorly constrained. Hence, I used proxy data of the composition of ancient seawater to drive the removal flux. I considered Sr/Ca ratios (Fig. 2.1, left ordinate) specifically derived from marine carbonate data (Steuber, 2002) and Ca concentrations (Fig. 2.1, right ordinate) reconstructed from

brine inclusion data (Horita et al., 2002). Afterwards the strontium removal flux was adjusted to produce Sr/Ca ratios in seawater consistent with the proxy data:

$$F_B^{Sr} = k_B^{Sr} * \left(\frac{cSr_{MOD}}{cCa_{DAT}} - \left(\frac{cSr}{cCa} \right)_{DAT} \right), \quad (2.18)$$

where cSr_{MOD} is the strontium concentration in seawater calculated in the model, while $(cSr/cCa)_{DAT}$ and cCa_{DAT} describe the concentrations recorded in marine carbonates and brine inclusions. The kinetic constant k_B^{Sr} is set to a large value ($850 * 10^{18}$ mol Sr Ma^{-1}), guaranteeing a very small deviation between measured and modeled isotopic rates.

This varied strontium submodel considers a new approach for the removal of strontium from the ocean (F_B^{Sr}), the approaches from Wallmann (2001) for hydrothermal Sr release (F_{HY}^{Sr}), as well as continental silicate and carbonate weathering (F_{WS}^{Sr} , F_{WC}^{Sr}):

$$\frac{dSr}{dt} = F_{HY}^{Sr} + F_{WS}^{Sr} + F_{WC}^{Sr} - F_B^{Sr}. \quad (2.19)$$

In consequence I calculated the $^{87}Sr/^{86}Sr$ ratio of ancient seawater using strontium fluxes, which were scaled by the corresponding ^{87}Sr mole fractions (Φ^{87}) (for a detailed listing of the used parameter see Appendix A2.1 - A2.3):

$$\frac{d^{87}Sr/^{86}Sr}{dt} = \Phi_{HY}^{87} * F_{HY}^{Sr} + F_{WS}^{87Sr} + \Phi_{WC}^{87} * F_{WC}^{Sr} - \Phi_{SW}^{87} * F_B^{Sr}. \quad (2.20)$$

The isotopic strontium removal flux out of oceanic water is scaled with the changing mole fraction of seawater calculated in the model (Φ_{SW}^{87}) assuming that removed Sr has the isotope composition of coeval seawater.

The hydrothermal strontium isotope flux and the flux of strontium isotopes released during weathering of volcanic rocks are closely related to the prevailing tectonic/volcanic activity (f_{VO}) (Wallmann, 2001; Wallmann, 2004). Therefore, the seawater $^{87}Sr/^{86}Sr$ ratio reacts very sensitive to a varying tectonic/volcanic activity (f_{VO}). Thus I determined its changing rate by forcing the calculated $^{87}Sr/^{86}Sr$ ratio of seawater to track the marine isotope record (Veizer et al., 1999):

$$f_{VO} = k_{VO} * ((^{87}Sr/^{86}Sr)_{MOD} - (^{87}Sr/^{86}Sr)_{DAT}), \quad (2.21)$$

where $(^{87}Sr/^{86}Sr)$ characterizes the isotope composition of ancient seawater calculated in the model ($(^{87}Sr/^{86}Sr)_{MOD}$) and recorded in marine carbonates ($(^{87}Sr/^{86}Sr)_{DAT}$ Fig. 2.3) (Veizer et al., 1999). The corresponding kinetic constant k_{VO} is set to a large value (10^5 Ma^{-1}), guaranteeing a very small deviation between measured and modeled isotope ratios for all model runs (Wallmann, 2004). This kind of calculation allows to adjust the volcanic/tectonic variable dynamically and to track the changing strontium isotopic seawater composition (Wallmann, 2001).

2.2.5 Oxygen model

The evolution of atmospheric oxygen is strongly coupled to the evolution of biological and geological processes on Earth's surface. Via redox processes oxygen controls long-term geochemical cycles of carbon and sulfur (Berner and Canfield, 1989).

Due to the use of the simplified sulfur model by Hansen and Wallmann (2003) (see section 2.2.1.), some of the oxygen-sulfur-coupled parameterizations have been changed too. The new oxygen submodel considers the essential burial and weathering fluxes of particulate organic carbon (F_{BO} , F_{WO}) and sedimentary pyrite (F_{BP} , F_{WP}) (Berner et al., 2003). It also takes into account the oxygen consumption due to the oxidation of Fe(II) during oceanic crust alteration (O_{Fe}), the oxygen consumption due to the oxidization of SO_2 emitted from intraplate volcanoes as well as the oxidation of H_2S and SO_2 emitted from subduction zone volcanoes (O_S). The change of atmospheric oxygen with time can be calculated as:

$$\frac{dO_2}{dt} = -O_{WP} - O_S + O_{BP} - F_{WO} + F_{BO} - O_{Fe}, \quad (2.22)$$

with O_{WP} as the consumption of oxygen during sedimentary pyrite weathering and O_{BP} as the release of oxygen during sedimentary pyrite precipitation (Hansen and Wallmann, 2003) (detailed information Appendix A2.1 - A2.3).

2.3 External forcing of the model

The model includes twenty-three external forcings, summarized in Tab. 2.3 (see also Figs. 2.1 - 2.3). These are one terrestrial-biota, five geological, and 17 physico-chemical forcings. All of the forcings except the seawater concentrations and the isotope values are normalized to prehuman time values. They are mainly taken from GEOCARB III (Berner and Kothavala, 2001) and from the model by Wallmann (2004), except the coal distribution, which was established within this article (see chapter 2.2.2.).

2.4 Results and Discussion

In order to analyze the model results, a standard case was developed representing the best agreement between model results and independent data. To obtain this standard case, model parameters were tuned within the ranges given in Tabs. 2.1 - 2.3 until the model reproduced the Quaternary values for atmospheric pO_2 and pCO_2 , modern concentrations of PO_4 and dissolved inorganic carbon in seawater and the marine $\delta^{13}C$ and $\delta^{34}S$ records (Hayes et al., 1999; Horita et al., 2002; Royer et al., 2001).

Additionally, for better understanding of the processes occurring in this coupled system and their connection to each other, I run sensitivity tests with varied parameter sets to demonstrate their impact on the particulate cycle.

2.4.1 Sulfur model

2.4.1.1 Standard case

Figure 2.4 shows the predictions of Phanerozoic marine evaporite net burial flux. The net burial flux increases during the Middle Cambrian, followed by a decrease with a minimum during the Permian-Carboniferous cold period, and a second peak during the Lower Mesozoic. The net burial flux of marine evaporites during the Cambrian and Triassic is two-and-a-half times higher than today. Evaporation and evaporite formation are controlled by the climate conditions (Gordon, 1975). Thus, the hotter and dryer the climate is, the more evaporation occurs, while evaporation is inhibited under cold and wet conditions.

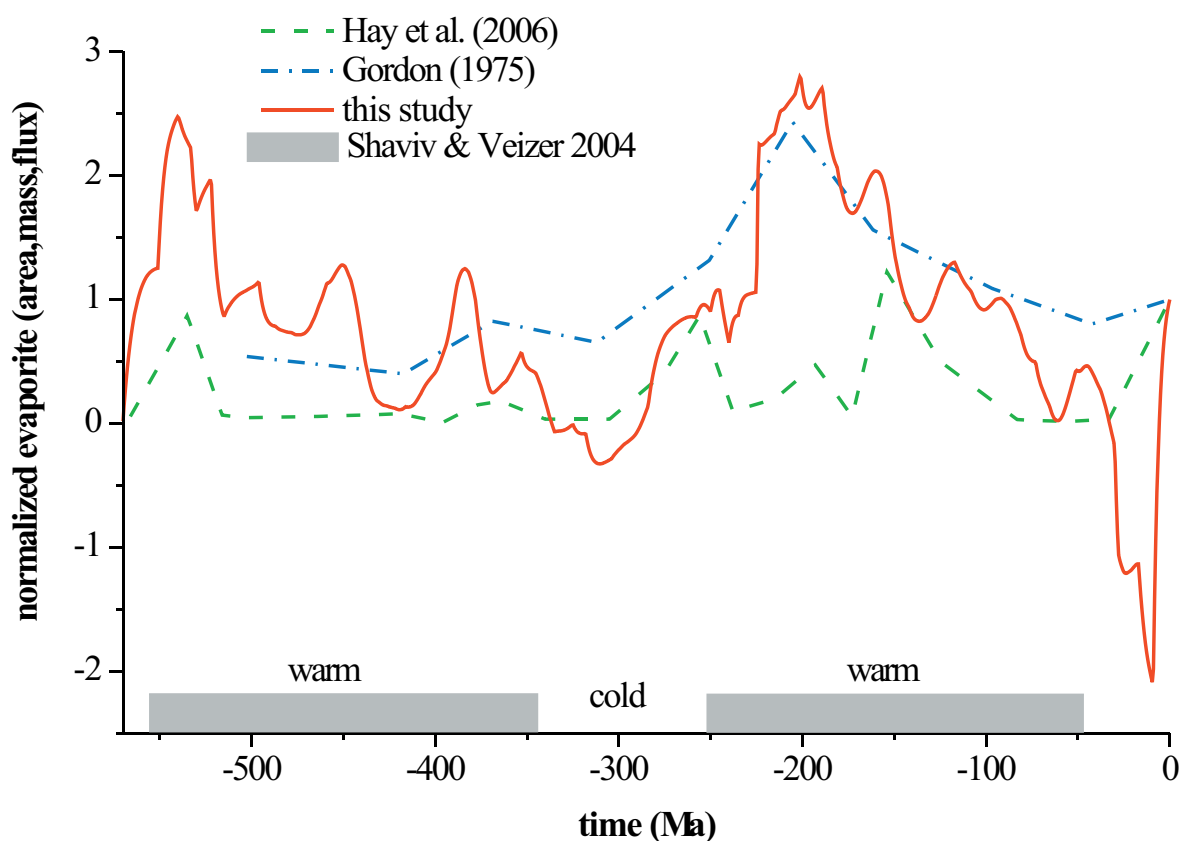


Figure 2.4: To the Quaternary value normalized changes in net marine evaporite fluxes ($netF_{BE}$) (Quaternary value = $0.23 * 10^{18} \text{ mol Ma}^{-1}$), in the standard case (solid line), compared to the distribution of evaporites (Quaternary value = $10^4 \text{ km}^2 \text{ Ma}^{-1}$, (Gordon, 1975)) (dotted & dashed line), evaporite masses - (Quaternary value = $10^{15} \text{ kg Ma}^{-1}$, (Hay et al., 2006)) (dashed line), and generalized climate conditions (Shaviv and Veizer, 2004) (shaded area).

In comparison to the climate conditions during the Phanerozoic (Shaviv and Veizer, 2004) accordance's between warmer climates and enhanced net evaporite burial occur, and during the Permo-Carboniferous-Ice-Age a decrease of net marine evaporite burial flux occurs (Fig. 2.4). Noticeable is also the strong drop during the Tertiary. This shift in marine evaporite net burial flux reflects the enormous global changes in Paleoclimates and -geography. The conditions of the Early Tertiary to the Upper Tertiary transforms from arid climate and large variations of oceanic transgression and regression, to cold wet climate with huge denudation of rising mountains and stagnation of oceanic level (Stanley, 1989).

There is reasonably good agreement between the model-predicted net marine evaporite burial flux (netF_{BE}) and distribution of marine evaporites (Gordon, 1975), especially during the Mesozoic, a warm period within the Phanerozoic (Fig. 2.4). My Cambrian, Permian and Jurassic model results are also confirmed by the recent reconstruction of evaporite volumes published by Hay et al. (2006). This reconstruction is based on the composition and accumulation rates of sedimentary rocks deposited over the Phanerozoic as compiled by Ronov (1993). During the Triassic my model results and the independent reconstructions of Hay et al. (2006) disagree. The model prediction shows maximum fluxes for the entire Phanerozoic at this time, whereas the calculated masses (Hay et al., 2006) also show an excursion but not as significant. Considering that ancient evaporites are easily lost by erosion and weathering, it is not surprising that periods of intensive evaporation are not always documented in the geological record.

The isotope ratios of sulfur fluxes and the analogous mole fractions for Phanerozoic times are shown in Figure 2.5. The sulfur isotope burial flux of ancient sedimentary pyrite ($\delta^{34}\text{SO}_{4\text{BP}}$) changes through time, it decreases continuously from -1 ‰ in the Cambrian up to -30 ‰ in the Permian, followed by an increase to the current value of about -15 ‰. The isotope values of mantle derived sulfur and sedimentary pyrite subjected to weathering were set to constant values over the entire Phanerozoic (0 ‰ and 20 ‰). Via flux calculation and isotope variations of buried and released sulfur I am able to recreate successfully the Phanerozoic seawater sulfur isotope values ($\delta^{34}\text{S}$), although the detail is not. Figure 2.5 shows the recreation of the overall changes of composition of predicted $\delta^{34}\text{S}$ over the entire Phanerozoic, compared to the record of marine carbonates (Strauss, 1999), with a decrease of about 15 ‰ in the Early Phanerozoic during the advent of land plants from 30 ‰ to the slightest values during the Permo-Triassic of about 12 ‰, as well as an increase of 10 ‰ in the Mesozoic and Cenozoic up to the current value (20.5 ‰). The overall amplitude of $\delta^{34}\text{S}$ is well portrayed, although Lower Phanerozoic predictions are a few per mil to low, whereas the predictions in the Middle Phanerozoic are a few per mil to high. The sharp Devonian/Carboniferous shift from maximum (28 ‰) to minimum (15 ‰) during a geological short time (10 Ma) is missing in My prediction, this could be due to inadequately modeling of geochemical changes due to the advent of the first land plants. Similarly misfit of model- and proxy data occurs during the change of Paleozoic to Mesozoic.

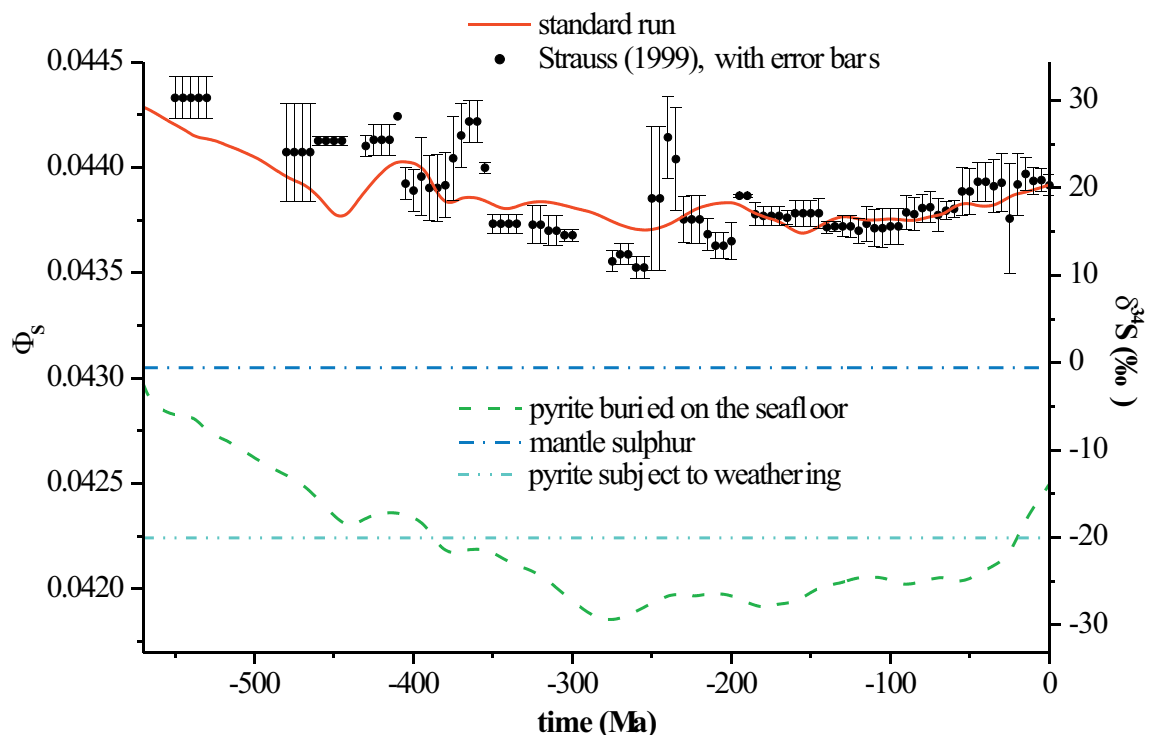


Figure 2.5: Changes in mole fractions (Φ) and corresponding $\delta^{34}\text{S}$ values in Phanerozoic seawater, used in the standard case for the calculation of the sulfur isotope seawater inventory, with sedimentary pyrite buried on the seafloor (Φ^{P_b}) (dashed line), deposited pyrite subjected to weathering (Φ^{P_w}) (dashed & double dotted line), mantle derived sulfur (Φ^{P_M}) (dashed & dotted line), and the isotopic composition in seawater ($\Phi^{\text{P}_{\text{SO}_4}}$) (solid line).

2.4.1.2 Sensitivity tests

The overall trend of the net marine evaporite burial flux (netF_{BE}) (Figs. 2.4 & 2.6) is strongly coupled to the climate conditions (Gordon, 1975; Gorshkov and Makarieva, 2006). But it is also driven by the supply of soluble seawater ingredients, e.g. sulfur. The test results due to the hypothetical lack of sedimentary pyrite in the global sulfur cycle reflects in detail the overall trend of the standard case with a positive displacement of about 10 % (Fig. 2.6). Hence sedimentary pyrite represents a significant sulfur sink in the global long-term sulfur cycle. Whereas the test results with eliminated sulfur from the mantle reflects - but not in detail - the overall trend of the standard case with a negative displacement of about 50 %. Because mantle sulfur only acts as a considerable source (250 ppmV, Alt and Shanks III (1998)), its impact on global sulfur cycle is more significant than the impact due to recyclable sedimentary pyrite. Both predictions reflect the overall trend with two heights in Cambrian and Jurassic, but in the prediction without volcanic sulfur degassing the small excursions during the Ordovician, Devonian, Permian, and in the Cenozoic are lost (Fig. 2.6). These predictions clearly show the dependency of the marine evaporite net burial flux to the sulfur concentration in seawater as well as the different impact of sedimentary pyrite net burial fluxes and mantle sulfur on

the seawater SO_4 inventory, but also emphasize the essential impact of climate conditions. Therefore, although the main seawater sulfur is eliminated, the significant heights of the net evaporite burial flux are displayed.

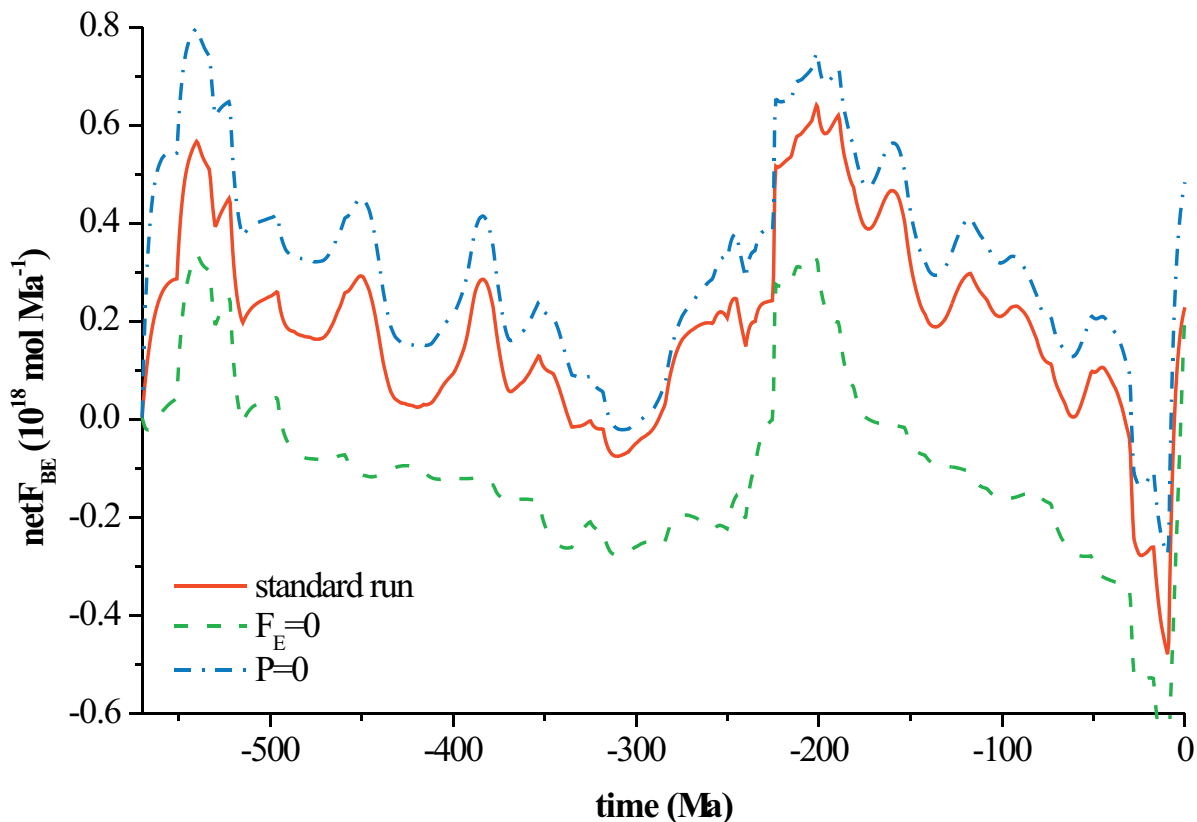


Figure 2.6: Changes in Phanerozoic marine evaporite net burial fluxes (netF_{BE}) used in the standard case (solid line), compared to the netF_{BE} without input of sulfur via volcanic emission ($F_{\text{E}}=0$) (dashed line), and to the prediction with eliminated pyrite burial and weathering fluxes ($P=0$) (dotted & dashed line).

As already annotated above the here described long-term sulfur cycle interacts with the cycles of carbon and oxygen. In particular, the POC burial mainly controls the formation of sedimentary pyrite (Berner and Berner, 1996). Both processes (POC burial and formation of sedimentary pyrite) are associated with oxygen release. Due to POC burial as a result of organic matter production and photosynthesis, and due to burial of sedimentary pyrite as a result of bacterial sulphate reduction high amounts of O_2 are released. In turn, oxygen is consumed during weathering of these substances.

Due to the marine evaporite net burial flux sulfur isotopes become removed out of seawater. For modeling I predicted no isotope fractionation during the removal of sulfur out of seawater during evaporation. Figure 2.7 illustrates the prediction of sulfur isotope concentration of seawater over the Phanerozoic with an eliminated influence by the net marine evaporite burial flux. The shown trend varies from about 5 ‰ during Ordovician up to 10 ‰ during Jurassic from the standard case. It implies that marine evaporite net burial flux affects the isotopic composition of seawater only slightly.

Moreover Figure 2.7 shows the significant effect of mantle sulfur on the seawater $\delta^{34}\text{S}$ value due to the emission of sulfur out of volcanoes on land and arc volcanoes. The variation of the predicted trend ranges between 15 ‰ during Devonian and 22 ‰ during Jurassic, when compared to the trend of the standard case. Figure 2.7 also clearly indicates the significant impact of mantle sulfur on the $\delta^{34}\text{S}$ seawater concentration during the overall trend, but also its significant effect on the detailed excursions during time. In contrast to the impact of mantle sulfur causes not only an elimination of the sedimentary pyrite net burial flux and a strong decrease in ancient $\delta^{34}\text{S}$ of 15 to 20 ‰, it also removes any variations in $\delta^{34}\text{S}$ over time. An elimination of the time-dependent supply of phosphorus from land via weathering ($F_w^{\text{PO}_4} = F_w^{\text{PO}_4}(q)$), has a small effect on seawater $\delta^{34}\text{S}$ only (Fig. 2.7). The latter prediction in Figure 2.7 shows a small displacement of the $\delta^{34}\text{S}$ trend, which almost follows the curve of the standard run, with one exception during the Permian.

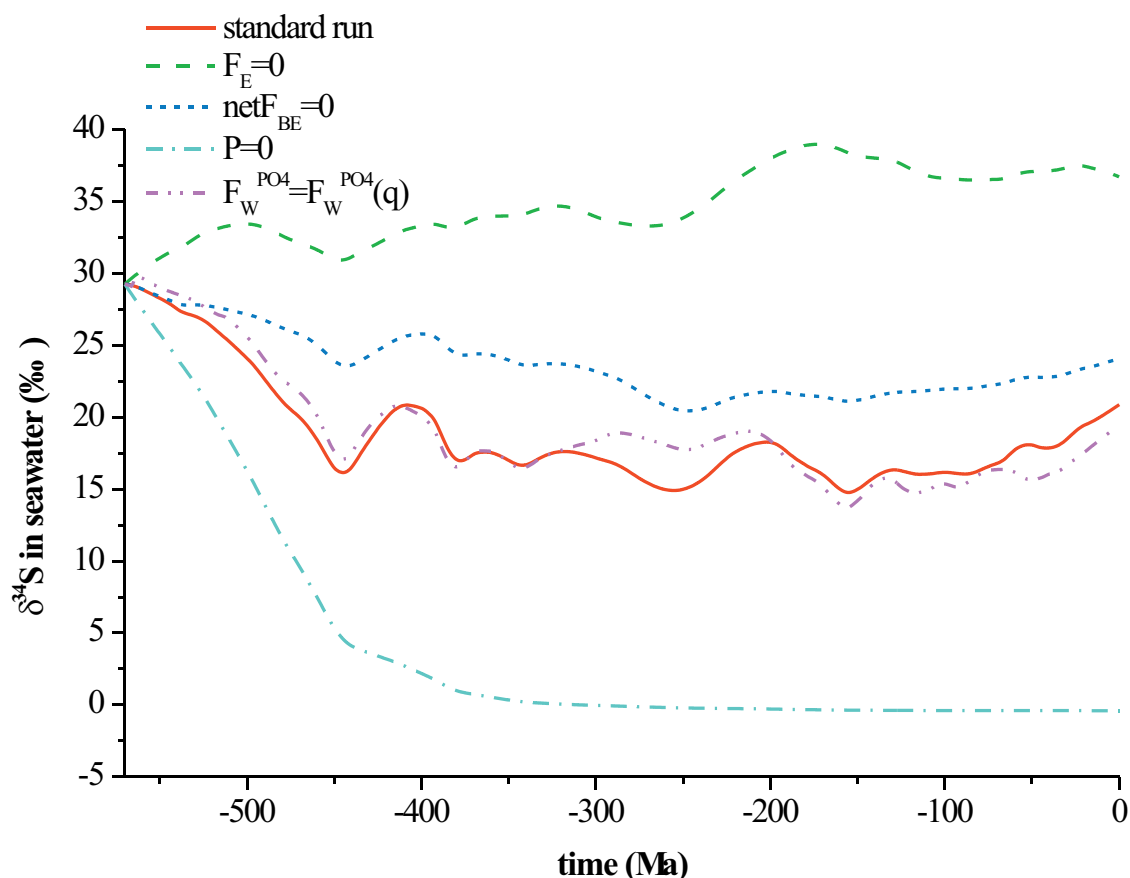


Figure 2.7: Changes in Phanerozoic seawater $\delta^{34}\text{S}$ concentration, in the standard case (solid line), compared to a run without sulfur emission via mantle degassing ($F_E=0$) (dashed line), and compared to a run without marine evaporite net burial fluxes ($\text{net}F_{\text{BE}}=0$) (dotted line), no pyrite weathering and burial fluxes ($P=0$) (dashed & dotted line), and constant weathering flux of phosphorus ($F_w^{\text{PO}_4} = F_w^{\text{PO}_4}(q)$) (dashed & double dotted line).

The overall results of these sensitivity tests is, that the effect of mantle sulfur and sedimentary pyrite net burial flux on seawater $\delta^{34}\text{S}$ ranges on a high magnitude, whereas the effect of the marine evaporite net burial flux on variations is significantly weaker. The impact of phosphorus weathering fluxes from land on seawater $\delta^{34}\text{S}$ via controlling the particulate organic matter burial

flux is negligible on geological timescales. It is conspicuous that the displacement of the prediction due to marine evaporite net burial fluxes reflects the overall trend of seawater $\delta^{34}\text{S}$, whereas neither the prediction using the lack of mantle sulfur, nor the prediction using the lack of sedimentary pyrite does so. Variances in $\delta^{34}\text{S}$ are affected by sedimentary pyrite and mantle sulfur. Thus, a balance between sedimentary pyrite net burial flux and mantle sulfur mainly controls the $\delta^{34}\text{S}$ of Phanerozoic seawater. Furthermore the conclusions shown in Figures 2.7 and 2.8 indicate that the burial of the sulfur inventory varies the seawater sulfur inventory little, but considerably affects the isotope fractionation of seawater $\delta^{34}\text{S}$.

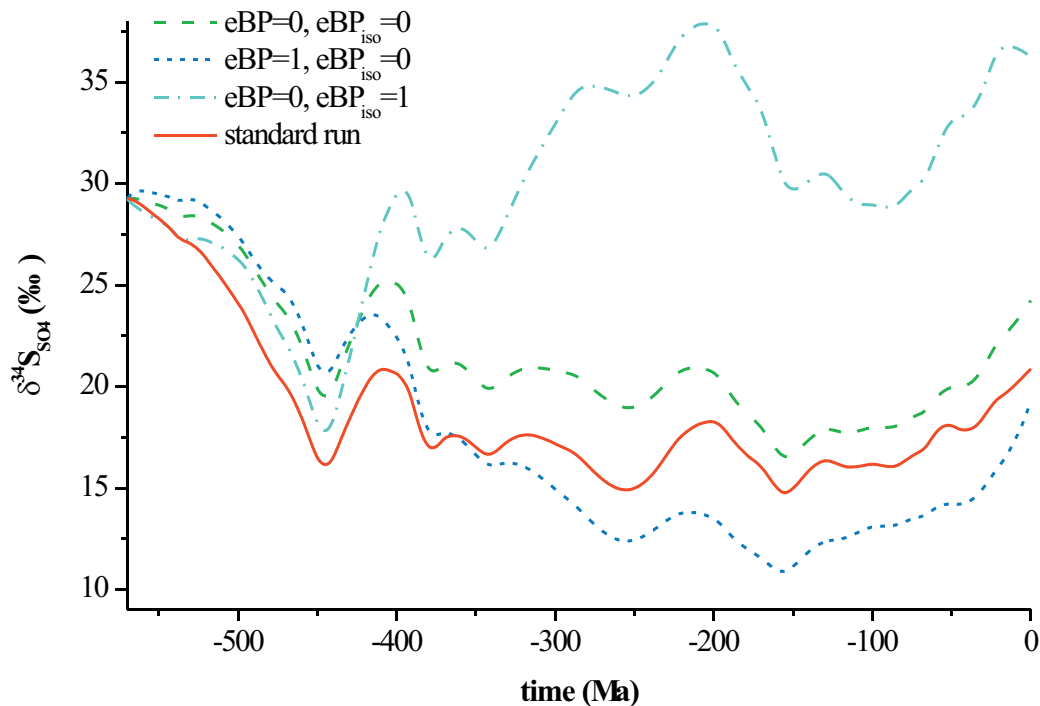


Figure 2.8: Changes in Phanerozoic seawater $\delta^{34}\text{S}$ concentration, in the standard case (solid line), compared to runs with different weightings in the linkage to the oxic and anoxic conditions, no linkage of $p\text{O}_2$ to sedimentary pyrite burial efficiency, and no fractionation effect during sedimentary pyrite burial ($e\text{BP}=0$, $e\text{BP}_{\text{iso}}=0$) (dashed line), a strong linkage to oxic conditions at the burial area and no isotopic fractionation linkage ($e\text{BP}=1$, $e\text{BP}_{\text{iso}}=0$) (dotted line), as well as to a run with no linkage of $p\text{O}_2$ to burial and a strong isotopic fractionation linkage ($e\text{BP}=0$, $e\text{BP}_{\text{iso}}=1$) (dashed & dotted line).

While Figure 2.7 distinguishes the significant effect of the sedimentary pyrite net burial flux on seawater $\delta^{34}\text{S}$, Figure 2.8 illustrates the significance of the sedimentary pyrite net burial flux on the $\delta^{34}\text{S}$ in dependency to $p\text{O}_2$. Sedimentary pyrite burial depends on the redox conditions at the precipitation area (Berner, 1980) - on one hand due to the change of oxic and anoxic conditions during burial processes at the precipitation area, and on the other hand due to the oxic and anoxic conditions influencing fractionation processes during the burial of the sulfur isotopes (Berner, 2001). Figure 2.8 demonstrates the impact of the particular connection. For a better comparison of both linkages the changes of the coupling parameter ($e\text{BP} \sim$ burial dependency & $e\text{BP}_{\text{iso}} \sim$ isotope fractionation dependency during burial) were compared to a run with no linkage to $p\text{O}_2$ ($e\text{BP}=0$ &

$eBP_{iso}=0$), than to the standard run ($eBP=1$ & $eBP_{iso}=0.5$), thus a weighting on sedimentary pyrite burial occurs when compared to fractionation processes ($eBP=1$ & $eBP_{iso}=0$ only linkage between pO_2 and burial efficiency, $eBP=0$ & $eBP_{iso}=1$ only linkage between pO_2 and isotopic fractionation). The prediction of seawater $\delta^{34}S$ values with an eliminated coupling of burial rates to pO_2 , is clearly coupled to the isotope fractionation and causes a strong increase compared to the standard run as well as to the case with no linkage (Fig. 2.8). The prediction of seawater $\delta^{34}S$ with a strong coupling of burial to pO_2 and an eliminated coupling to isotope fractionation decreases compared to the standard run and the case with no linkage. Summarized, the more intensive the coupling of sedimentary pyrite burial is to pO_2 , the lighter seawater $\delta^{34}S$ values get, what is caused by the burial of heavier isotopes (Fig. 2.8). The more intensive the coupling of the sulfur isotope fractionation is to the pO_2 , the heavier the seawater $\delta^{34}S$ values get. Hence it can be pointed out: the impact of oxygen conditions is more relevant for seawater sulfur isotope compensation, due to isotope fractionation processes, than for burial (Fig. 2.8). In conclusion seawater $\delta^{34}S$ is affected by sedimentary pyrite burial as well as by oxygen concentration.

2.4.2 Phosphorus model

2.4.2.1 Standard case

Figure 2.9a shows the prediction of phosphorus burial and weathering fluxes over the entire Phanerozoic. Parameter values were varied within the ranges listed in Table 2.1 & 2.2 until the best possible fit for phosphorus weathering ($F_W^{PO_4}$) and fixation ($F_{Bland}^{PO_4}$, $F_{Bsea}^{PO_4}$, $F_{Hy}^{PO_4}$) was obtained to reproduce the well known current values. Fluxes of weathering on land as well as burial on the seafloor generally follow an increasing trend, with slight excursions once in a while and noticeable heights during the beginning of the Cenozoic. The main loss of seawater phosphorus occurs due to its burial on the seafloor and, in small amounts, due to precipitation processes at hydrothermal systems. The originally negligible loss of phosphorus on land thus gains importance during the Carboniferous coal swamp era (Fig. 2.9a). Figure 2.9b shows the predicted phosphorus seawater concentration over the entire Phanerozoic. The prediction of seawater PO_4 concentration increase continuously over time, with concentrations below the well known pre-industrial Holocene value during the Lower Phanerozoic and during the Jurassic, and concentrations approaching the pre-industrial Holocene concentration ($2.03 \mu M PO_4$) during Middle and Upper Phanerozoic.

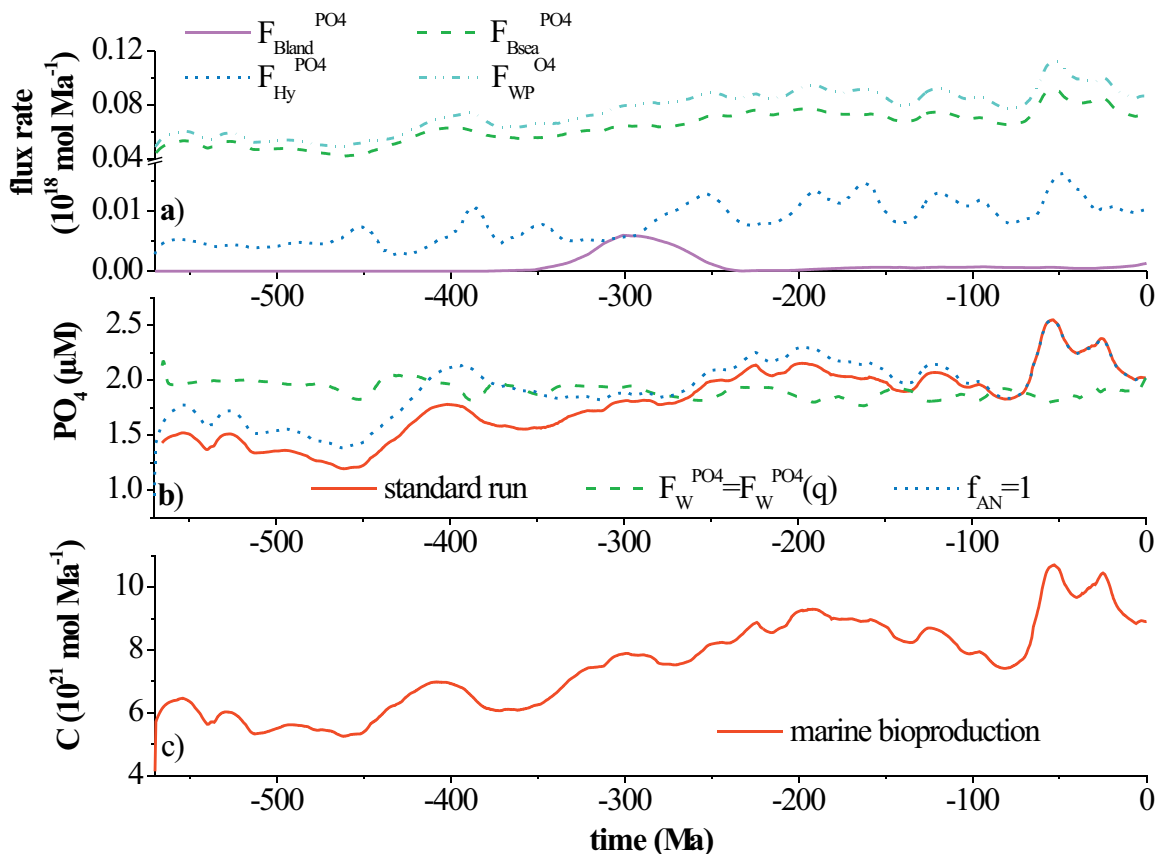


Figure 2.9 a-c: a) Changes in the Phanerozoic main flux rates of phosphorus burial on land ($F_{\text{Bland}}^{\text{PO}_4}$) (solid line), organic phosphorus burial on the seafloor ($F_{\text{Bsea}}^{\text{PO}_4}$) (dashed line), burial on the oceanic crust near hydrothermal systems ($F_{\text{Hy}}^{\text{PO}_4}$) (dotted line), and P release due to the weathering of sulfur bearing rocks ($F_{\text{W}}^{\text{PO}_4}$) (dashed & double dotted line), in the standard case. b) Changes in seawater concentration of phosphorus in the standard case (solid line), compared to the seawater concentration assuming constant phosphorus weathering on land ($F_{\text{W}}^{\text{PO}_4} = F_{\text{W}}^{\text{PO}_4}(q)$) (dashed line), as well as to a run with eliminated land plant evolution ($f_{\text{AN}} = 1$) (dotted line). c) Changes in marine bioproductivity.

2.4.2.2 Sensitivity tests

Weathering drives the seawater phosphorus concentration. Setting the phosphorus weathering flux from land to the high Quaternary value throughout the simulation period ($F_{\text{W}}^{\text{PO}_4} = F_{\text{W}}^{\text{PO}_4}(q)$) causes increasing seawater PO_4 concentration during the Paleozoic and decreasing seawater PO_4 concentration during the rest of the Phanerozoic, compared to the standard case (Fig. 2.9b). This prediction distinguishes, that the seawater PO_4 concentration strongly depends on the phosphorus supply from land, whereas the sinks depend on the seawater concentration. Furthermore Figure 2.9b emphasizes a shift of the evolution of phosphorus release due to weathering during the Phanerozoic - compared to Quaternary conditions, only a low nutrient release occurred until the appearances of land plants due to comparatively weak weathering. Since the great evolution of land plants the weathering conditions have changed, during almost the entire Mesozoic and Cenozoic the weathering conditions are weaker than in the Quaternary, but stronger than during the Early Paleozoic. As already

mentioned above, PO_4 is an essential nutrient for organisms, thus the bioproductivity depends on the supply by this nutrient (Fig. 2.9c). Otherwise, land plants control the weathering efficiency of PO_4 bearing rocks. Figure 2.9b shows predictions of PO_4 seawater concentrations due to an eliminated time-dependence of land plant evolution ($f_{\text{AN}}=1$). Increasing land plant activity results in increasing weathering rates, which caused an increased PO_4 seawater concentration prior the completed evolution of land plants during the Phanerozoic.

2.4.3 Carbon model

2.4.3.1 Standard case

Figure 2.10 shows the prediction of the total particulate organic carbon burial flux (F_{BO}), with its two subfluxes POC burial on land (F_{BOland}) and burial on the seafloor (F_{BOsea}). In general, the POC burial flux on land is very low, with an exception during the Carboniferous coal swamp era. The burial flux onto the seafloor increases over time, but decreases due to the advent of land plants, due to the increasing storage of particulate organic matter on land and the inhibited supply to the ocean by land plants. This contrary trend during the Carboniferous occurs after the height of land plants during the Carboniferous coal swamp era, the burial rates on the seafloor increase further

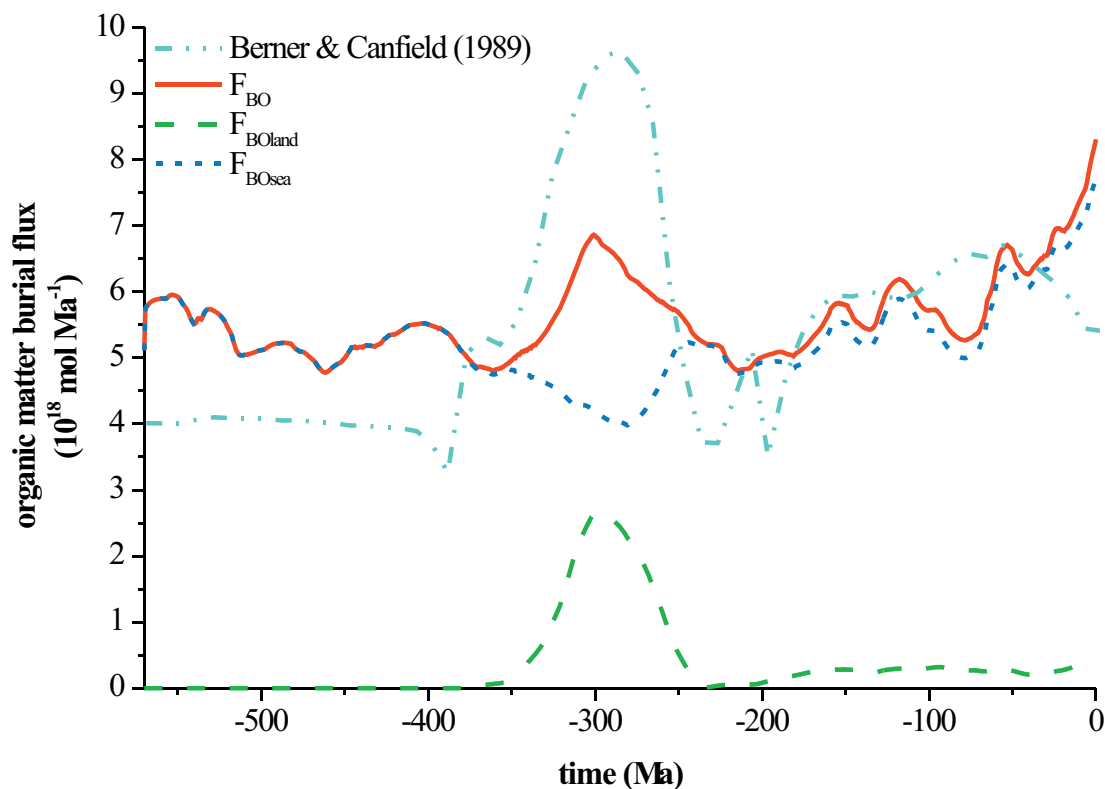


Figure 2.10: Changes of Phanerozoic particulate organic matter fluxes, buried on land (F_{BOland}) (dashed line) and on the seafloor (F_{BOsea}) (dotted line) as well as total particulate organic matter fluxes (F_{BO}) (solid line) used in the standard case, compared to the total organic carbon burial data by Berner and Canfield (1989) (dashed & double dotted line).

with positive excursions during the second evolution of land plants in the Cretaceous. Thus the total POC burial rates increase continuously over time, with significant heights during the advent of land plants at the border from the Devonian to the Carboniferous, and their second evolution during the Cretaceous. The appearance of land plants enhanced the supply of organic matter, but the formation of swamps inhibited the transport of organic matter to the oceans. In comparison to the prediction of Berner and Canfield (1989) only the character of both predictions are visible, whereas the amplitudes during the Paleozoic disagree. But under consideration of the large range ($5 - 10 \cdot 10^{18} \text{ mol C Ma}^{-1}$, Bergman et al. (2004)) of the current value and the unclarity about the detailed present processes, this disagreement is explainable and justifiable. Predictions for the carbon dioxide concentration rate (RCO_2) are displayed in Figure 2.11. The Phanerozoic begins with high RCO_2 values of up to 8, which decrease due to the advent of land plants during the Carboniferous reaching a minimum value of 2, staying on a low range of about 1 to 3. My prediction ranges within the calculations of different authors (e.g. Berner and Kothavala (2001) and Rothman (2002)).

Figure 2.12 illustrates the isotope ratios ($\delta^{13}\text{C}$) and the analogous mole fractions (Φ_c) of carbon fluxes. The secular isotope trends of POC subjected to weathering and POC buried on the seafloor ranges between -31 ‰ during Cambrian and -24 ‰ nowadays. The trends show some strong positive excursions in the Silurian (-25 ‰) and during the Carboniferous (-27 ‰), further heights

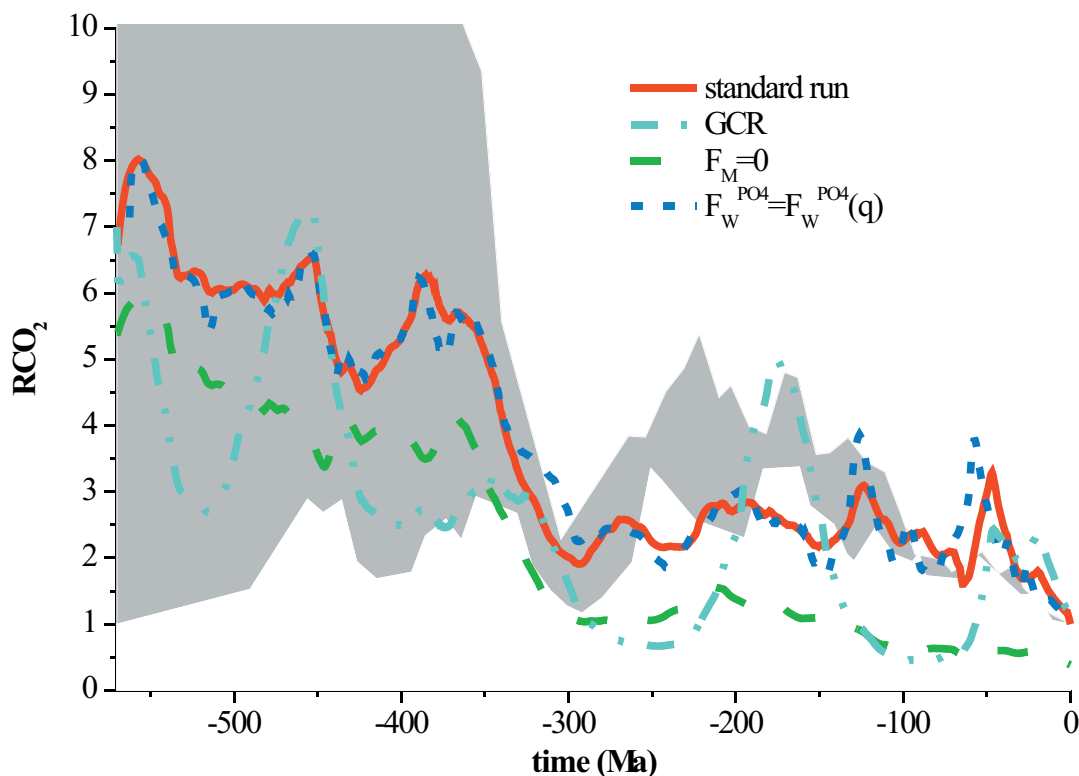


Figure 2.11: Changes in Phanerozoic RCO_2 in the standard case (solid line), compared to a run without degassing activity from volcanoes on land and arc volcanoes ($F_M=0$) (dashed line), constant phosphorus weathering on land ($F_w^{\text{PO}_4} = F_w^{\text{PO}_4}(q)$) (dotted line), and to a run with the impact on global surface temperature by galactic cosmic radiation (GCR) (dashed & double dotted line) (Wallmann, 2004). The shaded area represents the space between predicted RCO_2 by Berner and Kothavala (2001) and Rothman (2002).

are displayed during the Cretaceous (-25 ‰). The isotope value of mantle derived carbon was set to a constant value (-3.5 ‰). The isotope value of carbonate carbon subjected to weathering ranges between -3 ‰ in the Cambrian and 2 ‰ nowadays, with an increase during the Carboniferous up to 4 ‰. The combination of these isotope carbon fluxes results in the isotope seawater composition over the entire Phanerozoic ($\delta^{13}\text{C}$) (Fig. 2.12), with a strong increase during the Lower Cambrian, caused by the evolution of marine organisms, and a further increase during the advent of the first land plants during the Carboniferous. Compared to the data by Hayes et al. (1999), the overall trend is successfully recreated, although the finer detail is not (Fig. 2.12). Parameter values for this recreation were varied within the ranges listed in Table 2.1 & 2.3 until the best possible fit obtained.

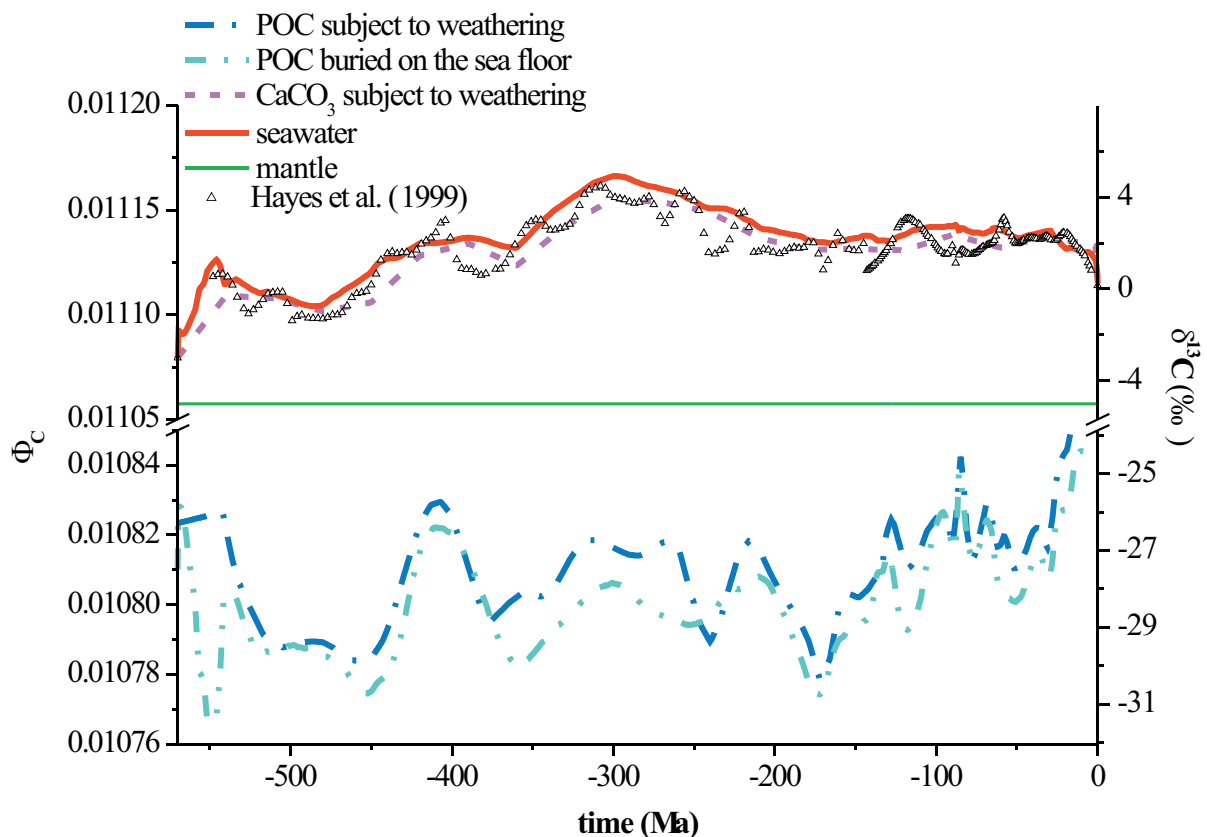


Figure 2.12: Changes in the mole fractions (Φ) and corresponding $\delta^{13}\text{C}$ values used for the calculation of the carbon isotope seawater inventory in the standard case; POC subjected to weathering (Φ^{13}_{POCin}) (dashed & dotted line), POC buried on the seafloor ($\Phi^{13}_{\text{POCout}}$) (dashed & double dotted line), CaCO_3 subjected to weathering (Φ^{13}_{Cin}) (dashed line), mantle (Φ^{13}_M) (thin solid line), and seawater (Φ^{13}_σ) (bulk solid line), reference values recorded in marine carbonates (Hayes, 1999) (triangle).

2.4.3.2 Sensitivity tests

Figure 2.11 shows the significant indirect influences of galactic cosmic radiation in RCO_2 . During the Early Phanerozoic a RCO_2 depletion was caused by galactic cosmic radiation, whereas

during the Cretaceous a significant enhancement has occurred. The excursions of the Cretaceous were documented in the geological record, whereas the depletion during the Early Phanerozoic overestimate the impact of cosmic radiation and varies significant from the geological record (Berner, 2004b; Royer et al., 2001; Wallmann, 2004).

As shown above, the burial of particulate organic matter is controlled by the supply of PO_4 to the ocean, as well as its release on land. In order to investigate the influence of the nutrient supply from land to the ocean the weathering flux of phosphorus was set to the moderate Quaternary value throughout the model simulation ($F_w^{\text{PO}_4} = F_w^{\text{PO}_4}(q)$) (Fig. 2.13), predicting the Phanerozoic total POC burial flux. The predictions are higher during the Cambrian, whereas the prediction during the Carboniferous and younger times are almost identically when compared to the standard case. POC burial is strongly coupled to the release of phosphorus, since the fluxes of phosphorus to the ocean during the Lower Phanerozoic is much lower than after the appearance of land plants, resulting in a lower POC burial during early times. This emphasizes the significant impact of land plants on the nutrient flux since their advent during the Carboniferous. The model also predicts a total particulate organic matter burial due to an eliminated time-dependent land plant evolution, the predicted trend is weaker as the latter one. This highlights that the land plants contribute to the weathering of phosphorus bearing rocks, but the main part is controlled by different processes, e.g. CO_2 .

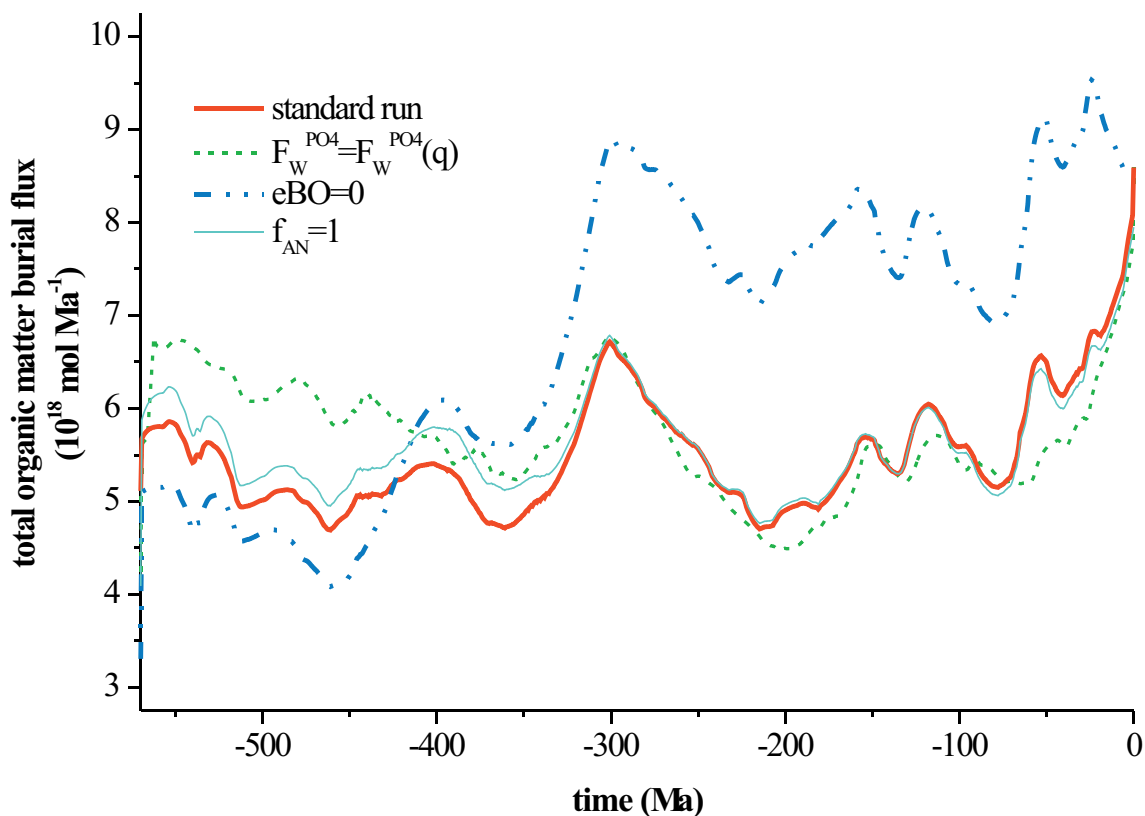


Figure 2.13: Changes in Phanerozoic particulate organic matter burial fluxes, in the standard case (solid line), compared to a run with time independent weathering and burial phosphorus fluxes ($F_w^{\text{PO}_4} = F_w^{\text{PO}_4}(q)$) (dotted line), to a run with eliminated coupling of $p\text{O}_2$ to particulate organic matter burial ($e\text{BO}=0$) (dashed & double dotted line), and to a run with eliminated land plant evolution ($f_{\text{AN}}=1$) (thin line).

The elimination of the pO_2 time-dependency ($eBO=0$) for POC burial generates decreasing particulate organic matter burial fluxes during the Paleozoic, and strong increasing fluxes during the Mesozoic and Cenozoic (Fig. 2.13). Due to this prediction a higher pO_2 inhibits the POC burial during the Early Phanerozoic, but lower pO_2 enhances POC burial during the Middle and Upper Phanerozoic compared to the standard case. Since the oxygen concentration is an important factor for the POC burial, the oxygen concentration should influence the seawater $\delta^{13}C$ by this way.

Figure 2.14 shows the prediction of the Phanerozoic $\delta^{13}C$ seawater trend, compared to the standard case. Surprisingly, the overall trend of the standard case is also reflected in detail with some small exceptions, only, e.g. during the Permo-Carboniferous, where a positive shift in $\delta^{13}C$ of up to 0.2 ‰ is displayed. The POC burial flux is controlled by the pO_2 , as highlighted above, but POC weathering is controlled by the pO_2 as well. The elimination of pO_2 time-dependency ($eBO=eWO=0$) for POC burial and weathering thus deciphers the significance of pO_2 on POC fluxes and their negative feedbacks (Fig. 2.14).

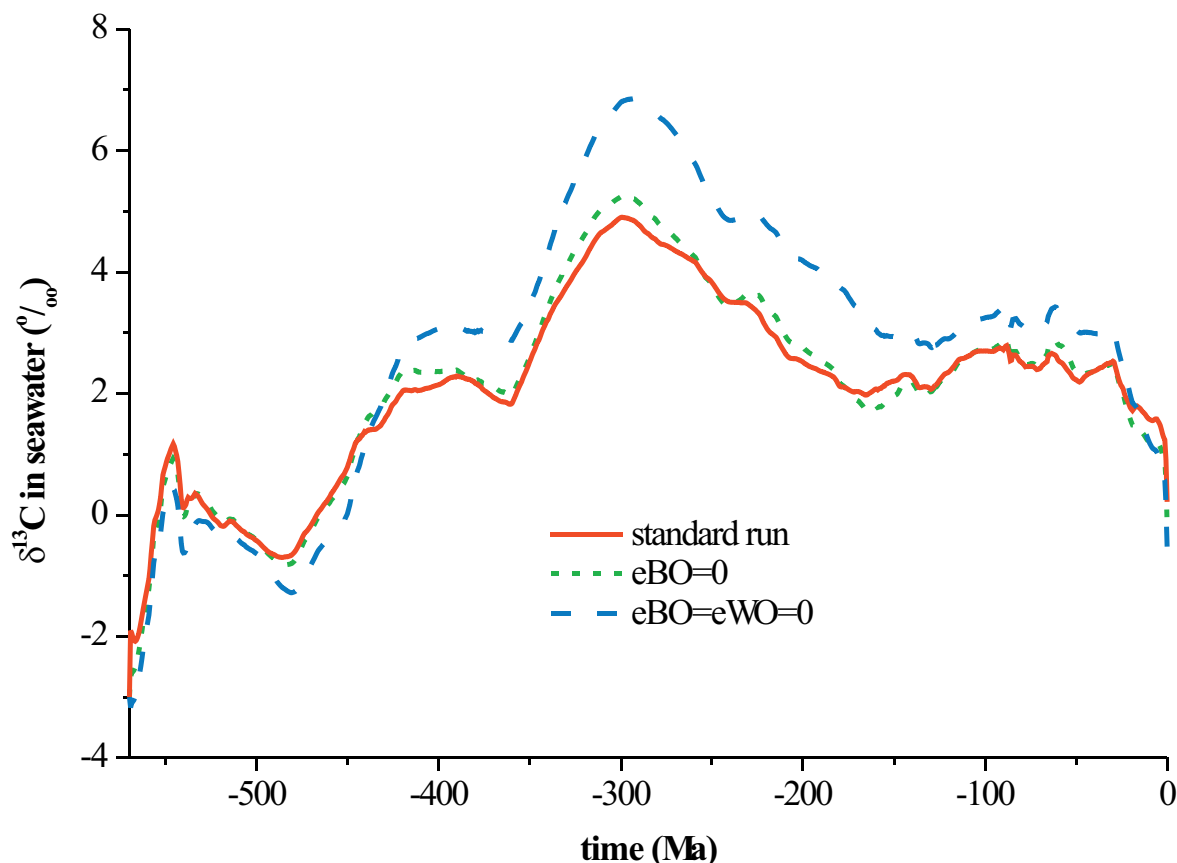


Figure 2.14: Changes in Phanerozoic seawater $\delta^{13}C$ trend in the standard run (solid line), compared to a run with eliminated coupling of pO_2 to particulate organic matter burial ($eBO=0$) (dotted line), and with eliminated coupling of pO_2 to particulate organic matter burial and weathering ($eBO=eWO=0$) (dashed line).

2.4.4 Strontium model

2.4.4.1 Standard case

The model predicts the Phanerozoic tectonic/volcanic activity. Figure 2.15 shows an oscillating trend over the Phanerozoic, with significant higher activity rates than today in each era, most notably in the Mesozoic and Cenozoic. Some maximum tectonic/volcanic activity rates coincide with maximum pulses of ocean crust production (Larson, 1991), whereas others occur during periods of flood basalts (Courtillot and Renne, 2003), and superplumes (Abbott and Isley, 2002). It is a puzzle to discover all accordance's between the particular events. Figure 2.15 also shows phases of significant low activity rates, lower than today. Just as well there are possible geological records for the “low phases”. For the accumulation of land masses it was assumed, that a tectonic recovery occurred, e.g. during Rodinia (570 Ma) and Pangäa (300 Ma) (Stanley, 1989; Torsvik, 2003). Considering that the ancient flood basalts and superplumes as well as oceanic crust production are not fully documented in the geological record, it is not surprising that periods of strong basaltic Sr release are not always accompanied by known magmatic events. The tectonic/volcanic values derived above reflect the release of isotopically depleted Sr from weathering volcanic rocks deposited on the continents and

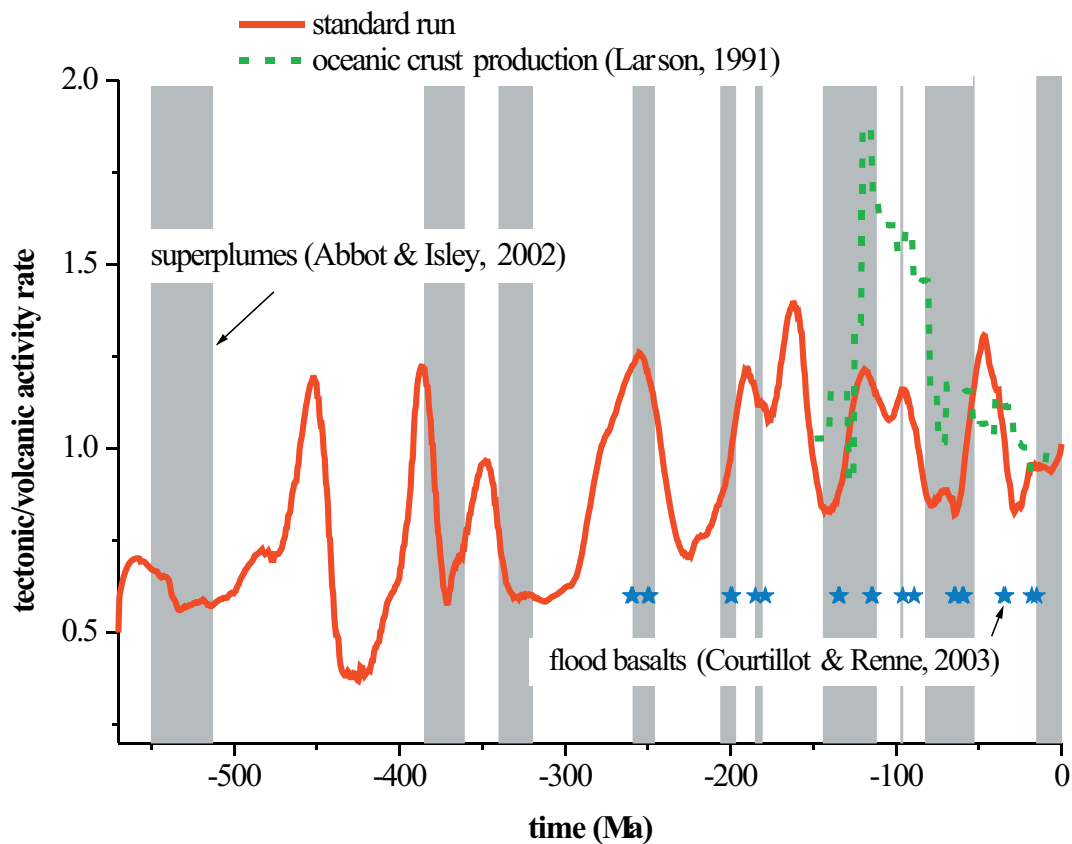


Figure 2.15: Changes in Phanerozoic volcanic and tectonic activity f_{vo} (solid line) in the standard case, calculated by using $^{87}\text{Sr}/^{86}\text{Sr}$ isotope data (Veizer et al., 1999), applying the data to equation 2.22. They are compared to the occurrence of superplumes (Abbott and Isley, 2002) (gray bars) and flood basalts (Courtillot and Renne, 2003) (stars), as well as to the production rate of oceanic crust (Larson, 1991) (dashed line).

basaltic basement rocks hydrothermal leached at submarine spreading centers. Thus they include the effect of volcanic activity both on land and on the seafloor. They cannot be used to distinguish between plum-related intraplate volcanism and spreading/subduction related volcanism occurring at active plate margins. Thus changes in spreading/subduction rate might differ from the reconstructed tectonic/volcanic values during periods of intense intraplate volcanism. Nevertheless, the changes in tectonic/volcanic activity reconstructed here from the marine $^{87}\text{Sr}/^{86}\text{Sr}$ record are arguably more valid than previously used proxies.

Figure 2.16 illustrates the prediction of the strontium isotope composition of non-silicate rocks and carbonate rocks subjected to weathering. The strontium isotope ratio of carbonate rocks decreases in an oscillating trend from Cambrian to Permian, followed by an increase up to the present value of $^{87}\text{Sr}/^{86}\text{Sr}=0.709$. The strontium ratio of non-volcanic silicate rocks was set to a constant value for the main part of the Phanerozoic and was increased at the Middle Paleocene up to the current value of 0.718 (Wallmann, 2001) (Fig. 2.16). Strontium mole fractions and the corresponding $^{87}\text{Sr}/^{86}\text{Sr}$ ratios in seawater, used for the prediction of ancient isotope strontium seawater inventory, were caused by non-volcanic silicate rock weathering (Φ_{S}^{87}), carbonate rock weathering (Φ_{WC}^{87}), and seawater (Φ_{SW}^{87}), with $\Phi_{\text{hy}}^{87}=0.06947$ and $^{87}\text{Sr}/^{86}\text{Sr}=0.704$ for hydrothermal fluids, and $\Phi_{\text{vo}}^{87}=0.06956$ and $^{87}\text{Sr}/^{86}\text{Sr}=0.705$ for volcanic deposits.

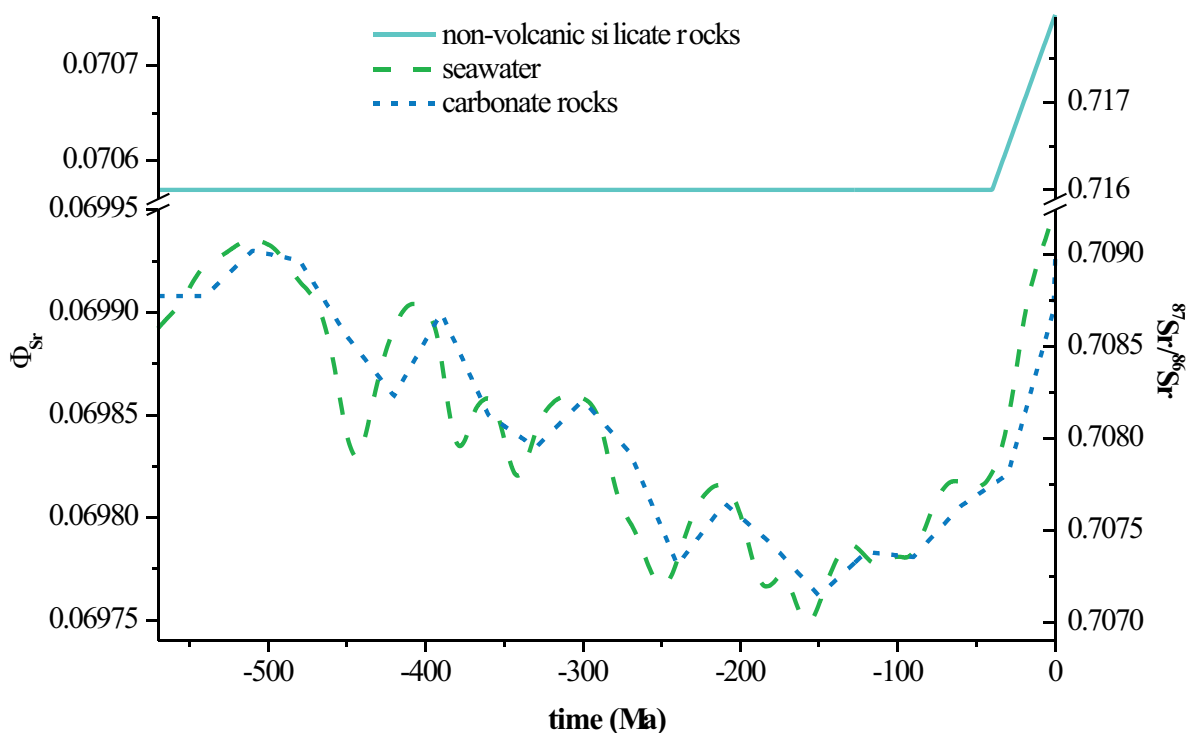


Figure 2.16: Changes in Phanerozoic strontium mole fractions (Φ) and the corresponding $^{87}\text{Sr}/^{86}\text{Sr}$ ratios in seawater used for the calculation of ancient strontium isotope seawater inventory, influenced by volcanic silicate rock weathering (Φ_{S}^{87}) (solid line), carbonate rock weathering (Φ_{WC}^{87}) (dotted line), and seawater (dashed line) (Φ_{SW}^{87}). (with $\Phi_{\text{hy}}^{87}=0.06947$ and $^{87}\text{Sr}/^{86}\text{Sr}=0.704$ for hydrothermal fluids, and $\Phi_{\text{vo}}^{87}=0.06956$ and $^{87}\text{Sr}/^{86}\text{Sr}=0.705$ for volcanic deposits).

2.4.5 Oxygen model

2.4.5.1 Standard case

Figure 2.17 shows the variation of the atmospheric partial pressure of oxygen (pO_2) during the Phanerozoic within a range between 0.17 and 0.35 atm. The low pO_2 during the Cambrian obtains a strong increase during the advent of the first land plants, a second increase up to the maximum pressure during the Carboniferous. After this height the pO_2 decreases with significant positive excursions in the Triassic and the Tertiary up to the atmospheric partial pressure of today (0.21 atm). The predicted pO_2 trend varies between a possible range of 0.17 - 0.35 atm, determined by burning experiments (Walker et al., 1981; Wildman et al., 2004), and agree with the general predictions for pO_2 trends of Bergman et al. (2004), Berner et al. (2003), and Kasting et al. (1979).

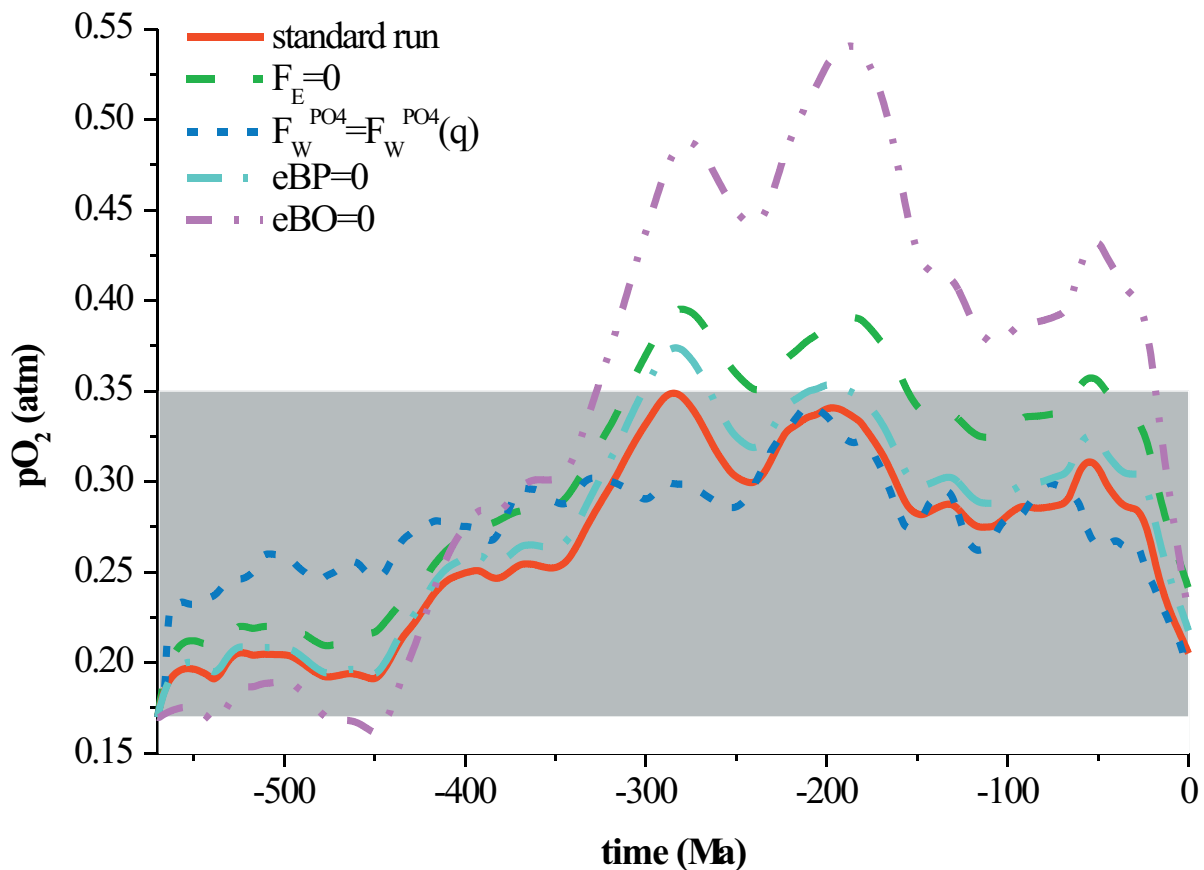


Figure 2.17: Changes in Phanerozoic atmospheric pO_2 in the standard case (solid line), compared to a run without sulfur degassing from volcanoes on land and arc volcanoes ($F_E=0$) (dashed line), to a run with constant phosphorus weathering on land ($F_W^{PO4}=F_W^{PO4}(q)$) (dotted line), to a run with an eliminated impact of pO_2 on sedimentary pyrite burial ($eBP=0$) (dashed & dotted line), and to a run with eliminated impact of pO_2 on particulate organic matter burial ($eBO=0$) (dashed & double dotted line). The shaded area represents the space between the predicted possible pO_2 concentrations (0.17 and 0.35) performed by Watson et al. (1978) and Wildman et al. (2004).

2.4.5.2 Sensitivity tests

Oxygen is consumed due to oxidation of sulfur emitted by volcanoes (Hansen and Wallmann, 2003). Figure 2.17 shows the increasing Phanerozoic pO_2 value, due to the prediction of eliminated sulfur emission by volcanoes on land and arc volcanoes. The predicted pO_2 of the case study increases during the Carboniferous up to 0.4 atm, 5 matm higher than in the standard case. The pO_2 affects the burial rates of particulate organic matter and burial of sedimentary pyrite, but due to oxygen consumption, particulate organic matter and sedimentary pyrite burial affects the pO_2 . Figure 2.17 shows the prediction of the pO_2 increase due to an eliminated coupling between POC as well as sedimentary pyrite burial and oxic-anoxic conditions. Both predictions show an increase in Phanerozoic pO_2 , whereas elimination of the coupling to the POC burial is of more significance, than the elimination of the coupling to the sedimentary pyrite burial. The latter one shows a small increase to the overall trend of up to 2 matm, whereas the previously predicted values increase up to a maximum of 0.55 atm. It should be mentioned the maximum value does not occur during the Cambrian, but 100 Ma later during the Triassic. Nevertheless, the three discussed predictions reflect the characteristics of the standard case, except for the particular displacement.

The prediction with an eliminated time-dependent phosphorus weathering flux ($F_w^{PO_4}=F_w^{PO_4}(q)$) shows a different Phanerozoic trend, the pO_2 increases during the Cambrian up to a concentration of 7.5 matm higher than the standard case. This prognosis did not show the sharp increase of the standard run due to the advent of land plants, its pressure change increases continuously up to the Permian. It reaches its maximum value during the Triassic, almost likewise the value of the standard case, afterwards it more or less follows the predictions of the standard case. These case tests illustrate the dependency of pO_2 to precipitation and dissolution processes. The dramatic impacts on pO_2 by different driving forces were buffered due to negative feedbacks between both participants, e.g. an enhanced pO_2 increase POC weathering, whereas POC weathering lowers the pO_2 .

2.5 Conclusions

The new record of evaporite turnover presented in this chapter covers the entire Phanerozoic and shows that evaporites are preferentially buried during warm periods while evaporite weathering prevails during cold periods. It confirms that evaporite cycling is controlled by the prevailing climatic conditions. It also indicates that the global inventory of evaporites increased over the Phanerozoic. As the concentration of NaCl in seawater is mainly controlled by the turnover of evaporites, this model result also suggests that the salinity of seawater probably decreased over the Phanerozoic.

My new Phanerozoic record of volcanic/tectonic activity shows distinct peaks during periods marked by a rapid decline in the seawater $^{87}Sr/^{86}Sr$ ratios. I applied the marine $^{87}Sr/^{86}Sr$ record to derive this record since the isotopic ratios of Sr in seawater are reliably documented in the geological record and because the marine $^{87}Sr/^{86}Sr$ record is closely coupled to the volcanic/tectonic activity

through the release of isotopically depleted Sr from mid-ocean ridges and young volcanic rocks. The new record shows a very poor correlation to the global sea-level curve suggesting that sea-level is a poor proxy for spreading and subduction rates.

The model shows that both the phosphate content and the productivity of the ocean have increased continuously over the Phanerozoic (Fig. 2.9c). This trend is neither observed in the burial of organic carbon nor in the marine $\delta^{13}\text{C}$ record showing that these parameters do not reliably reflect the ocean's changing productivity.

The marine $\delta^{34}\text{S}$ record is clearly determined by both volcanic and sedimentary processes while previous models often assumed that the evolution of seawater $\delta^{34}\text{S}$ values reflects the sedimentary cycling of sulfur, only. Hence, the marine $\delta^{34}\text{S}$ record should not be used as a proxy for the turnover of sedimentary pyrite and evaporites since changing rates of volcanic activity on land and at the seafloor also have a significant effect on the isotopic composition of seawater sulfate.

Atmospheric oxygen is more involved in both high-temperature and low-temperature geochemical processes than former tests suggest. It is stabilized by a number of negative feedbacks and strongly affects the chemical and isotopic composition of seawater and sedimentary rocks.

References

- Abbott D. H. and Isley A. E. (2002) The intensity, occurrence, and duration of superplume events and eras over geological time. *Journal of Geodynamics* 34, 265 - 307.
- Alt J. C., Shanks III W. C., and Jackson M. C. (1993) Cycling of sulfur in subduction zones: The geochemistry of sulfur in the Mariana Arc and back-arc trough. *Earth and Planetary Letters* 119, 477 - 494.
- Alt J. C. and Teagle D. A. H. (1999) The uptake of carbon during alteration of ocean crust. *Geochimica et Cosmochimica Acta* 63(10), 1527 - 1535.
- Archer D. E. (1996) An atlas of the distribution of calcium carbonate in sediments of the deep sea. *Global Biogeochemical Cycles* 10(1), 159-174.
- Bach W. and Edwards K. J. (2003) Iron and sulfide oxidation within the basaltic ocean crust: Implications for chemolithoautotrophic microbial biomass production. *Geochimica et Cosmochimica Acta* 67(20), 3871 - 3887.
- Berner E. K. and Berner R. A. (1996) *Global environment, water, air, and geochemical cycles.* Prentice - Hall, inc.
- Berner R. A. (1982) Burial of organic carbon and pyrite sulfur in the modern ocean: its geochemical and environmental significance. *American Journal of Science* 282, 451 - 473.
- Berner R. A. (1987) Models for carbon and sulfur cycles and atmospheric oxygen: application to Palaeozoic geologic history. *American Journal of Science* 287, 177 - 196.
- Berner R. A. (1994) GEOCARB II: A revised model of atmospheric CO₂ over Phanerozoic time. *American Journal of Science* 294, 56-91.
- Berner R. A. (1999) Atmospheric oxygen over Phanerozoic time. *Proceedings of the National Academy of Sciences of the United States of America* 96, 10955 - 10957.
- Berner R. A. (2004) The Phanerozoic carbon cycle: CO₂ and O₂.
- Berner R. A. and Canfield D. E. (1989) A new model for atmospheric oxygen over Phanerozoic time. *American Journal of Science* 289, 333-361.
- Berner R. A. and Kothavala Z. (2001) GEOCARB III: A revised model of atmospheric CO₂ over Phanerozoic time. *American Journal of Science*, 182-204.
- Carpenter S. J. and Lohmann K. C. (1997) Carbon isotope ratios of Phanerozoic marine cements: Re-evaluating the global carbon and sulfur Systems. *Geochimica et Cosmochimica Acta* 61(22), 4831 - 4846.
- Compton J., Mallinson D., Glenn C. R., Filipelli G., Föllmi K., Shields G., and Zanin Y. (2000) Variations in the global phosphorus cycle. *Marine Authogenesis: From Global to Microbial* 66, 21 - 33.
- Courtillot V. E. and Renne P. R. (2003) On the ages of flood basalt events. *Comptes Rendus Geosciences* 335, 113 - 140.
- Davis A. C., Bickle M. J., and Teagle D. A. H. (2003) Imbalance in the oceanic strontium budget. *Earth and Planetary Science Letters* 211(1 - 2), 173 - 187.

- Dessert C., Dupré B., Gaillardet J., Francois L. M., and Allègre C. J. (2003) Basalt weathering laws and the impact of basalt weathering on the global carbon cycle. *Chemical Geology* 202, 257 - 273.
- Gaillardet J., Dupré B., Louvat P., and Allègre C. J. (1999) Global silicate weathering and CO₂ consumption rates deduced from the chemistry of large rivers. *Chemical Geology* 159, 3-30.
- Gibbs M. T., Bluth G. J. S., and Fawcett P. J. (1999) Global chemical erosion over the last 250 my: Variations due to changes in palaeogeography, palaeoclimate, and palaeogeology. *American Journal of Science* 299, 611 - 651.
- Gordon W. A. (1975) Distribution by latitude of Phanerozoic evaporite deposits. *Journal of Geology* 83(6), 671 - 684.
- Graf H. F., Feichter J., and Langmann B. (1997) Volcanic sulfur emissions: Estimates of source strength and its contribution to the global sulfate distribution. *Journal of Geophysical Research* 102, 10727-10738.
- Halmer M. M., Schmincke H.-U., and Graf H.-F. (2002) The annual volcanic gas input into the atmosphere, in particular into the stratosphere: a global data set for the past 100 years. *Journal of Volcanology and Geothermal Research* 115, 511 - 528.
- Hansen K. W. and Wallmann K. (2003) Cretaceous and Cenozoic evolution of seawater composition, atmospheric O₂ and CO₂: A model perspective. *American Journal of Science* 303, 94 - 148.
- Hay W. W. (1998) Carbonate sedimentation through the late Precambrian and Phanerozoic. *Zentralblatt der Geologischen und Paläontologischen Vereinigung Teil 1*(Heft 5 - 6), 435 - 445.
- Hay W. W., Migdisov A., Balukhovskiy A. N., Wold C. N., Floegel S., and Soeding E. (2006) The decline in salinity of the ocean during the Phanerozoic: implications for climate, ocean circulation and life. *Marine Geology*.
- Hay W. W., Sloan J. L., and Wold C. N. (1988) Mass/age distribution and composition of sediments on the ocean floor and the global rate of sediment subduction. *Journal of Geophysical Research* 93(B12), 14933-14940.
- Hayes J. M., Strauss H., and Kaufman A. J. (1999) The abundance of ¹³C in marine organic matter and isotopic fractionation in the global biogeochemical of carbon during the past 800 Ma. *Chemical Geology* 161, 103 - 125.
- Horita J., Zimmermann H., and Holland H. D. (2002) Chemical evolution of seawater during the Phanerozoic: Implications from the record of marine evaporites. *Geochimica et Cosmochimica Acta* 66(21), 3733 - 3756.
- Jones C. E. and Jenkyns H. C. (2001) Seawater strontium isotopes, oceanic anoxic events, and seafloor hydrothermal activity in the Jurassic and Cretaceous. *American Journal of Science* 301, 112 - 149.

- Larson R. L. (1991) Latest pulse of Earth: Evidence for a mid-Cretaceous superplume. *Geology* 19, 547 - 550.
- Lenton T. M. and Watson A. J. (2000) Redfield revisited, 1. Regulation of nitrate, phosphate, and oxygen in the ocean. *Global Biogeochemical Cycles* 14(1), 225 - 248.
- Petsch S. T. and Berner R. A. (1998) Coupling the geochemical cycles of C, P, Fe, and S: The effect on atmospheric O₂ and the isotopic records of carbon and sulfur. *American Journal of Science* 298, 246-262.
- Rothman D. H. (2002) Atmospheric carbon dioxide levels for the last 500 million years. *Proceedings of the National Academy of Sciences of the United States of America* 99(7), 4167 - 4171.
- Shaviv N. J. and Veizer J. (2004) CO₂ as a primary driver of Phanerozoic climate: Comment. *Geological Society of America* 14(7), 18 - 22.
- Steuber T. and Veizer J. (2003) A Phanerozoic record of plate-tectonic control of seawater chemistry and carbonate sedimentation. *Geology* 30, 1123 - 1126.
- Strauss H. (1999) Geological evolution from isotope proxy signals - sulfur. *Chemical Geology* 161, 89 - 101.
- Veizer J., Ala D., Azym K., Bruckschen P., Buhl D., Bruhn F., Carden G. A. F., Diener A., Ebner S., Godderies Y., Jasper T., Korte C., Pawellek F., Podleha O. G., and Strauss H. (1999) ⁸⁷Sr/⁸⁶Sr, $\delta^{13}\text{C}$ and $\delta^{18}\text{O}$ evolution of Phanerozoic seawater. *Chemical Geology* 161, 59-88.
- Wallmann K. (1999) Die Rolle der Subduktionszonen im globalen Wasser- und Kohlenstoffkreislauf. Habilitation, Christian-Albrechts-Universität.
- Wallmann K. (2001a) Controls on the Cretaceous and Cenozoic evolution of seawater composition, atmospheric CO₂ and climate. *Geochimica et Cosmochimica Acta* 65(18), 3005 - 30025.
- Wallmann K. (2001b) The geological water cycle and the evolution of marine $\delta^{18}\text{O}$ values. *Geochimica et Cosmochimica Acta* 65(15), 2469 - 2485.
- Wallmann K. (2004) Impact of atmospheric CO₂ and galactic cosmic radiation on Phanerozoic climate change and the marine $\delta^{18}\text{O}$ record. *Geochemistry, Geophysics, Geosystem, an electronic journal of the Earth sciences* 5(1), 30.
- Watson A. J., Lovelock J. E., and Margulis L. (1978) Methanogenesis, fires, and the regulation of atmospheric oxygen. *Biosystems* 10, 293-298.
- Wheat C. G., Feely R. A., and Mottl M. J. (1996) Phosphate removal by oceanic hydrothermal processes: An update of the phosphorus budget in the oceans. *Geochimica et Cosmochimica Acta* 60(16), 3593 - 3608.
- Wildman J. R. A., Hickey L. J., Dickinson M. B., Berner R. A., Robinson J. M., Dietrich M., Essenhigh R. H., and Wildman C. B. (2004) Burning of forest materials under late Paleozoic high atmospheric oxygen levels. *Geological Society of America* 32(5), 457 - 460.

Appendix

Appendix A2.1: Fluxes of carbon, strontium, oxygen, phosphorus, and sulfur (10^{18} mol Ma^{-1} , 10^{16} mol Ma^{-1} for Sr, mol/kg for concentration) considered in the Box Model.

Description	Equation
C input into the ocean	$F_{Cin} = F_M + F_{SC} + F_{MC} + F_{WC} + F_{WO} + F_{EO} - F_{BO}$
Ca fixation during crust alteration	$F_{ALT} = \frac{CO(rec)}{CO} * (r_{ALT} * (f_{VO} - 1) + 1) * F_{ALT}(q)$
CaCO ₃ subduction into the mantle	$F_{SM} = f_{VO} * k_{SC} * CO * (1 - r_S)$
Carbonate accumulation	$F_{BC} = k_{BC} * \frac{cCa * Co_3}{K_d^{SP}} - 1$
Carbonate accumulation on continental crust	$F_{BCC} = f_{BCC} * F_{BC}$
Carbonate accumulation on oceanic crust	$F_{BCO} = (1 - f_{BCC}) * F_{BC}$
Carbonate weathering	$F_{WC} = f_{ER}^{eWC} * f_{BB}CO_2 * f_{LA} * f_D * f_{AN} * k_{WC} * CC$
CO ₂ exchange between ocean and atmosphere	$F_{EX} = k_{EX} * (pCO_2^{SW} - pCO_2^{atm})$
CO ₂ release during metamorphism of continental carbonates	$F_{MC} = k_{MC} * CC$
CO ₂ release from subducted CaCO ₃	$F_{SC} = f_{VO} * r_S * k_{SC} * CO$
CO ₂ release from subducted POC	$F_{EO} = f_{VO} * k_{EO} * POC * f_{ER}^{eWO}$
CO ₂ release via mantle degassing	$F_M = f_{VO} * F_M(q)$
POC burial	$F_{BO} = F_{BOland} + F_{BOsea}$
POC burial at the sea floor	$F_{BOsea} = F_{Bsea}^{PO_4} * 106 * RO_2$
POC burial on land	$F_{BOland} = F_{Bland}^{PO_4} * 450$
POC flux into subduction zones	$F_{SZO} = f_{VO} * k_{SZO} * POC * f_{ER}^{eWO}$
POC weathering	$F_{WO} = f_{ER}^{eWO} * k_{WO} * POC * f_A * RO_2$
Silicate weathering	$F_{WS} = f_B CO_2 * f_D^{0.65} * f_{AN} * f_{ER}^{eWS} * (F_{WS}^{VO}(q) * (f_{VO} * (f_{VO} - 1) + 1) + F_{WS}^S(q))$
O ₂ consumption due to oxidation of Fe ²⁺ during oceanic crust alteration	$F_{Fe}^O = f_{VO} * F_{Fe}(q)$
O ₂ consumption due to pyrite weathering	$F_{WP}^O = Z_{15/8} * F_{WP}$
O ₂ consumption during oxidation of SO ₂ emitted from intraplate volcanoes and H ₂ S and SO ₂ emitted from spreading centers	$F_S^O = F_E * (Z_{1/2} + r_{1/2} * Z_{1/2} + (1 - r_{1/2}) * Z_2)$
O ₂ release during pyrite burial	$F_{BP}^O = Z_{15/8} * F_{BP}$
Net evaporite burial	$netF_{BE} = (cSO_4 - (cSO_4)_{DAT}) * k_{BE}$
Pyrite accumulation	$F_{BP} = F_{BOsea} * r_{BOAN} * \left(\frac{S}{C}\right)_M * \left(\frac{1}{RO_2}\right)^{eBP} * RSO_4^{eBS}$
Pyrite weathering	$F_{WP} = f_A * f_{ER}^{eWP} * F_{WP}(rec) * 0.5^{eWP}$

Appendix A2.1: Continued

Description	Equation
Dissolved phosphorus loss at hydrothermal plumes	$F_{Hy}^{PO_4} = F_{Hy}^{PO_4}(q) * f_{VO} * RPO_4$
Dissolved phosphorus released due to weathering	$F_W^{PO_4} = \frac{F_{WO} + F_{WS} + F_{WC}}{F_{WO}(q) + F_{WS}^S(q) + F_{WS}^{VO}(q) + F_{WC}(q)} * F_W^{PO_4}(q)$
Organic P burial in marine sediments	$F_{Bsea}^{PO_4} = k_B^{PO_4} * PO_4$
Organic P burial on land	$F_{Bland}^{PO_4} = f_{ER} f_{coal} * f_{PO_4} * F_W^{PO_4}$
P buried in authigenic CFA	$F_{BCa}^{PO_4} = F_{BCa}^{PO_4}(q) * (117 * PO_4)^2$
P sorbed on iron and manganese oxides	$F_{BFe}^{PO_4} = F_{BFe}^{PO_4}(q) * \frac{1 - anox}{0.86}$
⁸⁷ Sr release during silicate weathering	$F_{WS}^{87} = f_B CO_2 * f_D^{0.65} * f_{AN} * f_{ER}^{eWS} * \left(\Phi_{VO}^{87} * F_{WS}^{VO}(q) * (f_{VO} * (f_{VO} - 1) + 1) + \Phi_S^{87} * F_{WS}^S(q) \right)$
Sr release at spreading centers	$F_{Hy}^{Sr} = f_{VO} * F_{Hy}^{Sr}(q)$
Sr release during carbonate weathering	$F_{WC}^{Sr} = r_{Sr} * 100 * F_{WC}$
Sr release during silicate weathering	$F_{WS}^{Sr} = f_B CO_2 * f_D^{0.65} * f_{AN} * f_{ER}^{eWS} * \left(F_{WS}^{SrVO}(q) * (f_{VO} * (f_{VO} - 1) + 1) + F_{WS}^{SrS}(q) \right)$
Sr removal from the seawater	$F_B^{Sr} = k_B^{Sr} * \left(\frac{Sr}{Ca_{DAT}} - \frac{Sr_{DAT}}{Ca_{DAT}} \right)$

Appendix A2.2: Variables used in the definition of carbon, strontium, oxygen, phosphorus, and sulfur fluxes considered in the box model.

Description	Equation
¹³ C mole fraction of TC	$\Phi^{13C} = \frac{^{13}TC}{TC}$
¹³ C ratio during POC accumulation	$R^{POC} = \left(\frac{\delta^{13C} + \Delta POC_H + 1}{1000} \right) * RPDB$
¹³ C ratio of buried CaCO ₃	$R^C = \left(\frac{\delta^{13C}}{1000} + 1 \right) * RPDB$
Carbonate alkalinity at the surface of ocean (mol/kg)	$CA^S = CA^d - 0.1 * DC$
Carbonate alkalinity in the deep ocean (mol/kg)	$CA^d = CA * con$
Carbonate ion concentration in seawater (mol/kg)	$CO_3 = \frac{CA^d * (K_1^d - 4 * K_2^d) - K_1^d * TC^d + \sqrt{K_1^d * (CA^d * (K_1^d - 4 * K_2^d)) * (CA^d - 2 * TC^d) + K_1^d * TC^{d^2}}}{2 * (K_1^d - 4 * K_2^d)}$
CO ₂ effect on weathering after the appearance of vascular land plants	$f_{CO_2}^a = 1 - \frac{1}{1 + e^{-\frac{t+325}{5}}}$
CO ₂ effect on weathering before the appearance of vascular land plants	$f_{CO_2}^b = \frac{1}{1 + e^{-\frac{t+325}{5}}}$
CO ₂ influence on weathering	$f_{CO_2} = f_{CO_2}^b * RCO_2^{0.5} + f_{CO_2}^a * \left(\frac{2 * RCO_2}{1 + RCO_2} \right)^{0.4}$
Isotopic fractionation during POC burial	$\Delta POC = \Delta POC_H + 1 - G * \frac{O}{38 * 10^{18}}$
Mole fraction of ¹³ C in marine carbonates subject to weathering, metamorphism and subduction	$\Phi^{13C}_{in} = \frac{1000 + \delta^{13}CaCO_3}{89990 + \delta^{13}CaCO_3}$
Mole fraction of ¹³ C in POC buried at the sea floor	$\Phi^{13}_{POC} = \frac{\alpha_{POC} * \Phi^{13}C}{\alpha_{POC} * \Phi^{13}C + 1 - \Phi^{13}C}$
Mole fraction of ¹³ C in POC subject to weathering, metamorphism and subduction	$\Phi^{13}C_{POC_{in}} = \frac{1000 + \delta^{13}POC}{89990 + \delta^{13}POC}$
pCO ₂ in surface waters	$pCO_2^{SW} = \frac{K_1^S * (TC^S - CA^S) - K_2^S * (4 * CA^S - 8 * TC^S) + \sqrt{K_1^S * (CA^S * (K_1^S - 4 * K_2^S)) * (CA^S - 2 * TC^S) + K_1^S * TC^{S^2}}}{2 * K_0 * (K_1^S - 4 * K_2^S)}$
pCO ₂ influence on carbonate weathering	$f_{BB}CO_2 = f_C(T) * f_{CO_2}$
pCO ₂ influence on silicate weathering	$f_BCO_2 = f_S(T) * f_{CO_2}$
pCO ₂ normalized on the recent value in atmosphere	$RCO_2 = \frac{CO_2}{CO_2(q)}$
pH in deep waters	$pH^d = -\log \left(\frac{K_1^d * (TC^d - CA^d) + \sqrt{K_1^d * (CA^d * (K_1^d - 4 * K_2^d)) * (CA^d - 2 * TC^d) + K_1^d * TC^{d^2}}}{2 * CA^d} \right)$

Appendix A2.2: Continued

Description	Equation
Sr/Ca ratio in seawater	$R_{Ca}^{Sr} = \frac{cSr}{cCa}$
Total dissolved carbon concentration in deep waters (mol/kg)	$TC^d = TC * con$
Total dissolved carbon concentration in surface waters (mol/kg)	$TC^S = TC^d - \Delta C$
$\delta^{13}C$ in seawater	$\delta^{13}C = \frac{88990 * \Phi^{13}C}{1 - \Phi^{13}C} - 1000$
Anoxic fraction in the oceans	$anox = 1 - 0.86 * RO_2 * 117 * PO_4$
pO_2 dependent fractionation factor for pyrite accumulation	$O_{38}^{eBP} = \left(\frac{O}{38 * 10^{18}} \right)^{eBP}$
pO_2 in ocean and atmosphere (ppmV)	$pO_2 = \frac{O}{181.4 * 10^{18}}$
pO_2 normalized on the recent value in atmosphere	$RO_2 = \frac{O_2}{O_2(q)}$
^{34}S isotopic ratio of evaporites buried on the continental crust	$R^{BE} = \left(\frac{\delta^{34}SO_4 + \Delta_{BE}}{1000} + 1 \right) * RCDT$
^{34}S isotopic ratio of seawater	$R^{SO_4} = \left(\frac{\delta^{34}SO_4}{1000} + 1 \right) * RCDT$
^{34}S mole fraction of evaporites deposited on continental crust	$\Phi_{BE} = \frac{\alpha_{BE} * \Phi_{SO_4}}{\alpha_{BE} * \Phi_{SO_4} + 1 - \Phi_{SO_4}}$
^{34}S mole fraction of pyrite buried in sediments	$\Phi_{BP} = \frac{\alpha_{BP} * \Phi_{SO_4}}{\alpha_{BP} * \Phi_{SO_4} + 1 - \Phi_{SO_4}}$
^{34}S mole fraction of seawater	$\Phi_{SO_4} = \frac{\delta^{34}SO_4}{SO_4}$
$\delta^{34}S$ of accumulated sedimentary pyrite	$\delta^{34}S_{BP} = \frac{22220 * \Phi_{BP} - 1000}{1 - \Phi_{BP}}$
$\delta^{34}S$ value of seawater	$\delta^{34}S_{SW} = \frac{22220 * \Phi_{SO_4} - 1000}{1 - \Phi_{SO_4}}$
P normalized on the recent value in oceans	$RPO_4 = \frac{PO_4}{PO_4(q)}$
^{87}Sr ratio in seawater	$R^{87}SW = \frac{9.43 + \Phi^{87}SW}{1 - \Phi^{87}SW}$
Mole fraction of ^{87}Sr in seawater	$\Phi_{SW}^{87Sr} = \frac{^{87}Sr}{Sr}$
Mole fraction of ^{87}Sr in weathering carbonate rocks	$\Phi_{WC}^{87Sr} = \frac{R^{87}Sr_{WC}^{CaCO_3}}{9.43 + R^{87}Sr_{WC}^{CaCO_3}}$
Mole fraction of ^{87}Sr released during the	$\Phi_{VO}^{87Sr} = \frac{R^{87}Si}{9.43 + R^{87}Si}$

Appendix A2.2: Continued

Description	Equation
Conversion from 10^{18} mol in concentration (mol/kg)	$con = \frac{10^{18} * 1.024}{Volume_{seawater}}$
Global average surface temperature	$Temp_s = \Gamma * \ln(RCO_2) - W_s * \left(\frac{-t}{570}\right) + T(q) + GEOG$
Temperature influence on carbonate weathering	$f_C(T) = 1 + 0.087 * (T - T(q))$
Temperature influence on silicate weathering	$f_S(T) = e^{0.09 * (T - T(q))} * (1 + RUN * (T - T(q)))^{0.65}$
Temperature prevailing at the saturation level, related to the surface temperature	$Temp_d = Temp_s - \Delta T$

Appendix A2.3: Quaternary parameter ranges used in the definition of carbon, strontium, oxygen, phosphorus, and sulfur fluxes considered in the box model, with the value used for the standard run.

Parameter / constant	Description	Range	Reference	Value
CC(q)	Quaternary value for carbonates on continental crust (10^{18} mol)	-	Berner (1987)	3000
CO(rec)	Recent value CaCO_3 in and on oceanic crust (10^{18} mol Ma^{-1})	1000 - 1200	Berner (2004)	1200
$F_{\text{ALT}}(\text{q})$	Quaternary rate of crust alteration (10^{18} mol Ma^{-1})	1.5 - 2.4	Wallmann (2001a)	2
$F_{\text{BCO}}(\text{q})$	Quaternary carbonate accumulation (10^{18} mol Ma^{-1})	10 - 11	Archer (1996)	10.5
$F_{\text{BO}}(\text{q})$	Quaternary rate of POC burial (10^{18} mol Ma^{-1})	5 - 10	Wallmann (2001a)	6
$F_{\text{WS}}^{\text{S}}(\text{rec})$	Recent CO_2 consumption during weathering of silicate rocks (10^{18} mol Ma^{-1})	5.85 - 11.7	Gaillardet et al. (1999)	10
$F_{\text{WS}}^{\text{VO}}(\text{rec})$	Recent CO_2 consumption during weathering of volcanic deposits (10^{18} mol Ma^{-1})	-	Dessert et al. (2003)	4.08
$\text{pCO}_2(\text{q})$	Quaternary partial pressure of carbon dioxide (atm)	-	Berner (2004)	0.00023
POC(q)	Quaternary POC mass on continental and oceanic crust (10^{18} mol)	-	Berner (1982)	1250
$\text{O}_{\text{Fe}}(\text{q})$	Quaternary O_2 consumption due to oxidation of Fe^{2+} during oceanic crust alteration (10^{18} mol Ma^{-1})	0.1 - 0.9	Bach and Edwards (2003)	0.5
$\text{pO}_2(\text{q})$	Quaternary partial pressure of oxygen (atm)	-	Berner (1999)	0.21
$F_{\text{BP}}(\text{q})$	Quaternary rate of pyrite burial (10^{18} mol Ma^{-1})	0.55 - 1.08	Wallmann (2001a)	1.08
$F_{\text{E}}(\text{q})$	Quaternary S release due to volcanic emission (10^{18} mol Ma^{-1})	0.29 - 0.85	Graf et al. (1997)	0.3
$F_{\text{H}_2\text{S}}(\text{q})$	Quaternary H_2S release at spreading centers (10^{18} mol Ma^{-1})	0.055 - 0.244	Alt et al. (1993)	0.15
$F_{\text{BCa}}^{\text{PO}_4}(\text{q})$	Quaternary burial of CFA at sea-floor (10^{18} mol Ma^{-1})	-	Lenton and Watson (2000)	0.015
$F_{\text{BFePO}_4}(\text{q})$	Quaternary burial of P in sedimentary iron-manganese-oxides (10^{18} mol Ma^{-1})	-	Lenton and Watson (2000)	0.006
$F_{\text{BHy}}^{\text{PO}_4}(\text{q})$	Quaternary loss of dissolved phosphorus at hydrothermal plumes (10^{18} mol Ma^{-1})	0.0119 - 0.0161	Wheat et al. (1996)	0.012
$F_{\text{Borg}}^{\text{PO}_4}(\text{q})$	Quaternary rate of organic phosphorus burial (10^{18} mol Ma^{-1})	-	Lenton and Watson (2000)	0.015
$F_{\text{W}}^{\text{PO}_4}(\text{q})$	Quaternary dissolved phosphorus, riverine and eolian input into the ocean via weathering (10^{18} mol Ma^{-1})	0.026 - 0.155	Compton et al. (2000)	0.08
$F_{\text{HY}}^{\text{Sr}}(\text{q})$	Quaternary release of Sr at spreading centers (10^{16} mol Ma^{-1})	0.5 - 1.5	Davis et al. (2003)	1.45
T(q)	Quaternary average global temperature ($^{\circ}\text{C}$)	-	Wallmann (2001b)	13.5

Chapter III

**A model of atmospheric methane over
the entire Phanerozoic**

Abstract

A simple geochemical box model for the global cycle of methane (CH_4) has been developed and applied to reconstruct the evolution of atmospheric methane over the entire Phanerozoic. According to the model, the partial pressure of atmospheric methane ($p\text{CH}_4$) increased up to approx. 10 ppmV during the Carboniferous coal swamp era. This implies a maximum radiative forcing of about 3.5 W m^{-2} via methane. By its radiative forcing and due to its decomposition into CO_2 , methane caused an increase of the average global surface temperature by up to 1°C during the Permian-Carboniferous. The elevated $p\text{CH}_4$ values during the Permian-Carboniferous cold period may have moderated the temperature decline caused by the coeval draw-down of atmospheric CO_2 . Both the decrease in $p\text{CO}_2$ and the increase in $p\text{CH}_4$ are intimately linked to the spread of land plants during the Permian and Carboniferous. The high methane emissions from swamps during this period may have prevented the development of a “snowball earth” state repeatedly encountered during the Precambrian prior to the advent of land plants. Additional runs with a global carbon model indicate that the heating induced by elevated $p\text{CH}_4$ favored the draw-down of atmospheric $p\text{CO}_2$ via enhanced rates of silicate weathering. The effects of episodic gas hydrate decomposition were investigated using an extended model simulating the evolution of $\delta^{13}\text{C}$ values in seawater and marine carbonates. These model runs confirm that the negative $\delta^{13}\text{C}$ excursions documented in the geological record were indeed accompanied by a significant increase in atmospheric $p\text{CH}_4$ and $p\text{CO}_2$ values.

3.1 Introduction

Migeotte (1948) was one of the first who identified methane (CH_4) in the atmosphere by its infrared absorption band in the solar spectrum. CH_4 is the most abundant hydrocarbon gas in the atmosphere and plays an important role in climate regulation (Seinfeld and Pandis, 1998). It probably was one of the greenhouse gases, emitted by methanogenic bacteria, which warmed the early Earth's surface to unexpected high temperatures (Pavlov et al., 2000). Being a greenhouse gas, CH_4 molecules do not interact with short-wave radiation, such as UV-radiation, but trap reflected outgoing long-wave radiation from the Earth's surface (Fogg, 2003). Thus the troposphere gets warmer while the methane content increases - the direct effect of CH_4 on the average global temperature (Lelieveld et al., 1998). Furthermore an increase in tropospheric CH_4 enhances the partial pressures of carbon dioxide and water vapor in the stratosphere and the tropospheric ozone concentration (Blake and Rowland, 1988). These changes force additional global warming (Harvey, 1993) - the indirect effect of CH_4 on the average global temperature (Gassmann, 1994). Thus Methane both affects climate and is affected by climate. Moreover CH_4 plays an important role in the global organic carbon cycle (Kvenvolden, 2002).

Data from ice cores illustrate an increase in atmospheric CH_4 concentration due to human activity (Dickinson and Cicerone, 1986). Human activities like agriculture, livestock domestication,

and biomass burning triggered the initial increase in atmospheric CH₄. The following industrialization and the resulting air pollution have reinforced this trend. Isotopic composition (Graedel and Crutzen, 1995) and spatial distribution confirm that two third of the present annual emissions are of anthropogenic origin (IPCC, 2001).

Except for the anthropogenic emission, CH₄ is emitted from waterlogged soils, by termites, out of the oceans and the sea-floor, from shallow water regions of the oceans, out of lakes (Berner and Berner, 1996), as well as from magmatic and mud volcanoes (Ehhalt, 1974). In pre-human times, wetlands, particularly swamps and peat, were the prime emitters. In times of reduced terrestrial plant coverage, mud volcanoes might have been the most important source (Kopf, 2003). Furthermore, a sudden catastrophic release of methane caused by the thermal decomposition of gas hydrates might have happened occasionally and could have changed the global atmospheric methane concentration significantly. This kind of eruption may have triggered a global climate warming (Jiang et al., 2003) and/or “snowball” Earth glaciations (Schrag et al., 2002) in the geological past. Negative carbon-isotope excursions ($\delta^{13}\text{C}$) which were found in fossil benthic foraminifera and the remains of other calcareous organisms during several Phanerozoic events (Beerling et al., 2002; Bice and Marotzke, 2002; Hesselbo et al., 2000; Jahren et al., 2001; Jahren et al., 2005; Kennett et al., 2000; Kirschvink and Raub, 2003; Padden et al., 2001; Ryskin, 2003) may reflect a massive injection of ¹²C depleted methane into oceans and atmosphere. It should, however, be considered that alternative mechanisms such as the thermogenic decomposition of sedimentary organic matter due to intrusion of mantle derived melts have been evoked to explain these negative carbon-isotope excursions (Svensen et al., 2004).

Methane is produced during the decomposition of organic matter of both animal and herbal origin. Cleavage of polymeric into monomer organic matter and the fermentative transformation by microorganisms produce simple compounds, such as hydrogen, carbon dioxide, formic acid, acetic acid, methanol, and methylamine (Stanley, 1989). Methanogenic archaea represent the end of the anaerobic respiratory chain and transform the mentioned substrates into gaseous CH₄ and CO₂ (Graedel et al., 1986). Methanogenesis occurs only in anoxic environments, such as swamps, marshes, wetlands, peat lands, anoxic marine sediments, permafrost soils, bottoms of freshwater lakes with a high sedimentation rate, and the digestive tract of herbivores and insects (Berner and Berner, 1996; Ehhalt, 1974). Methane production is suppressed in the presence of dissolved sulfate. Hence, marine environments - where seawater sulfate is abundant - tend to have lower methane production rates than freshwater environments with lower sulfate contents. Rates of methanogenesis depend on the prevailing temperature, the amount of organic matter, the metabolic activity of anoxic microorganisms and the aerial extent as well as the temporal duration of anoxic conditions in certain terrestrial environments (Fey et al., 2004). The abiologically produced CH₄ can be neglected, since only a small part of the emitted CH₄ is caused by thermal breakdown or by volcanism. The latter process contributes less than 1 % to the total release (Ehhalt and Heidt, 1973). Most of the natural methane emission into the atmosphere is driven by biological activity.

Because of the impact of atmospheric CH₄ on climate (Lelieveld et al., 1998) on both long

and on short time scales, several models for the global CH₄ cycle have been developed. These include models addressing tropospheric CH₄ oxidation (Jacob, 2000), modern atmospheric CH₄ change (Dlugokencky et al., 1998), the future evolution of atmospheric CH₄ (Dickinson and Cicerone, 1986), and Precambrian pCH₄ levels (Pavlov et al., 2003).

In this chapter I attempt the first reconstruction of the atmospheric CH₄ level over the entire Phanerozoic (570 Ma) with the main focus on biological sources and on sudden methane emissions by collapsing gas hydrates. With my new model I also evaluate the possible effects of methane on Phanerozoic climate evolution.

3.2 Set-up of the methane model

The box model presented in this chapter is built on previous models of the global carbon cycle (Wallmann, 2001a; Wallmann, 2004) and an updated version of these models developed by the author (Bartdorff and Wallmann, submitted). New parameterizations are introduced to simulate the global methane cycle. Hence, fluxes of methane into the atmosphere are related to external parameters such as changes in land area, plant coverage and volcanic/tectonic activity. The influence of sudden methane release from dissociating gas hydrates is tested and evaluated using the $\delta^{13}\text{C}$ values recorded in the carbonate shells of marine fossils (Hayes et al., 1999). A simple model of atmospheric methane oxidation is included to calculate, finally, the atmospheric partial pressures of methane over the Phanerozoic and the radiative forcing induced by this greenhouse gas. A complete description of all model equations and parameters is given in the Appendix.

3.2.1 Sources of atmospheric methane

Atmospheric CH₄ is mainly released from biological sources hosted in terrestrial environments. Our understanding of atmospheric methane cycling is, however, to a large extent limited by a poor quantification of these sources.

3.2.1.1 Wetlands

Wetlands are the main natural sources of atmospheric CH₄. Coals are formed from plant material deposited in swamps and terrestrial wetland. Coals and coal basin sediments - which are preserved in the geological record - are, thus, a proxy for the abundance of methane-producing wetlands in the past.

Ronov (1993) investigated the abundance of terrigenous sedimentary rocks, including coal basin sediments, deposited over the various periods of the Phanerozoic and preserved till today (S_p).

These data were later updated and re-compiled by W. W. Hay (personnel communication) and applied by Berner and Kothavala (2001) and Berner (2004). It should, however, be considered that a large fraction of the initially deposited sediments was not preserved but converted into metamorphic rocks and lost by erosion and subduction. Previous studies on sedimentary rock cycling showed that this loss follows a simple first order decay law (Veizer and Jansen, 1979). Hence, the initial terrigenous sedimentation rate S_i was calculated as (Wallmann, 2001a):

$$S_i = S_p \cdot e^{b \cdot t}, \quad (3.1)$$

using the S_p values listed in Berner and Kothavala (2001) while the decay constant (b) was set to the value $5 \times 10^{-3} \text{ Ma}^{-1}$ previously derived by Gregor (1985) and Wallmann (2001a). The resulting S_i values plotted in Fig. 3.1a were then multiplied with the fraction of terrigenous sediments deposited in coal basins (Fig. 3.1b) taken from Berner (2004) to calculate the accumulation rate of coal basin sediments over the Phanerozoic. These values were finally normalized to the values derived for the most recent period considered in Ronov's compilations (the Pliocene) to calculate the relative change in coal basin sedimentation over the Phanerozoic ($f_{ER} f_{coal}$, Fig. 3.1c).

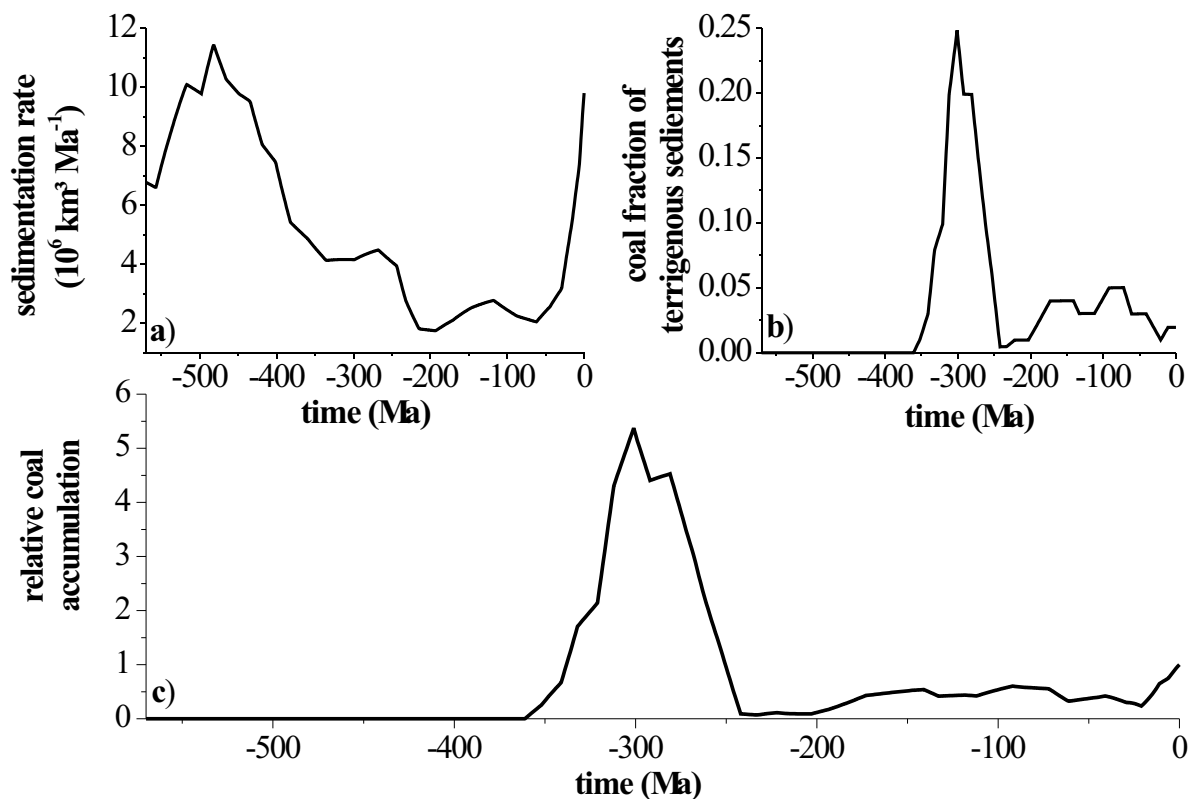


Figure 3.1a-c: Changes in a) Sedimentation rate (Berner, 2004), b) coal fraction of terrigenous sediments (Berner and Kothavala, 2001), c) relative coal accumulation derived from a) and b) and normalized (see text).

Christensen et al. (2003) investigated the CH_4 production in wetlands at different temperatures. Their data show an exponential growth in the production rate of CH_4 with increasing temperature (Fig. 3.2a). I normalized this exponential dependency to the Quaternary average global temperature of about 13.5°C (Wallmann, 2001b) to describe the relative influence of ambient temperature on the CH_4 emission from waterlogged soils. I chose a simple exponential function to describe this dependency (Fig. 3.2b). Thus the dimensionless temperature-dependent parameter (f_{Wetland}) for CH_4 production out of waterlogged soils can be described as:

$$f_{\text{Wetland}} = 0.111 * \exp^{0.1635 * \text{Temp}}, \quad (3.2)$$

where the exponent Temp is the time-dependent global average surface temperature (Fig. 3.3a) over the Phanerozoic calculated by Bartdorff and Wallmann (submitted). For the average Quaternary surface temperature this equation yields a value of unity so that f_{Wetland} can be applied to calculate the effect of temperature change on methane emissions from wetlands with respect to the recent temperature.

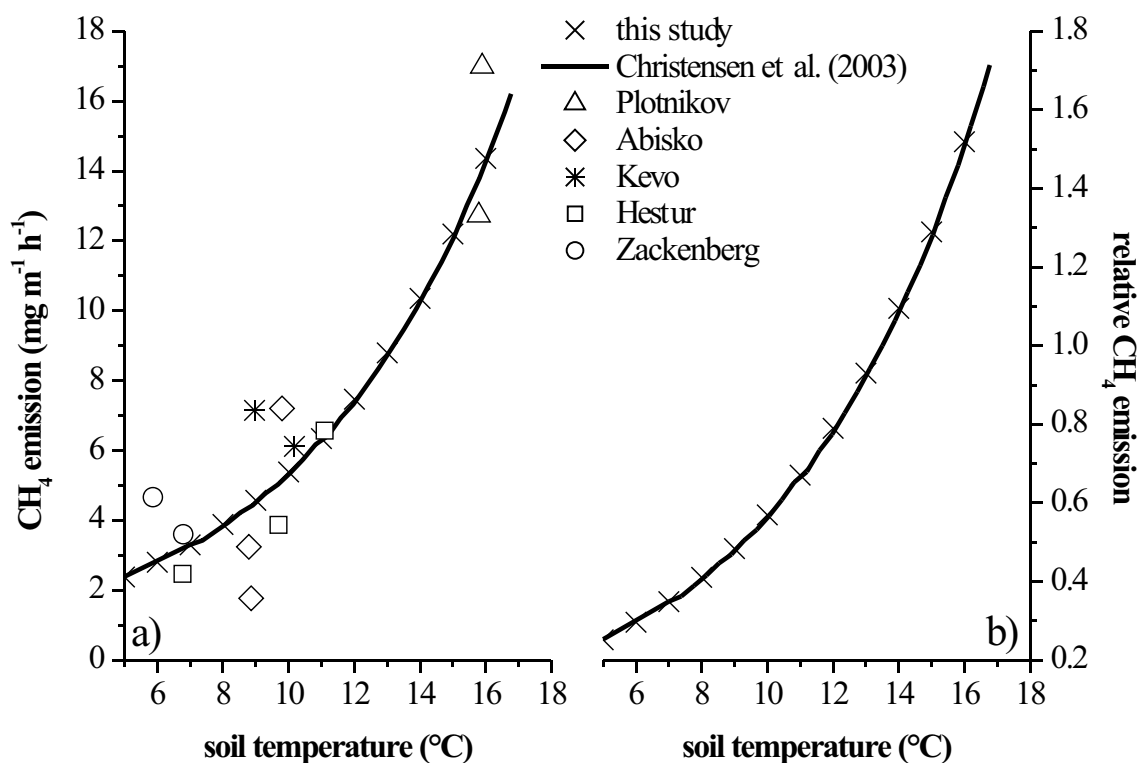


Figure 3.2a-b: Dependency of CH_4 emission from waterlogged soils on the surrounding temperature a) according to Christensen et al. (2003), b) normalized on the Quaternary average global temperature (13.5°C , Wallmann (2001)) which was used as an exponential expression for the calculation of temperature dependent CH_4 emission from wetlands, with “1” at temperature 13.5°C in equation 3.2.

The CH_4 production in ancient wetlands ($F_{\text{wetland}}^{\text{CH}_4}$) is calculated using the previously derived change in coal basin sedimentation ($f_{\text{ER}} f_{\text{coal}}$), the parameter f_{Twetland} describing the effect of temperature on the methane release from wetlands, and the recent CH_4 production rate of waterlogged soils and swamps ($F_{\text{wetland}}^{\text{CH}_4}(q)$):

$$F_{\text{wetland}}^{\text{CH}_4} = F_{\text{wetland}}^{\text{CH}_4}(q) * f_{\text{ER}} f_{\text{coal}} * f_{\text{Twetland}} \quad (3.3)$$

The modern value is estimated to fall into the range of 55 to 150 Tg $\text{CH}_4 \text{ yr}^{-1}$ according to Seinfeld and Pandis (1998).

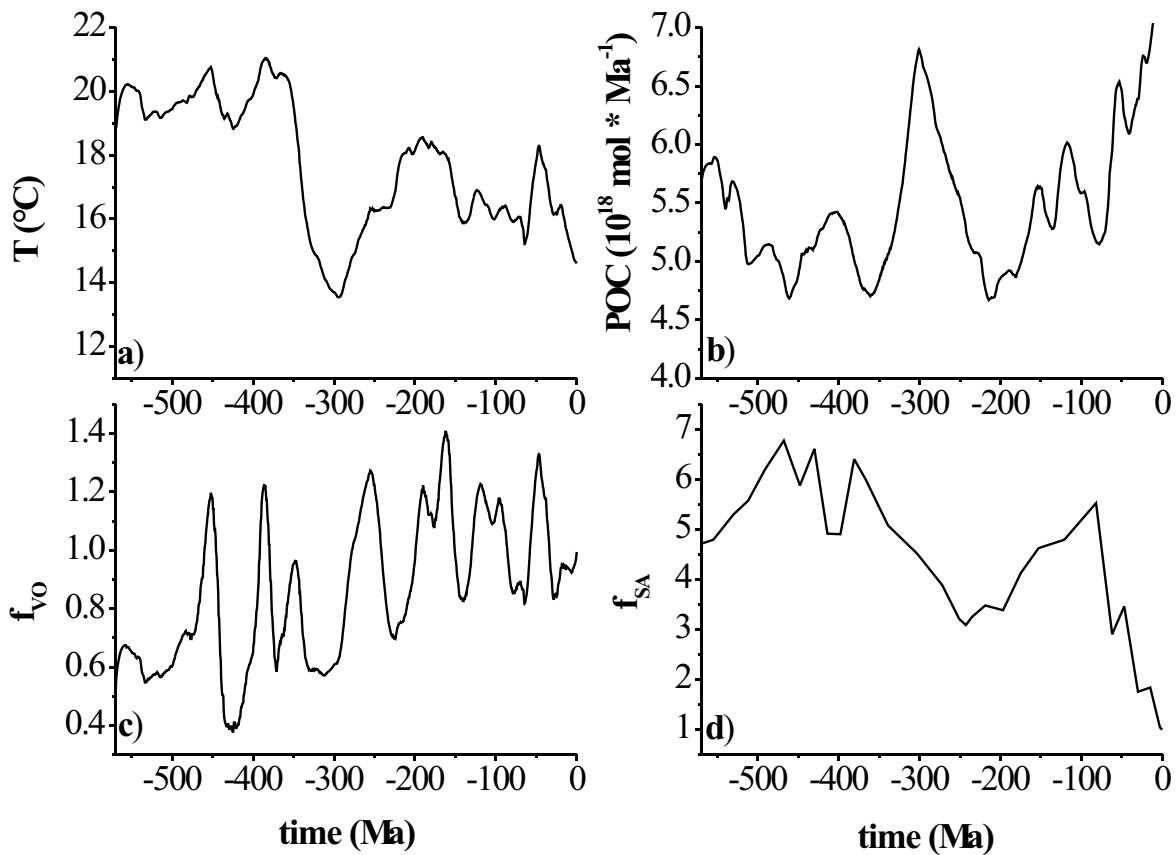


Figure 3.3a-d: Changes in a) average global temperature (Bartdorff and Wallmann, sub.), b) POC accumulation on the sea-floor (Bartdorff and Wallmann, sub.), c) normalized sea covered area (Ronov, 1994); d) tectonic activities (Bartdorff and Wallmann, sub.), used as external forcings.

3.2.1.2 Marine sources

Compared to the terrestrial emissions the marine settings play a minor role. The recent CH_4 release from the oceans (10 - 15 Tg $\text{CH}_4 * \text{yr}^{-1}$; IPCC (2001)) is mainly driven by the biogenic production in anoxic micro-environments located in “marine snow” particles sinking through the upper water

column. The accumulation rate of particulate organic carbon (Fig. 3.3b) is used to define the methane release from sinking particles in the upper water column because the methane-generating particle flux is reflected in POC accumulation:

$$F_{ocean}^{CH_4} = \frac{F_B^{POC}}{F_B^{POC}(q)} * F_{ocean}^{CH_4}(q), \quad (3.4)$$

where F_B^{POC} is the burial rate used as a proxy for biological productivity of the oceans over time (Fig. 3.3b), $F_B^{POC}(q)$ is the Quaternary burial rate of POC ($6 * 10^{18} \text{ mol} * \text{Ma}^{-1}$; Wallmann (2003)), and $F_{ocean}^{CH_4}(q)$ is the recent CH_4 release from of the photic zone.

Marine methane generated in the pore space of sediments migrates towards the surface to be trapped in sea-floor bounded reservoirs, such as gas hydrates, or escapes through natural gas seeps or mud volcanoes as dissolved methane or free gas. Some of this CH_4 is emitted from shallow water environments such as marginal seas and mud flats. According to Judd et al. (2002), the amount of CH_4 released in shallow water environments is influenced by sea-level change. During a falling sea-level these potential CH_4 production areas decrease, while due to transgression the size of shallow water environments increases. Thus for modeling I constrain the changing size of the shelf-bounded sources over time by simply coupling the recent CH_4 emission rate of these environments with the change of shelf area covered by the oceans over time and the changing rate of organic carbon burial:

$$F_{shelf}^{CH_4} = F_{shelf}^{CH_4}(q) * f_{SA} * \frac{F_B^{POC}}{F_B^{POC}(q)}, \quad (3.5)$$

where f_{SA} is the proxy data (Ronov, 1994) normalized to the recent value for the covered sea-floor over time (Fig. 3.3c), and $F_{shelf}^{CH_4}$ ($0.4 - 12.2 \text{ Tg } CH_4 * \text{yr}^{-1}$; Judd et al. (2002)) is the recent emission of CH_4 out of the shallow water environments.

3.2.1.3 Mud volcanoes

Some CH_4 is emitted during quiescent and eruptive periods from mud volcanoes on land, placed mainly along convergent plate margins where fluid-rich sediments accumulate (Kopf, 2002). Marine mud volcanoes with a recent releasing rate of up to $61.3 \text{ Tg } CH_4 * \text{yr}^{-1}$ (Kopf, 2003) are probably less important because methane is almost completely oxidized near the seafloor and in the water column. With a changing sea-level the CH_4 stability conditions change as well. Moreover, a falling sea-level would enhance CH_4 fluxes out of mud volcanoes on land (Boles et al., 2001) but inhibit a further deposition of organic-rich sediments in these areas. However, the main controlling factor on mud volcanism is probably the rate and spatial extent of subduction and plate convergence providing

the pressure gradients necessary for fluid and mud ascent. Therefore, I calculate the evolution of the CH₄ release from mud volcanoes for the past by using the recent CH₄ emission from terrestrial mud volcanoes and the changing rates of subduction and organic matter accumulation:

$$F_{mud}^{CH_4} = F_{mud}^{CH_4}(q) * \frac{F_B^{POC}}{F_B^{POC}(q)} * f_{VO}, \quad (3.6)$$

where $F_{mud}^{CH_4}(q)$ is the recent emission of CH₄ via mud volcanism including both quiescent and eruptive degassing (6 - 9 Tg CH₄ * yr⁻¹; Etiope and Milkov (2004)), and f_{VO} (Fig. 3.3d) is the calculated tectonic/extrusive activity over the entire Phanerozoic (Bartdorff and Wallmann, submitted).

3.2.1.4 Volcanic emissions

Because of the minor release, the volcanic CH₄ emissions into the atmosphere by continental magmatic volcanism (0.8 – 6.2 Tg CH₄ * yr⁻¹; Judd et al. (2002)) is only of minor importance. To calculate the volcanic CH₄ release over the Phanerozoic, I assume the CH₄ emission via eruptive volcanism to be proportional to the activity of magmatic volcanoes. Thus the recent emissions of volcanoes and the calculated trend of activity of the continental volcanoes (f_{VO}) over time (Bartdorff and Wallmann, submitted), give the following expression for the emission in the past:

$$F_{volcano}^{CH_4} = f_{VO} * F_{volcano}^{CH_4}(q). \quad (3.7)$$

3.2.1.5 Gas hydrates

Methane gas hydrates are the greatest CH₄ reservoir on earth (Milkov, 2004) and are low-level permanent but catastrophic temporary emitters with a rather low annual average release of up to 3 Tg CH₄ (Judd et al., 2002). Methane from hydrates can reach the ocean surface in form of gas bubbles and buoyant hydrate floats (Paull et al., 2002) whereas dissolved methane is almost completely oxidized in the water column before it can reach the atmosphere (Valentine et al., 2001). Gas hydrates are generated under high pressure and/or low temperature when a liquid (water on/in the sea floor) and a gas (methane) react to form clathrates (Sloan, 1997). These conditions are found in permafrost regions on land and in marine sediments. A sudden catastrophic release due to a breakdown of almost all of the oceanic CH₄ reservoirs in the sea-floor may have triggered global climate warming and the rapid negative carbon-isotope ($\delta^{13}C$) excursion found in fossil benthic foraminifera and the remains of other calcareous organisms in the Lower Cambrian (Kirschvink and Raub, 2003), in the Upper Permian (Ryskin, 2003), in the Lower Jurassic (Hesselbo et al., 2000), in the Upper Jurassic (Padden et al., 2001), in the Lower Cretaceous (Beerling et al., 2002; Jahren et al., 2001; Jahren et al., 2005), and in the Lower Eocene (Bice and Marotzke, 2002; Kennett et al., 2000) (Tab. 3.1). During such

an event solid, dissolved, and gaseous CH₄ are released into the ocean and some CH₄ may escape oxidation in the water column to be emitted into the atmosphere.

Catastrophic methane release from gas hydrates may be triggered by changing tectonic activity (Jahren et al., 2005; Padden et al., 2001), sea-level changes, and ocean warming (Bice and Marotzke (2002), and Dickens (2001)). Another potential CH₄ production mechanism is the thermogenic breakdown of organic matter due to intrusion of mantle derived melts into carbon rich sediments (Svensen et al., 2004). Some authors (Bains et al., 1999; Jahren et al., 2001; Ryskin, 2003) assume that also the punctuated mass extinction and noticeable facies changes during the Phanerozoic (Katz et al., 1999) might have been caused by a sudden release of methane from decomposing gas hydrates and the following changes in global temperature and spread of anoxic conditions in the ocean.

Table 3.1: Methane release out of methane gas hydrates and other natural CH₄ sources;

I) during the particular epoch;

II) at the estimated time frames;

III) published by:

1 - Kirschvink and Raub (2003), 2 - Bice and Marotzke (2002),

3 - Jahren et al. (2001), 4 - Beerling et al. (2002),

5 - Padden et al. (2001), 6 - Hesselbo et al. (2000),

7 - Ryskin (2003);

IV) the estimated emission amount of CH₄ out of gas hydrates in mol at the particular estimated emission time; V) in the model calculated total release of CH₄ out of other sources to the atmosphere in 10¹⁸ mol Ma⁻¹ at the particular epoch; VI) part of the estimated emission due to sudden methane release by gas hydrates compared to the estimated recent store of methane in gas hydrates; VII) model calculated enhanced volcanic activity relative to the recent activity, f_{VO} (Bartdorff and Wallmann, sub.) according to the (Harland et al., 1990) time scale, to compare emission events with enhanced tectonic activity.

*** PETM – Paleocene-Eocene-Thermal-Maximum*

Epoch	Age of the event (Ma)	Ref.	Total CH ₄ release from gas hydrates (mol)	Duration (kyr)	CH ₄ flux, as release from gas hydrates (10 ¹⁶ mol 10 kyr ⁻¹)	CH ₄ flux, as release of other natural sources (10 ¹¹ mol 10 kyr ⁻¹)	Periods of enhanced and <u>maximal</u> tectonic activity (Ma)
Lower Eocene	PETM ** (~55)	2	1.67 * 10 ¹⁷	20	8.35	4.66	59 – <u>51</u> – 37
Upper Paleocene	55	1	6.23 * 10 ¹⁷	100	6.23	4.26	79 – <u>69</u> – 64
Lower Cretaceous	117	3	1.87 * 10 ¹⁶	1000	0.0187	5.73	135 – <u>118</u> – 88
	120	4	1.87 * 10 ¹⁷	200	0.935		
Upper Jurassic	157.6 – 157.3	5	6.23 * 10 ¹⁷	100	6.23	5.8	203 – <u>162</u> – 148
Lower Jurassic	183.6 – 181.4	4	3.17 * 10 ¹⁷	200	1.59	3.36	203 – <u>190</u> – 148
	183	6	1.25 * 10 ¹⁷ – 2.25 * 10 ¹⁷	400	0.125 – 0.225		
Upper Permian	251	7	6.23 * 10 ¹⁶ – 6.23 * 10 ¹⁷	-	-	9.31	286 – <u>255</u> – 235
Lower Cambrian	540	1	6.23 * 10 ¹⁷	100	6.23	1.73	> 565

In this chapter I include different scenarios to show the influence of sudden CH₄ release from dissociating gas hydrates. The chosen values correspond to the maximum values given in the literature (Beerling and Royer, 2002; Bice and Marotzke, 2002; Hesselbo et al., 2000; Jahren et al.,

2001; Jahren et al., 2005; Kennett et al., 2000; Kirschvink and Raub, 2003; Padden et al., 2001; Ryskin, 2003). To estimate the maximum effect of gas hydrate destabilization on atmospheric $p\text{CH}_4$ values, methane is released directly in the atmosphere without considering the oxidation in the oceans. A series of methane pulses into the atmosphere is defined in the model using the estimated masses of methane released by gas hydrate destabilization and the duration of these events (Tab. 3.1):

$$F_{gun}^{CH_4} = F_{gun}^{CH_4}(table) \quad (\text{Tab. 3.1}). \quad (3.8)$$

3.2.1.6 Insects

Another important source of modern CH_4 are insects (mainly termites) producing $20 \text{ Tg CH}_4 \cdot \text{yr}^{-1}$ (IPCC, 2001). Since the first appearance of insects, these animals have influenced the partial pressure of CH_4 in the atmosphere (Grimaldi, 2001), especially in phases with a notable gigantism as known from insects in the early Paleozoic (Dudley, 1998). There are, however, a lot of uncertainties about the evolution and abundance of ancient insects and their alkane production rate. In the model I assume that termites have been the main emitter of CH_4 among all insects, and I couple the evolution of termites and their recent CH_4 emission value ($F_{\text{termite}}^{\text{CH}_4}(q)$), IPCC (2001) to calculate their Phanerozoic influence:

$$F_{\text{termite}}^{CH_4} = f_{IN} * F_{\text{termite}}^{CH_4}(q). \quad (3.9)$$

The evolution of termites began in the Cretaceous (Grimaldi, 2001). Hence, the parameter f_{IN} is set to zero for the Paleozoic and early Mesozoic and is increased to 1 during the Cretaceous.

3.2.1.7 Methane release

In my model, the overall pre-human CH_4 emission into the atmosphere (Figs. 3.4a-f) is thus given as (equation 3.2 to 3.8):

$$F_{\text{release}}^{CH_4} = F_{\text{mud}}^{CH_4} + F_{\text{gun}}^{CH_4} + F_{\text{volcano}}^{CH_4} + F_{\text{ocean}}^{CH_4} + F_{\text{shelf}}^{CH_4} + F_{\text{wetland}}^{CH_4} + F_{\text{termite}}^{CH_4}. \quad (3.10)$$

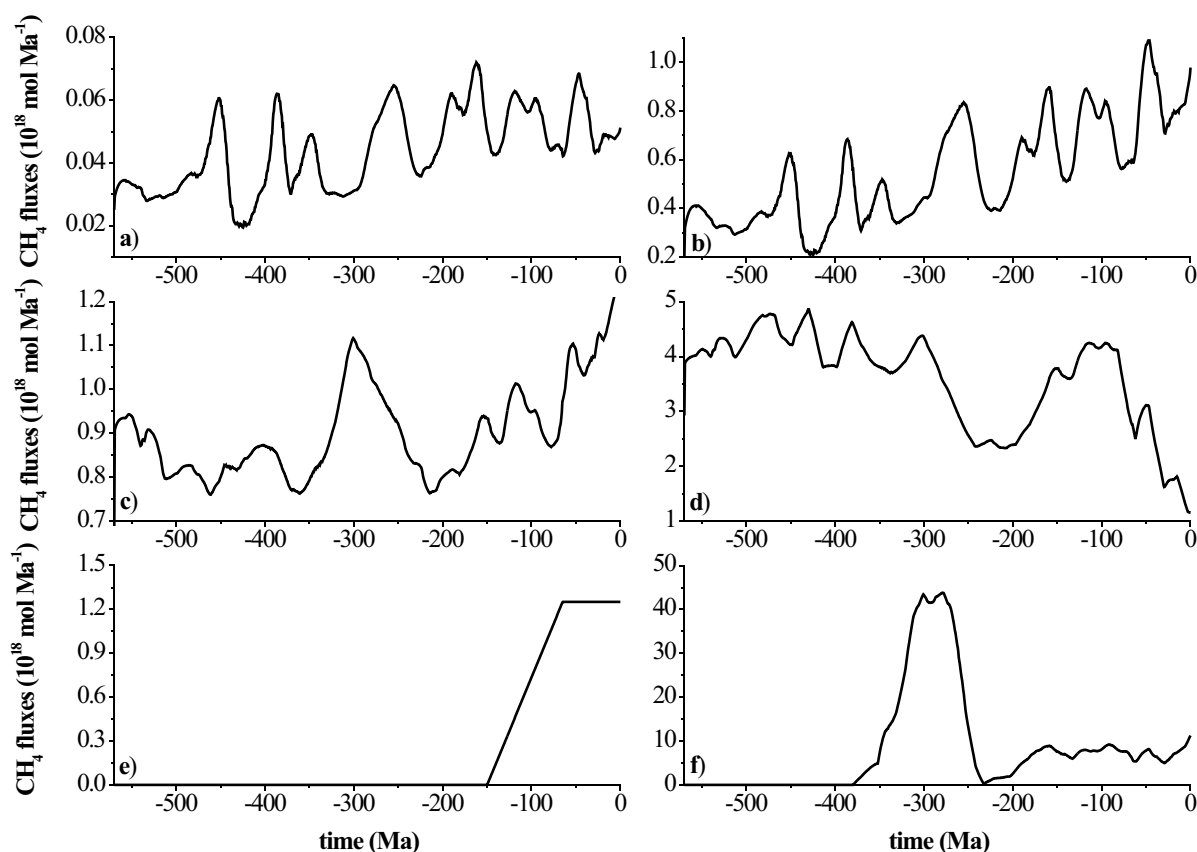


Figure 3.4: Changes in CH_4 fluxes into the atmosphere, out of a) volcanoes on land, b) mud volcanoes in shallow water environments, c) the photic zone of the oceans, d) shelf-zones, e) digestive tracts of insects, f) wetlands; used for the calculation of atmospheric methane concentration.

3.2.2 Sinks of atmospheric methane

The main destruction of CH_4 reaching the atmosphere presently occurs in the modern troposphere ($360 - 530 \text{ Tg CH}_4 \cdot \text{yr}^{-1}$; Seinfeld and Pandis (1998)), because more than 80 % (Sudo et al., submitted) of the cleaning power of the atmosphere is housed in its lower 16 km (Budyko et al., 1987). A minor part of atmospheric CH_4 is consumed within the soils.

3.2.2.1 Oxidation in the atmosphere

Some (e.g. OH , O_2 , NO) of the reactants in the reaction chain of methane destruction are formed in the troposphere (Jacob, 2000), others, e.g. O_3 - one of the main agents in tropospheric chemistry (Wang et al., 1997) - move from the stratosphere into the troposphere (Schultz et al., 1998). There are two types of triggers for the whole reaction chain of CH_4 destruction/oxidization: One is the solar flux, which triggers the photolytic reactions, and other ones are radicals, which affect the chain reaction. Due to the decomposition of atmospheric methane into atmospheric carbon dioxide a large

amount of interstage products is produced. These interstage products are also decomposed within a very short time (ranging between seconds and hours). For long time modeling only the initial- and the end-product account. The reaction chain for the production of the oxidizing agents is very complex and is discussed in Seinfeld and Pandis (1998). The main oxidizing agents removing methane from the atmosphere are hydroxyl radicals produced in these chain reactions.

In the context of my model, it is important to note that the effectiveness of the CH₄ oxidation by hydroxyl radicals (OH) increases as the amount of the hydrocarbon molecules decreases (Jacob, 2000; Lawrence et al., 2001). Due to the rapid recycling rate of hydroxyl radicals at moderate CH₄ levels, the oxidization processes, mentioned above, do not significantly deplete the hydroxyl radicals (Lelieveld et al., 2002). However, at high CH₄ concentrations the cleaning power of the atmosphere decreases substantially. Consequently, the atmosphere adjusts to pollution when moderate CH₄ emissions prevail while CH₄ accumulates in the atmosphere during times of enhanced emission.

I postulate a steady state for modeling the loss of methane out of the atmosphere on geological time scale. The loss ($F_{atmosphere}^{CH_4}$) of methane out of the atmosphere is proportional to the atmospheric content of methane (RCH_4), and a kinetic constant ($k_{atmosphere}$), which also depends the atmospheric methane content:

$$\frac{F_{atmosphere}^{CH_4}}{F_{loss}^{CH_4}(q)} = k_{atmosphere} * RCH_4. \quad (3.11)$$

Schmidt and Shindell (2003) applied atmospheric chemistry modeling to quantify the exponential decrease in atmospheric OH abundance and methane oxidation caused by increasing partial pressures of CH₄ (Fig. 3.5). Figure 3.5 shows the decreasing tropospheric oxidation with increasing atmospheric methane concentration. I fitted a third order exponential term to the model results of Schmidt and Shindell (2003) to define a kinetic constant for atmospheric methane oxidation depending on the prevailing atmospheric CH₄ level:

$$k_{atmosphere} = 0.07925 + 0.61712 * e^{\frac{-RCH_4}{5.43812}} + 0.62564 * e^{\frac{-RCH_4}{0.41025}} + 0.35927 * e^{\frac{-RCH_4}{39.436}}. \quad (3.12)$$

The RCH_4 parameter appearing in this equation gives the partial pressure of methane in the atmosphere normalized to the prehuman value (0.7 ppmV).

The loss of CH₄ ($F_{atmosphere}^{CH_4}$) by atmospheric oxidation is described by the relation between the kinetic constant for oxidation and the prehuman loss rate. I assume that the prehuman loss ($F_{loss}^{CH_4}(q)$) and the prehuman emission are balanced (225 Tg CH₄ * yr⁻¹; Schmidt and Shindell (2003)):

$$F_{atmosphere}^{CH_4} = k_{atmosphere} * F_{loss}^{CH_4}(q) * RCH_4. \quad (3.13)$$

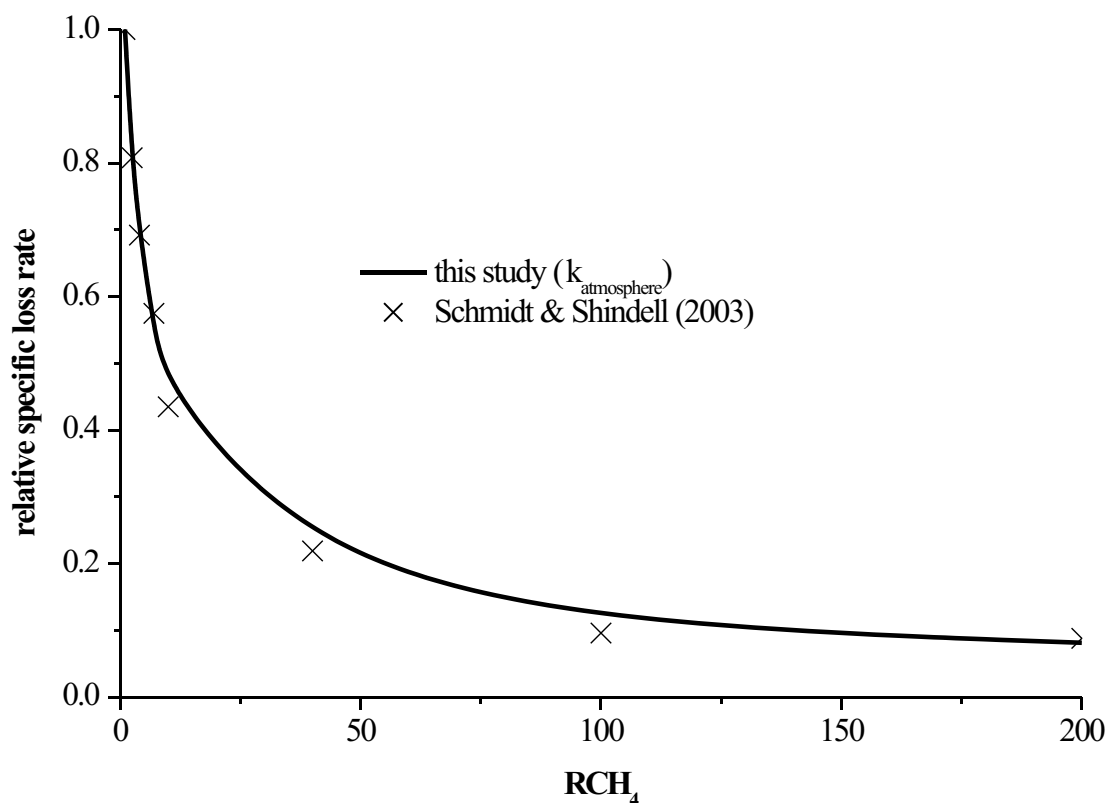


Figure 3.5: Decrease in loss rate of CH₄ out of the atmosphere in dependency to the atmospheric CH₄ concentration (Schmidt and Shindell, 2003).

3.2.2.2 Oxidation within the soils

A small part (1 – 10 %; Lelieveld et al. (1998)) of the atmospheric CH₄, mainly the CH₄ in the soil air and/or in the air near the Earth's surface, gets decomposed by soil organisms. Weathering processes in contact with the atmosphere develops soils. The decomposing organisms live in the humus-rich and aerated part of soils. The humus layer is formed by plants, thus there is a dependency between the plant evolution and the humus-rich layer evolution in the soils (Stanley, 1989). The more plants are growing, the more humus layers are developed. Berner (1994) reconstructed the rise and evolution of the vascular land plants during the entire Phanerozoic. These non-dimensional data (f_{AN}) and the recent uptake of CH₄ by soil organisms ($F_{soil}^{CH_4}(q) = 30 - 40 \text{ Tg CH}_4 \cdot \text{yr}^{-1}$; King and Schnell (1994)) describe the CH₄ oxidation for the past ($F_{soil}^{CH_4}$):

$$F_{soil}^{CH_4} = F_{soil}^{CH_4}(q) * f_{AN}, \quad (3.14)$$

3.2.2.3 Loss of atmospheric methane

Methane gets decomposed due to oxidation processes in the atmosphere, and within the soils. The reduction in the CH₄ inventory located in the lower atmosphere due to physical transport processes (Ehhalt, 1974), such as the Hadley circulation and eddy diffusion (together < 60 Tg CH₄ * yr⁻¹), is not resolved in my model, because of the lack of information on the atmospheric circulation processes in the Phanerozoic. I include the transported CH₄ mass (7 - 11 % of total destroyed CH₄, Lelieveld et al., (1998)) in the total recent chemical destruction processes of about 392 – 578 Tg CH₄ * yr⁻¹ Seinfeld and Pandis (1998).

Accordingly, the destruction of CH₄ in the lower and upper atmosphere via the atmospheric cleaning power ($F_{atmosphere}^{CH_4}$) and the uptake by soil organisms ($F_{soil}^{CH_4}$) during the entire Phanerozoic (equation 3.11 + 3.12) can be described as:

$$F_{loss}^{CH_4} = F_{soil}^{CH_4} + F_{atmosphere}^{CH_4}. \quad (3.15)$$

3.2.3 Budget of atmospheric methane

Based on the terms above, sources and sinks (equation 3.9 & 3.14), the changing inventory of CH₄ in the atmosphere over the Phanerozoic can be calculated as:

$$\frac{dMCH_4}{dt} = F_{release}^{CH_4} - F_{loss}^{CH_4}, \quad (3.16)$$

where $F_{release}^{CH_4}$ is the total release of CH₄ into the atmosphere, and $F_{loss}^{CH_4}$ is the consumption of atmospheric CH₄. Because of the fast consumption rate (Jacob, 2000) and the resulting short lifetime of CH₄ in the atmosphere (Sudo et al., submitted), almost all of the released CH₄ gets decomposed. Thus the atmospheric CH₄ amount ($F_{release}^{CH_4} - F_{loss}^{CH_4}$) is in a quasi steady state:

$$\frac{dMCH_4}{dt} = 0, \quad (3.17)$$

$$F_{release}^{CH_4} - F_{soil}^{CH_4} - k_{atmosphere} * F_{loss}^{CH_4}(q) * RCH_4 = 0. \quad (3.18)$$

Solving for RCH₄ results in:

$$RCH_4 = \frac{F_{release}^{CH_4} - F_{soil}^{CH_4}}{k_{atmosphere} * F_{loss}^{CH_4}(q)}. \quad (3.19)$$

This term is analytical insolvable, because of the exponents in the term $k_{atmosphere}$ (see eq. 3.10), thus I solve this term numerical (Tab. 3.2 & Fig. 3.6) with Mathematica 5.0. For the given values of CH₄ release and CH₄ soil consumption:

$$F_{release}^{CH_4} - F_{soil}^{CH_4} = netrelease, \quad (3.20)$$

I calculate the CH_4 concentration in the atmosphere. Fig. 3.6 shows the RCH_4 value as a function of the net release of CH_4 . RCH_4 increases exponentially with increasing net release.

For modeling the atmospheric CH_4 amount (RCH_4), the CH_4 release, the consumption by soil organisms, and the kinetic constant for the atmospheric loss are the working parameters.

Table 3.2: Numerical solved term (eq. 3.16 & 3.23), RCH_4 netrelease (on prehuman values normalized) = $F_{release}^{CH_4} - F_{soil}^{CH_4}$; the resulting RCH_4 is the normalized CH_4 content in the atmosphere.

RCH_4 release	0	0.1	0.5	1	2	3	4	5	6	7	8	9	10	12	15	20
RCH_4	0	0.1	0.4	1	2.5	4.5	7.6	12.3	18.5	25.8	35.2	49.6	76.1	129.4	180.9	250.4

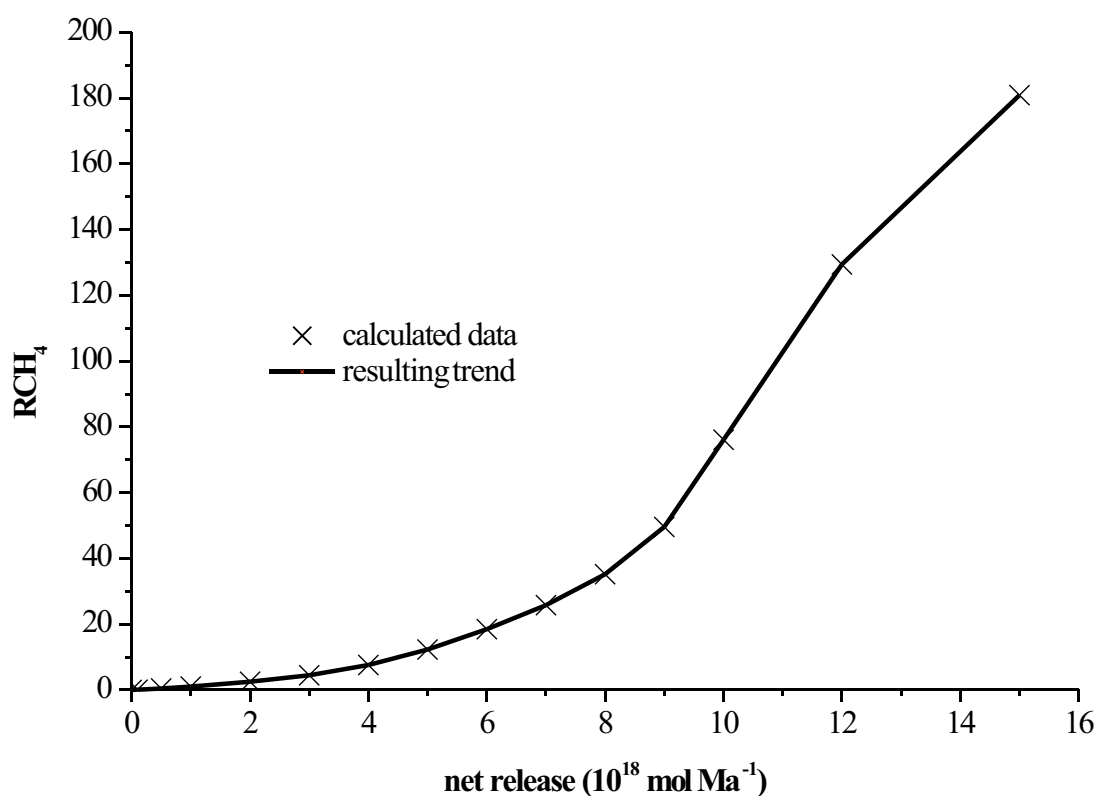


Figure 3.6: Changes in dependency of atmospheric methane on methane net release (Tab. 3.2)

3.2.4 Isotope modeling

Carbon isotope modeling is performed as in Wallmann (2001a) considering also the release and oxidation of depleted methane from magmatic volcanoes and gas hydrates. Model calculations are validated using the oceanic $\delta^{13}C$ trend reconstructed by Hayes et al. (1999). To calculate the carbon

isotopic composition of seawater, oceanic and atmospheric input and output fluxes are multiplied with the corresponding mole fraction of ^{13}C (Φ), which is defined as:

$$\Phi = \frac{^{13}\text{C}}{^{13}\text{C} + ^{12}\text{C}} = \frac{1000 + \delta^{13}\text{C}}{89990 + \delta^{13}\text{C}}. \quad (3.21)$$

For carbon release due to CH_4 degassing of magmatic volcanoes ($F_{\text{volcano}}^{\text{CH}_4}$) a constant average $\delta^{13}\text{C}_{\text{volcano}}$ of $-4.5\text{‰} \pm 0.5\text{‰}$ (Dickens, 2003) is used, and for carbon release due to sudden degassing via gas hydrate dissolution a constant average $\delta^{13}\text{C}_{\text{hydrate}}$ of $-70\text{‰} \pm 20\text{‰}$ (Gautier and Claypool, 1984) is applied. The turnover of these reservoirs is calculated as:

$$\frac{\delta^{13}\text{CH}_4}{dt} = \Phi_{\text{hydrate}} * F_{\text{gun}}^{\text{CH}_4} + \Phi_{\text{volcano}} * F_{\text{volcano}}^{\text{CH}_4}. \quad (3.22)$$

This calculation approach is coupled with the output of the model run of the geochemical model by Bartdorff and Wallmann (submitted).

The organic carbon cycle is included in the isotope model of Wallmann (2001a) considering burial and weathering of organic matter only. Production and microbial degradation of organic matter are important processes on short time scales. On the long geological time scales of the model, these processes are, however, not relevant because only the organic matter that is permanently buried in sediments and sedimentary rocks has an effect on the long-term evolution of the global carbon cycle. Hence, isotopically depleted methane and enriched CO_2 formed during the microbial degradation of young organic matter are also not included in the present carbon isotope model. Only those methane fluxes originating from ancient carbon reservoirs such as the earth's mantle and gas hydrates are considered.

3.2.5 Climate effects of methane

Atmospheric CH_4 is an important greenhouse gas and affects the global average surface temperatures by its radiative forcing. The radiative forcing by CH_4 can be estimated as (Thorpe et al., 1996):

$$RF = 0.0411 * (\sqrt{p\text{CH}_4} - \sqrt{p\text{CH}_4(q)}), \quad (3.23)$$

where RF is the radiative forcing ($\text{W} * \text{m}^{-2}$) and $p\text{CH}_4$ and $p\text{CH}_4(q)$ are the atmospheric partial pressures of methane changing over time and the reference prehuman level (350 ppbV). In the absence of climate feedbacks, the climate sensitivity parameter λ ($0.30 \text{ K} * (\text{W} * \text{m}^{-2})^{-1}$, Seinfeld and Pandis (1998)) can be used to calculate the impact of methane on the average global surface temperature (ΔT^{CH_4}):

$$\Delta T^{\text{CH}_4} = \lambda * RF. \quad (3.24)$$

3.3 Results and Discussion

3.3.1 The Phanerozoic evolution of atmospheric methane

This study comprises the first attempt to describe the atmospheric methane evolution over the entire Phanerozoic. During the Carboniferous coal swamp era the methane release reached the maximum value for the entire Phanerozoic. The atmospheric methane content increased to 10 ppmV (Fig. 3.7). The next two peaks were reached in the Cretaceous and Jurassic with maximum contents of 1.5 ppmV approaching the methane level prevailing in the modern atmosphere.

The main trend of atmospheric methane may be influenced by the appearance of land plants and the coeval spread of swamps on the continents. During the Permian and Carboniferous, when plants first flourished on the continents and large continental areas were covered by wetlands, vast amounts of methane were formed in these swamps and wetlands by the microbial degradation of plant remains. According to the model, the atmospheric partial pressure of CH_4 was up to 28 times higher than in prehuman times (Fig. 3.7).

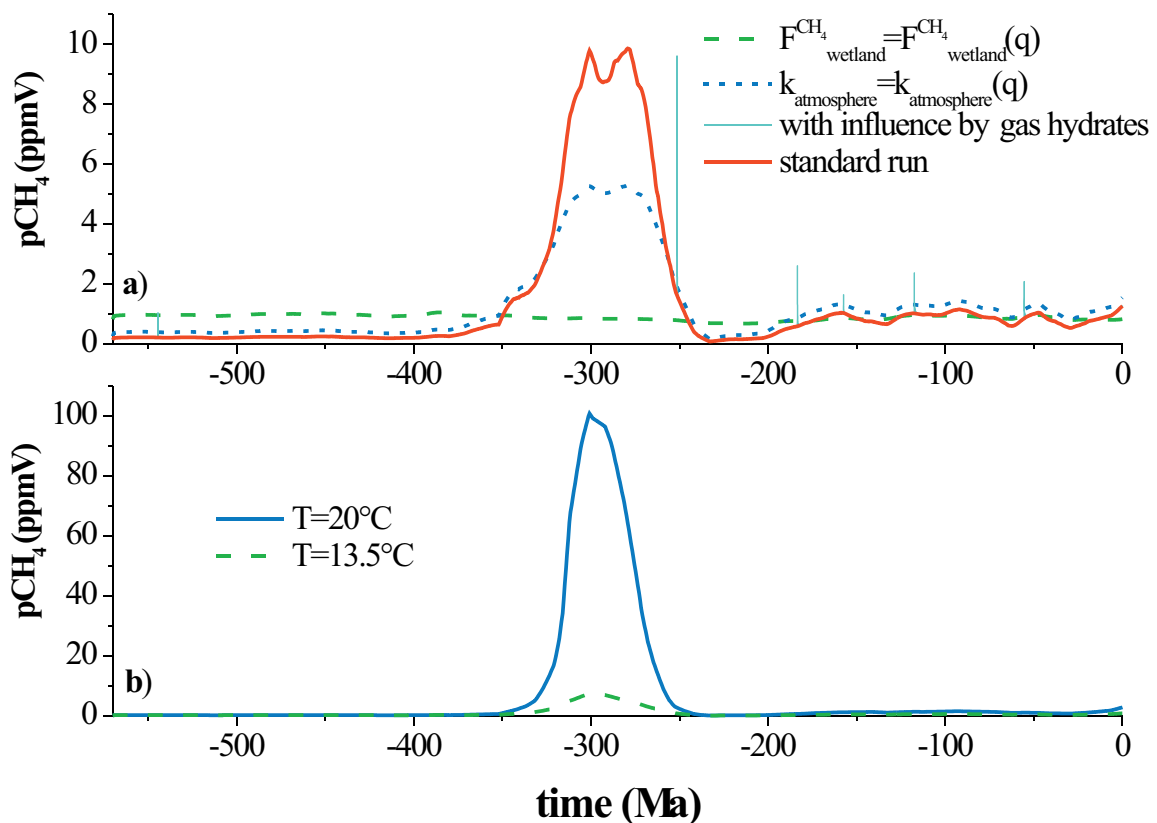


Figure 3.7a-b: Changes in $p\text{CH}_4$ in a) standard run, a constant kinetic loss of CH_4 out of the atmosphere ($k_{\text{atmosphere}} = k_{\text{atmosphere}}(q)$), a constant emission rate out of the main emitter, the wetlands ($F_{\text{wetland}}^{\text{CH}_4} = F_{\text{wetland}}^{\text{CH}_4}(q)$), and the impact of sudden methane release by gas hydrates with an emission time of about 10 kyr_(PETM-value) (Tab. 3.3), b) model runs with a constant temperature (13.5 and 20°C).

3.3.2 Effects of atmospheric methane on global average surface temperatures

During the coal swamp era, the rising methane level caused a strong and positive radiative forcing (Fig. 3.8) inducing a temperature increase of up to 1°C. I derive a term (Eq. 3.23) for the influence of atmospheric methane on the average global temperature. It is possible to include this expression in the existing calculation of Berner and Kothavala (2001) for a secular temperature calculation:

$$T = \Gamma * \ln RCO_2 - W_s * \frac{t}{-570} + T(q) + GEOG + \Delta T^{CH_4}, \quad (3.25)$$

where Γ gives the relation between temperature and RCO_2 , RCO_2 is the atmospheric partial pressure of CO_2 normalized to the Quaternary value (230 μatm), W_s defines the impact of increasing solar luminosity on surface temperature, $GEOG$ describes the effect of paleogeography on albedo and surface temperature, and $T(q)$ is the average Quaternary surface temperature (13.5°C). In times of low methane emission the influence is consequently low, but in times with high methane emission rates, and low atmospheric loss, the influence becomes significant, especially in the Carboniferous coal swamp era. The direct effect of CH_4 on the global temperature is obvious (Fig. 3.9), but there is also an indirect effect on the RCO_2 . As a result of the methane-driven temperature increases, the consumption of CO_2 due to silicate weathering increases too. The RCO_2 , therefore, decreases in times

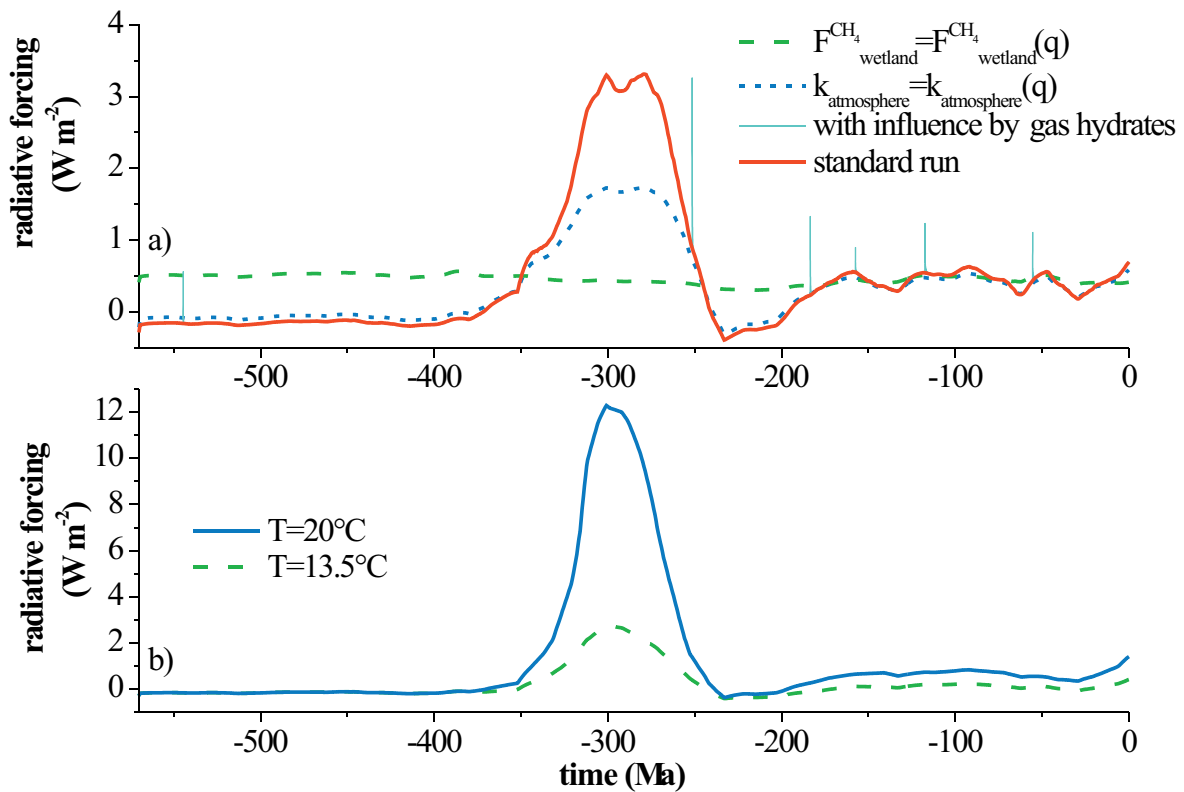


Figure 3.8a-b: Changes in radiative forcing (RF), in a) standard run, and in a constant kinetic loss of CH_4 out of the atmosphere ($k_{atmosphere} = k_{atmosphere}(q)$), a constant emission rate out of the main emitter, the wetlands ($F_{wetland}^{CH_4} = F_{wetland}^{CH_4}(q)$), and the impact of sudden methane release by gas hydrates with an emission time of about 10 kyr ($PETM$ -value) (Tab. 3.3), b) model runs with a constant temperature (13.5 and 20°C).

with high methane release rates (Fig. 3.9). This is an unexpected result, as one expects the RCO_2 to increase due to increasing pCH_4 . Since its decomposition products, and its lowering effects due to enhanced weathering efficiency, as a result of increasing temperature, are far more significant. This negative feedback is not balanced; the direct warming effect is stronger than the indirect cooling effect. Because of the short residence time of methane in the atmosphere the warming effect by this greenhouse gas occurs only on a small timescale. Because of the further cooling due to decreasing RCO_2 , and the feedback of silicate weathering, methane could even act as a trigger for the “Snowball Earth effect” as discussed by Schrag et al. (2002).

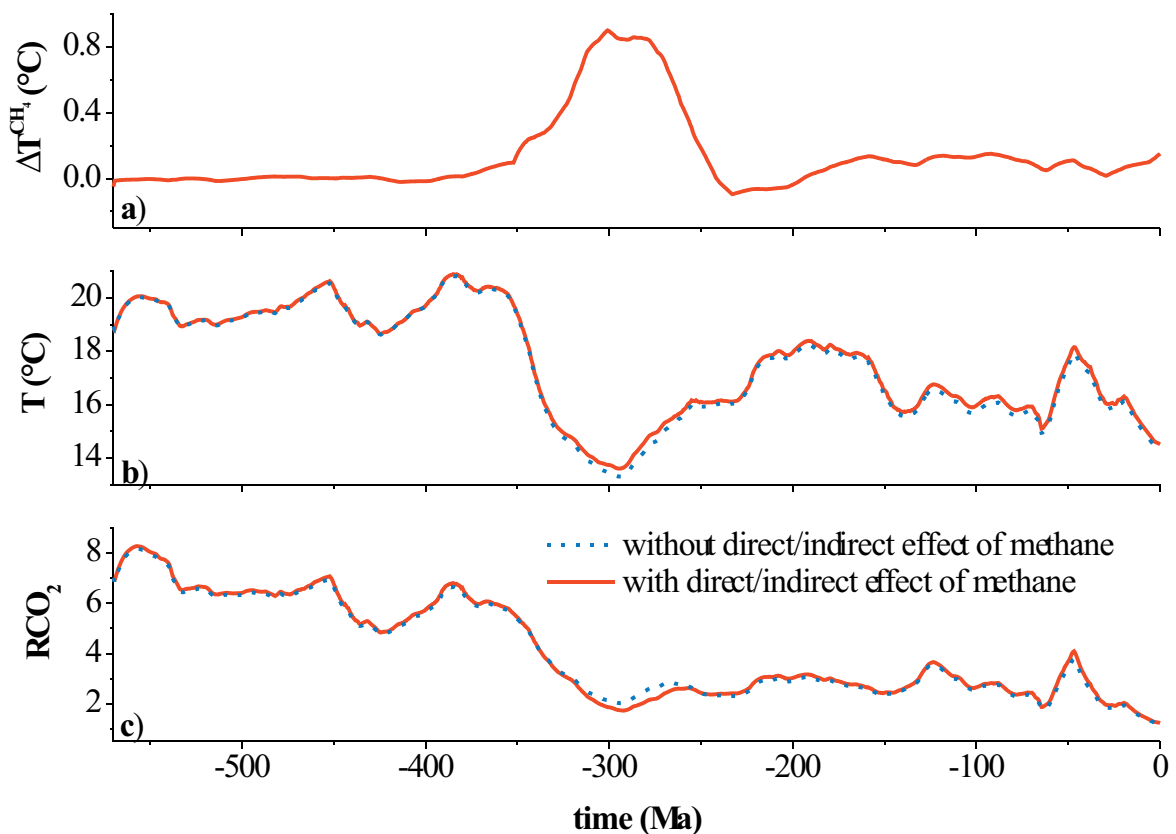


Figure 3.9a-c: Changes in a) temperature change due to atmospheric methane, b) average global temperature, calculated by the impact of CO_2 , without CH_4 (Bartdorff & Wallmann sub.), and calculated with the impact of CH_4 , c) RCO_2 , induced due to different silicate erosion efficiency forced by different average global temperature.

3.3.3 Methane oxidation in the Phanerozoic atmosphere

The increase of atmospheric methane on one hand is caused by a greater amount of emission, but on the other hand it is due to the decreasing cleaning power of the atmosphere. Another sensitivity test runs with a time-independent kinetic constant of CH_4 out of the atmosphere ($k_{\text{atmosphere}} = k_{\text{atmosphere}}(q)$). This case offers a high loss rate of CH_4 removal out of the atmosphere, not considering the particular

CH₄ emission into the atmosphere. The resulting atmospheric concentration reaches lower values (Fig. 3.7) than in the standard run. That demonstrates how sensitive the cleaning power of the atmosphere reacts on pollution. The “cleaning effectiveness” loses its power due to increasing pollution. These results are the reason for a further sensitivity test, an elimination of the time-depending main emitter ($F_{\text{wetland}}^{\text{CH}_4} = F_{\text{wetland}}^{\text{CH}_4}(q)$). As expected, the atmospheric CH₄ content and the RF stays on a level, lower than reached for the standard run (Figs. 3.7 & 3.8).

3.3.4 Gas hydrate dissociation

In many previous publications the influence of methane gas hydrates on the atmospheric amount of alkanes are discussed. This proposed link is based on the assumption that the hard to explain $\delta^{13}\text{C}$ excursions are caused by the sudden release of gas by methane gas hydrates (Clathrate Gun Hypothesis). Because of the minor amount of the released gas on a geological time scale there is only a little influence on the atmospheric methane amount, but because of the strong negative isotope ratio it is possible that the mentioned excursion is caused by such an event. The model runs six different sceneries (included in the common carbon model by Bartdorff and Wallmann (submitted)), one without a sudden methane release (standard run), another one including the sudden releases with a maximum release as it is generally published (Tab. 3.1), with no oxidation in the oceans at time spans of 10, 50, 100, 150 kyr (Tab. 3.3), and a run with an emission time of 10 kyr and a emission rate of the best researched value for these events, as calculated for Paleocene-Eocene Thermal Maximum (PETM).

Table 3.3: Changes in $p\text{CH}_4$ induced due to sudden methane release by gas hydrates; at the given point in time (cp. Tab. 3.1), the different emission times for these events, and the resulting maximum $p\text{CH}_4$, the temperature change due to methane derived (ΔT_{CH_4}) radiative forcing, and the change of average global temperature (ΔT_{total}) in the atmosphere.

** Model run with the best recorded amount of the released CH_4 , used for all estimated points in time (cp. Tab. 3.1)*

Point in time (Ma)	Time frame for CH ₄ emission due to sudden CH ₄ release by gas hydrates (kyr)														
	150			100			50			10			10(PETM-value)*		
	$p\text{CH}_4$	ΔT_{CH_4}	ΔT_{total}	$p\text{CH}_4$	ΔT_{CH_4}	ΔT_{total}	$p\text{CH}_4$	ΔT_{CH_4}	ΔT_{total}	$p\text{CH}_4$	ΔT_{CH_4}	ΔT_{total}	$p\text{CH}_4$	ΔT_{CH_4}	ΔT_{total}
55	1.01	0.16	0.29	1.08	0.18	0.35	1.29	0.21	0.35	3.31	0.48	0.19	3.31	0.48	0.2
65	0.72	0.1	0.14	0.76	0.11	0.17	0.82	0.12	0.16	1.4	0.23	0.08	2.98	0.44	0.29
117	1.2	0.2	0.34	1.29	0.21	0.41	1.52	0.25	0.4	4.19	0.57	0.22	3.68	0.52	0.2
157	1.11	0.18	0.41	1.14	0.19	0.45	1.23	0.2	0.44	1.82	0.19	0.33	3.8	0.53	0.61
183	0.81	0.12	0.87	0.64	0.08	1.03	1.2	0.2	1.01	4.24	0.57	0.58	2.89	0.43	0.43
251	2.89	0.43	1.89	3.35	0.48	2.23	5.08	0.65	2.19	43.08	2.33	1.33	5.08	0.65	0.35
544	0.25	-0.04	0.14	0.26	-0.03	0.17	0.31	-0.01	0.16	0.82	0.12	0.11	2.16	0.34	0.3
	Maximum $p\text{CH}_4$ (ppmV), ΔT_{CH_4} – temperature change due to radiative forcing (°C), ΔT_{total} – change of average global temperature (°C) at the time of emission														

Table 3.3 illustrates the maximum reached values of $p\text{CH}_4$, ΔT^{CH_4} , and the resulting change of average global temperature (ΔT^{total}) with respect to the direct and indirect effects for these events. The increasing influence on the $p\text{CH}_4$ with a decreasing emission time span becomes clear. With decreasing emission time the atmospheric methane concentration increases. Due to the same emission amount and the resulting increasing emission flux the atmospheric cleaning power become less effective. Considerable is the change in $p\text{CH}_4$ due to emission fluxes at the 10 kyr time span, up to 43 ppmV, twenty five times higher than the concentration today. The temperature effect of methane (ΔT^{CH_4}) also increases with decreasing emission time up to 2.3°C. Surprisingly is the trend of the total temperature change (ΔT^{total}), as a result of direct and indirect effects of atmospheric methane. At geological long emission times (150 – 50 kyr) the total temperature change is higher than the temperature change only by atmospheric methane, because of the effects of CH_4 and its decomposition product CO_2 . But at an emission time of 10 kyr, the total temperature change is lower than the effect driven only by methane. This unexpected behavior is caused by the enhanced consumption of CO_2 due to silicate weathering and the resulting drop of $p\text{CO}_2$. This mechanism buffers the temperature increase due to methane degassing.

Table 3.3 also shows the effect of atmospheric methane accumulation and the loss of the effectiveness of the atmospheric cleaning power. The run with the 10 kyr time span (10 kyr_(PETM/ value)) and a constant emission flux, as assumed for the Paleocene-Eocene-Thermal-Maximum-Event (Kirschvink and Raub, 2003), for all several events clearly point out the enhanced effects of a continuous CH_4 emission (e.g. from wetlands) and sudden methane releases. Because of the accumulation of all the emitted methane and the decreasing atmospheric cleaning power, the impact of the sudden methane releases is significant in periods with higher continuous emission fluxes. This unexpected different increase is based on the different effectiveness of the cleaning power of the atmosphere. It results in an enhanced atmospheric methane concentration, e.g. in the Permian, with high methane degassing by wetlands and high releases by gas hydrates.

The latter results only demonstrate the operation mode of the model, and the postulated behavior, especially the failure of the cleaning system of the atmosphere, they neither reinforce nor deny the Clathrate Gun Hypothesis. The amount of the released methane due to several pumps is under debate. The assumed amount ranges between 60 and 70 % of the estimated recent global storage of CH_4 on the sea-floor. Indisputable is the appearance of the sudden methane clathrate breakdown to explain the significant negative peaks of the $\delta^{13}\text{C}$ trend over Phanerozoic time. I am now able to calculate the potential emission flux for these events, by coupling the present methane model to the carbon model by Bartdorff and Wallmann (submitted). Thus I create five 10 kyr model runs with a particular constant isotopic carbon ratios (60, 70, 80, 90, 100 ‰) of CH_4 emitted out of gas hydrates, and adjust the emission fluxes to the best fit to achieve the recorded $\delta^{13}\text{C}$ value at the particular time (Fig. 3.10). Because of the consideration of all main carbon fluxes in the common carbon model by Bartdorff and Wallmann (submitted) the calculated emission methane fluxes out of the gas hydrates are the best assumptions for these events (Tab. 3.4).

Table 3.4: Best fit calculation for the estimated events of sudden methane release by gas hydrates (cp. Tab. 3.1); with the estimated point in time, and the different isotopic carbon ratio of CH_4 (60 – 100 ‰); and the corresponding emission rate to fulfill the request; that the negative excursion of the $\delta^{13}\text{C}$ (Fig. 3.10) are originated by the breakdown of gas hydrates.

Point in time (Ma)	Carbon ratio in CH_4 emitted due to sudden methane release by gas hydrates (‰)				
	60	70	80	90	100
55	7.9	6.8	5.6	5	4.4
117	7.3	5.9	5.1	4.5	4
157	2.8	2.4	2	1.9	1.6
183	10	8.5	7.3	6.3	5.6
251	14	11.8	10	8.8	8.4
540	7.9	6.8	5.8	5	4.5
Emission rate (10^{18} mol 10kyr^{-1})					

Generally, the influence of carbon out of naturally originated CH_4 on the global $\delta^{13}\text{C}$ is negligible, all biologically produced methane occurs due to decomposition of organic matter. It only causes a rearrangement of the isotopic carbon content, e.g. plants remove carbon out of the atmosphere, thus the atmospheric ratio becomes heavier, and due to decomposition the atmospheric isotopic compensation becomes lighter in the same order. Only extraordinary events, with heavy and sudden CH_4 releases, also the thermogenic, abiologically produced methane carbon, influences the global $\delta^{13}\text{C}$ trend.

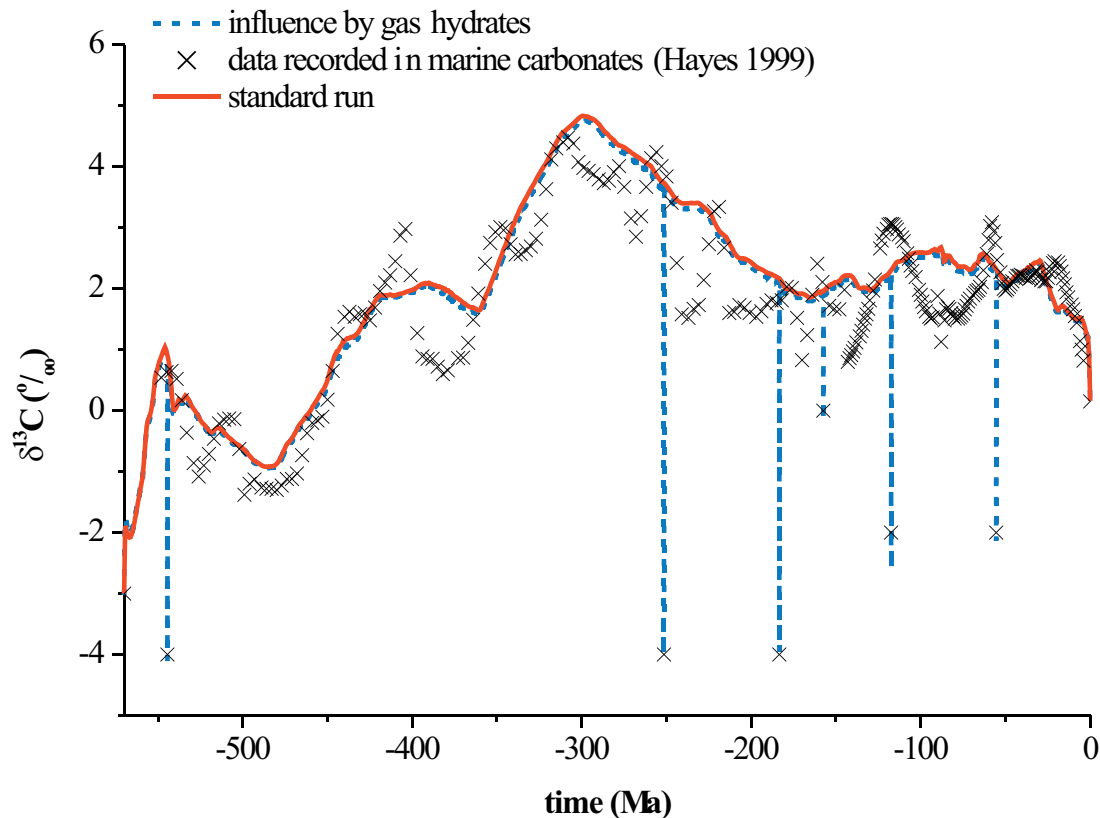


Figure 3.10: Changes in $\delta^{13}\text{C}$, recorded in marine carbonates (Hayes et al., 1999), calculated in the common carbon model (Bartdorff and Wallmann, sub.) used for the standard run, and the calculated model including the case study with sudden methane release by gas hydrates with an emission time of about 10 kyr and 70‰ isotopic carbon ratio of methane (Tab. 3.4).

Table 3.3 shows the direct and indirect influences of the assumed events on the $p\text{CH}_4$ and the average global temperature at different emission time frames. The results are obvious, with decreasing time frames the emission flux increases, thus the effects become more significant. But there is a big lack of evidence for these changes. However, whether the influence of released methane by gas hydrates on the atmosphere is significant or not, the influence on the global isotopic carbon trend is given, because of the high negative isotopic ratio.

The triggers for the sudden methane release are under debate (Beerling et al., 2002; Bice and Marotzke, 2002; Hesselbo et al., 2000; Jahren et al., 2001; Jahren et al., 2005; Kennett et al., 2000; Padden et al., 2001; Ryskin, 2003). One initial step could be caused by magmatic intrusions (cp. Svensen et al. (2004)), or bulging of seafloor due to enhanced subduction (Jahren et al., 2005). The comparison of Fig. 3.11a and Fig. 3.11c suggest some eye-catching coincidences between the epoch with the sudden methane release and the calculated tectonic / volcanic activity (Bartdorff and Wallmann, submitted) (Tab. 3.1). In times with the assumed releases, maxima of tectonic activity occur, except for LPTM. The accordances reinforce the assumption of Svensen et al. (2004) that magmatic intrusions could have triggered sudden methane release events. Based on this I calculate a model run with a sudden methane release at the calculated tectonic maxima (Fig. 3.11) at an emission time span of about 10 kyr. The fluxes of this approach are based on the resulted emission fluxes of an isotopic carbon ration of CH_4 of about 70 ‰ (Tab. 3.4). Out of this calculation I offer some possible “new” carbon isotope excursions for the past.

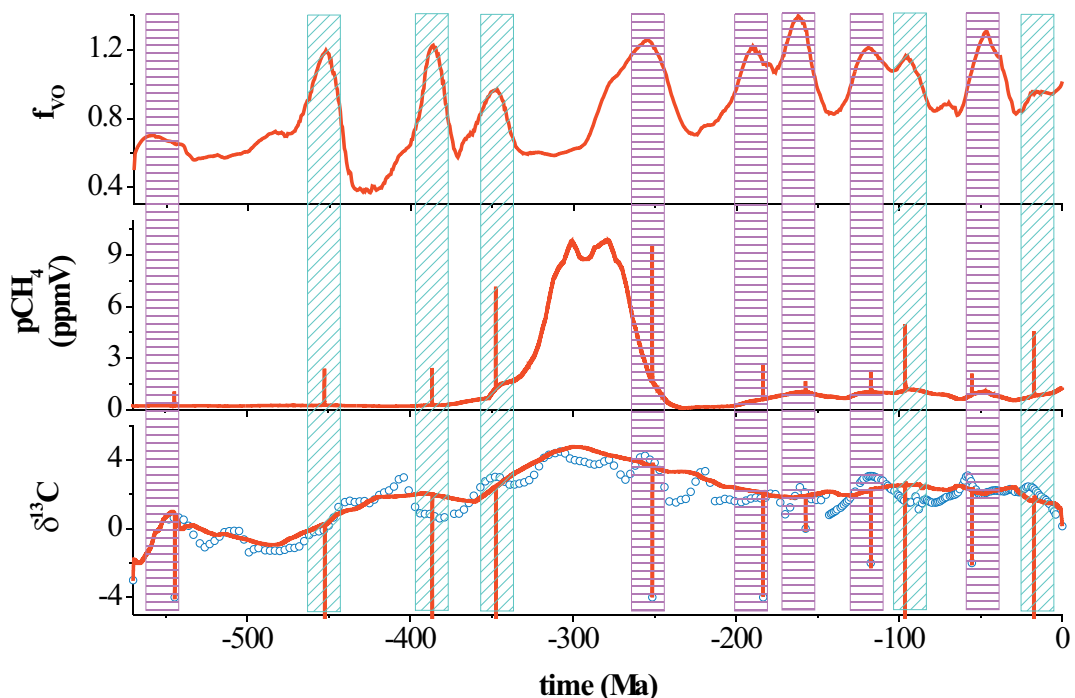


Figure 3.11a-c: Changes in a) volcanic/tectonic activity (f_{vo}) (Bartdorff and Wallmann, sub.), b) methane concentration in the atmosphere including sudden methane release by gas hydrates triggered by enhanced volcanic activity, c) $\delta^{13}\text{C}$ in seawater with carbon input from sudden methane release by gas hydrates triggered by enhanced volcanic activity, circles are proxy data (Hayes et al., 1999), dashed lines are the calculated data of the carbon output (Bartdorff and Wallmann, sub.); horizontal hatched bars show the correlation between enhanced volcanism and recorded $\delta^{13}\text{C}$ excursions, angular hatched bars show the assumed $\delta^{13}\text{C}$ excursions at times with enhanced volcanism.

3.3.5 Feedbacks between methane and climate change

Low surface temperatures prevailed during the Carboniferous coal swamp era (Fig. 3.3a). As the microbial methane production in swamps is temperature dependent (Fig. 3.2a), the methane emissions were mitigated by the climatic conditions of the Permian-Carboniferous cold period. Under warmer conditions, the atmospheric partial pressure of methane calculated in the model would have been even higher than indicated in the standard run (Fig. 3.7a).

It is conspicuous, that in times of low temperature (Fig. 3.3a) the $p\text{CH}_4$ increases (Fig. 3.7). Because of the enhanced humidity on land due to decreasing temperature, the coal-swamp distribution increased and forced the CH_4 emission. It is obvious that the increasing emissions slow down the lowering trend of temperature as a function of the heating properties of the greenhouse gas, and may have prevented an upcoming ice age in the Carboniferous.

I run two sensitivity tests to show the dependency of CH_4 emission to the average global temperature. In both runs the time dependency of the temperature is eliminated, one runs with a “low” Quaternary value of about 13.5°C , and the other one runs with an arbitrary temperature of about 20°C for the entire Phanerozoic. It becomes obvious how influential the surrounding temperature could be (Fig. 3.7). The atmospheric CH_4 content increases exponentially due to increasing temperature. At a constant temperature of about 13.5°C , the $p\text{CH}_4$ reaches max. 7.3 ppmV a variance lower of about 2.3 ppmV in the standard run at the same time, but a constant temperature of about 20°C results in an atmospheric CH_4 concentration of about 100 ppmV. This is caused by the exponential dependency of the methane emission and its atmospheric accumulation. The resulting RF significantly enhanced the surrounding temperature. The maximum value at a constant average global temperature is about 12 W m^{-2} , which is 25 times higher than the RF of CH_4 today - and eight times higher than the RF of CO_2 today (Fig. 3.8). For these test runs I excluded the positive feedback of increasing methane emission due to an increasing surrounding temperature and the increasing temperature due to an increasing methane emission. This effect would further enhance the $p\text{CH}_4$, thus RF, in the case of constant temperature, as mentioned above. These runs point out the strong dependency of methane emission to the surrounding temperature but are far away from realistic conditions. As mentioned before the distribution of waterlogged soils increase with increasing humidity due to decreasing temperature. Thus due to increasing temperature the distribution of waterlogged soils decreases, resulting in a total emission amount decrease, although the emission rate increases.

There are positive and negative feedbacks on the climate caused by the discussed greenhouse gas. In times of warm climate melting of CH_4 gas stores, trapped in permafrost soils and under ice sheets, forces the warming trend as a positive feedback. In times of cold climate the amounts of freezing stores increase and inhibit the CH_4 release as a positive feedback. A negative feedback happens during cold as well as warm climates. Due to a sinking sea-level the stability conditions of the gas hydrates trapped on the sea-floor are changing. Thus an enhanced release and a following climate warming are contrary to the sea-level lowering processes, like ice sheet growing. This means

a negative feedback to the global warming results at the same time in a forced CH_4 release inhibited by a rising sea-level and by changing the stability conditions of gas hydrates. Simultaneously a higher CH_4 amount in the water column forces a decrease of the marine biological activities, enhances the amount of organic matter and therefore also the CH_4 release as a positive feedback. With a shift from colder to warmer climates the source aspects for wetlands are becoming more significant, because the temperature is rising as well as the humidity. Thus the released methane causes the temperature to rise. Since the air is getting dryer with rising temperature, the source aspects change to worse conditions, what it is likewise for cooling conditions. Hence, it is obvious that a change in source aspects is linked to the climate with positive and negative feedbacks.

3.4 Conclusions

The present model describes the secular CH_4 trend over the entire Phanerozoic and reflects the importance of the wetlands. The atmosphere is able to adjust moderate emission rates, but up to a specific value, alkanes become accumulated exponentially in the atmosphere. In times with significant accumulation, and with a sudden release of great methane amounts, the pollution more or less affects the average global temperature, and RCO_2 . In times with high organic matter production, the atmospheric CH_4 content increases. This was the case during the Carboniferous coal swamp era, when the atmospheric methane content increased up to 10 ppmV. The high atmospheric methane concentration during the Carboniferous implies a maximum radiative forcing of about 3.5 W m^{-2} via methane, which is twice as high as the recent radiative forcing of atmospheric CO_2 . The model results show conspicuously, that the RCO_2 did not increase proportional to pCH_4 due to increasing methane emission, as expected due to its decomposition products. In contrast, during the Carboniferous, atmospheric methane increased and the RCO_2 decreased. By its radiative forcing and due to its decomposition into CO_2 , methane heated the average global surface temperature up to 1°C . Due to increasing surface temperature, the silicate weathering increases, which consumes atmospheric CO_2 . The elevated pCH_4 values during the Permian-Carboniferous cold period may have moderated the temperature decline caused by the coeval draw down of atmospheric CO_2 . Both, the decrease in pCO_2 and the increase in pCH_4 are intimately linked to the spread of land plants during the Permian and Carboniferous. The high methane emissions from swamps during this period may have prevented the development of a “snowball earth” state repeatedly encountered during the Precambrian prior to the advent of land plants.

The trigger for the sudden methane release is under debate, as well as its influence on the global atmospheric methane budget, and on the global temperature, but it is comprehensible that it had an influence on the secular $\delta^{13}\text{C}$ trend, because of the very light carbon content. I can calculate the emitted carbon via methane degassing by gas hydrates concerning to overall carbon cycle with respect to isotopic carbon excursions.

Chapter III

Because of the decomposition of such great amounts of methane, degassed from the ocean floor, a massive oxygen reduction in seawater occurs, which precludes an anoxic ocean event, which could result in mass extinctions.

Generally, the direct effects of atmospheric methane are less important, more important are the indirect effects, e.g. due to the production of water vapor and CO₂.

References

- Bains S., Corfield R. M., and Norris R. D. (1999) Mechanisms of climate warming at the end of the Palaeocene. *Science* 285, 724 - 727.
- Bartdorff O. and Wallmann K. (submitted) Modeling the chemical evolution of seawater (S, P, C, Sr, O) over the Phanerozoic.
- Beerling D. J., Lomas M. R., and Gröcke D. R. (2002) On the nature of methane gas-hydrates dissociation during the Torarcian and Aptian oceanic anoxic events. *American Journal of Science* 302, 28 - 49.
- Beerling D. J. and Royer D. L. (2002) Fossil plants as indicators of the Phanerozoic global carbon cycle. *Annual Reviews of Earth and Planetary Sciences* 30, 527 - 556.
- Berner E. K. and Berner R. A. (1996) *Global environment, water, air, and geochemical cycles*. Prentice - Hall, inc.
- Berner R. A. (1994) GEOCARB II: A revised model of atmospheric CO₂ over Phanerozoic time. *American Journal of Science* 294, 56-91.
- Berner R. A. (2004) The Phanerozoic carbon cycle: CO₂ and O₂.
- Berner R. A. and Kothavala Z. (2001) GEOCARB III: A revised model of atmospheric CO₂ over Phanerozoic time. *American Journal of Science*, 182-204.
- Bice K. L. and Marotzke J. (2002) Could changing ocean circulation have destabilized methane hydrate at the Palaeocene / Eocene boundary? *Paleoceanography*.
- Blake D. R. and Rowland F. S. (1988) Continuing worldwide increase in tropospheric methane, 1978 to 1987. *Science* 239, 1129 - 1131.
- Boles J. R., Clark J. F., Leifer I., and Washburn L. (2001) Temporal variation in natural methane seep rate due to tides, Coal Oil Point area, California. *Journal of Geophysical Research* 106(C11), 27,077 - 27,086.
- Budyko M. I., Ronov A. B., and Yanshin A. L. (1987) *History of the earth's atmosphere*. Springer-Verlag.
- Christensen T. R., Ekberg A., Ström L., Mastepanov M., Panikov N., Öquist M., Svensson B. H., Nykänen H., Martikainen P. J., and Oskarsson H. (2003) Factors controlling large scale variations in methane emissions from wetlands. *Geophysical Research Letters* 30(7, 1414), 67,1 - 67-4.
- Dickens G. R. (2001) On the fate of past gas: What happens to methane released from bacterially mediated gas hydrate capacitor? *Geochemistry, Geophysics, Geosystem, an electronic journal of the Earth sciences* 2.
- Dickens G. R. (2003) Rethinking the global carbon cycle with a large, dynamic and microbially mediated gas hydrate capacitor. *Earth and Planetary Science Letters* 213, 169 - 183.
- Dickinson R. E. and Cicerone R. J. (1986) Future global warming from atmospheric trace gases. *Nature* 319, 109 - 115.

- Dlugokencky E. J., Masarie K. A., Lang P. M., and Tans P. P. (1998) Continuing decline in the growth rate of atmospheric methane. *Nature*.
- Dudley R. (1998) Atmospheric oxygen, giant Palaeozoic insects and the evolution of aerial locomotor performance. *Journal of Experimental Biology* 201, 1043 - 1050.
- Ehhalt D. H. (1974) The atmospheric cycle of methane. *Tellus XXVI*(1 - 2), 58 - 70.
- Ehhalt D. H. and Heidt L. E. (1973) Vertical Profiles of CH₄ in the Troposphere and Stratosphere. *Journal of Geophysical Research* 78(24), 5265 - 5271.
- Etiopo G. and Milkov A. V. (2004) A new estimate of global methane flux from onshore and shallow submarine mud volcanoes to the atmosphere. *Environmental Geology* 46, 997 - 1002.
- Fey A., Claus P., and Conrad R. (2004) Temporal change of ¹³C-isotope signatures and methanogenic pathways in rice field soil incubated anoxically at different temperatures. *Geochimica et Cosmochimica Acta* 68(2), 293 - 306.
- Fogg P. G. T. (2003) General behaviour and origins of greenhouse and significant trace gases. In *Chemicals in the Atmosphere - Solubility, sources and reactivity* (ed. P. G. T. Fogg and J. Sangster), pp. 1 - 18. International Union of Pure and Applied Chemistry.
- Gassmann F. (1994) *Was ist los mit dem Treibhaus Erde?* Verlag der Fachvereine Zürich.
- Gautier D. L. and Claypool G. E. (1984) Interpretation of methanic diagenesis in ancient sediments by analogy with processes in modern diagenetic environments. In *Clastic Diagenesis*, Vol. 37 (ed. D. A. McDonald and R. C. Surdam), pp. 111 - 123. American Association of Petroleum Geologists.
- Graedel T. E. and Crutzen P. J. (1995) *Atmosphere, Climate, and Change*. Scientific American Library.
- Graedel T. E., Hawkins D. T., and Claxton L. D. (1986) *Atmospheric chemical compounds, sources, occurrence, and bioassay*. Academic Press, Inc.
- Gregor C. B. (1985) The mass-age distribution of Phanerozoic sediments. In *The chronology of the geologic record* (ed. N. J. Snelling), pp. 284 - 288. Geological Society.
- Grimaldi D. (2001) Insect evolutionary history from Handlirsch to Hennig and beyond. *Journal of Palaeontology* 75(6), 1152 - 1160.
- Harvey L. D. D. (1993) A guide to global warming potentials (GWPs). *Energy policy*, 24 - 34.
- Hayes J. M., Strauss H., and Kaufman A. J. (1999) The abundance of ¹³C in marine organic matter and isotopic fractionation in the global biogeochemical of carbon during the past 800 Ma. *Chemical Geology* 161, 103 - 125.
- Hesselbo S. P., Gröcke D. R., Jenkyns H. C., Bjerrum C. J., Farrimond P., Morgans Bell H. S., and Green O. R. (2000) Massive dissociation of gas hydrate during a Jurassic oceanic event. *Nature* 406, 392 - 395.
- IPCC. (2001) *Climate change 2001: The scientific basis*. Cambridge University Press.
- Jacob D. J. (2000) The oxidizing power of the atmosphere. In *Handbook for the weather, climate and water* (ed. T. Potter, B. Colman, J. Fishman, and M.-G. Hill).

- Jahren A. H., Arens N. C., Sarmiento G., Guerrero J., and Amundson R. (2001) Terrestrial record of methane hydrate dissociation in the Early Cretaceous. *Geology* 29(2), 159 - 162.
- Jahren A. H., Conrad C. P., Arens N. C., Mora G., and Lithgow-Bertelloni C. (2005) A plate tectonic mechanism for methane hydrate release along subduction zones. *Earth and Planetary Science Letters* 236, 691 - 704.
- Jiang G., Kennedy M. J., and Christie-Blick N. (2003) Stable isotopic evidence for methane seeps in Neoprotozoic postglacial cap carbonates. *Nature* 426, 822 - 826.
- Judd A. G., Hovland M., Dimitrov L. I., Garcia Gill S., and Jukes V. (2002) The geological methane budget at continental margins and its influence on climate change. *Geofluids* 2, 109 - 126.
- Katz M. E., Pak D. K., Dickens G. R., and Miller K. G. (1999) The source and fate of massive carbon input during the latest Paleocene Thermal Maximum. *Science* 286, 1531 - 1533.
- Kennett J. P., Cannariato K. G., Hendy I. L., and Behl R. J. (2000) Carbon isotopic evidence for methane hydrate instability during quaternary interstadials. *Science* 288, 128 - 132.
- King G. M. and Schnell S. (1994) Effect of increasing atmospheric methane concentration on ammonium inhibition of soil methane consumption. *Nature* 370, 282 - 284.
- Kirschvink J. L. and Raub T. D. (2003) A methane fuse for the Cambrian explosion: carbon cycles and true polar wander. *Comptes Rendus Geoscience* 335, 65 - 78.
- Kopf A. J. (2002) Significance of mud volcanism. *Reviews of Geophysics* 40(2), 2,1 - 2,52.
- Kopf A. J. (2003) Global methane emission through mud volcanoes and its past and present impact on the Earth's climate. *International Journal of Earth Science (Geologische Rundschau)* 92, 806 - 816.
- Kvenvolden K. A. (2002) Methane hydrate in the global organic carbon cycle. *Terra Nova* 14, 302 - 306.
- Lawrence M. G., Jöckel P., and Kuhlmann R. (2001) What does the global mean OH concentration tell us? *Atmospheric Chemistry and Physics* 1, 37 - 49.
- Lelieveld J., Crutzen P. J., and Dentener F. J. (1998) Changing concentration, lifetime and climate forcing of atmospheric methane. *Tellus* 50(B), 128 - 150.
- Lelieveld J., Peters W., Dentener F. J., and Krol M. C. (2002) Stability of tropospheric hydroxyl chemistry. *Journal of Geophysical Research* 107(D23), 17,1 - 17,11.
- Migeotte M. V. (1948) Spectroscopic evidence of methane in the Earth's atmosphere. *Physical Review Letters* 73, 519 - 520.
- Milkov A. V. (2004) Global estimates of hydrate-bound gas in marine sediments: how much is really out there? *Earth Science Reviews* 66(3-4), 183 - 197.
- Padden M., Weissert H., and Rafelis M. (2001) Evidence for Late Jurassic release of methane from gas hydrate. *Geology* 29(3), 223 - 226.

- Paull C. K., Brewer P. G., Ussler III W., Peltzer E. T., Rehder G., and Clauge D. (2002) An experiment demonstrating that marine slumping is a mechanism to transfer methane from seafloor gas-hydrate deposits into the upper ocean and atmosphere. *Geo-Marine Letters*, 13.
- Pavlov A. A., Hurtgen M. T., Kasting J. F., and Arthur M. A. (2003) Methane-rich Proterozoic atmosphere. *Geological Society of America* 31(1), 87 - 90.
- Pavlov A. A., Kasting J. F., Brown L. L., Rages K. A., and Freedmann R. (2000) Greenhouse warming by CH₄ in the atmosphere of early Earth. *Journal of Geophysical Research* 105(E5), 11,981 - 11,990.
- Ronov A. B. (1993) *Stratisfera ili osadochnaya obolochka zemli (kolichestvennoe issledovanie)* (ed. Nauka), pp. 1 - 144.
- Ronov A. B. (1994) Phanerozoic transgressions and regressions on the continents: A quantitative approach based on areas flooded by the sea and areas of marine and continental deposition. *American Journal of Science* 294(Summer), 777 - 801.
- Ryskin G. (2003) Methane-driven oceanic eruptions and mass extinctions. *Geological Society of America* 31(9), 741 - 744.
- Schmidt G. A. and Shindell D. T. (2003) Atmospheric composition, radiative forcing, and climate change as a consequence of a massive methane release from gas hydrates. *Paleoceanography* 18(1), 4,1 - 4,9.
- Schrag D. P., Berner R. A., Hoffmann P. F., and Halverson G. P. (2002) On the initiation of a snowball Earth. *Geochemistry, Geophysics, Geosystem*, an electronic journal of the Earth sciences 3(6).
- Schultz M. G., Jacob D. J., Wang Y., Logan J. A., Atlas E., Blake D. R., Blake N. J., Bradshaw J. D., Browell E. V., Fenn M. A., Flocke F., Gregory G. L., Heikes B. G., Sachse G. W., Sandholm S. T., Shetter R. E., Singh H. B., and Talbot R. W. (1998) On the Origin of Tropospheric Ozone and NO_x over the Tropical South Pacific. *Journal of Geophysical Research*.
- Seinfeld J. H. and Pandis S. N. (1998) *Atmospheric chemistry and physics; from air pollution to climate change*. John Wiley & Sons, Inc.
- Sloan E. D. (1997) *Clathrate hydrates of natural gases*, second edition, revised and expanded. Marcel Dekker, Inc.
- Stanley S. M. (1989) *Earth and live through time*. W.H. Freeman and Company.
- Sudo K., Takahashi M., and Akimoto H. (submitted) CHASER: A global chemical model of the troposphere, 2. Model results and evaluation. *Journal of Geophysical Research*.
- Svensen H., Planke S., Malthé-Sorensen A., Jamtveit B., Myklebust R., Eidem T. R., and Rey S. S. (2004) Release of methane from volcanic basin as a mechanism for initial Eocene global warming. *Nature* 429, 542 - 545.
- Thorpe R. B., Law K. S., Bekki S., and Pyle J. A. (1996) Is methane-driven deglaciation consistent with the ice core records? *Journal of Geophysical Research* 101(D22), 28,627 - 28,635.

- Valentine D. L., Blanton D. C., Reeborgh W. S., and Kastner M. (2001) Water column methane oxidation adjacent to an area of active hydrate dissociation, Eel River Basin. *Geochimica et Cosmochimica Acta* 65(16), 2633 - 2640.
- Veizer J. and Jansen S. L. (1979) Basement and sedimentary recycling and continental evolution. *Journal of Geology* 87, 341 - 370.
- Wallmann K. (2001a) Controls on the Cretaceous and Cenozoic evolution of seawater composition, atmospheric CO₂ and climate. *Geochimica et Cosmochimica Acta* 65(18), 3005 - 30025.
- Wallmann K. (2001b) The geological water cycle and the evolution of marine d¹⁸O values. *Geochimica et Cosmochimica Acta* 65(15), 2469 - 2485.
- Wallmann K. (2003) Feedbacks between oceanic redox states and marine productivity: A model perspective focused on benthic phosphorus cycling. *Global Biogeochemical Cycles* 17(3), 10,1 - 10,18.
- Wallmann K. (2004) Impact of atmospheric CO₂ and galactic cosmic radiation on Phanerozoic climate change and the marine δ¹⁸O record. *Geochemistry, Geophysics, Geosystem*, an electronic journal of the Earth sciences 5(1), 30.
- Wang C., Prinn R. G., and Sokolov A. P. (1997) A global interactive chemistry and climate model. *Journal of Geophysical Research*.

Appendix

Appendix A3.1: Fluxes of methane (10^{18} mol Ma^{-1}) considered in the Box Model.

Description	Equation
Amount of ^{13}C in atmospheric CH_4 (‰)	$^{13}C = \Phi^{13}C_{gun}^{CH_4} * F_{gun}^{CH_4} + \Phi^{13}C_{volcano}^{CH_4} * F_{volcano}^{CH_4}$
Atmospheric CH_4 content	$pCH_4 = RCH_4 * pCH_4(r)$
Atmospheric CH_4 loss	$F_{atmosphere}^{CH_4} = k_{atmosphere} * F_{loss}^{CH_4}(q) * RCH_4$
Atmospheric CO_2 amount, induced due to emitted methane	$C = F_{gun}^{CH_4} + F_{volcano}^{CH_4}$
Atmospheric partial pressure of CH_4	$pCH_4 = \frac{CH_4}{180 * 10^{18}}$
Average global temperature, induced due to CO_2 and CH_4	$Temp = \Gamma * \ln RCO_2 + \Delta T_{RF} - 7.4 * \frac{t}{-570} + 13.5 + GEOG$
Consumption of CH_4 within the soils	$F_{soils}^{CH_4} = F_{soils}^{CH_4}(q) * f_{AN}$
Kinetic constant calculation for methane loss in the atmosphere	$k_{atmosphere} = 0.07925 + 061712 * e^{\frac{-RCH_4}{5.43812}} + 0.65264 * e^{\frac{-RCH_4}{0.41025}} + 0.35927 * e^{\frac{-RCH_4}{39.436}}$
Mole fraction of released ^{13}C in CH_4 out of methane gas hydrates	$\Phi^{13}C_{gun}^{CH_4} = \frac{1000 + \delta^{13}C_{CH_4gun}}{89990 + \delta^{13}C_{CH_4gun}}$
Mole fraction of released ^{13}C in CH_4 out of terrestrial volcanoes	$\Phi^{13}C_{volcano}^{CH_4} = \frac{1000 + \delta^{13}C_{CH_4volcano}}{89990 + \delta^{13}C_{CH_4volcano}}$
Net input of CH_4 out of the releaser into the atmosphere	$netinput = \frac{F_{release}^{CH_4} - F_{soil}^{CH_4}}{F_{release}^{CH_4}(q) - F_{soil}^{CH_4}(q)}$
Quaternary release of CH_4 to the atmosphere	$F_{release}^{CH_4}(q) = F_{mud}^{CH_4}(q) + F_{gun}^{CH_4}(q) + F_{volcano}^{CH_4}(q) + F_{shelf}^{CH_4}(q) + F_{ocean}^{CH_4}(q) + F_{wetland}^{CH_4}(q) + F_{termite}^{CH_4}(q)$
Quaternary total atmospheric CH_4 loss	$F_{loss}^{CH_4}(q) = -F_{soil}^{CH_4}(q) - F_{atmosphere}^{CH_4}(q)$
Radiative forcing, induced due to atmospheric methane	$RF = 0.0411 * \sqrt{pCH_4} - \sqrt{pCH_4(q)}$
Relation between temperature change and radiative forcing	$\Delta T_{RF} = \lambda * RF$
Release of CH_4 out of digestive tracks of insects	$F_{termite}^{CH_4} = F_{termite}^{CH_4}(q) * f_{IN}$
Release of CH_4 out of mud volcanoes	$F_{mud}^{CH_4} = F_{mud}^{CH_4}(q) * \frac{F_B^{POC}}{F_B^{POC}(q)} * f_{VO}$
Release of CH_4 out of shallow water environments	$F_{shelf}^{CH_4} = F_{shelf}^{CH_4}(q) * f_{SA} * \frac{F_B^{POC}}{F_B^{POC}(q)}$
Release of CH_4 out of terrestrial volcanoes	$F_{volcano}^{CH_4} = F_{volcano}^{CH_4}(q) * f_{VO}$

Appendix A3.1: Continued

Description	Equation
Release of CH ₄ out of the photic zone of the oceans	$F_{ocean}^{CH_4} = \frac{F_B^{POC}}{F_B^{POC}(q)} * F_{ocean}^{CH_4}(q)$
Release of CH ₄ out of wetlands, particularly swamps	$F_{wetland}^{CH_4} = F_{wetland}^{CH_4}(q) * f_{T_{wetland}} * f_{ER} f_{coal}$
Sudden release of CH ₄ out of methane gas hydrates (Tab. 3.2)	$F_{gun}^{CH_4} = F_{gun}^{CH_4}(table)$
Temperature dependent releasing rate of CH ₄ out of wetlands	$f_{T_{wetland}} = 0.111 * e^{0.1635 * T_{temp}}$
Total atmospheric CH ₄ loss	$F_{loss}^{CH_4} = -F_{soil}^{CH_4} - F_{atmosphere}^{CH_4}$
Total release of CH ₄ to the atmosphere	$F_{release}^{CH_4} = F_{mud}^{CH_4} + F_{gun}^{CH_4} + F_{volcano}^{CH_4} + F_{shelf}^{CH_4} + F_{ocean}^{CH_4} + F_{wetland}^{CH_4} + F_{termite}^{CH_4}$

Appendix A3.2: Parameter of methane considered in the Box Model.

Parameter	Description	Reference	Value
$pCH_4(p)$	Preindustrial partial pressure of CH ₄ (ppmV)	Raynaud et al. (1993)	0.7
$F_B^{POC}(q)$	Quaternary POC accumulation (10 ¹⁸ mol Ma ⁻¹)	Wallmann (2004)	5.8
$F_{soil}^{CH_4}(q)$	Quaternary CH ₄ consumption of soils (10 ¹⁸ mol Ma ⁻¹)	IPCC (2001)	2.37
$F_{termite}^{CH_4}(q)$	Quaternary CH ₄ release out of digestive tracks of insects (10 ¹⁸ mol Ma ⁻¹)	IPCC (2001)	1.25
$F_{mud}^{CH_4}(q)$	Quaternary CH ₄ release out of mud volcanoes (10 ¹⁸ mol Ma ⁻¹)	Etiopie and Milkov (2004)	0.37 - 0.56 (0.56)
$F_{shelf}^{CH_4}(q)$	Quaternary CH ₄ release out of shallow water environments (10 ¹⁸ mol Ma ⁻¹)	Ehhalt and Heidt (1973)	0.0436 - 0.873 (0.473)
$F_{volcano}^{CH_4}(q)$	Quaternary CH ₄ release out of terrestrial volcanoes (10 ¹⁸ mol Ma ⁻¹)	Judd et al. (2002)	0.0499 - 0.387 (0.387)
$F_{ocean}^{CH_4}(q)$	Quaternary CH ₄ release out of the photic zone of the oceans (10 ¹⁸ mol Ma ⁻¹)	IPCC (2001)	0.623 - 0.935 (0.935)
$F_{wetland}^{CH_4}(q)$	Quaternary CH ₄ release out of wetlands, particularly swamps (10 ¹⁸ mol Ma ⁻¹)	Seinfeld and Pandis (1998)	3.43 - 9.35 (7.5)
$pCH_4(q)$	Quaternary partial pressure of CH ₄ (ppmV)	Raynaud et al. (1993)	0.355
$pCO_2(q)$	Quaternary partial pressure of CO ₂ (ppmV)	Berner and Berner (1996)	230
$pCH_4(r)$	Recent partial pressure of CH ₄ (ppmV)	Berner and Berner (1996)	1.71
$pCO_2(r)$	Recent partial pressure of CO ₂ (ppmV)	Berner and Berner (1996)	380
$\delta^{13}C_{gun}^{CH_4}$	$\delta^{13}C$ value of catastrophically released CH ₄ by methane gas hydrates (‰)	Gautier and Claypool (1984)	-100 to -50 (-50)
$\delta^{13}C_{volcano}^{CH_4}$	$\delta^{13}C$ value of released CH ₄ by terrestrial volcanoes (‰)	Gautier and Claypool (1984)	-5 to -4 (-4.5)

Appendix A3.3: External time-dependent variables considered in the Box Model.

<i>Variable</i>	<i>Description</i>
$f_{ER} f_{coal}$	Changes in coal distribution
$Temp$	Changes in global surface temperature
RCO_2	changes in normalized pCO_2
F_B^{POC}	Changes in POC accumulation on the sea-floor
f_{SA}	Changes in sea-level
Γ	Constant relating pCO_2 to surface temperature
f_{AN}	Effect of the rise and evolution of vascular land plants
f_{gun}	Temporary release of CH_4 out of methane gas hydrates

Chapter IV

**Evolution of oxygen concentrations in the deep
ocean and marine nutrient inventories over the
entire Phanerozoic**

Abstract

A new model for the turnover of molecular oxygen and nutrients in the global ocean has been developed. It includes a surface water and a deep water box and marine surface sediments deposited on the continental shelf, slope and rise, and on the deep-sea floor. It calculates the concentrations of dissolved oxygen, nitrate and phosphate in the two water boxes and in the pore waters of marine sediments. The surface water box receives nutrients from land and exchanges oxygen with the atmosphere. Moreover, nitrogen fixation adds nitrate to the surface ocean. Nutrients are removed from surface waters by marine export production. In the deep water box, oxygen is consumed and nutrients are released by the degradation of exported organic matter while nitrate is consumed via denitrification. Dissolved species are exchanged between the two water boxes by vertical mixing and the underlying sediments exchange solutes with the surface and deep ocean by molecular diffusion across the sediment/water interface.

The model was calibrated using Holocene data and was tested to decipher the sensitivity of the marine biogeochemical system with respect to external perturbations. These tests showed that marine productivity, nutrient inventories and the oxygen content of the deep ocean react very sensitive to changes in ocean ventilation whereas nutrient inputs from land have a comparably small effect on the oceans. Reducing sediments are a more important source of phosphate to the oceans than river input. Therefore, the positive feedback between ocean anoxia and eutrophication, which is rooted in the redox-dependent phosphorus turnover in sediments, dominates the evolution of the marine biogeochemical system. This model result implies that the state of the ocean is mainly regulated by climatic conditions and the O₂ content of the atmosphere. It was also applied to reconstruct the Phanerozoic evolution of the oceans. According to the model, the deep ocean was almost completely anoxic during the Early Paleozoic because the low oxygen concentrations in the early Paleozoic surface ocean - which were caused by low atmospheric pO₂ values and high surface temperatures - inhibited an effective ventilation of the deep ocean. The ocean evolved into a fully oxic state during the Permian-Carboniferous cold period when the oxygen concentration in surface water ventilating the deep ocean was very high because of high atmospheric pO₂ and low surface temperature values. Since these atmospheric and climatic conditions were probably caused by the spread of land plants (Bernier, 2004), the development of a fully oxic deep ocean should be regarded as an additional - and previously not recognized - consequence of this major ecological transition. The model also predicts that the nutrient N : P ratio in seawater changes with the redox state of the ocean and that nitrogen fixation cannot fully compensate for these changes. Thus, the nutrient N : P ratios were low in the anoxic oceans of the early Paleozoic and attained very high values during the Permian-Carboniferous cold period. Finally, the model was applied to investigate the triggering of oceanic anoxic events (OAEs). My model could only reproduce the Early Aptian OAE 1a when several important changes occur coevally. Nutrient inputs from the continents and ocean ventilation had to be changed simultaneously by 60 % to attain a fully anoxic Cretaceous ocean.

4.1 Introduction

Molecular oxygen is fundamental for life as we know it. It is mainly produced by organogenic processes and is consumed by geochemical breakdown processes and biological respiration. Atmosphere, hydrosphere, and pedosphere contain significant amounts of oxygen.

The evolution of atmospheric oxygen is strongly coupled to the biological evolution on land (Berner et al., 2003). The Phanerozoic atmospheric oxygen trend underlies the interplay of oxygen production due to photosynthesis and weathering, thus it has considerably varied over the past (Berner, 2004). The oceanic oxygen concentration in surface as well as deep water is linked to the atmospheric oxygen content (Fig. 4.1).

Contrary to former assumptions, e.g. by Holland (1978), the ocean's water composition has varied multiple times on a geological time scale (Martin, 1996). Because of the lack of evidence for these events in the geological record, the knowledge of the marine productivity of ancient seawater is very sparse. Even if there is considerable evidence for a consistently changing ocean water composition, such as dramatic changes in the biodiversity, like mass extinction and flourishing (Martin, 1996), unfortunately there is no information on the driving forces. The Phanerozoic advent for instance was assumed to mark such a big biogeochemistry change of the atmosphere as well as of the oceans (Kershaw and Cundy, 2000; Martin, 1996).

It has been assumed that the biodiversity is connected to the nutrient levels of the oceans (Martin, 2003), which are controlled by the efficiency of runoff, denudation, erosion and weathering rates. In the past the supply of dissolved nutrients from land has been small (Otto-Bliesner, 1995), likewise the biodiversity (Jackson and Johnson, 2001). Rigby and Milsom (2000) assumed that the nutrients in the Early Phanerozoic resided in a fast cycle in the upper surface, or were lost to deeper regimes, where they were decomposed, but under usage of large amounts of oxygen. Furthermore the sparsely produced oxygen was consumed shortly after its release (Kershaw and Cundy, 2000; Martin, 2003; Payne and Finnegan, 2006).

However, the knowledge of the composition and allocation of nutrients and oxygen within the ancient oceans is very limited, but it is distinct that an enhanced nutrient supply from the continents fed the oceanic life almost immediately and affected the entire ocean chemistry.

In general, the oxygen rich surface layer of the ocean is currently replenished by oxygen from the atmosphere (Houghton, 1997). The ventilation of deep seawater mainly occurs due to the sinking of oxygen rich dense seawater and vertical seawater mixing (Fig. 4.1). The ventilation by oxygen enriched water mainly prevails at the polar ice caps, due to the cooling of the surrounding seawater. The intensity of the ventilation rate strongly depends on the temperature gradient between the Equator and the polar caps (Kuypers et al., 1999).

The vertical flux of particles within the water column determines the distribution of biogeochemical elements in seawater (Chester, 2000). The decomposition and dissolution of particles during sinking processes together with ocean circulation control the diversification of oxygen, nutrients and other seawater ingredients (Frogner et al., 2001). Understanding the processes

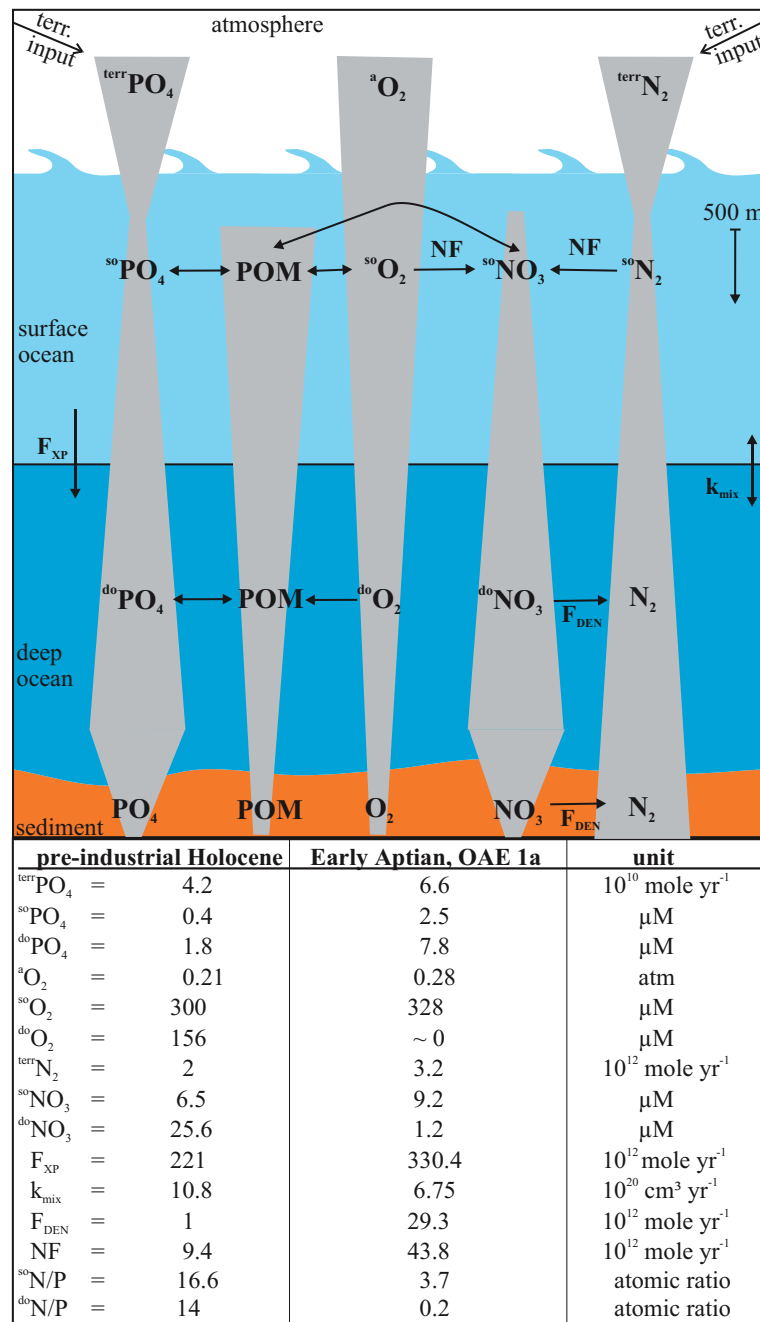


Figure 4.1: Biogeochemical pathways: The upper part illustrates schematically the biogeochemical pathways of phosphate (PO_4), nitrogen (N_2) and nitrate (NO_3), oxygen (O_2), and particulate organic matter (POM), and their control factors nitrogen fixation (NF), denitrification (F_{DEN}), export production (F_{XP}), and vertical mixing (k_{mix}) with respect to the river and aeolian input, atmosphere, oceanic surface water (< 500 m), oceanic deep water, and the oceanic sediment.

The lower part lists the comparison of pre-industrial Holocene to Early Aptian (OAE 1a) of oceanic fluxes and concentrations.

The shaded bars indicate the changes of the prevailing component, the superscripted letters assign the concentration and fluxes to the particular environment: terr – terrigenous input via rivers and aeolian transport, a – atmosphere, so – surface ocean, do – deep ocean, and se – sediment (the number for the component within the sediments belong to different environments, shallow seafloor, continental rise, deep seafloor). Pre-industrial Holocene river inputs and aeolian fluxes were taken from Berner and Berner (1996) and Compton et al. (2000) respectively. Marine export production and depositional fluxes were taken from Schlitzer (2000). (For further details see Appendix A4.6)

controlling particle formation in the upper ocean as well as their transport and transformation within the water column is crucial in determining the role of the oceans in global cycles of carbon and other associated elements.

Dissolved nutrients, carbon, phosphorus, and nitrogen are mainly removed out of the photic zone by photosynthesis. The driving force for changes of the oceanic nutrient inventory is the primary production, since it is limited by the amount of available nutrients, growing by the supply of phosphorus delivered due to weathering or by nitrogen fixation (Fennel et al., 2005). Dissolved and particulate nutrients from the upper oceanic water column are part of the recycling process inside the food chain, or sink to the seafloor as marine snow (Kerr, 2002). The main part of the descending particulate organic matter is remineralized. Parts of the recycled organic matter (POM) of the deeper water regime return into the food chain. The remaining part sinks to the seafloor, where it is decomposed or buried (Fig. 4.1). Because of the permanent consumption in the upper layer and sinking of the remaining parts, a depletion of nutrients in the upper water column results. Today the recycling of sinking matter within the photic zone buffers the depletion. But an increasing export production of nutrients out of the photic zone enhances the bacterial oxygen consumption. This exhaustion as well as the further usage of oxygen due to the decomposition of sinking organic matter results in an oxygen depletion of the ocean and thus probably in an extinction of marine life in the upper water column (Payne and Finnegan, 2006). The character of such an ocean transforms into eutrophic conditions. Descending organic matter, from the upper water column to the deep seafloor, is no longer consumed under oxic conditions, but decomposed due to the consumption of nitrogen under anoxic conditions. The remaining buried matter is covered by sediments and creates organic rich sediments which probably are followed by black shales or/and oil rich sediments, and which can be found in the geological record nowadays (Stanley, 1989).

During the past, recurrent shifts between oxic and anoxic seawater environments have occurred (Oceanic Anoxic Event - OAE). It is conspicuous that the anoxic events always lasted around three million years (Handoh and Lenton, 2003). During these widespread anoxic events almost all of the marine livings become extincted (Foote, 2003).

Anoxic events commonly occur during periods of warm climate (Jablonski, 2004), meaning high atmospheric CO₂ levels, limited polar ice caps, a small temperature gradient from the poles to the Equator (Kuypers et al., 1999), and thus an inhibited Thermohaline-circulation (Broecker, 1997). Oxygen solubility decreases with increasing temperature (Broecker and Peng, 1982). Furthermore marine animals in shallow water environments, such as shelf areas, consume the small amount of the dissolved oxygen, depending on the efficiency of the primary production (Payne and Finnegan, 2006). Because of a strong stratification of the ocean layers the transfer of oxygen to deep water environments is inhibited or nonexistent. Usually descending oxygen rich cold water at the polar caps feeds the deep water environments with oxygen (Broecker, 1997). During phases of warm global climate these polar ice caps melt more or less completely (Stanley, 1989). Because of the absence of these ice shields no or only little cooled water sinks into the deeper water column, automatically lowering the ventilation of deep water environments.

OAEs are accompanied with an enhanced tectonic and volcanic activity (Pálffy and Smith, 2000), documented in variations of strontium isotopes in marine carbonates (Jones and Jenkyns, 2001). During crust production and volcanic degassing more nutrients reach the ocean, force the organic matter production (Duggen et al., submitted) and enhance the formation of marine snow. In addition, crust formation increases the relative area of shallow seas and shelves (Rowley, 2002) and thus the distribution of populated marine environments (Payne and Finnegan, 2006). Furthermore the atmospheric CO₂ content increases due to enhanced volcanic degassing. A higher CO₂ content results in a higher global average temperature, leading to more complex consequences like enhanced weathering rates (Walker et al., 1981) and a decreased ocean circulation (Anderson and Archer, 2002).

Further evidences for possible OAEs in the past are abrupt positive $\delta^{13}\text{C}$ excursions in ancient ocean water (Kuypers et al., 2004). Generally organic matter sedimentation has increased during the OAEs (Kuypers et al., 1999). Due to the enhanced sedimentation, organic matter controlled the atmospheric CO₂ content in a negative feedback loop.

It is under debate what kind of triggers create anoxic oceans. On one hand it has been assumed that the initial impact originated on the seafloor (Renard et al., 2005), but on the other hand may have been caused by processes beyond the ocean floor (Bice et al., submitted), by processes on land (Morgan et al., 2004), as well as by extraterrestrial processes, such as precession (Aguillera-Franco and Allison, 2005; Kuypers et al., 2004; Tsikos et al., 2004). The differences become apparent in strontium, oxygen, and carbon isotopes recorded in marine carbonates. An enhanced release of methane out of clathrates within the seafloor results in an enormous negative $\delta^{13}\text{C}$ excursion (Sloan, 1997), in contrast, climatic impacts, e.g. significant global warming, results in a positive $\delta^{13}\text{C}$ excursion (Bailey et al., 2003), whereas the ratio of strontium isotopes decreases due to an enhanced light strontium release out of the mantle (Pálffy et al., 2002). The precession affects the climate, and thus, amongst other factors, the oxygen isotope ratio too (Nunez et al., 2006). The initial trigger mechanism of an OAE is still unknown, similarly to the main driving forces, but the resulting phenomena and their consequences have been recorded and will be discussed below.

Here a new model for oxygen, phosphorus, nitrogen and particulate organic carbon in oceans and their sediments is presented. The model predicts nutrient and oxygen concentration over the entire Phanerozoic. The presented regimes comprise the ocean surface layer down to a depth of 500 m and the deep ocean water box. Furthermore the model deciphers the influence factors to suffocate global oceans, as occurred during oceanic anoxic events.

4.2 Set up of the model

This model is based on the coupled benthic-pelagic three-box model by Wallmann (2003). The three-box model (high- and low-latitude surface reservoir and a deep water box) for the global ocean was simplified into a two-box model (ocean surface and ocean deep water box), whereas the benthic

model was expanded to simulate the turnover of oxygen, nutrients and carbon not only in bioturbated surface sediments but also in deeper sediment layers. The model was used to simulate the changing oxygen and nutrient inventories of the ocean over the entire Phanerozoic (570 Ma). External driving forces such as continental nutrient inputs and atmospheric oxygen concentrations (Figs. 4.1 & 4.2a - f) were taken from a new model simulating the Phanerozoic evolution of oceans and atmosphere (Bartdorff and Wallmann, submitted-b).

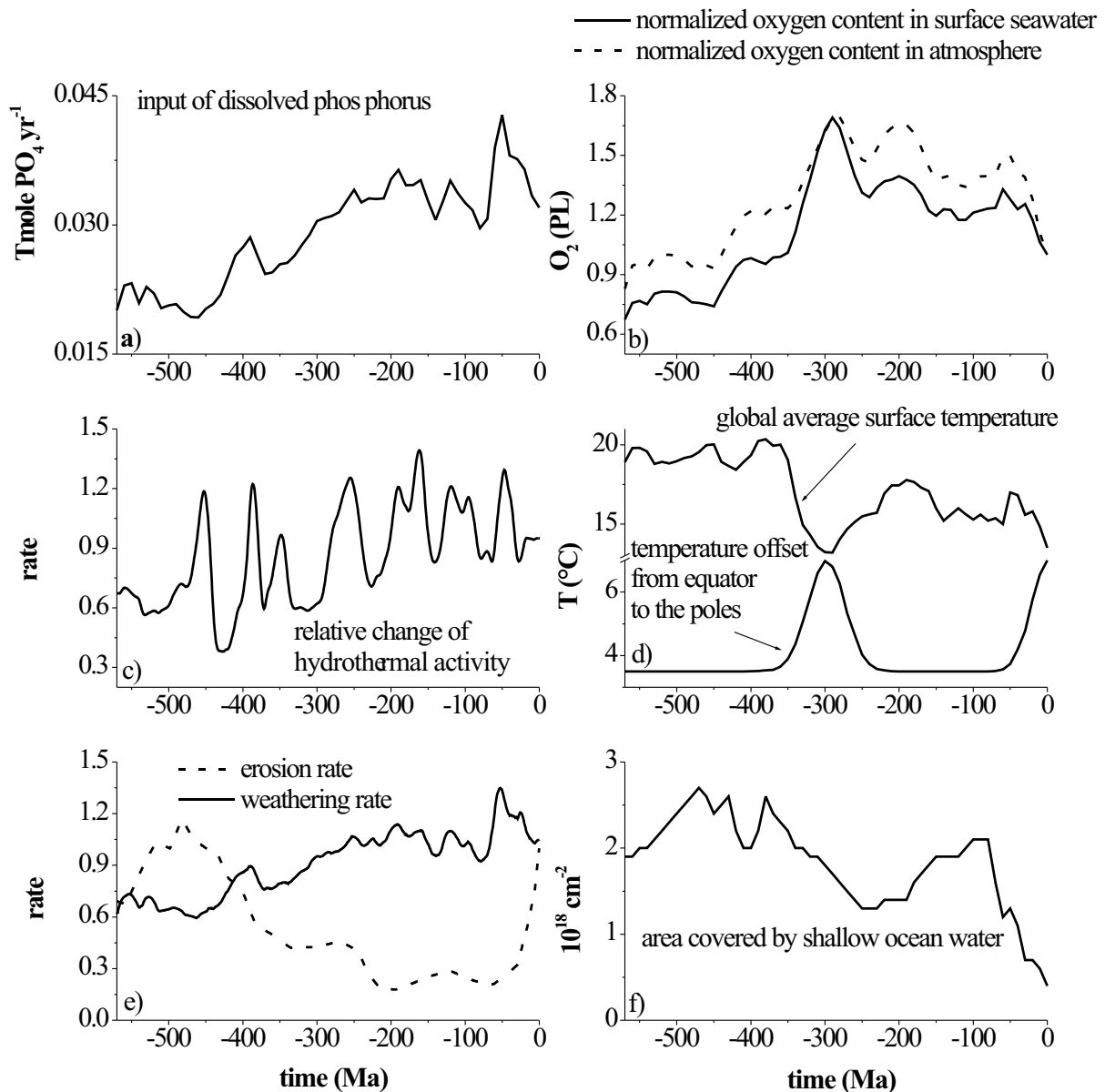


Figure 4.2a - f: External input of changes during the Phanerozoic a) of dissolved phosphorus into the surface water box ($< 500 \text{ m}$) (Bartdorff and Wallmann, sub.), b) oxygen content in surface water ($< 500 \text{ m}$) and atmosphere normalized on pre-industrial Holocene level (PL) ($300 \mu\text{M}$, 0.21 atm), c) relative change of hydrothermal activity (Bartdorff and Wallmann, sub.), d) global average surface temperature (Shaviv and Veizer, submitted) and temperature gradient from the equator to the poles, e) erosion efficiency and weathering rate (Bartdorff and Wallmann, sub.), f) area covered by shallow ocean water ($< 500 \text{ m}$) (Ronov, 1994), considered for modeling.

Below I describe the principle set-up of the two boxes, the surface and deep water layer, and the benthic processes considered in the model. The complete set up of the model, the differential equations, flux equations, and parameter values used in the model are summarized in Figure 4.1 and Table 4.1 as well as in Appendix A4.1 – A4.6. The detailed description of the model approaches can be found in Wallmann (2003). For model development I used Mathematica 5.2 by Wolfram Research.

*Table 4.1: Differential equations defining the turnover of phosphate, nitrate and oxygen in the water column. *: N_{sw} , N_{dw} , P_{sw} , P_{dw} , O_{sw} , O_{dw} are concentrations of dissolved nitrate (N), phosphate (P) and oxygen (O) in surface waters (sw), and deep water (dw). Additional parameters and parameter values are listed in Appendix A4.1 – A4.6. Shelf deposits extend down to a water depth of 500 m.*

Parameter	Equation*
Phosphate in surface water	$\frac{dP_{sw}}{dt} = (F_P - F_{XP}) * \frac{1}{Vol_{sw}} + \frac{area_{sh}}{Vol_{sw}} * \varphi_0 * \varphi_0^\theta * D_{P,sh} * \frac{\partial P_{sh}}{\partial t} \Big _{x=0} + trans_{P,sw}$
Phosphate in deep water	$\frac{dP_{dw}}{dt} = \frac{F_{XP}}{Vol_{sw}} * (-f_{D,ds} - f_{D,r} - f_{D,sh}) * \frac{Vol_{sw}}{Vol_{dw}} - k_{hy} * P_{dw} + \varphi_0 * \varphi_0^\theta * \left(\frac{area_{ds}}{Vol_{dw}} * D_{P,ds} * \frac{\partial P_{ds}}{\partial t} \Big _{x=0} + \frac{area_r}{Vol_{dw}} * D_{P,r} * \frac{\partial P_r}{\partial t} \Big _{x=0} \right) + trans_{P,dw}$
Nitrate in surface water	$\frac{dN_{sw}}{dt} = (F_N - 16 * F_{XP}) * \frac{1}{Vol_{sw}} + F_{NF} + \frac{area_{sh}}{Vol_{sw}} * \varphi_0 * \varphi_0^\theta * D_{N,sh} * \frac{\partial N_{sh}}{\partial t} \Big _{x=0} + trans_{N,sw}$
Nitrate in deep water	$\frac{dN_{dw}}{dt} = \frac{F_{XP}}{Vol_{sw}} * (-f_{D,ds} - f_{D,r} - f_{D,sh}) * 16 * \frac{Vol_{sw}}{Vol_{dw}} - \frac{F_{DEN}}{Vol_{dw}} + \varphi_0 * \varphi_0^\theta * \left(\frac{area_{ds}}{Vol_{dw}} * D_{N,ds} * \frac{\partial N_{ds}}{\partial t} \Big _{x=0} + \frac{area_r}{Vol_{dw}} * D_{N,r} * \frac{\partial N_r}{\partial t} \Big _{x=0} \right) + trans_{N,dw}$
Oxygen in deep water	$\frac{dO_{dw}}{dt} = -\frac{106}{rO} * \frac{O_{dw}}{O_{dw} + K_{O_2}} * \left(\frac{F_{XP}}{Vol_{sw}} * (-f_{D,ds} - f_{D,r} - f_{D,sh}) * \frac{Vol_{sw}}{Vol_{dw}} \right) + \varphi_0 * \varphi_0^\theta * \left(\frac{area_{ds}}{Vol_{dw}} * D_{O,ds} * \frac{\partial O_{ds}}{\partial x} \Big _{x=0} + \frac{area_r}{Vol_{dw}} * D_{O,r} * \frac{\partial O_r}{\partial x} \Big _{x=0} \right) - \frac{k_{mix}}{Vol_{dw}} * (O_{dw} - O_{sw})$

4.2.1 Surface water box

The surface layer spans the upper water column down to a depth of 500 m. It receives continental nutrient inputs via rivers and eolian transport. The nitrate and phosphate concentrations are calculated as internal model parameters considering the terrestrial inputs of nutrients, marine export production, nitrogen fixation, and the exchange processes with the underlying deep water box and shelf sediments (Tab. 4.1). Liebig's Law is implemented in the model such that export production is limited either by nitrate or phosphate (Wallmann, 2003). Nitrogen fixation depends only on dissolved phosphate concentrations and is inhibited by high dissolved nitrate concentrations (Wallmann 2003). With this parameterization, nitrogen fixation serves to stabilize both the nitrate concentration and the N : P ratio in the surface layer.

Oxygen concentrations calculated for the surface layer are not related to the biogeochemical processes occurring in the surface water but are controlled by externally prescribed atmospheric pO_2 values and surface temperatures (Fig. 4.2d). They are included in the model to simulate the ventilation of the deep ocean box. In the modern ocean, the supply of oxygen from surface water to deep water regimes mainly occurs at high-latitudes due to the cooling of the surface water by the surrounding polar ice caps. The oxygen content of this descending cold seawater is higher than the oxygen content of low-latitude seawater (Joos et al., 2003). The intensity and thus the effectiveness of this oxygen pump depend on the temperature gradient between the Equator and the polar caps (Boccaletti et al., 2003). The oxygen content of seawater is around $260 \mu\text{M}$ at an average Quaternary surface temperature of about 13.5°C (Broecker and Peng, 1982). Assuming that high-latitude surface waters ventilating the deep ocean are 7°C colder than the average surface water, these water masses attain an oxygen saturation content of about $300 \mu\text{M}$ (Broecker and Peng, 1982). During warmer periods, e.g. greenhouse periods (Norris et al., 2002), the temperatures at high-latitudes are strongly enhanced, therefore the descending water masses are much warmer and the temperature offset is reduced to smaller values (Fig. 4.2d). I predicted a temperature offset ranging from $3.5 - 7^\circ\text{C}$, in dependency to the global average temperature. The resulting oxygen concentrations in surface water used in the model (Fig. 4.2b) represent the values in surface waters at high latitudes ventilating the deep ocean rather than the concentrations in global average surface water. The highest oceanic surface oxygen content ($500 \mu\text{M}$) occurred during the icehouse era in the Upper Paleozoic (Fig. 4.2b). During the Mesozoic and Cenozoic the oceanic surface oxygen content decreased continuously down to the average content of the pre-industrial Holocene (about $300 \mu\text{M}$).

4.2.2 Deep water box

The deep water box spans the regime below 500 m water depth down to the seafloor. Nutrient concentrations in the deep ocean are enhanced by the re-mineralization of organic matter exported from the surface layer. They are diminished by the uptake of phosphate in hydrothermal plumes and axial circulation systems and by the loss of nitrate through microbial denitrification at low dissolved oxygen concentrations in the deep ocean (Tab. 4.1). Oxygen is consumed by the degradation of sinking organic matter. Moreover, nutrient and oxygen concentrations in the deep ocean box are affected by exchange processes with the surface box and the underlying slope and deep-sea sediments (Tab. 4.1).

4.2.3 Benthic model

The benthic submodel accounts for the turnover of dissolved oxygen, nitrate, and phosphate, particulate organic matter and particulate phosphorus in surface sediments deposited on the shelf,

continental slope and deep-sea floor (Wallmann, 2003). It is closely couple to the two water boxes. Sediments receive marine particulate organic matter produced within the surface water and not degraded within the deep water column. They exchange dissolved nutrients and oxygen with the surface water box (shelf sediments) and the deep water box (slope and deep-sea deposits) across the sediment/water interface. Terrigenous particles, including POC and reactive P, are also deposited at the sediment surface. Within the sediment, oxygen is consumed and nutrients are released in the pore water by the degradation of organic matter. Phosphate is fixed in authigenic minerals and in iron oxides while nitrate is consumed by denitrification. Overall, the benthic model does not follow simple Redfield stoichiometry. It rather predicts that nutrient fluxes from sediments into the water column depend on sedimentary redox conditions. Phosphate is preferentially recycled into the ocean under reducing conditions while nitrate recycling is enhanced under oxic conditions (Wallmann, 2003).

The benthic transport-reaction model of Wallmann (2003) was modified and extended to 20 cm depth, because redox-dependent processes controlling the turnover of nutrients also occur below a sediment depth of 10 cm. Each model column is now separated into 100 segments using an uneven grid (0.05 cm at the surface and 0.35 cm at depth). Porosity and tortuosity decrease with sediment depth and affect the transport of dissolved species via molecular diffusion and the transport of solids via burial. Bioturbation is limited to the upper 10 cm of the sediment column. Organic matter raining to the seafloor is degraded using simple first order kinetics within the bioturbated surface layer (0 – 10 cm) and age-dependent kinetics (Middelburg, 1989) in the underlying layer (10 – 20 cm).

4.3 Results and Discussion

The results of different model applications are presented and discussed in the following section. In the first subsection below I illustrate the oceanic pre-industrial Holocene current state for oxygen and nutrients in seawater. In section 4.3.2 I decipher the impact of the principal external driving forces on the marine biogeochemical system while the Phanerozoic evolution of oxygen and nutrient inventories and marine productivity are reconstructed in section 4.3.3. In the final subsection oceanic anoxic events (OAE) are described, and the parameters that may have driven the suffocation of ancient oceans (considering as an example, OAE 1a, Early Aptian, 120 Ma) are discussed.

4.3.1 Holocene oxygen and nutrient budgets

The rather well known state of the pre-industrial Holocene ocean was used to tune poorly constrained model parameters including the kinetic constants for export production, nitrogen fixation and denitrification (App. A4.4). The model results for the Holocene ocean obtained with these optimized parameter values compare well with observations (Fig. 4.1).

Figure 4.3 illustrates the results of the benthic model as calculated in the standard case for the pre-industrial Holocene. Dissolved oxygen concentrations (Fig. 4.3a) decrease with sediment depth due to the microbial degradation of POC (Fig. 4.3b). Due to the high depositional rates of organic matter, the oxygen content of sediment pore waters on shelves and continental rises is exhausted within the upper 2 cm, whereas oxygen is not completely consumed in deep-sea sediments receiving a much smaller flux of organic matter. Because of the oxygen depletion in the sediments phosphorus is released into the solution. On the shelves and continental slopes it is enriched below the oxygen penetration depth whereas dissolved phosphate is depleted in deep-sea sediments because oxygen penetrates to the base of the model column (Fig. 4.3c). These conditions also control the reactive phosphorus inventory of the sediment, since reactive phosphorus turns into dissolved phosphate under oxygen depletion, whereas under oxic conditions this process is reversed (Fig. 4.3d).

Nitrate is released into the pore water during oxic degradation of organic matter and is consumed below the oxygen penetration depth by denitrification (Fig. 4.3e). The nitrate content in the upper 2 cm is about 15 μM in shelf sediments, and 20 μM in continental rise sediments, while both environments are depleted in nitrate below 5 cm sediment depth. Whereas under oxic conditions, the nitrate content in deep sea sediments increases from 20 μM in the upper layer up to 35 μM in the deeper layer.

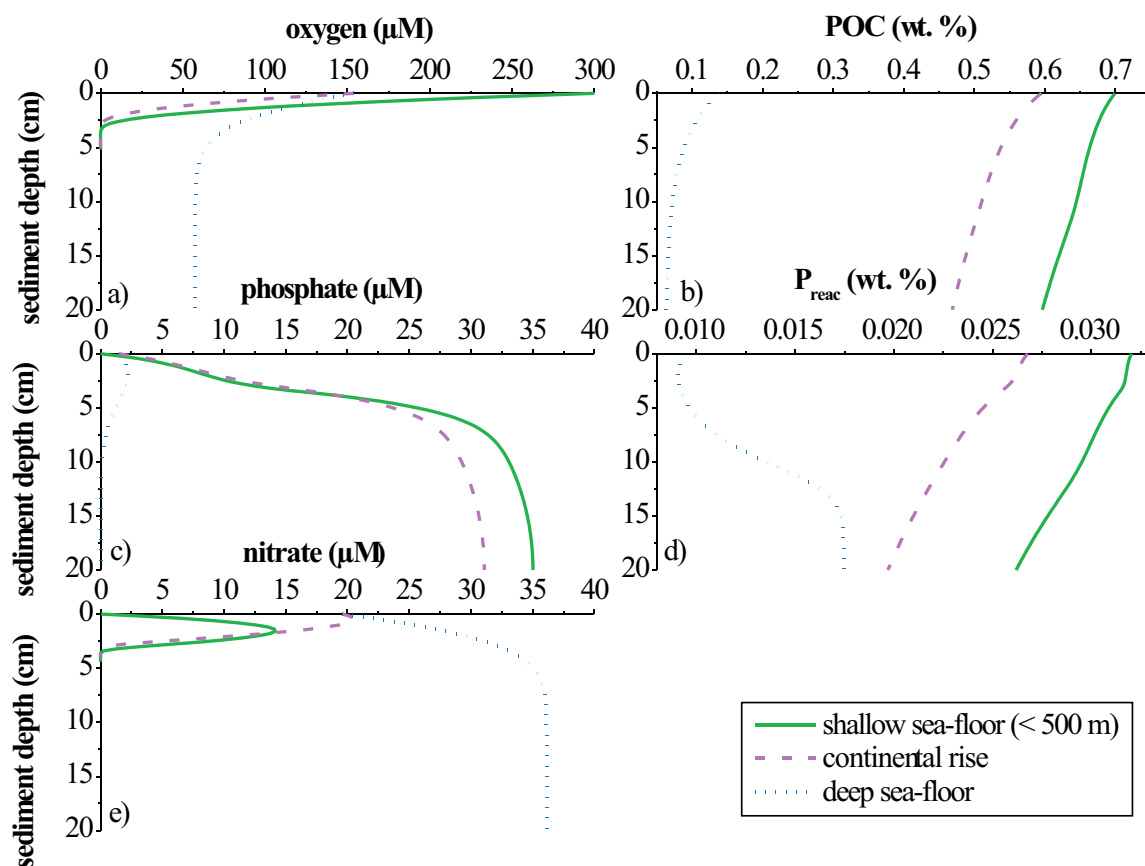


Figure 4.3a - e: Changes in pre-industrial Holocene benthic species of a) oxygen content, b) POC fraction, c) phosphate content, d) reactive phosphate fraction, e) nitrate concentration, versus 20 cm oceanic sediment depth on the shelves, continental rise, and on the deep seafloor.

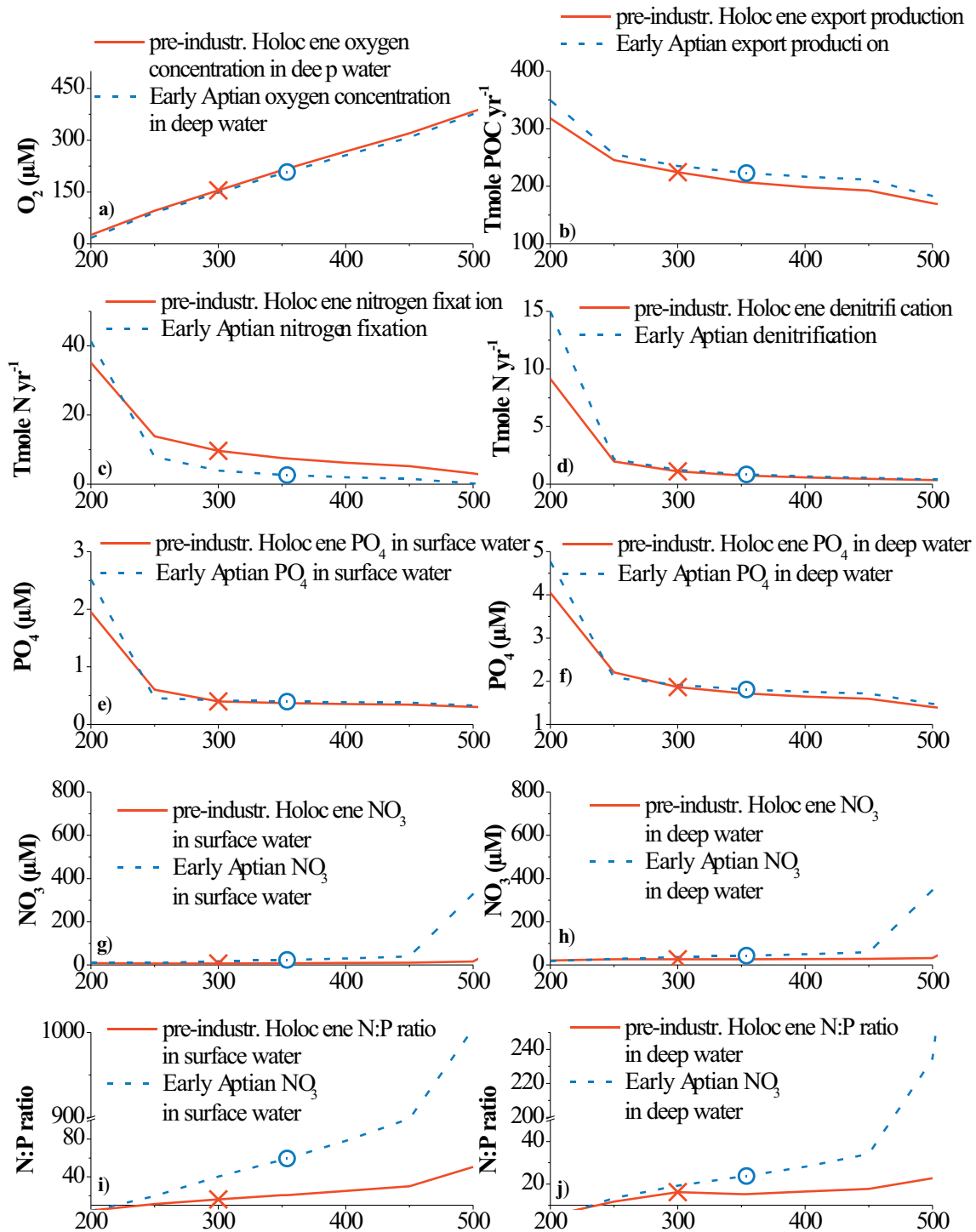
4.3.2 Sensitivity tests

In the following I explore the sensitivity of the marine biogeochemical system – as represented in my model - with respect to changes in *deep water ventilation* through oxygenated surface waters, *dissolved phosphate input* from land, *sedimentation rate*, and the *vertical mixing*. I applied the standard case for the pre-industrial Holocene (Fig. 4.1 & App. A4.6), and changed the corresponding parameter values to cover the range of values that may have prevailed during different periods of the Phanerozoic.

Deep water ventilation. - The oxygen content of deep water is directly proportional to the oxygen concentration in surface waters ventilating the deep ocean (Fig. 4.4a). The nutrient inventories and the rates of biogeochemical processes show a more complicated and highly coupled response to changing oxygen concentrations in surface waters. Thus, nitrate concentrations tend to increase with increasing ventilation (Figs. 4.4g & 4.4h) because denitrification - which serves as the major nitrate sink - is inhibited at high oxygen levels (Fig. 4.4d). Phosphate concentrations show the reverse trend since phosphorus is preferentially fixed and buried in sediments under oxic conditions (Figs. 4.4e & 4.4f). In response to these changes in nutrient inventories, the marine export production decreases significantly with increasing ventilation (Fig. 4.4b). This overall behavior indicates that phosphorus is in general the limiting nutrient in the model ocean and that nitrogen fixation usually provides sufficient nitrate for marine export production.

However, at very low concentrations of oxygen in the surface water ventilating the deep ocean ($< 250 \mu\text{M}$), nitrate is the limiting nutrient because nitrogen fixation can not compensate for the nitrate deficit caused by enhanced rates of denitrification in the deep ocean and in marine sediments. Under these conditions, the phosphate inventory is greatly expanded (Figs. 4.4e & 4.4f) because phosphate released at the seafloor is only partly fixed in organic matter.

The N : P ratios in surface and deep water are stabilized by nitrogen fixation over a broad range of redox conditions (Figs. 4.4i & 4.4j). The ratios are, however, much higher than the Redfield ratio under very oxic conditions ($\text{O}_2 > 450 \mu\text{M}$). Nitrate accumulates in the ocean under these conditions because the terrestrial input of nitrate is larger than the removal of nitrate by organic matter burial and denitrification. Even the complete shut-down of nitrogen fixation cannot inhibit the built-up of high nitrate concentrations in the ocean under fully oxic and oligotrophic conditions. Under reducing and eutrophic conditions nitrate is rapidly consumed by denitrification while phosphate is preferentially released at the seafloor. Even though nitrogen fixation is greatly enhanced under these conditions, the N : P ratio is significantly reduced indicating that nitrogen fixation can not fully compensate for enhanced denitrification and phosphate release.



O₂ concentration in surface water ventilating the deep ocean (μM)

Figure 4.4a - h: Changes in a) oxygen concentration in deep water; b) export production from surface water box to the deep water box; c) nitrogen fixation in surface water (< 500 m); d) denitrification in oceanic sediments and deep water; e) phosphate concentration in surface water (< 500 m) f) phosphate concentration in deep water; g) nitrate concentration in surface water (< 500 m); h) nitrate concentration in deep water; i) N:P atomic ratio in surface water; j) N:P atomic ratio in deep water; in dependency to changing deep water ventilation. The solid lines illustrate the sensitivity tests for the pre-industrial Holocene, the dashed lines illustrate the sensitivity tests for Early Aptian OAE 1a. The x-marks represent the ventilation during pre-industrial Holocene. The circles represent the ventilation during the Early Aptian OAE 1a.

Dissolved phosphate input. - Figure 4.5 illustrates the changing composition of the selected species of the submodel in dependency to changing input of dissolved phosphate from land via rivers and aeolian transport. Marine export production increases in response to the enhanced P input (Fig. 4.5b). Due to the enhanced marine snow production, the oxygen consumption in deep water increases, resulting in diminished oxygen contents (Fig. 4.5a). The increasing phosphate input into the ocean causes only a small increase in the dissolved phosphate content of surface and deep waters (Figs. 4.5e - h) because phosphate is fixed in marine organic matter buried at the seafloor. Nitrogen fixation in surface water increases in response to the enhanced supply of phosphate (Fig. 4.5c) while denitrification in deep water increases because of the transition towards more reducing and eutrophic conditions. Nitrogen fixation compensates for denitrification so that N : P ratios are maintained close to the Redfield value. Overall, increasing fluxes of dissolved phosphate from the continents into the oceans have only a rather small effect on the marine biogeochemical system. The export production increased by less than 20 % upon a twofold change in phosphate input (Fig. 4.5b), whereas a corresponding change in the oxygen concentration in surface water caused much larger changes in marine productivity, oxygen and nutrient inventories (Fig. 4.4). Thus, the marine biogeochemical system reacts more sensitive towards changes in the oxygenation of surface waters than towards inputs of dissolved phosphate from the continents.

Sedimentation rate. - The sedimentation rate and depositional flux of terrigenous phosphate and particulate organic matter at the shallow seafloor (< 500 m water depth) were changed simultaneously to simulate the effects of increasing continental erosion and terrigenous sedimentation on the ocean (Fig. 4.6). While the deposition of terrigenous organic matter and reactive phosphorus should enhance the release of dissolved phosphate from shelf sediments into the ocean, the coeval increase in sedimentation rate causes a more efficient burial of phosphorus and organic matter at the seafloor. The sensitivity test shows that the increase in sedimentation rate is the dominant effect reducing the phosphate fluxes from sediments into the ocean. Consequently, marine productivity and nutrient concentrations decrease with increasing shelf sedimentation while the oxygen concentration in the deep ocean increases significantly (Fig. 4.6).

The effects of terrigenous sedimentation change in sign and magnitude when the terrigenous matter is deposited on the continental slope and rise rather than the continental shelf (Fig. 4.7). Deposited on the slope and rise (> 400 m water depth), terrigenous sediments enhance the consumption of oxygen in deep water, the productivity of the ocean, the nutrient inventories, as well as the fixation of nitrogen and denitrification (Figs. 4.7a - h). This opposing effect is probably related to the oxygen cycle. The microbial degradation of terrigenous organic matter consumes oxygen. At shallow water depth, the oxygen is rapidly replenished from the atmosphere whereas the oxygen content of deep water is significantly reduced by benthic respiration processes because of restricted ventilation. In response to the more reducing conditions in the deep ocean, phosphate is released from slope and rise sediments to eventually trigger a transition towards more eutrophic conditions. Thus, enhanced rates of continental erosion and terrigenous sedimentation may either favor eutrophic or oligotrophic conditions pendent on the prevailing depositional area.

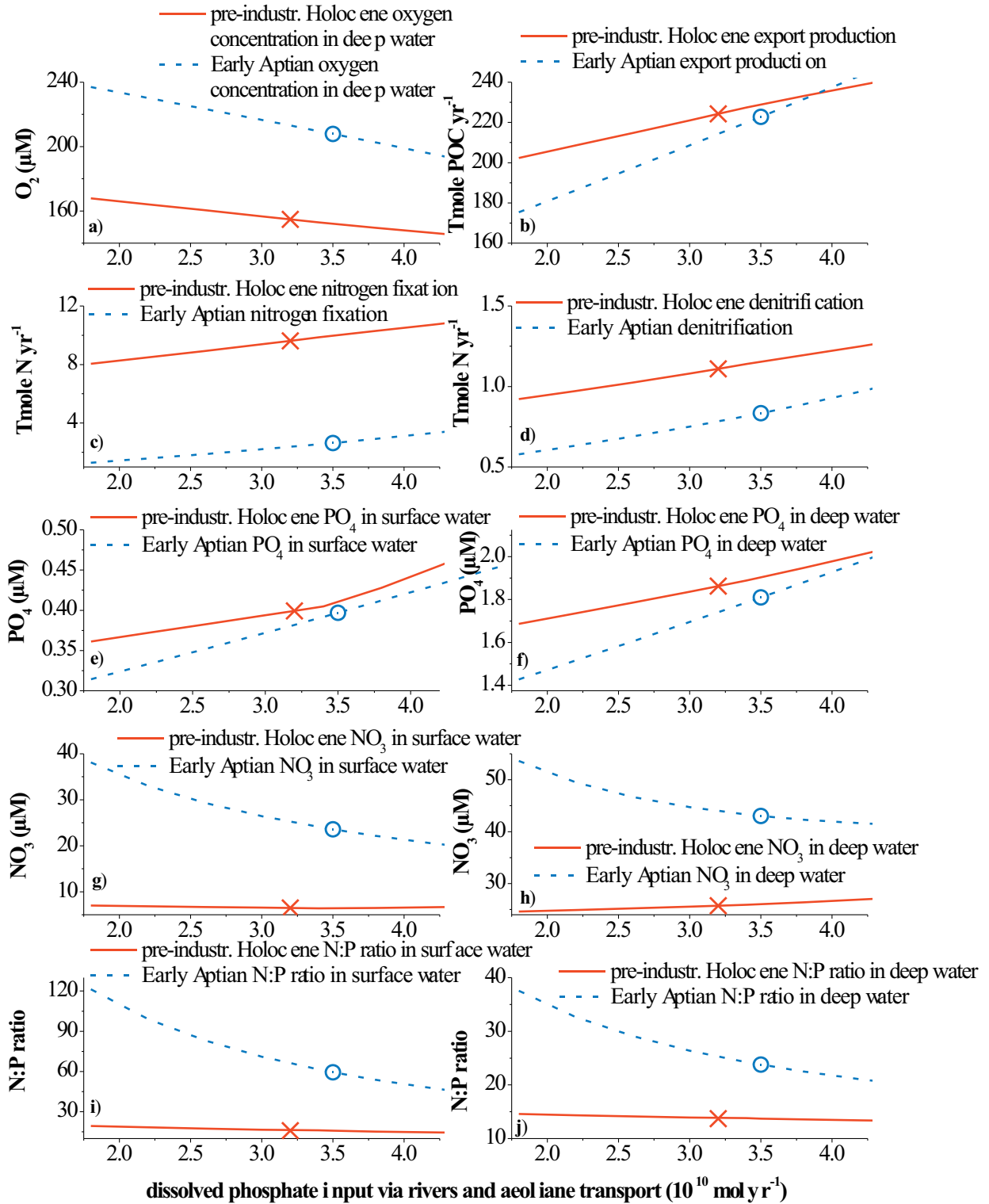


Figure 4.5a - h: Changes in a) oxygen concentration in deep water, b) export production from surface water box to the deep water box, c) nitrogen fixation in surface water (< 500 m), d) denitrification in oceanic sediments and deep water, e) phosphate concentration in surface water (< 500 m) f) phosphate concentration in deep water, g) nitrate concentration in surface water (< 500 m), h) nitrate concentration in deep water, i) N:P atomic ratio in surface water, j) N:P atomic ratio in deep water; in dependency to changing dissolved phosphorus input via river and aeolian transport. The solid lines illustrate the sensitivity tests for the pre-industrial Holocene, the dashed lines illustrate the sensitivity tests for Early Aptian OAE 1a. The x-marks represent the river and aeolian input during pre-industrial Holocene. The circles represent the river and aeolian input during the Early Aptian OAE 1a.

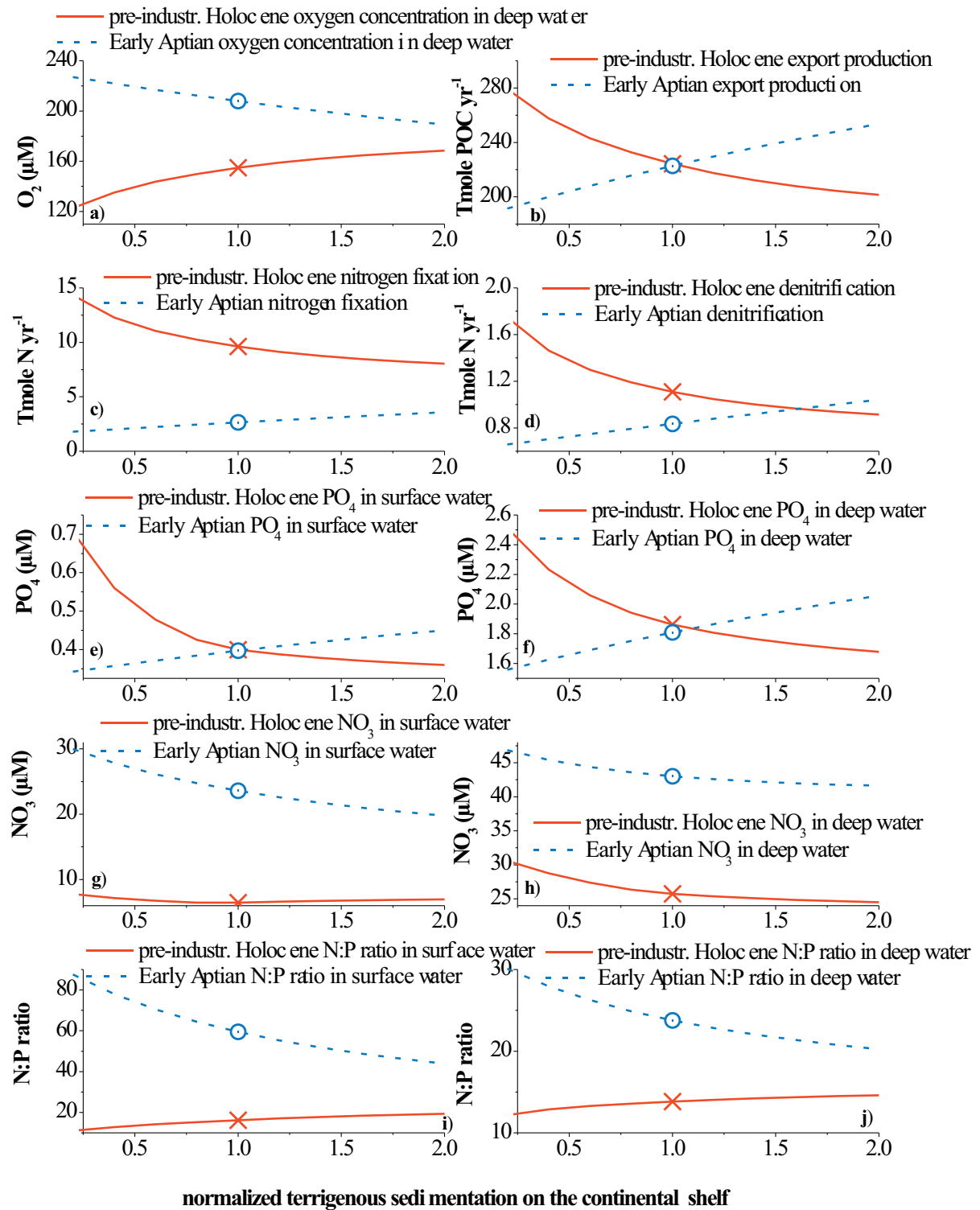
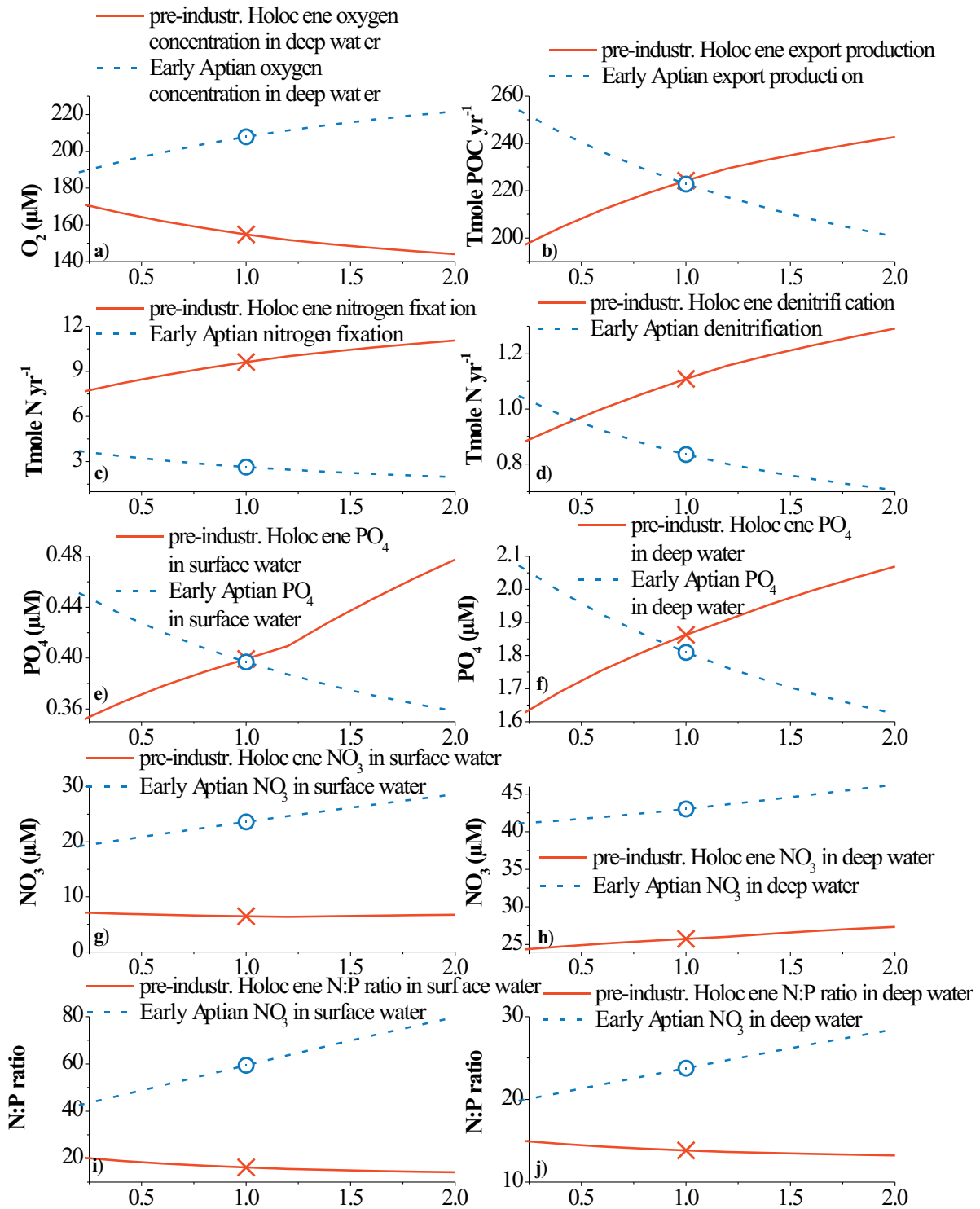


Figure 4.6a - h: Changes in a) oxygen concentration in deep water, b) export production from surface water box to the deep water box, c) nitrogen fixation in surface water (< 500 m), d) denitrification in oceanic sediments and deep water, e) phosphate concentration in surface water (< 500 m) f) phosphate concentration in deep water, g) nitrate concentration in surface water (< 500 m), h) nitrate concentration in deep water, i) N:P atomic ratio in surface water, j) N:P atomic ratio in deep water; in dependency to changing of normalized terrigenous sedimentation on shallow seafloor. The solid lines illustrate the sensitivity tests for the pre-industrial Holocene, the dashed lines illustrate the sensitivity tests for Early Aptian OAE 1a. The x-marks represent the terrigenous sedimentation on shallow seafloor during pre-industrial Holocene. The circles represent the terrigenous sedimentation on shallow seafloor during the Early Aptian OAE 1a.



normalized terrigenous sedimentation on continental slope and rise

Figure 4.7a - h: Changes in a) oxygen concentration in deep water; b) export production from surface water box to the deep water box, c) nitrogen fixation in surface water (< 500 m), d) denitrification in oceanic sediments and deep water; e) phosphate concentration in surface water (< 500 m) f) phosphate concentration in deep water; g) nitrate concentration in surface water (< 500 m), h) nitrate concentration in deep water; i) N:P atomic ratio in surface water; j) N:P atomic ratio in deep water; in dependency to changing of normalized terrigenous sedimentation on continental rise. The solid lines illustrate the sensitivity tests for the pre-industrial Holocene, the dashed lines illustrate the sensitivity tests for Early Aptian OAE 1a. The x-marks represent the terrigenous sedimentation on continental rise during pre-industrial Holocene. The circles represent the terrigenous sedimentation on continental rise during the Early Aptian OAE 1a.

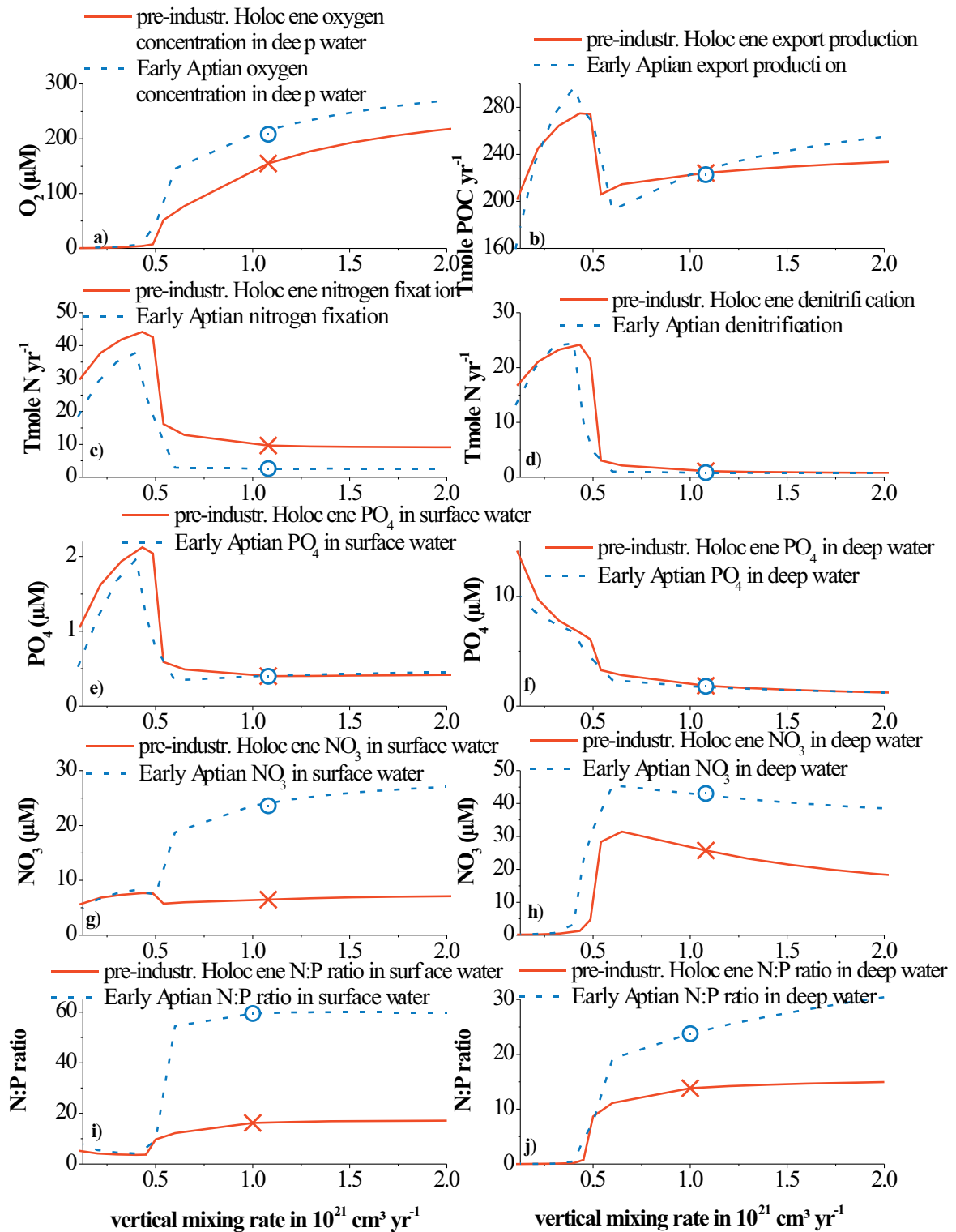


Figure 4.8a - h: Changes in a) oxygen concentration in deep water, b) export production from surface water box to the deep water box, c) nitrogen fixation in surface water (< 500 m), d) denitrification in oceanic sediments and deep water, e) phosphate concentration in surface water (< 500 m) f) phosphate concentration in deep water, g) nitrate concentration in surface water (< 500 m), h) nitrate concentration in deep water; i) N:P atomic ratio in surface water; j) N:P atomic ratio in deep water; in dependency to changing vertical mixing rate. The solid lines illustrate the sensitivity tests for the pre-industrial Holocene, the dashed lines illustrate the sensitivity tests for Early Aptian OAE 1a. The x-marks represent the vertical mixing rate during pre-industrial Holocene. The circles represent the vertical mixing rate during the Early Aptian OAE 1a.

Vertical mixing rate. - The ocean reacts very sensitive with respect to changes in the vertical mixing rate (Fig. 4.8). The vertical mixing rate defines the exchange of nutrients between the two water boxes and the ventilation of the deep water. Low vertical mixing results in a suffocation of the deep ocean (Fig. 4.8a) and a corresponding increase in the dissolved phosphate inventory (Figs. 4.8e & 4.8f). Marine productivity and the transport of nutrients from the deep ocean into the productive surface waters are favored by the expansion of the phosphate inventory in the deep ocean but restricted by the decrease in vertical mixing. The overall effect is a strong maximum in productivity at a moderately low rate of vertical mixing (Fig. 4.8b). The nitrate inventory is reduced at low mixing rates because of enhanced denitrification and nitrate rather than phosphate is the limiting nutrient under reducing conditions as also shown by the low N : P ratios.

In conclusion, the biogeochemical system of the model ocean reacts very sensitive to changes in ocean ventilation caused either by a change in the oxygen concentration of surface waters or in the rate of vertical mixing. Changing inputs from land (dissolved and particulate) have a comparably small effect on nutrient and oxygen dynamics and marine productivity.

4.3.3 Phanerozoic evolution

The model previously calibrated (section 4.3.1) and tested (section 4.3.2), is now applied to simulate the Phanerozoic evolution of the marine biogeochemical system. In this model application, parameters used for the external forcing of the model were varied systematically to reproduce the changing external conditions during the different periods of the Phanerozoic (Fig. 4.2). The end of the model simulation ($t=0$) reproduces the well known pre-industrial Holocene values.

Figure 4.9a shows the oxygen content of deep seawater over the entire Phanerozoic. According to the model, the oceans were almost completely anoxic during the Early Paleozoic. Oxygen values started to rise during the Silurian when the first land plants evolved. The oxygen concentration difference between deep water and surface water varied through time and reached a maximum value of about 230 μM during the Early Paleozoic (Fig. 4.9b), while the deep ocean was more or less anoxic (Fig. 4.9a). Subsequently, the oxygen content difference between both layers decreased to a Triassic value of 125 μM and attained a value of 145 μM during the Holocene. The deep water oxygen content is mainly controlled by the microbial degradation of marine particulate organic matter exported from the surface ocean. Thus, the oxygen gradient (Fig. 4.9b) and the marine export production (Fig. 4.9f) are highly correlated. Eutrophication and the spread of anoxic conditions are related to each other in a positive feedback loop rooted in the redox-dependent turnover of phosphorus in marine sediments (Wallmann, 2003). Thus, the low oxygen concentrations in the Early Paleozoic surface ocean - which were caused by low atmospheric $p\text{O}_2$ values and high surface temperatures - favored the release of phosphate from sediments and thereby promoted an increase in marine productivity. The oxygen concentrations in the deep ocean were further reduced by the increase in marine productivity and respiration so that more phosphorus was released at the

seafloor inducing higher productivity and lower oxygen values in a positive feedback loop.

The ocean evolved into a fully oxic state during the Permian-Carboniferous cold period (Fig. 4.9a) when the oxygen concentration in surface water was very high (Fig. 4.2a) because of high atmospheric pO_2 and low surface temperature values. Since these atmospheric and climatic conditions were probably caused by the spread of land plants (Berner 2004), the development of a fully oxic deep ocean should be regarded as an additional - and previously not recognized - consequence of this major ecological transition.

The sensitivity tests showed that the phosphate inventory of the ocean is mainly regulated by ocean ventilation rather than by the continental inputs (section 4.3.2). The Phanerozoic model simulations confirm this conclusion. The input of dissolved phosphate into the ocean increased over time (Fig. 4.2a) while the phosphate inventory and marine productivity decreased over the Phanerozoic (Figs. 4.9d & 4.9f) The evolution of the marine biogeochemical system is thus mainly regulated by climatic and atmospheric changes affecting the ventilation of the deep ocean.

The high N : P ratios suggest that the ocean was PO_4 limited over most periods of the Phanerozoic. The ratios are correlated to the oxygen concentrations in the deep ocean (Figs 4.9a & 4.9e). Under fully oxic conditions N : P ratios were very high because phosphate was fixed in sediments while denitrification was strongly suppressed. Under anoxic conditions N : P ratios decreased because of enhanced denitrification and benthic phosphate release. Nitrate was the limiting nutrient under anoxic conditions even though nitrogen fixation increased under these conditions prevailing during the Early Paleozoic. The nitrogen limitation inhibited a further increase in productivity and allowed for the built up of high phosphate concentrations in the ocean. The positive feedback rooted in the benthic phosphorus cycle was thus limited by the negative feedback imbedded in the nitrogen cycle.

In the modern ocean, the N : P ratio of seawater is close to the planktonic N : P ratio (Redfield, 1958). It has been postulated that this relation also held in the past and has always been maintained by nitrogen fixation (Tyrrell, 1999). However, my model predicts that the nutrient N : P ratio in seawater changes with the redox state of the ocean and that nitrogen fixation cannot fully compensate for these changes. The N : P ratios in ancient seawater are unknown. My model results can, thus, not be validated by independent data. My model uses a fixed planktonic N : P ratio. It is, however, possible that the average elemental composition of plankton is not constant over time but evolved as a consequence of changing nutrient ratios in seawater. Thus, unexpected high plankton N : P ratios (Gönülol and Obali, 1998) occur in fresh water algae and the N : P ratio of primary producers may be determined by the nutrient supply (Hall et al., 2005). It is, therefore, possible that, both, the N : P ratio in plankton and in seawater changed over the Phanerozoic. In this case, the changes in seawater would be less extreme than calculated in my model because a nutrient dependent N : P ratio in plankton would provide further negative feedback for the nutrient ratio in seawater.

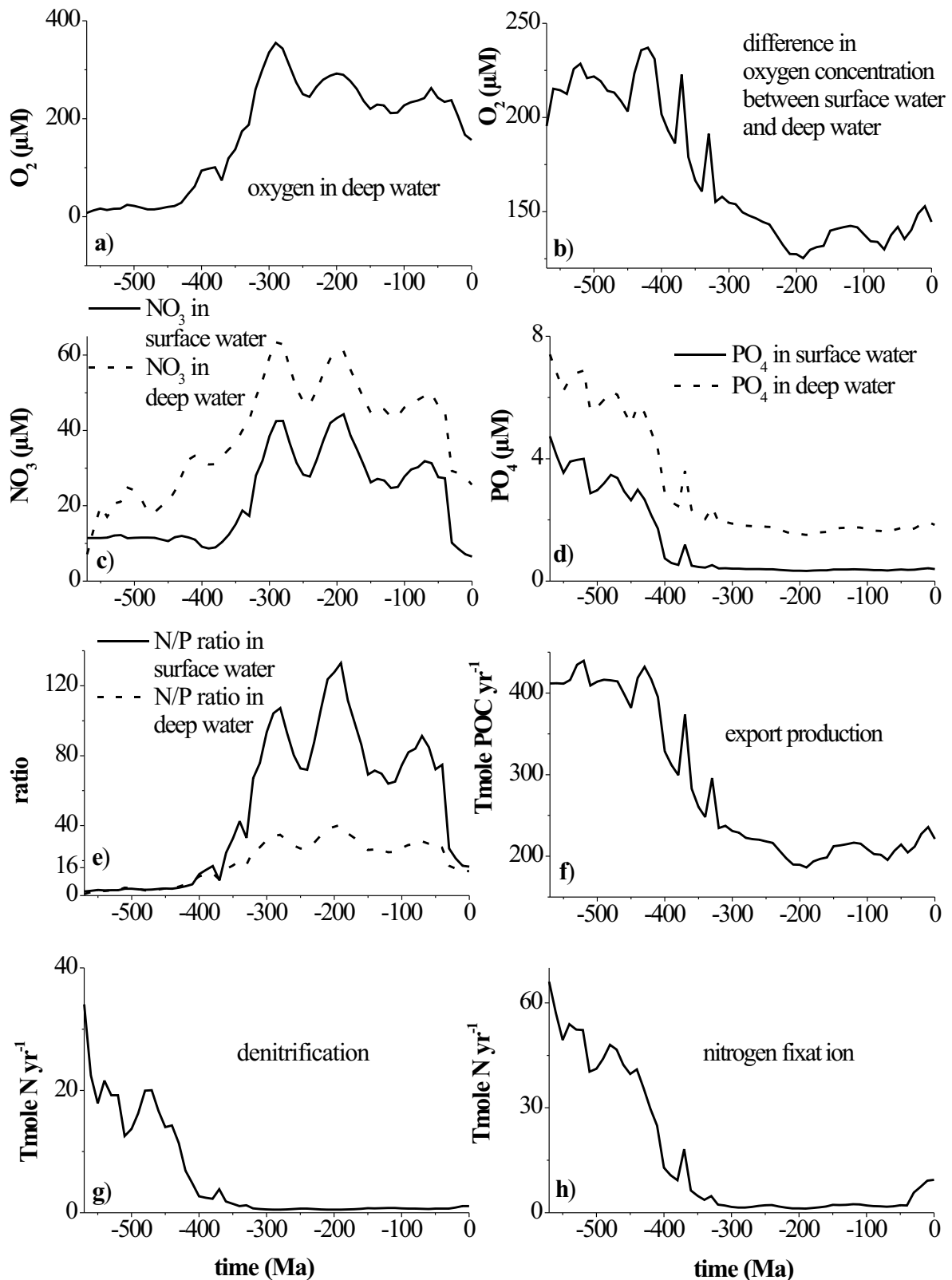


Figure 4.9a - h: Changes in Phanerozoic a) oxygen content in deep water; b) oxygen discrepancy between surface and deep water; c) nitrate content in surface (< 500 m) and deep water; d) phosphate content in surface (< 500 m) and deep water; e) N/P ratio in surface (< 500 m) and deep water; f) export production from surface water box into the deep water box; g) denitrification in oceanic sediments and deep water; h) nitrogen fixation in surface water (< 500 m).

4.3.4 Oceanic Anoxic Events (OAEs)

There is clear evidence that the long-term evolution of Phanerozoic oceanic oxygen conditions was interrupted by several brief periods of significant oxygen depletion (Bralower et al., 2002b), so called oceanic anoxic events (OAEs). These are characterized by the wide-spread occurrence of black shales (Langrock et al., 2003) and are often accompanied by sharp positive $\delta^{13}\text{C}$ and negative $\delta^{18}\text{O}$ excursions (Beerling et al., 2002; Kuypers et al., 2004; Bailey et al., 2003), sea-level changes (Hallam and Wignall, 1999), variations in $^{87}\text{Sr}/^{86}\text{Sr}$ (Jones and Jenkyns, 2001; Pálffy et al., 2002), the occurrences of widespread igneous rocks (Morgan et al., 2004; Wignall, 2001), dramatic changes in the oceanic circulation system (Hotinski et al., 2001; Overpeck et al., 2005), as well as global mass extinctions (Rampino and Haggerty, 1995; Ryskin, 2003).

Anoxic conditions in the deep ocean are either caused by enhanced rates of oxygen respiration or reduced rates of oxygen supply (ventilation). One possible process that could enhance the rate of respiration is the sudden methane release by gas hydrates followed by microbial methane oxidation. According to Bartdorff and Wallmann (submitted-a) the methane flux varied during the OAE 1a between 4 and $7.3 \cdot 10^{14}$ mole $\text{CH}_4 \text{ yr}^{-1}$, during a time frame of 10 k years, and between 1.8 and $3.2 \cdot 10^{12}$ mole $\text{CH}_4 \text{ yr}^{-1}$, during a time frame of 150 k years. Under consideration of a complete methane oxidation in the water column the oxygen consumption ranged between 8 and $14.6 \cdot 10^{14}$ mole $\text{O}_2 \text{ yr}^{-1}$, during a time frame of 10 k years, and between 3.6 and $6.5 \cdot 10^{12}$ mole $\text{O}_2 \text{ yr}^{-1}$, during a time frame of 150 k years. The ventilation of oxygen during the Early Aptian was about $1.54 \cdot 10^{14}$ mole $\text{O}_2 \text{ yr}^{-1}$. Thus, the oxygen consumption was ninefold greater, than the supply, during a short time frame, whereas during a longer time frame the consumed oxygen is a fourth to a half of the ventilated oxygen. Hence, sudden methane release by gas hydrates could exhaust the regenerated oxygen in deep water, if the time frame for the prevailing event occurs on a short time scale (e.g. 10 k years). During larger time frames the consumption is significant, but not sufficient to exhaust the complete oxygen out of the oceans.

$^{87}\text{Sr}/^{86}\text{Sr}$ data suggest that OAEs are significantly influenced by changes in tectonic activity (Benton and Twitchett, 2003; Pálffy and Smith, 2000; Pálffy et al., 2002). Such changes could cause changes in the main oceanic current systems, which are important for the maintenance of deep water regimes (Gille et al., 2004). Furthermore such isotopic shifts display a changed input of mantle material into the atmosphere and ocean. Such an enhanced release of mantle derived material could have changed the climate by greenhouse gases and aerosols, the surface conditions due to the covering with volcanic matter, but also the oceanic balance due to the fertilization of surface water and the deposition of volcanic material on the seafloor (Van Cappellen and Ingall, 1994). Changed climate conditions affect the thermo-haline circulation (Toggweiler, 1994), which, among other factors, is mainly controlled by the temperature gradient between the equator and the poles (Hotinski et al., 2001). Furthermore, erosion and denudation depend on the global surface temperature, thus the aeolian and river input of terrestrial matter into the ocean also depends on the global temperature (Van Cappellen and Ingall, 1994). This input changes the oceanic nutrient inventory and the deposition of

organic and inorganic detritus (Bailey et al., 2003; Berner and Berner, 1996; Bralower et al., 2002b; Herrle et al., 2003). Additionally volcanic ashes feed the ocean with detritus and nutrients. (Duggen et al., submitted; Frogner et al., 2001) estimated how fast nutrients are released out of volcanic ashes after their deposition in oceanic surface waters. These dissolved nutrients enhance the biological activity (Duggen et al., submitted; Sarmiento, 1993; Wu et al., 2000), likewise as the nutrient input from land (Berner and Berner, 1996). All these dramatically short term changes result in an inhibited or stagnated ocean circulation, and an explosion of bioproductivity in the surface layer. Both effects, particularly combined, are followed by a sudden suffocation of deep water regimes (Bralower et al., 2002a).

Table 4.2: Comparison of fluxes and constants, which were used for modeling the standard run the exemplarily OAEs. The first row shows the parameters, which were detected as possible driving forces for the overturning of an oxic ocean into an anoxic ocean. The second row represents the values for the prevailing parameters, which were used for the standard run for the Cretaceous ocean at 120 Ma. The third row represents the calculated values for the prevailing parameters, which were used to overturn the ancient ocean at 120 Ma. The fourth row represents the calculated values for the prevailing parameters, which were used for the standard run for the pre-industrial Holocene ocean. The last row represents the values for the prevailing parameters, which were used to hypothetical overturn the pre-industrial Holocene ocean.

Parameter	standard case (120 Ma)	OAE 1a (120 Ma)	standard case (Holocene)	“OAE” (Holocene)
Volume of surface water box (10^{23} cm ³)	1.81	2.89	1.81	2.53
Vertical mixing rate (10^{21} cm ³ yr ⁻¹)	1.08	0.68	1.08	0.77
Oxygen concentration in surface water (mmol cm ⁻³)	354	328	300	256
River and aeolian input of dissolved P (10^{13} mmol yr ⁻¹)	4.5	7.2	4.2	5.88
River and aeolian input of dissolved N (10^{15} mmol yr ⁻¹)	2	3.2	2	2.8
Kinetic constant for export production (yr ⁻¹)	0.03	0.048	0.07	0.098
Kinetic constant for nitrogen fixation (mmol PO ₄ cm ⁻³ yr ⁻¹)	1	1.6	1.2	1.68
Hydrothermal P-uptake (10^{13} mmol yr ⁻¹)	1.3	2.08	1.04	1.46
Area of shallow seafloor (10^{18} cm ²)	1.9	3.04	0.4	0.56
Sedimentation rate on the shelves (10^{-3} cm yr ⁻¹)	2.3	2.3	47	47
Sedimentation rate on continental rise (10^{-3} cm yr ⁻¹)	14.9	23.8	28	39.2
Sedimentation rate on the deep seafloor (10^{-3} cm yr ⁻¹)	1.9	3	1.9	2.66
Deposition of terrigenous POC on the shelves (10^{-4} mmol cm ⁻² yr ⁻¹)	5.9	5.9	100	100
Deposition of terrigenous POC on continental rise (10^{-4} mmol cm ⁻² yr ⁻¹)	22	36	80	112
Deposition of terrigenous P _{reac} on the shelves (10^{-4} mmol cm ⁻² yr ⁻¹)	0.14	0.14	2.3125	2.3125
Deposition of terrigenous P _{reac} on continental rise (10^{-4} mmol cm ⁻² yr ⁻¹)	0.51	0.82	0.18	2.52
Deposition of terrigenous P _{reac} on the deep seafloor (10^{-4} mmol cm ⁻² yr ⁻¹)	0.01	0.021	0.00463	0.006482

Considering these premises for an adequate OAE-modeling, I evaluated the parameters (Tab. 4.2), which could induce an exhaustion of oxygen in the deep ocean. Thus, I considered a simultaneous increase in volcanic activity, nutrient input into the ocean, surface temperature, and sea-level (Friedrich et al., 2005; Hallam and Wignall, 1999; Handoh and Lenton, 2003; Bailey et al., 2003; Bralower et al., 2002b). Additionally, I diminished the oxygen content in surface water ventilating the deep ocean and the vertical mixing rate whereas the particulate nutrient deposition and the sedimentation rate were enhanced (Tab. 4.2). The modeling showed that the corresponding parameters have to be changed by 60 % with respect to their Holocene values to stimulate an OAE.

The sensitivity of the Cretaceous model ocean with respect to the various external forcings is depicted in Figs. 4.4 - 4.8. In general, the Cretaceous ocean showed a similar sensitivity towards external perturbations as in the Holocene ocean. However, the net effects of terrigenous sedimentation on the biogeochemical system differed in sign between the two simulations. This significant discrepancy in more or less all specific parameters is caused by the different spatial extent of the shelf areas at the prevailing time. The area covered by shallow seas during the Cretaceous was around five times larger than during the pre-industrial Holocene (Fig. 4.2f). The sensitivity tests also indicate, that the ocean was more stable during the Lower Cretaceous than during the Holocene (Figs. 4.4 - 4.8). Because of this result I run an added suffocation test. Several model tests were run until the Holocene ocean was depleted in oxygen, comparable to the Cretaceous event. Whereas the Cretaceous ocean “needs” changes up to 60 % to suffocate, the pre-industrial Holocene ocean only “needs” about 40 % to reach the same anoxic conditions (Tab. 4.2).

4.4 Conclusions

Systematic sensitivity tests of the new model presented in this chapter revealed that marine productivity, nutrient inventories and the oxygen content of the deep ocean react very sensitively to changes in ocean ventilation whereas inputs from land (dissolved and particulate nutrients) have a comparably small effect on the oceans.

Reducing sediments are a more important source of phosphate to the oceans than river input. Therefore, the positive feedback between ocean anoxia and eutrophication, which is rooted in the redox-dependent phosphorus turnover in sediments, dominates the evolution of the marine biogeochemical system. This model result implies that the state of the ocean is mainly regulated by climatic conditions and the O₂ content of the atmosphere.

The model was also applied to reconstruct the Phanerozoic evolution of the oceans. According to the model, the deep ocean was almost completely anoxic during the Early Paleozoic. The low oxygen concentrations in the early Paleozoic surface ocean - which were caused by low atmospheric pO₂ values and high surface temperatures - inhibited an effective ventilation of the deep ocean and thereby favored the release of phosphate from sediments. The oxygen concentrations in the deep ocean were further reduced by the phosphate-triggered increase in marine productivity and

respiration so that more phosphorus was released at the seafloor inducing higher productivity and lower oxygen values in a positive feedback loop.

The ocean evolved into a fully oxic state during the Permian-Carboniferous cold period when the oxygen concentration in surface water ventilating the deep ocean was very high because of high atmospheric pO_2 and low surface temperature values. Since these atmospheric and climatic conditions were probably caused by the spread of land plants (Berner, 2004), the development of a fully oxic deep ocean should be regarded as an additional - and previously not recognized - consequence of this major ecological transition.

In the modern ocean, the N : P ratio of seawater is close to the planktonic N : P ratio (Redfield, 1958). It has been postulated that this relation also held in the past and has always been maintained by nitrogen fixation (Tyrrell, 1999). However, my model predicts that the nutrient N : P ratio in seawater changes with the redox state of the ocean and that nitrogen fixation cannot fully compensate for these changes. Thus, the nutrient N : P ratios were low in the anoxic oceans of the Early Paleozoic and attained very high values during the Permian-Carboniferous cold period.

OAEs are a sign of dramatic changes in global biogeochemistry. My model could only reproduce the Early Aptian OAE 1a when several important changes were assumed to occur coevally. Nutrient inputs from the continents and ocean ventilation had to be changed simultaneously by 60 % to attain a fully anoxic Cretaceous ocean. The initial trigger could have been a dramatic change in tectonic/volcanic activity, documented by $^{87}\text{Sr}/^{86}\text{Sr}$ shifts. An enhanced tectonic/volcanic activity affects the climate and thereby ocean circulation through the release of large amounts of CO_2 into the atmosphere. It may also cause changes in oceanic currents due to significant changes in the oceanic topography. The nutrient input into the ocean is enhanced by the deposition and weathering of volcanic ashes and by CO_2 -induced climate change. A significant addition of nutrients to the oceans is also caused by the direct input of volcanic matter into the ocean.

The fertilization of the ocean, the boost of the marine bioproductivity, as well as the storage of huge amounts of carbon on the seafloor restore former conditions via negative feedbacks. This implies that an OAE is not only a dramatic event causing the suffocation of the deep sea but also part of a global regulation system stabilizing the Earth.

Moreover, it could be derived by the model that methane which is suddenly released from the seafloor - as discussed in the "clathrate gun hypothesis" - , exhausts the entire oxygen replenished by ventilation due to its almost immediate oxidation. The oxygen consumption could be ninefold greater than its supply when considering a short time frame of 10 kyr for methane degassing, whereas during a longer time frame (150 kyr) the consumed oxygen is a fourth to a half of the ventilated oxygen. Hence, sudden methane releases by gas hydrates could exhaust the regenerated oxygen in deep water, if the time frame for the prevailing event occurs on a short time scale < 10 kyr. Due to the suffocation of the ocean mass extinctions of almost all marine animals could be initiated. During larger time frames the consumption is significant, but not sufficient to exhaust the complete oxygen out of the oceans.

References

- Aguillera-Franco N. and Allison P. (2005) Events of the Cenomanian-Turonian Succession, Southern Mexico. *Journal of Iberian Geology* 31(1), 25 - 50.
- Anderson D. M. and Archer D. (2002) Glacial-interglacial stability of ocean pH inferred from foraminifer dissolution. *Nature* 416, 70 - 73.
- Anderson L. A. and Sarmiento G. (1994) Redfield ratios of remineralization determined by nutrient data analysis. *Global Biogeochemical Cycles* 8(1), 65 - 80.
- Bailey T. R., Rosenthal Y., McArthur J. M., Schootbrugge van de B., and Thirlwall M. F. (2003) Paleooceanographic changes of the Late Pliensbachian-Early Toarcian interval: a possible link to the genesis of an Oceanic Anoxic Event. *Earth and Planetary Science Letters* 212, 307 - 320.
- Bartdorff O. and Wallmann K. (submitted-a) A model of atmospheric methane over the Phanerozoic.
- Bartdorff O. and Wallmann K. (submitted-b) Modeling the chemical evolution of seawater (S, P, C, Sr, O) over the Phanerozoic.
- Berling D. J., Lomas M. R., and Gröcke D. R. (2002) On the nature of methane gas-hydrates dissociation during the Torarcian and Aptian oceanic anoxic events. *American Journal of Science* 302, 28 - 49.
- Benton M. J. and Twitchett R. J. (2003) How to kill (almost) all life: the end-Permian extinction event. *Trends in Ecology and Evolution* 18(7), 358 - 365.
- Berner E. K. and Berner R. A. (1996) *Global environment, water, air, and geochemical cycles*. Prentice - Hall, Inc..
- Berner R. A. (2004) The Phanerozoic carbon cycle: CO₂ and O₂.
- Berner R. A., Beerling D. J., Dudley R., Robinson J. M., and Wildman J. R. A. (2003) Phanerozoic atmospheric oxygen. *Annual Reviews of Earth and Planetary Sciences* 31, 105 - 134.
- Bice K. L., Birgel D., Meyers P. A., Dahl K. A., Hinrichs K. U., and Norris R. D. (submitted) A multiple proxy and model study of Cretaceous upper ocean temperatures and atmospheric CO₂ concentrations.
- Boccaletti G., Pacanowski R. C., Philander S. G. H., and Fedorov A. V. (2003) The thermal structure of the upper ocean. *Journal of Physical Oceanography* 34(4), 888 - 902.
- Boudreau B. P. (1997) *Diagenetic models and their implementation, Modelling transport and reactions in aquatic sediments*. Springer-Verlag.
- Bralower T. J., Kelly D. C., and Leckie R. M. (2002a) Biotic effects of abrupt Paleocene and Cretaceous climate events. *ODP Legacy*.
- Bralower T. J., Silva I. P., and Malone M. J. (2002b) New evidence for abrupt climate change in the Cretaceous and Paleogene: An Ocean Drilling Program expedition to Shatsky Rise, northwest Pacific. *GSA Today*, 4 - 10.

- Broecker W. S. (1997) Thermohaline circulation, the Achilles Heel of our climate system: Will man-made CO₂ upset the current balance? *Science* 278, 1582 - 1588.
- Broecker W. S. and Peng T.-H. (1982) *Tracers in the sea*. Eldigio Press.
- Chester R. (2000) *Marine Geochemistry*. Blackwell Science Ltd.
- Compton J., Mallinson D., Glenn C. R., Filipelli G., Föllmi K., Shields G., and Zanin Y. (2000) Variations in the global phosphorus cycle. *Marine Authogenesis: From Global to Microbial* 66, 21 - 33.
- Duggen S., Croot P., Schacht U., and Hoffmann L. (submitted) Subduction zone volcanic ash can fertilize the surface ocean and stimulate phytoplankton growth: Evidence from biogeochemical experiments and satellite data. *Science*.
- Fennel K., Follows M. J., and Falkowski P. G. (2005) The co-evolution of the nitrogen, carbon and oxygen cycles in the Proterozoic ocean. *American Journal of Science* 305, 526 - 545.
- Foote M. (2003) Origination and extinction through the Phanerozoic: A new approach. *Journal of Geology* 111, 125 - 148.
- Friedrich O., Nishi H., Pross J., Schmiedel G., and Hemleben C. (2005) Millennial- to Centennial-Scale Interruptions of the Oceanic Anoxic Event 1b (Early Albian, mid-Cretaceous) Inferred from Benthic Foraminiferal Repopulation Events. *Palaios* 20, 64 - 77.
- Frogner P., Gíslason S. R., and Óskarsson N. (2001) Fertilizing potential of volcanic ash in ocean surface water. *Geological Society of America* 29(6), 487 - 490.
- Gille S. T., Metzger E. J., and Tokmakian R. (2004) Seafloor topography and ocean circulation. *Oceanography* 17(1), 47 - 54.
- Gönülol A. and Obali O. (1998) Seasonal variations of phytoplankton blooms in Suat Ugurlu (Samsun - Turkey). *Turkish Journal of Botany* 22, 93 - 97.
- Hall S. R., Smith V. H., Lytle D. A., and Leibold M. A. (2005) Constraints on primary producer N:P stoichiometry along N:P supply ratio gradients. *Ecology* 86(7), 1894 - 1904.
- Hallam A. and Wignall P. B. (1999) Mass extinctions and sea-level changes. *Earth and Planetary Science Letters* 48, 217 - 250.
- Handoh I. C. and Lenton T. M. (2003) Periodic mid-Cretaceous oceanic anoxic events linked by oscillations of the phosphorous and oxygen cycles. *Global Biogeochemical Cycles* 17(4), 3/1 - 3/11.
- Herrle J. O., Pross J., Friedrich O., and Hemleben C. (2003) Short-term environmental changes in the Cretaceous Tethyan Ocean: micropalaeontological evidence from the Early Albian Oceanic anoxic event 1b. *Terra Nova* 15, 14 - 19.
- Holland D. H. (1978) *The chemistry of the atmosphere and oceans*. John Wiley & sons, Inc.
- Hotinski R. M., Bice K. L., Kump L. R., Najjar R. G., and Arthur M. A. (2001) Ocean stagnation and end-Permian anoxia. *Geological Society of America* 29(1), 7 - 10.
- Houghton J. T. (1997) *Globale Erwärmung*. Springer Verlag.
- Jablonski D. (2004) Extinction: past and present. *Nature* 427, 589.
- Jackson J. B. C. and Johnson K. G. (2001) Measuring past biodiversity. *Science* 293, 2401 - 2404.

- Jahnke R. A. (1996) The global ocean flux of particulate organic carbon: Areal distribution and magnitude. *Global Biogeochemical Cycles* 10(1), 71 - 88.
- Jones C. E. and Jenkyns H. C. (2001) Seawater strontium isotopes, oceanic anoxic events, and seafloor hydrothermal activity in the Jurassic and Cretaceous. *American Journal of Science* 301, 112 - 149.
- Joos F., Plattner G.-K., Stocker T. F., Körtzinger A., and Wallace D. W. R. (2003) Trends in marine dissolved oxygen: Implications for ocean circulation changes and the carbon budget. *EOS, Transaction, American Geophysical Union* 84(21), 197 - 204.
- Kerr R. A. (2002) Inconstant ancient seas and life's path, seawater composition has changed over geological time, geochemists more realize. Has biological evolution changed along with it? *Science* 298, 1165 - 1166.
- Kershaw S. and Cundy A. (2000) *Oceanography, an Earth science perspective*. Stanley Thornes.
- Kuypers M. M. M., Lourens L. J., Rijpstra W. I. C., Pancost R. D., Nijhenshuis I. A., and Sinninghe Damsté J. S. (2004) Orbital forcing of organic burial in the proto-North Atlantic during oceanic anoxic event 2. *Earth and Planetary Science Letters* 228, 465 - 482.
- Kuypers M. M. M., Pancost R. D., and Sinninghe Damsté J. S. (1999) A large and abrupt fall in atmospheric CO₂ concentration during Cretaceous time. *Nature* 399, 342 - 345.
- Langrock U., R. S., Lipinski M., and Brumsack H.-J. (2003) Paleoenvironment and sea-level change in the early Cretaceous Barents Sea—implications from near-shore marine sapropels. *Geo-Mar Letters* 23, 34 - 42.
- Martin R. E. (1996) Secular increase in nutrient levels through the Phanerozoic: Implications for productivity, biomass, and diversity of the marine biosphere. *Palaios* 11, 209 - 219.
- Martin R. E. (2003) The fossil record of biodiversity: nutrients, productivity, habitat area and differential preservation. *Lethaia* 36, 179 - 194.
- Menard H. W. and Smith S. M. (1966) Hypsometry of ocean basin provinces. *Journal of Geophysical Research* 71, 4305 - 4325.
- Meybeck M. (1993) C, N, and P, and S in rivers: From sources to global inputs. In *Interactions of C, N, P, and S in Biogeochemical Cycles and Global Change* (ed. R. Wollast, F. T. MacKenzie, and L. Chou), pp. 163 - 193. Springer Verlag.
- Middelburg J. J. (1989) A simple rate model for modeling organic matter decomposition in marine sediments. *Geochimica et Cosmochimica Acta* 53, 1577 - 1581.
- Middelburg J. J., Soetaert K., and Herman P. M. J. (1996) Empirical relationships for use in global diagenetic models. *Deep Sea Research Part I*(44(2)), 327 - 344.
- Morgan J. P., Reston T. J., and Ranero C. R. (2004) Contemporaneous mass extinctions, continental flood basalts, and 'impact signals': are mantle plume-induced lithospheric gas explosions the causal link? *Earth and Planetary Science Letters* 217, 263 - 284.
- Norris R. D., Bice K. L., Magno E. A., and Wilson P. A. (2002) Jiggling the tropical thermostat in the Cretaceous hothouse. *Geological Society of America* 30(4), 299 - 302.

- Nunez S., Abarca del Rio R., Lange C., Hebbeln D., and Marchant M. (2006) Milankovitch-scale variability of stable carbon and oxygen isotopes off northern Chile during the last 1 Myr. *Geophysical Research Abstracts* 8, 09925.
- Otto-Bliesner B. L. (1995) Continental drift, runoff and weathering feedbacks: Implications from climate model experiments. *Journal of Geophysical Research* 100(D6), 11,357 - 11,548.
- Overpeck J. T., Strum M., Francis J. A., Perovich D. K., Serreze M. C., Benner R., Carmack E. C., Chapin III F. S., Gerlach S. C., Hamilton L. C., Hinzman L. D., Holland M., Huntington H. P., Key J. R., Lloyd A. H., MacDonald G. M., McFadden J., Noone D., Prowse T. D., Schlosser P., and Vörösmarty C. (2005) Arctic system on trajectory to new, seasonally ice-free state. *EOS, Transaction, American Geophysical Union* 86(34), 309 - 316.
- Pálffy J. and Smith P. L. (2000) Synchrony between Early Jurassic extinction, oceanic anoxic event, and the Karoo-Ferrar flood basalt volcanism. *Geology* 28(8), 747 - 750.
- Pálffy J., Smith P. L., and Mortensen J. K. (2002) Dating the end-Triassic and Early Jurassic mass extinctions, correlative large igneous provinces, and isotopic events. In *Catastrophic events and mass extinctions: impacts and beyond*, Vol. 356 (ed. C. Koeberle and K. G. MacLeod), pp. 523 - 532. Geological Society of America.
- Payne J. L. and Finnegan S. (2006) Controls on marine animal biomass through geological time. *Geobiology* 4, 1 - 10.
- Rampino M. R. and Haggerty B. M. (1995) Mass extinctions and periodicity. *Science* 269(Letters), 617 - 618.
- Redfield A. C. (1958) The biological control of chemical factors in the environment. *American Scientist* 46, 205 - 221.
- Renard M., Raëflis de M., Emmanuel L., Moullade M., Masse J.-P., Kuhnt W., Bergen J. A., and Tronchetti G. (2005) Early Aptian $\delta^{13}\text{C}$ and manganese anomalies from the historical Cassis-La Bédoule stratotype sections (S.E. France): relationship with a methane hydrate dissociation event and stratigraphic implications. *Carnets de Géologie / Notebooks on Geology* 04.
- Rigby S. and Milsom C. V. (2000) Origins, evolution, and diversification of zooplankton. *Annual Reviews of Ecological Systems* 31, 293 - 313.
- Ronov A. B. (1994) Phanerozoic transgressions and regressions on the continents: A quantitative approach based on areas flooded by the sea and areas of marine and continental deposition. *American Journal of Science* 294(Summer), 777 - 801.
- Rowley D. B. (2002) Rate of plate creation and destruction: 180 Ma to present. *Geological Society of America* 114(8), 927 - 933.
- Ryskin G. (2003) Methane-driven oceanic eruptions and mass extinctions. *Geological Society of America* 31(9), 741 - 744.
- Sarmiento J. L. (1993) Atmospheric CO_2 stalled. *Nature* 365, 697 - 698.

- Schlitzer R. (2000) Applying the adjoint method for biochemical modeling: Export of particulate organic matter in the world ocean. In *Inverse Methods in Global Biogeochemical Cycles*, Vol. 114 (ed. P. Kasibhatla), pp. 107 - 124. American Geophysical Union.
- Shaviv N. J. and Veizer J. (submitted) The relative influence of atmospheric CO₂ and galactic cosmic rays on the low-latitude sea surface temperature over the Phanerozoic.
- Sloan E. D. (1997) *Clathrate hydrates of natural gases*, second edition, revised and expanded. Marcel Dekker, Inc.
- Stanley S. M. (1989) *Earth and life through time*. W.H. Freeman and Company.
- Toggweiler J. R. (1994) The ocean's overturning circulation. *Physics Today*, 54 - 50.
- Toggweiler J. R. (1999) Variation of atmospheric CO₂ by ventilation of the ocean's deepest water. *Paleoceanography* 14(5), 671 - 588.
- Tsikos H., Jenkyns H. C., Walsworth-Bell B., Petrizzo M. R., Forster A., Kolonic S., Erba E., Premolisilva I., Baas M., Wagner T., and Sinninghe Damste J. S. (2004) Carbon-isotope stratigraphy recorded by the Cenomanian–Turonian Oceanic Anoxic Event: correlation and implications based on three key localities. *Journal of the Geological Society* 161, 711 - 719.
- Tyrrell T. (1999) The relative influences of nitrogen and phosphorus on the oceanic primary production. *Nature* 400, 525 - 531.
- Van Cappellen P. and Ingall E. D. (1994) Benthic phosphorus regeneration, net primary production, and ocean anoxia: A model of the coupled marine biogeochemical cycles of carbon and phosphorus. *Paleoceanography* 9(5), 677 - 692.
- Walker J. C. G., Hays P. B., and Kasting J. F. (1981) A negative feedback mechanism for the long-term stabilization of Earth's surface temperature. *Journal of Geophysical Research* 86(C10), 9776 - 9782.
- Wallmann K. (2003) Feedbacks between oceanic redox states and marine productivity: A model perspective focused on benthic phosphorus cycling. *Global Biogeochemical Cycles* 17(3), 10,1 - 10,18.
- Wheat C. G., Feely R. A., and Mottl M. J. (1996) Phosphate removal by oceanic hydrothermal processes: An update of the phosphorus budget in the oceans. *Geochimica et Cosmochimica Acta* 60(16), 3593 - 3608.
- Wignall P. B. (2001) Large igneous provinces and mass extinctions. *Earth Science Reviews* 53, 1 - 33.
- Wu J., Sunda W., Boyle E. A., and Karl D. M. (2000) Phosphate depletion in the Western North Atlantic Ocean. *Science* 289, 759 - 762.

Appendix

Appendix A4.1: Flux equations for the water column used in the model. ‡ - Export production (F_{XP}) depends on either nitrate or phosphate concentration considering Liebig's minimum law. The corresponding parameter values are listed in Tabs. A4.2 – A4.6. Depositional fluxes (in $\text{mmol cm}^{-2} \text{ yr}^{-1}$) are defined as fractions of export production. Benthic fluxes of dissolved species s (oxygen, nitrate and phosphate) are calculated for each depositional environment e (shelf, slope & rise, deep-sea) using the benthic model defined in Tab. A4.5. These fluxes are a function of depositional fluxes and affect the concentration of dissolved species in the water column.

Parameter	Equation [‡]
Anoxic POC degradation in deep water	$F_{AND} = 106 * F_{XP} - r_O * F_{O,dw} - \frac{5}{4} * F_{DEN}$
Denitrification in the deep water column	$F_{DEN} = Vol_{dw} * \frac{106}{r_O} * \frac{4}{5} * \frac{K_{O_2}}{O_{dw} + K_{O_2}} * \frac{N_{dw}}{N_{dw} + K_{NO_3}} * F_{XP}$
Export production	$F_{XP} = Vol_{sw} * k_{max} * Min \left(\frac{N_{sw}}{16} * \frac{N_{sw}}{K_{NO_3} + N_{sw}}, P_{sw} * \frac{P_{sw}}{K_P + P_{sw}} \right)$
N ₂ -fixation at low latitudes	$F_{NF} = Vol_{sw} * k_{fix} * 16 * P_{sw} * \frac{P_{sw}}{K_P + P_{sw}} * \frac{K_{NF}}{K_{NF} + N_{sw}}$
Oxygen respiration in deep water	$F_{O,dw} = \frac{106}{r_O} * \frac{O_{dw}}{O_{dw} + K_{O_2}} * F_{XP} * (1 - f_{D,ds} - f_{D,r} - f_{D,sh})$
Transport for species in deep water	$trans_{s,dw} = - \frac{k_{mix}}{Vol_{dw}} * ((P_{dw}, N_{dw}) - (P_{sw}, N_{sw}))$
Transport for species in surface water	$trans_{s,sw} = \frac{k_{mix}}{Vol_{sw}} * ((P_{dw}, N_{dw}) - (P_{sw}, N_{sw}))$

Appendix A4.2: Flux equations for benthos used in the model. The corresponding parameter values are listed in Tabs. A4.2 – A4.6. Benthic fluxes of dissolved species s (oxygen, nitrate and phosphate) are calculated for each depositional environment e (shelf, slope & rise, deep-sea) using the benthic model defined in Tab. A4.5.

Parameter	Equation
Benthic fluxes for dissolved species s (mmol yr ⁻¹)	$F_{BE,s,e} = area_s * \Phi * D_{s,e} * \left. \frac{\partial C_{s,e}}{\partial x} \right _{x=0}$
Bioturbation coefficient as function of depth (cm ² yr ⁻¹)	$D_{B,s,e} = D_{B,e} * e^{\frac{-x_e^2}{2 * xB}}$
Burial rate at the sediment/water interface (cm yr ⁻¹)	$v_{s,e} = (1 - \varphi_f) * \frac{w_e}{1 - \varphi_0}$
Factor relating POC concentration in wt.% to oxygen concentration (mmol cm ⁻³)	$r_{C,e} = 1.2 * r_O * \frac{\varphi_e}{(1 - \varphi_e) * \rho}$
Factor relating POC concentration in wt.% to phosphate concentration (mmol cm ⁻³)	$r_{P,e} = 3.097 * \frac{\varphi_e}{(1 - \varphi_e) * \rho}$
First derivative of bioturbation coefficient as function of depth (cm ² yr ⁻¹)	$f'(D_{B,s,e}) = D_{B,e} * e^{\frac{-x_e^2}{2 * xB}} * \frac{x_e}{xB}$
First derivative of fluid flow with depth	$f'(upw_{s,e}) = -\varphi_f * w_e * \frac{\varphi_e}{\varphi_e^2}$
First derivative of porosity change with depth x	$f'(\varphi) = -p\varphi x * (\varphi_0 - \varphi_f) * e^{-p\varphi x * x_e}$
First derivative of solid volume fraction with depth x	$f'(\varphi_{solid,e}) = p\varphi x * (\varphi_0 - \varphi_f) * e^{-p\varphi x * x_e}$
Fluid flow due to steady state compaction (cm yr ⁻¹)	$upw_{s,e} = \varphi_f * \frac{w_e}{\varphi_e}$
Kinetic constants for POC degradation with depth (yr ⁻¹)	$k_e = k_0 * e^{\frac{-x_e^2}{2 * xB}} + 0.16 * \left(\frac{xB}{w_e} + \frac{x_e}{vs_e} \right)^{-0.95}$
Kinetic constants for POC degradation with depth interval (yr ⁻¹)	$k_{x,e} = k_0 * e^{\frac{-x^2}{2 * xB}} + 0.16 * \left(\frac{xB}{w_e} + \frac{x}{(1 - \varphi_f) * w_e / (1 - \varphi_x)} \right)^{-0.95}$
Sediment porosity (as a function of depth x)	$\varphi_e = \varphi_f + (\varphi_0 - \varphi_f) * e^{-p\varphi x * x_e}$
Volume fraction of solids	$\varphi_{solid,e} = 1 - \varphi_e$

*Appendix A4.3: Differential equations defining the turnover of POC, P, oxygen, nitrate and phosphate in surface sediments (< 20 cm). * - Dissolved oxygen, nitrate and phosphate concentrations in pore waters are given in mmol (cm³ pore water)⁻¹, reactive P and POC concentrations are calculated in wt-%. The five differential equations describing the benthic processes are solved for three different depositional areas. The index e in these equations stands for ds (deep-sea), r (continental rise and slope), and sh (shelf). The corresponding parameter values are listed in Tab. A4.1 – A4.6. The upper boundary conditions of the benthic P and POC models are given by the corresponding depositional fluxes (Tab. A4.6) provided by the pelagic model (Tab. A4.1) whereas the upper boundary of the pore water models for oxygen, nitrate and phosphate are given by the corresponding concentrations in the overlying water reservoirs also calculated in the pelagic box model (Tab. A4.1). These fluxes and concentrations change through time providing a dynamic upper boundary for the benthic model and a close benthic-pelagic coupling. Shelf bottom water concentrations were calculated as averages of deep water and low-latitude surface water concentrations. Zero gradients are used as lower boundary condition at the bottom of the modeled sediment column (20 cm sediment depth).*

Parameter	Equation*
POC in Sediments	$\frac{\partial POC_e}{\partial t} = -k_{s,e} * POC_e$
Reactive P in sediments	$\frac{\partial Pr_e}{\partial t} = -k_{s,e} * \alpha * \left(1 - \frac{PO_{4e}}{PO_{4e}^{SAT}}\right) * Pr_e + r_{Pr,e} * PO_{4e} * \frac{k_{up,s,e} * NO_{3e}}{NO_{3e} + K_{NO_3}}$
Oxygen in pore water	$\frac{\partial O_{2,e}}{\partial t} = -k_{s,e} * \frac{POC_e}{r_{C,e}} * \frac{O_{2,e}}{O_{2,e} + K_{O_2}}$
Nitrate in pore water	$\frac{\partial NO_{3,e}}{\partial t} = k_{s,e} * \frac{POC_e}{r_{C,e}} * r_N * r_O * \frac{O_{2,e}}{O_{2,e} + K_{O_2}} - k_{s,e} * \frac{POC_e}{r_{C,e}} * \frac{4}{5} * \frac{K_{O_2}}{O_{2,e} + K_{O_2}} * \frac{NO_{3,e}}{NO_{3,e} + K_{NO_3b}}$
Phosphate in pore water	$\frac{\partial PO_{4,e}}{\partial t} = k_{s,e} * \alpha * \left(1 - \frac{PO_{4,e}}{PO_{4e}^{SAT}}\right) * \frac{Pr_e}{r_{Pr,e}} * -k_{up,s,e} * PO_{4,e} * \frac{NO_{3,e}}{NO_{3,e} + K_{NO_3b}}$

Appendix A4.4: Parameter values of the pelagic model used for the standard simulation.

Parameter/Symbol	Value	Reference
Kinetic constant for export production k_{max} (yr ⁻¹)	0.03	this work
Kinetic constant for hydrothermal phosphate uptake k_{hw} (yr ⁻¹)	$6 * 10^{-6}$	Wheat et al. (1996)
Kinetic constant for N ₂ -fixation k_{fix} (mmol cm ³ yr ⁻¹)	1	this work
Molar ratio between oxygen consumption and POC degradation rate r_O	1	Anderson and Sarmiento (1994)
Monod constant for N ₂ -fixation K_{NF} (μM)	$5 * 10^{-8}$	this work
Monod constants for export production K_P (μM)	$1 * 10^{-8}$	this work
Oxygen concentration in surface water $O_{2,sw}$ (μM)	300	this work
Ratio between P and N in organic matter r_{PN}	16/106	this work
Riverine input and from aeolian dust of dissolved N F_N (mol yr ⁻¹)	$2 * 10^{+12}$	Meybeck (1993)
Riverine input and from aeolian dust of dissolved P F_P (mol yr ⁻¹)	$3.2 + 1 * 10^{+10}$	Meybeck (1993)
Vertical mixing rate k_{mix} (cm ³ yr ⁻¹)	$1.08 * 10^{21}$	this work
Volume of deep water box Vol_{dw} (cm ³)	$1.17 * 10^{24}$	Toggweiler (1999)
Volume of surface water box (< 500 m) Vol_{sw} (cm ³)	$1.81 * 10^{23}$	Toggweiler (1999)

Appendix A4.5: Parameter values used in the modeling of sedimentary processes in different depositional environments.

Parameter	Deep-sea	Slope & rise	Shelf	References
Area of the seafloor area _e (m ²)	270 * 10 ⁺¹²	50 * 10 ⁺¹²	40 * 10 ⁺¹²	Menard and Smith (1966)
Bioturbation coefficient D _{B,e} (cm ² yr ⁻¹)	1	5	25	Middelburg et al. (1996)
Coefficient for the calculation of tortuosity using Archie's θ	3	3	3	this work
Coefficient for the exponential decrease of porosity with depth Pφ _x (cm ⁻²)	0.1	0.1	0.1	this work
Density of dry solids ρ (g cm ⁻³)	2.6	2.6	2.6	this work
Depositional flux of terrigenous P F _{dep} P _{re} (mol yr ⁻¹)	2.5 * 10 ¹⁰	18 * 10 ¹⁰	18.5 * 10 ¹⁰	this work
Depositional flux of terrigenous POC F _{dep} POC _e (mol yr ⁻¹)	0	4 * 10 ¹²	4 * 10 ¹²	this work
Diffusion coefficient of nitrate in sediments D _{NO₃,e} (cm ² yr ⁻¹)	224	224	448	Boudreau (1997)
Diffusion coefficient of oxygen in sediments D _{O,e} (cm ² yr ⁻¹)	274	274	548	Boudreau (1997)
Diffusion coefficient of phosphate in sediments D _{PO₄,e} (cm ² yr ⁻¹)	97	97	194	Boudreau (1997)
Fraction of export production deposited at the seafloor f _{D,e}	0.1	0.1	0.25	Jahnke (1996)
Kinetic constant for phosphate uptake k _{up,e} (yr ⁻¹)	50	50	150	this work
Kinetic constant for POC and P _{reac} degradation k _{0,e} (yr ⁻¹)	0.04	0.04	0.1	this work
Monod constants K _{NO₃,b} (μM)	0.1	0.1	0.1	this work
Monod constants K _{O₂} , K _{NO₃} (μM)	1	1	1	this work
Porosity at infinitive depth φ _f	0.7	0.7	0.7	this work
Porosity at zero depth φ ₀	0.8	0.8	0.8	this work
Preferential degradation of P _{reac} versus POC α	2	2	2	this work
Saturation concentration of PO ₄ in pore water PO ₄ ^{SAT} (μM)	150	150	150	this work
Sedimentation rate w _e (cm kyr ⁻¹)	1.9	28	47	this work

Appendix A4.6: Pre-industrial Holocene river inputs, aeolian fluxes, ice transport and hydrothermal fluxes were taken from Berner and Berner (1996) and Compton et al. (2000) respectively. Marine export production and depositional fluxes were taken from Schlitzer (2000). Fluxes are given in 10¹⁰ mol P (N) yr⁻¹. Burial rates were calculated from sediment accumulation rates (Berner and Berner, 1996) assuming an average P content of 0.07 wt-%.

Symbol	Flux	Value
F _p	Input of dissolved P into the ocean via rivers and aeoliane transport	3.2
F _n	Input of dissolved N into the ocean via rivers and aeoliane transport	2
F _{hv}	Removal of dissolved P via hydrothermal processes	1.3
F _{xp}	Marine export production of POP	220
F _{dep} POC _{sh}	Deposition flux of terrigenous POC to the shallow (< 500 m) seafloor	400
F _{dep} POC _r	Deposition flux of terrigenous POC to continental rise seafloor	400
F _{dep} P _{sh}	Deposition flux of terrigenous reactive P to the shallow (< 500 m) seafloor	18.5
F _{dep} P _r	Deposition flux of terrigenous reactive P to the continental rise seafloor	18
F _{dep} P _{ds}	Deposition flux of terrigenous reactive P to the deep-sea floor	2.5

Chapter V

Conclusions

The present study contributes to an improved understanding of the Phanerozoic evolution of the exosphere. Via three new stand-alone geochemical box models it was possible to evaluate and reconstruct the evolution of ancient seawater (dissolved inorganic carbon, alkalinity, nutrients, and oxygen), the isotope composition of seawater sulfate and dissolved inorganic carbon, as well as the partial pressures of oxygen (pO_2), carbon dioxide (pCO_2), and methane (pCH_4) in the atmosphere. Moreover, the models were used to reconstruct the volcanic and tectonic activity, and for the first time to reconstruct the net evaporite burial and the productivity of ancient oceans over the entire Phanerozoic (570 Ma). They were applied to identify the main drivers of the sulfur cycle, the chemical consequences of sudden marine methane releases as discussed in the “Clathrate Gun Hypothesis (Kennett et al., 2003)”, and the mechanisms driving an aerated ocean into an anoxic ocean (e.g. during an OAE, Beerling et al. (2002)).

Systematic sensitivity tests of the new models suggest that marine productivity, nutrient inventories and the oxygen content of the deep ocean react very sensitive to changes in ocean ventilation whereas inputs from land (dissolved and particulate nutrients) have a comparably small effect on the ocean’s chemistry. The models confirm the point of view that the positive feedback between oceanic anoxia and eutrophication dominates the evolution of the marine biogeochemical system. This system is mainly controlled by the redox-dependent phosphorus turnover in sediments because reducing sediments are a more important source of phosphate to the oceans than rivers. The models show that both the phosphate content and the productivity of the ocean, have increased continuously over the Phanerozoic, although this trend is neither observed in the burial of organic carbon nor in the marine $\delta^{13}C$ record, showing that these parameters do not reliably reflect the ocean’s changing productivity.

According to the three models presented in this thesis, the deep ocean was almost completely anoxic during the Early Paleozoic. The low oxygen concentration in the early Paleozoic surface ocean - caused by low atmospheric pO_2 values and high surface temperatures - inhibited an effective ventilation of the deep ocean and thereby favored the release of phosphate from sediments. The oxygen concentration in the deep ocean was further reduced by the phosphate-triggered increase in marine productivity and respiration, causing an even bigger release of phosphorus at the seafloor and thus inducing higher productivity and lower oxygen values in a positive feedback loop. The ocean evolved into a fully oxic state during the Permian-Carboniferous cold period when the oxygen concentration in surface water ventilating the deep ocean was very high because of a high atmospheric pO_2 and a low surface temperature. Since these atmospheric and climatic conditions were probably caused by the spread of land plants (Berner, 2004), the development of a fully oxic deep ocean should be regarded as an additional - and previously not recognized - consequence of this major ecological transition.

In the modern ocean, the nitrogen and phosphorus (N : P) ratio of seawater is close to the planktonic N : P ratio (Redfield, 1958). It has been postulated that this relation never significantly changed in the past, always maintained by nitrogen fixation (Tyrrell, 1999). But because of the dependency of seawater phosphate concentration on the redox state of the ocean, the models presented

here predict for the first time that the nutrient N : P ratio in seawater has varied in the ancient ocean. The nutrient N : P ratio was low in the anoxic oceans of the Early Paleozoic and attained very high values during the Permian-Carboniferous cold period.

Additionally to the oceanic anoxic state in the Early Paleozoic the global oceans passed repeatedly through oceanic anoxic states. These oceanic anoxic events (OAEs) are an indicator for dramatic changes in global biogeochemistry. As an example, one of the three models could reproduce the Early Aptian OAE 1a when several important changes were assumed to occur coevally. Nutrient inputs from the continents and ocean ventilation had to be changed simultaneous by 60 % to attain a fully anoxic Cretaceous ocean. The initial trigger could have been a dramatic change in tectonic/volcanic activity, which is documented by $^{87}\text{Sr}/^{86}\text{Sr}$ shifts in the geological record (Jones and Jenkyns, 2001). An enhanced tectonic/volcanic activity affects the climate and thereby ocean circulation through the release of large amounts of CO_2 into the atmosphere. It may also cause changes in oceanic currents due to significant changes in the oceanic topography. The nutrient input into the ocean is enhanced by the deposition and weathering of volcanic ashes and by CO_2 -induced climate change. A significant addition of nutrients to the oceans is also caused by the direct input of volcanic matter into the ocean (Duggen et al., submitted). The fertilization of the ocean, the boost in marine bioproductivity, as well as the storage of huge amounts of carbon on the seafloor restore former conditions via negative feedbacks. This implies that an OAE is not only a dramatic event causing the suffocation of the deep sea but also part of a global regulation system stabilizing Earth's climate.

Other model applications suggest that atmospheric oxygen is more involved in temperature dependent geochemical processes than previously believed. It is stabilized by a number of negative feedbacks and strongly affects the chemical and isotopic composition of seawater and sedimentary rocks. The marine $\delta^{34}\text{S}$ record is clearly determined by both, volcanic and sedimentary processes, while previous models often assumed that the evolution of seawater $\delta^{34}\text{S}$ values reflects the sedimentary cycling of sulfur, only. Hence, the marine $\delta^{34}\text{S}$ record should not be used as a proxy for the turnover of sedimentary pyrite and evaporites since changing rates of volcanic activity on land and at the seafloor also have a significant effect on the isotopic composition of seawater sulfate.

A frequent occurrence of marine sulfur sinks and sources are marine evaporite rocks. New records of evaporite turnover cover the entire Phanerozoic and show that evaporites are preferentially buried during warm periods while evaporite weathering prevails during cold periods (Gordon, 1975). The modeling confirms these trends and shows that evaporite cycling is controlled by the prevailing climatic conditions. It also indicates that the global inventory of evaporites increased over the Phanerozoic. As the concentration of NaCl in seawater is mainly controlled by the turnover of evaporites, this model result also suggests that the salinity of seawater probably decreased over the Phanerozoic.

Another component which is controlled by climate conditions as well as the redox state in the sediments is methane. The models presented here describe the secular CH_4 trend and reflect the importance of waterlogged soils, e.g. the wetlands. In times with high organic matter production,

the atmospheric CH_4 content increases. This was the case during the Carboniferous coal swamp era, when the atmospheric methane content increased up to 10 ppmV. The atmosphere is able to adjust moderate emission rates, but after exceeding a specific value, alkanes become accumulated exponentially in the atmosphere. In times with significant accumulation, and with a sudden release of great methane amounts, the pollution more or less affects the average global temperature by its radiative forcing, and diminishes RCO_2 due to enhanced silicate weathering. The model results clearly show, that the RCO_2 did not increase proportional to pCH_4 due to increasing methane emission. If the impact on average global surface temperature by methane is significant, the RCO_2 decreases, because of the methane derived temperature increase and of the following CO_2 consumption due to enhanced weathering.

The probable triggers for a sudden methane release are under debate - as well as their influence on the global atmospheric methane budget, and on the global temperature. But it is comprehensible that they had an influence on the secular $\delta^{13}\text{C}$ trend, because of the methane's very light isotopic composition. Hence, methane derived carbon emitted into ocean and atmosphere was calculate considering a full model of the global carbon cycle and applying the well constrained isotopic carbon data from the geological record

Because of the decomposition of such great amounts of methane degassed from the ocean floor a massive oxygen reduction in seawater will occur, precluding an anoxic ocean event and possibly resulting in mass extinctions. Generally, the direct effects of atmospheric methane are less important, more important are the indirect effects, e.g. due to the production of water vapor and CO_2 .

As exposed by several model runs, the movement of Earth's crust significantly influences a large number of processes, not only abiotic, but also biotic processes. Up to now, reconstructions of tectonic and volcanic activity over the Phanerozoic remained controversial. Hence, the marine $^{87}\text{Sr}/^{86}\text{Sr}$ record was applied to derive a new record of volcanic/tectonic activity since the isotopic ratios of Sr in seawater are reliably documented in the geological record and because the marine $^{87}\text{Sr}/^{86}\text{Sr}$ record is closely coupled to the volcanic/tectonic activity through the release of isotopically depleted Sr from mid-ocean ridges and young volcanic rocks. The new Phanerozoic record of volcanic/tectonic activity presented here shows distinct peaks during periods marked by a rapid decline in the seawater $^{87}\text{Sr}/^{86}\text{Sr}$ ratios. It shows little correlation to the global sea-level curve suggesting that sea-level changes are a poor proxy for spreading and subduction rates.

Outlook

The present study portrays in detail the development, configuration, functionality, and the results of three new biogeochemical box models. Because of the complexity of the considered global biogeochemical processes these three stand-alone models were used to produce manageable mathematical descriptions of the considered processes. Each of the three models is coherent in itself, but they are configured to the outputs of the different models as external forcings.

Further research on this kind of biogeochemical topics, including the use of these models of cause, should combine the process-descriptions of the single models to an overall-model, with a simplification of the main processes, and a fortified elimination of negligible processes. Besides that an expansion of the future model on several processes would be scientifically precious.

Just to mention one example, it could be interesting for the future to decipher the amount of ancient gas hydrates in dependency to the deposition of organic matter, and their possible positive feedback. In the work presented here the amount of gas hydrates was derived by using recorded carbon isotopes. A nature-orientated model should be calculated via a mathematical description of organic matter input, burial, and decomposition into methane over time. After that, a correlation to the significant carbon isotope excursions could confirm the model approach.

As shown with the help of this one example, for the future it would be useful to detach the model calculations from external forcings. Moreover, it becomes obvious, that there are many biogeochemical processes, neither considered in the above mentioned model approach nor in several other models known to me.

However, science is an ongoing contribution to the understanding of natural processes, we have to expand our knowledge about our environment, never hesitating to solve open questions – even mathematically.

Danksagung

Für das Gelingen dieser Arbeit war, wie es im allgemeinen üblich ist, die Mithilfe anderer erforderlich, im Folgenden möchte ich den Beteiligten danken.

Als erstes gebührt mein Dank meinem Doktorvater Herr Prof. Dr. Klaus Wallmann. Sein beständiges Interesse und seine Diskussionsbereitschaft haben diese Arbeit entscheidend geprägt. Er stand mir jederzeit mit zahlreichen Ratschlägen, Hilfestellungen und modellierspezifischen Tipps zur Verfügung.

Ferner möchte ich PD Dr. Thor Hansteen für die Übernahme des Zweitgutachtens und für wesentliche Ergänzungen danken, die diese Arbeit durch seine Anmerkungen erhalten hat.

Die SFB 574 Mitgliedern Dr. Susan Mau, Thomas Hammerich, Dr. Steffen Kutterolf, Dietmar Bürk, Emelina Corrales Cordero, Dr. Warner Brückmann und Frank Schellig unterstützen mich fürsorglich, mit ihnen führte ich viele spannende und hilfreiche Fachdiskussionen. Von ihnen bekam ich auch in schwierigen Phasen die notwendige moralische Unterstützung. Hervorzuheben sind die guten Seelen des SFB's, Dr. Steffen Kutterolf und Dr. Emanuel Söding, ohne die für uns Doktoranden weder das Verweilen noch das Arbeiten eine so große Freude gewesen wäre.

An dieser Stelle gilt ein besonderer Dank Herrn Dr. Roger Luff, der sich mit viel Einsatz und fundiertem Wissen bemüht hat meine Arbeit voranzutreiben, und bestrebt war, mir mit seinem Kritikbewusstsein und seinen Anregungsvorschlägen zu zeigen, wie eine wissenschaftliche Struktur in meine Modellbeschreibungen und -präsentationen zu bringen ist. Ebenso danke ich Herrn Dr. Christian Hensen, der sich dem Wirrwarr meiner Modellpräsentationen angenommen hat, und mir für das wissenschaftliche Schreiben hilfreiche Tipps gegeben hat.

Frau Dr. Ulrike Schacht gilt ein besonderer Dank, ihre fachlichen Tipps, vor allem wenn ich mich in den Weiten der Geochemie verloren habe, führten mich wieder zurück zum Wesentlichen. Des Weiteren hat sie unermüdliche Ausdauer und Mühe beim Korrekturlesen meiner Schriftstücke bewiesen, und erheblich zum Gelingen dieser Arbeit beigetragen.

Außerdem gilt mein Dank den Mitgliedern der Prüfungskommission, für ihre Bereitschaft, sich mit meiner Arbeit kritisch auseinander zusetzen.

Besonderer Dank gilt meinen Eltern und meinen Freunden, im Besonderen Joachim und Susanne Schöffler, Till Seehusen, Katharina Treyse, Nils Künne, Silke Steph, Kathrin Neumann, und all den anderen die mich über die Jahre moralisch unterstützt haben, und in Phasen großer Widerstände wieder aufgebaut haben. Hervorheben möchte ich an dieser Stelle das entgegengebrachte Vertrauen und die unermüdliche Unterstützung meiner Eltern, ohne die weder das Studium, noch diese Arbeit möglich gewesen wäre. Großer Dank gilt auch meinem Patenkind Jaron Schöffler und seinen beiden Geschwistern Tamino und Noemi, sie zeigten mir oft, dass man auch mit Sand Modelle erstellen kann, und dass auch diese mitunter Sinn machen.

Die Arbeit wurde von der DFG im Rahmen des SFB 574 „Volatile und Fluide in Subduktionszonen: Klima-Rückkopplungen und Auslösemechanismen von Naturkatastrophen“ gefördert.

Hiermit erkläre ich an Eides statt, dass ich die vorliegende Doktorarbeit selbständig erstellt und keine anderen als die angegebenen Hilfsmittel verwendet habe. Ferner habe ich weder diese noch eine ähnliche Arbeit an einer anderen Stelle im Rahmen eines Prüfungsverfahrens vorgelegt, veröffentlicht oder zur Veröffentlichung eingereicht.

Oliver Bartdorff

Lebenslauf

Oliver Bartdorff

geb. am 19.12.1968

in Berlin

Staatsangehörigkeit: deutsch

wohnhaft in Ottendorf, Schleswig-Holstein

1983 - 1991	Grundschule und Gymnasium in Berlin Abitur im Juni 1991
Okt. 1991 – Okt. 1993	Technische Universität Berlin Grundstudium der Energie- und Verfahrenstechnik
Okt. 1993 – Nov. 1999	Technische Universität Berlin Studium der Geologie/Ingenieurgeologie Vordiplom im April 1996 Diplom im November 1999 Diplomarbeitsthema: „Ingenieurgeologische Untersuchung zur Klüftung im Salinar des Bergwerkes Bischofferode (Thüringer Becken)“ bei der K-UTECH GmbH
Okt. 2000 – Juli 2002	Institut für Pflanzenernährung und Bodenkunde der Christian-Albrechts Universität zu Kiel Wissenschaftlicher Angestellter Arbeitsthema: „Böden als Quelle und Senken von CO ₂ “
seit Aug. 2002	IFM-GEOMAR, Christian-Albrechts Universität zu Kiel; Wissenschaftlicher Angestellter im Sonderforschungsbereich 574